INAUGURAL-DISSERTATION

zur

Erlangung der Doktorwürde

der

Naturwissenschaftlich-Mathematischen Gesamtfakultät

der

Ruprecht-Karls-Universität Heidelberg

vorgelegt von

Diplom-Chemikerin Nina Dovalil

aus Waibstadt

Tag der mündlichen Prüfung 19.11.2010

Copper(II) Coordination Chemistry
of
Cyclic Pseudo Hexa- and Octapeptides

Gutachter:

Prof. Dr. Peter Comba

Prof. Dr. Roland Krämer

This thesis was accomplished performed in at the Inorganic Chemistry Department of the Ruprecht-Karls-University in Heidelberg from July 2007 until September 2010 and was supervised by Prof. Dr. Peter Comba.

Experimental work was also accomplished at the Centre for Advanced Imaging (former CMR) at the University of Queensland, Brisbane, Australia under supervision of Prof. Dr. Graeme Hanson.

Publications:

Comba, Peter; Dovalil, Nina; Haberhauer, Gebhard; Hanson, Graeme R.; Kato, Yuki; Taura, Toshiaki "*Complex formation and stability of westiellamide derivatives with copper(II)"* **2010,** Journal of Biological Inorganic Chemistry.

Talks:

„Kupfer(II)-Koordinationschemie zyklischer Peptide"
At the annual"Weihnachtskolloqium" of the Graduate College 850, December 2008.

„Kupfer(II)-Koordinationschemie zyklischer Peptide"
At the „Koordinationschemikertreffen 2010" in Mainz, February 2010

Posters:

"Copper(II) Chemistry of Cyclic Peptides: Towards Understanding the Metabolic Role of Patellamides"
At Lecturetour Korea, Japan 2009

"Copper(II) Chemistry of Cyclic Peptides: Towards Understanding the Metabolic Role of Patellamides"
Presented at the International Conference of Bio Inorganic Chemistry, Nagoya, Japan, 2009

"*Copper(II) coordination Chemistry of Cyclic Peptides: Understanding the Metabolic Role of Patellamides?"*
Presented at the European Conference of Bio-Inorganic Chemistry, Thessaloniki, Greece, 2010

Für Mama und Oma

Acknowledgements/Danksagungen

Als erstem möchte ich Prof. Dr. Peter Comba danken, für das interessante Thema, die Möglichkeit nach Brisbane zu gehen, die Konferenzen zu denen ich durfte und vor allem für die mir gewährten Freiräume bei der Erforschung der zyklischen Peptide. Es hat mir sehr viel Spaß gemacht. Danke auch, für die vielen Gespräche und Diskussionen und dafür, dass deine Tür immer offen steht.

Dr. Marion Kerscher sei gedankt dafür, dass sie sich durch die ganzen Seiten durchgelesen hat, trotz fehlender oder zu vieler Kommata und für das rote Knäul. Danke dass du dich durchgekämpft hast.

Dass der DFT Teil nicht nur eine halbe Seite lang ist, verdanke ich Dr. Bodo Martin und Sascha Hausberg, die meine Rechenfragen mit Geduld beantworten haben. Dr. Prabha Vadivelu, sei dank für die MM Berechnungen in Kapitel 4.

Ein riesen Dankeschön an Marlies von Schönebeck-Schilli und Karin Stelzer, die mich durch den ganzen Verwaltungsdschungel geführt haben und ohne die mir bestimmt heute noch Unterschriften oder Verwaltungskrams für die Annahme als Doktorand fehlen würden.

Prof. Dr. Haberhauer, möchte ich herzlich für die Bereitstellung der Makrozyklen ($\mathbf{H_3L^2}$, $\mathbf{H_3L^3}$, $\mathbf{H_4L^{ox}}$) danken, sowie Yuri Kato für die Messung der ITC Daten und Michael Westphal für die Messung einiger ESR und CD Daten.

Miau und Danke Marta! Ohne dich wär's im Mopslabor maximal halb so schön gewesen. In den letzten drei Jahren bist du mir echt ans Herz gewachsen – Liebe Frau Zett, die Frau D wird dich ganz schön vermissen.

Prof. Graeme Hanson was a big help with all the EPR stuff, he corrected my English, accommodated me in Brisbane, and has become a friend. It was a great time at the CMR and in Brisbane! Of course I'd also like to thank all people at the CMR (or now CAI) for making me feel at home, during my stay there. A special thank goes to Dr. Christopher Noble, for all the help with the EPR, especially helium EPR, for giving me a ride, for throwing snowballs at me and for taking me to the stuff club for lunch. It was really fun! Ross Barnard, Luke Guddat, Tony Miscamble, Gary Schenk, and Chris I'd like to thank you guys for those productive (lunch) times, all the jokes, the high quality conversations and of course all the muffins (Would you please say hi to Kim from me?).

Außerdem ein herzliches Dankeschön an den kompletten AK Comba, der mein Chaos ertragen hat, mit dem ich viel Spaß hatte und den ich vermissen werde. Natürlich auch danke an die „Nachbarn/Mitbewohner“ den AK Linti (für Steine Kocher, seid ihr echt lustig ;)). Vor allem geht mein Dank an Philipp der meinen ganzen Schleim gemessen hat, immer und immer wieder… Euch allen danke ich für die schöne Zeit, die ich in 503 verbracht habe. Hierzu gehört natürlich auch Björn Seibold: auch wenn du schon ne ganze Weile nimmer da bist, war ‘ne echt schöne Zeit mit dir im Labor und das Thema ist auch ein schönes.

Allen Mitarbeitern der chemischen Institute, die in der Analytik beschäftigt sind, möchte ich vielmals danken, vor allem der OC-Massenabteilung, ohne euch würde meine Analytik nicht existieren. Desweiteren ein Dankeschön an den AK Klein, dessen CD Spektrometer ich verwenden durfte und natürlich an meine Forschungspraktikanten Max Hanke, Marta Wolczyk, Laura Waigel und Franziska Schenk. Danke für Eure Hilfe bei Laborarbeiten.

Ein Dank dem kleinen Gecko dafür, dass er mir nen neuen Faden geschickt hat, nachdem ich schon keinen hatte. Und außerdem Nervennahrung und dass du weißt, wie man oinkt.

Thanks George for correcting my English and proofreading my thesis.

Pubsch. Hierfür gibt’s keine richtigen Worte. Danke, dass du auch da bist, wenn alles aus ist. Wenn’s nur noch KO und Maulen im Doppelpack gibt und überhaupt: Ohne Dich wär doof. Ich bin froh, dass ich dich hab.

Der illustren Reihe der kochenden Chemiker, aka Kochzirkel, möchte ich für die ganzen Pfunde danken, die ich in der Zeit zugelegt habe, ihr seid nicht ganz unschuldig. Aber lecker war es immer wieder.

Danke der DFG, der HGS und dem GK850 für die finanzielle Unterstützung.

Last but not least, gilt der wohl größte Dank meiner Familie: Tantili und Erich, den „Elfen“ (Cousinen), der „Schwabenfraktion“ und den „Sinsheimern“. Es ist schön, dass es euch gibt. Allen voran jedoch meiner Mutter und Oma, ohne euch wäre es mir nicht möglich gewesen zu studieren. Ihr habt immer zu mir gehalten und überhaupt: Ihr seid die Besten, ich liebe Euch!

Cyclic Pseudo Peptide Structures and Abbreviations

The following cyclic pseudo peptides are relevant for the present thesis.

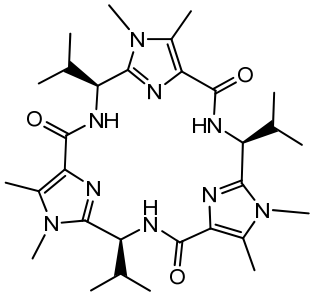

H_3L^1

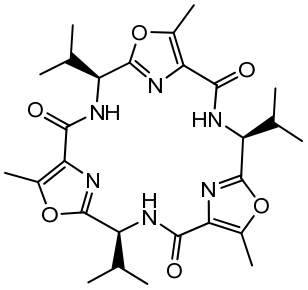

H_3L^2

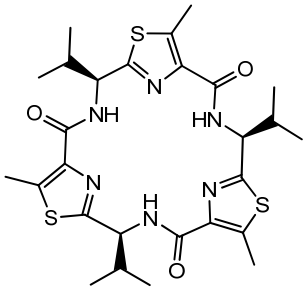

H_3L^3

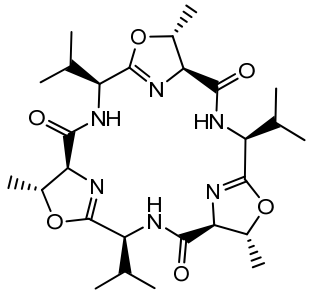

westiellamide
H_3L^{wa}

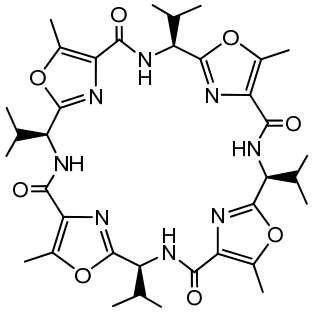

H_4L^{ox}

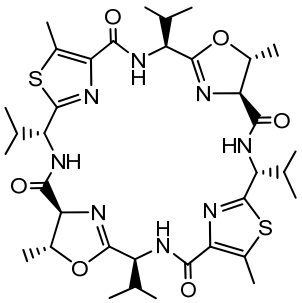

H_4L^{ascA}

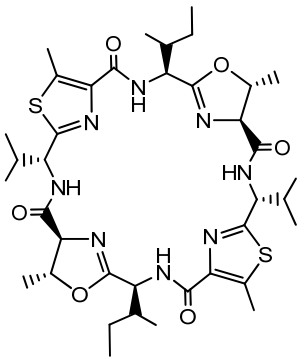

ascidiacyclamide
H_4L^{asc}

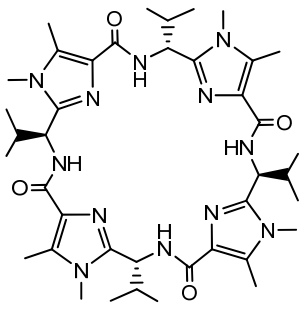

H_4L^{rs}

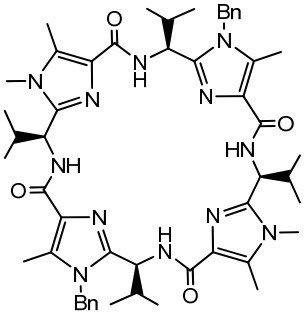

$H_4L^{4\text{-}bn}$

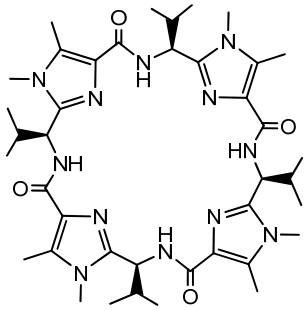

H_4L^4

Abstract

Cyclic pseudo peptides that can be isolated from the marine genus *lissoclinum* (*ascidians*) exhibit an interesting and versatile copper(II) coordination chemistry. They are highly preorganized, well suited for the complexation of copper(II) and are found to preferably form dinuclear copper(II) complexes. The accumulation of copper(II) in the *ascidians* and its complexation in the *ascidians* by cyclic pseudo peptides suggests a metabolic role of the copper(II) complexes of these interesting molecules. Recent findings imply the involvement of dinuclear copper(II) complexes in capture and/or hydrolysis of atmospheric CO_2. This thesis deals with the synthesis of the cyclic pseudo peptides $\mathbf{H_3L^1}$, $\mathbf{H_4L^4}$, $\mathbf{H_4L^{4\text{-}bn}}$, $\mathbf{H_4L^{rs}}$, and $\mathbf{H_4L^{ascA}}$ and with the investigation of the mono- and dinuclear copper(II) complexes of the cyclic pseudo hexa- and octapeptides $\mathbf{H_3L^{1\text{-}3}}$, $\mathbf{H_3L^{wa}}$, $\mathbf{H_4L^4}$, $\mathbf{H_4L^{rs}}$, $\mathbf{H_4L^{ox}}$, and $\mathbf{H_4L^{ascA}}$ and their potential as model systems for the natural macrocycles. The main focus is on the investigation of the dinuclear copper(II) complexes of cyclic pseudo octapeptides, their reaction with atmospheric CO_2 to the corresponding carbonato bridged species, and the differences in coordination chemistry that arise from their different molecular structures (Chapter 4).

An overview over the origin of the natural cyclic pseudo peptides, their preferred conformations, and their so far studied metal coordination chemistry together with the perspective of this thesis is given in Chapter 1. The syntheses of the artificial pseudo peptides ($\mathbf{H_3L^1}$, $\mathbf{H_4L^4}$, $\mathbf{H_4L^{4\text{-}bn}}$, $\mathbf{H_4L^{rs}}$, and $\mathbf{H_4L^{ascA}}$) are described in Chapter 2.

Chapter 3 deals with the mono- and dinuclear copper(II) complexes of the cyclic pseudo hexapeptides $\mathbf{H_3L^{1\text{-}3}}$ and $\mathbf{H_3L^{wa}}$. The stability constants of the copper(II) complexes of $\mathbf{H_3L^{1\text{-}3}}$ have been measured by ITC (Chapter 3.2.2) and, most interestingly, it was found that at low base concentrations $\mathbf{H_3L^2}$ coordinates copper(II) in an unusual way at the outside of the macrocycle. This coordination mode has not been reported before and was further investigated by EPR and NMR studies. The EPR spin Hamiltonian parameters of the mononuclear copper(II) complexes of $\mathbf{H_3L^{1\text{-}3}}$ and $\mathbf{H_3L^{wa}}$ were also calculated by DFT methods (see Chapter 3.2.4) and it was found that the accurate prediction of *g* and *A* tensors is complicated and in order to get reasonable results the consideration of the spin orbit coupling of copper is mandatory. However, no combination of functional and basis set was found that provides reliable results when used with a variety of cyclic pseudo peptides.

The coordination chemistry of the cyclic pseudo octapeptides $\mathbf{H_4L^4}$, $\mathbf{H_4L^{rs}}$, $\mathbf{H_4L^{ox}}$, and $\mathbf{H_4L^{ascA}}$ is described in Chapter 4. Although all cyclic pseudo octapeptides studied show a high cooperativity, the addition of base was found to be mandatory in order to achieve a complete complexation, as per coordinated copper(II) one amide of the macrocycles is deprotonated. Despite their similarity, there are significant differences in the copper(II) coordination chemistry and in the adopted conformations of the macrocycles. The configuration at C_α was found to substantially influence the adopted conformation of the macrocycles. This can be nicely seen, when the X-ray structures of the tetra-imidazole macrocycles $\mathbf{H_4L^4}$, $\mathbf{H_4L^{4\text{-}bn}}$, and $\mathbf{H_4L^{rs}}$ are compared (see Chapter 4.1). The combination of alternating R^*- and S^*-configured stereocenters in the linkers with imidazole rings seems to rigidify the macrocycle and leads to interesting EPR features of the dinuclear complexes. As a result of a so called magic angle setup, the copper(II) centers do not interact and thus exhibit an EPR spectrum that would usually be assigned to a mononuclear species (see Chapter 4.3.3). The assumed rigidity seems to influence the reaction with atmospheric CO_2, as $\mathbf{H_4L^{rs}}$ is the only cyclic pseudo octapeptide studied, where no formation of a carbonato bridged complex could be observed.

$\mathbf{H_4L^{ox}}$, the larger analogue of $\mathbf{H_3L^2}$, was also found to coordinate copper(II) from the outside of the macrocycle, thereby building $\mathbf{H_4L^{ox}}$/copper(II) 2:1 complexes (Chapter 4.4), comparable to the observed coordination chemistry of $\mathbf{H_3L^2}$. This coordination mode could not be observed for any of the other pseudo octapeptides studied and it is likely that the outside coordination is only present in cyclic pseudo peptides whose heterocycles are merely oxazoles, *e.g.* $\mathbf{H_3L^2}$ and $\mathbf{H_4L^{ox}}$. The dinuclear hydroxo complexes of the cyclic pseudo octapeptides $\mathbf{H_4L^4}$, $\mathbf{H_4L^{ox}}$ and $\mathbf{H_4L^{ascA}}$, $[\mathbf{H_2L^n}Cu^{II}_2(OH)]^+$ (n = 4, ox, ascA) were found to reversibly react with atmospheric CO_2 to the corresponding carbonato bridged species. This reaction had previously been observed for the natural pseudo peptide ascidiacyclamide and thus was studied in detail by experimental and computational methods (DFT and MM) by means of the copper(II) complexes of $\mathbf{H_4L^4}$, to probe whether the catalytic hydration of CO_2 was a metabolic function of natural cyclic pseudo peptides. However, the reaction of $\mathbf{H_4L^4}$ with CO_2 was found not to be catalytic. The fact that, besides $\mathbf{H_4L^{rs}}$, all studied cyclic pseudo octapeptides readily react with CO_2 suggests that copper(II) complexes of the natural cyclic pseudo peptides are related to a function that includes their reaction with CO_2, such as CO_2 transport or carbonate formation.

Kurzfassung

Die vorliegende Arbeit beschäftigt sich mit der Kupfer(II)-Koordinationschemie von zyklischen Pseudopeptiden, die aus Meeresorganismen, den *Ascidien*, isoliert werden können. Diese Pseudopeptide sind präorganisiert für die Koordination von Kupfer(II)ionen und weisen bei der Koordination einen ausgeprägten kooperativen Effekt auf, der sich in der bevorzugten Bildung zweikerniger Komplexe wiederspiegelt. Die hohe Konzentration an Kupfer(II) in den Organismen und dessen Komplexierung durch zyklische Pseudopeptide lassen vermuten, dass die Kupfer(II)komplexe eine Rolle im Metabolismus der *Ascidien* haben. Die genaue metabolische Aufgabe dieser Moleküle ist noch ungeklärt, jedoch weisen neuere Ergebnisse auf eine mögliche Beteiligung an der Hydrolyse oder Fixierung von atmosphärischem CO_2 hin. Im Rahmen dieser Arbeit wurden die synthetischen zyklischen Pseudopeptide $\mathbf{H_3L^1}$, $\mathbf{H_4L^4}$, $\mathbf{H_4L^{4\text{-}bn}}$, $\mathbf{H_4L^{rs}}$ und $\mathbf{H_4L^{ascA}}$ synthetisiert und die ein- und zweikernigen Kupfer(II)komplexe der zyklischen Pseudohexa- und -oktapeptide $\mathbf{H_3L^{1\text{-}3}}$, $\mathbf{H_3L^{wa}}$, $\mathbf{H_4L^4}$, $\mathbf{H_4L^{rs}}$, $\mathbf{H_4L^{ox}}$ und $\mathbf{H_4L^{ascA}}$ untersucht. Das Hauptaugenmerk galt der Reaktion der zweikernigen Kupfer(II)komplexe von zyklischen Pseudooktapeptiden mit atmosphärischem CO_2 zu den entsprechenden Karbonato-verbrückten Komplexen und den Besonderheiten in der Koordinationschemie der Makrozyklen, die sich aus deren unterschiedlicher Struktur ergibt (siehe Kapitel 4).

Der Kenntnisstand ist in Kapitel 1 zusammengefasst. Dort wird auf die Herkunft der natürlichen zyklischen Pseudopeptide eingegangen und ein Überblick über bereits untersuchte Pseudopeptide, sowie deren Metallkomplexe gegeben. Die Synthese der künstlichen Makrozyklen ($\mathbf{H_3L^1}$, $\mathbf{H_4L^4}$, $\mathbf{H_4L^{4\text{-}bn}}$, $\mathbf{H_4L^{rs}}$ und $\mathbf{H_4L^{ascA}}$) ist in Kapitel 2 beschrieben.

Die untersuchten ein und zweikernigen Komplexe der zyklischen Pseudohexapeptide $\mathbf{H_3L^{1\text{-}3}}$ und $\mathbf{H_3L^{wa}}$ werden in Kapitel 3 behandelt. Mittels ITC wurden die Komplexbildungskonstanten der ein und zweikernigen Kupfer(II)komplexe von $\mathbf{H_3L^{1\text{-}3}}$ gemessen (Kapitel 3.2.2). Unerwarteterweise wurde beobachtet, dass die Koordinationschemie von $\mathbf{H_3L^2}$ deutlich von der der anderen untersuchten Makrozyklen abweicht. Bei niedrigen Basenkonzentrationen koordiniert $\mathbf{H_3L^2}$ Kupfer(II) an der Außenseite des Makrozyklus mit den Sauerstoffen der Amidbindung und bildet dabei $\mathbf{H_3L^2}$/Kupfer(II) 2:1 Komplexe. Diese ungewöhnliche Koordinationsart wurde mittels ESR und NMR Studien eingehend untersucht. Die experimentell ermittelten ESR Parameter der einkernigen Kupfer(II)komplexe von $\mathbf{H_3L^{1\text{-}3}}$ und $\mathbf{H_3L^{wa}}$ wurden mit DFT Methoden berechnet (Kapitel 3.2.4). Die präzise Vorhersage der

Parameter erwies sich als schwierig, denn genaue Werte können nur erhalten werden, wenn die Spin-Bahn-Kopplung des Kupfers berücksichtig wird. Eine generell gültige Kombination aus Funktional und Basissatz, welche auf die Kupfer(II)komplexe aller zyklischen Peptide angewandt werden kann, konnte nicht gefunden werden.

Kapitel 4 befasst sich mit der Koordinationschemie der zyklischen Pseudooktapeptide $\mathbf{H_4L^4}$, $\mathbf{H_4L^{rs}}$, $\mathbf{H_4L^{ox}}$ und $\mathbf{H_4L^{ascA}}$. Alle Makrozyklen weisen eine ausgeprägte Kooperativität für die Koordination von Kupfer(II) auf, und bilden bevorzugt zweikernige Kupfer(II)-komplexe. Um eine vollständige Komplexierung zu erreichen, ist jedoch die Zugabe von Base zu den Komplexlösungen zwingend erforderlich, da pro koordiniertem Kupfer(II)ion ein Amid Stickstoff deprotoniert wird. Obwohl sich die Pseudooktapeptide sehr ähnlich sind, gibt es große Unterschiede in ihrer bevorzugten Konformation und darum in ihrer Koordinationschemie. Die Veränderung der Konfiguration an C_α führt zu einer beträchtlichen Änderung der Konformation des Makrozyklus. Dies wird besonders deutlich, wenn man die Kristallstrukturen der Makrozyklen $\mathbf{H_4L^4}$, $\mathbf{H_4L^{4\text{-}bn}}$ und $\mathbf{H_4L^{rs}}$ vergleicht (siehe Kapitel 4.1). Interessanterweise sind die zweikernigen Kupfer(II)komplexe von $\mathbf{H_4L^{rs}}$ die einzigen, für die keine Hinweise auf eine Reaktion mit atmosphärischem CO_2 oder Karbonationen gefunden werden konnte (siehe Kapitel 4.3). Es wird vermutet, dass der Makrozyklus aufgrund der Kombination von R^*- und S^*-konfigurierten C_α-Kohlenstoff Atomen und eingebauten Imidazolringen sehr rigide wird und die Kupfer(II)zentren deshalb nicht mehr mit Karbonat verbrückt werden können. Bemerkenswert sind die zweikernigen verbrückten Kupfer(II)-komplexe von $\mathbf{H_4L^{rs}}$, die Aufgrund einer „Magic Angle“ Ausrichtung der beiden Kupfer Zentren ein ESR Spektrum aufweisen, das dem eines einkernigen Komplexes gleicht.

$\mathbf{H_4L^{ox}}$, ein größeres Analogon des zyklischen Hexapeptids $\mathbf{H_3L^2}$, zeigt ebenfalls die ungewöhnliche Koordination von Kupfer(II) über die Außenseite des Ringsystems, die bereits für $\mathbf{H_3L^2}$ beobachtet wurde (Kapitel 4.4). Diese Koordinationsart konnte bei keinem der anderen zyklischen Oktapeptide beobachtet werden und wird von den eingebauten Oxazolringen verursacht. Die zweikernigen Hydroxokomplexe der Pseudopeptide $\mathbf{H_4L^4}$, $\mathbf{H_4L^{ox}}$ und $\mathbf{H_4L^{ascA}}$, $[\mathbf{H_2L^n}Cu^{II}_2(OH)]^+$ (n = 4, ox, ascA) reagieren mit atmosphärischem CO_2 zu den entsprechenden Karbonat-verbrückten Komplexen. Diese Reaktion wurde bereits bei den zweikernigen Komplexen des natürlichen Pseudooktapeptids Ascidiacyclamid beobachtet und wurde anhand der zweikernigen Kupfer(II)komplexe von $\mathbf{H_4L^4}$ im Detail untersucht, um herauszufinden, ob es sich hierbei um die metabolische Rolle der Pseudopeptide handelt. Die Reaktion ist reversibel, jedoch nicht katalytisch. Die Tatsache, dass abgesehen von $\mathbf{H_4L^{rs}}$ alle

untersuchten Makrozyklen bereitwillig mit CO_2 zu den entsprechenden karbonatverbrückten Komplexen reagieren, lässt vermuten, dass die metabolische Aufgabe der zweikernigen Kupferkomplexe der natürlichen zyklischen Peptide mit CO_2 zusammenhängt. Hierbei könnte es sich um den Transport von CO_2 oder um die Bildung von Karbonat handeln.

Table of Contents

1. State of the Art

1.1. Introduction

The oceans have been a source of fascination for humanity over many years. They cover more than 70% of the Earth's surface and, when their depth is considered, they encompass about 300 times the habitable volume of the terrestrial habitats on Earth. Nevertheless we are still far away from understanding marine life and ecosystems – the majority of marine life is not discovered yet, particularly that of the deep sea, and of the discovered life forms few are studied in detail.

In the 1970s, secondary metabolites from marine organisms were found to have excellent antiviral and cytotoxic properties.[1-11] These findings and the fact that some of the drugs derived from them are able to overcome multidrug resistance or to act as antineoplastic agents has boosted the interest in molecules derived from marine organisms.[12] Prior to the discovery of the drug potential of marine derived molecules the pharmaceutical researches had almost exclusively focused on the investigation of terrestrial metabolites.[13-17] However, the molecular design of molecules of terrestrial origin is fairly well studied and new isolated substances often only repeat known themes.[18] Marine metabolites on the other hand seem to cleverly manipulate the molecular structure that we know, including unusual functional groups or stereochemical quirks.[19] With the discovery of their potential as anti cancer drugs the number of isolated marine substances increased significantly. In just ten years (between 1977 and 1987) approximately 2500 molecules were isolated from marine sources.[20] Since then their number has continuously increased up to 3700 in 2007.[13, 21] The sensitivity of the marine ecosystem and the low availability of most metabolites has created an increasing demand for viable synthetic routes to the natural products or their model systems.[22] Synthesized mimics help study the function of the metabolites in the marine organisms as their exact metabolic purpose is still under investigation – some of the molecules, that showed a high anti tumor activity, are thought to be initially responsible for metal ion complexation.[19] They have structural features that are predestinated for metal ion complexation, such as functional groups, for example amides, heterocycles or ethers and preorganized chelate or ring structures. This is unsurprising as the oceans are a rich source for

a variety of metal ions. However, the number of metal complexes directly isolated from marine organisms is quite small.[23-25]

In some organisms, *e.g. ascidians* (sea squirts), the metal ion concentration, compared to the surrounding seawater, was found to be increased to a large extent, especially the concentration of copper(II) up to a factor of 10^4.[26-28] This is amazing, particularly considering the fact that the toxic effect of copper(II) on organisms is already observable at concentration in the range of 10^{-7} to 10^{-6} M.[29] In the *ascidians* the copper(II) chelation occurs *in vivo* by cyclic pseudo peptides that are produced by a symbiotic *prochloron* organism.[26, 30] Besides the fact that copper(II) ions are accumulated, little is known so far about the actual complexation chemistry of the cyclic pseudo peptides and of the chemistry of the copper(II) complexes of cyclic pseudo peptides. The high enrichment of copper(II) is suggestive for a metabolic role of the copper(II) complexes in the *ascidians*.[5, 31-38] A major hindrance to examining the chemistry of the natural metabolites is their low availability from the organism, only available with expensive extraction from natural sources or complex synthesis of artificial compounds.

The work presented in this thesis focuses on the interaction of copper(II) ions with cyclic pseudo hexa- and octapeptides and the possible CO_2 fixation of the dinuclear copper(II) complexes of the cyclic pseudo octapeptides. The studied cyclic pseudo peptides are models of natural compounds that can be isolated from *ascidians*, invertebrate marine organisms.

1.2. Cyclic Pseudopeptides from *Lissoclinum Patella* and *Lissoclinum Bistratum*

Sea squirts are sessile, marine animals, thus they remain firmly attached to substratum such as rocks and shells. Their name is derived from the Greek word *ασκιδιον*, which means leather bottle and describes their physical appearance. They have a sac-like body structure, with a tough outer "tunic" made of the polysaccharide tunicin, which compared other to tunicates leads to a more rigid “exoskeleton”. *Ascidians* can be found all over the world, usually in shallow water with salinities over 2.5%, and are among those marine organisms whose copper(II) accumulation is high. The fact that copper(II) is found in the non-polar fractions

suggests its complexation by organic molecules, such as natural cyclic pseudo peptides, *e.g.* patellamides (see Figure 1.2). Indeed, the marine genus *lissoclinum* is a rich source of cyclopeptide alkaloids featuring multiple oxazoline, thiazoline, oxazole or thiazole rings that have interesting properties.[39]

In 1980, Ireland and Scheuer reported the structure of ulicyclamide, that was isolated from a *lissoclinum patella* tunicate found near the Palau Islands in the Pacific Ocean (Figure 1.1).[40] In the following years, the patellamides A-E were isolated from various species of the genus *lisoclinum patella* (Figure 1.2).[41-46]

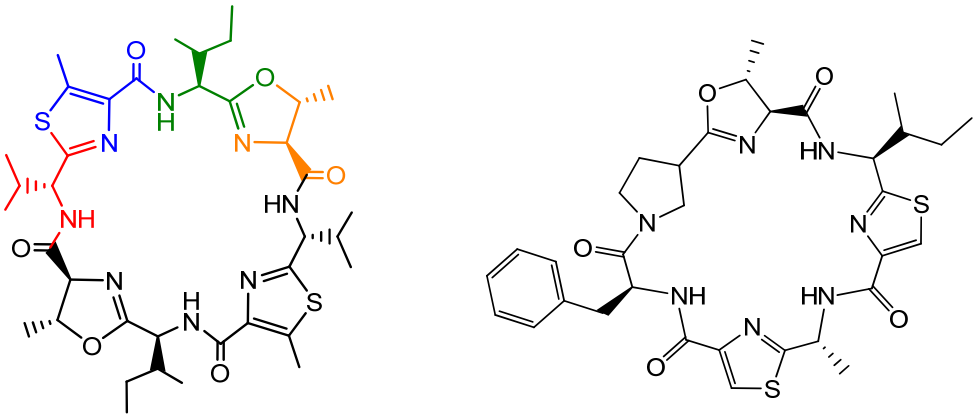

Figure 1.1. Chemical structure of the cyclic pseudopeptides ascidiacyclamide (left) and ulicyclamide. The different amino acids that build up a cyclic pseudo octapeptide are color coded in the structure of ascidiacyclamide (left): *D*-valine (red), *L*-cysteine (blue), *L*-isoleucine (green) and *D*-threonine (orange).[40, 45]

Five-membered heterocyclic rings are incorporated in the natural metabolites and alternate in the ring sequence with amino acid residues. The five-membered heterocyclic rings result from the condensation of serine, threonine and cysteine side chains with the preceding carbonyl groups in the peptide sequence. Due to these "disguised" peptide functionalities, the macrocycles are also referred to as pseudo peptides, *e.g.* patellamides are so called pseudo octapeptides as each of their heterocycles is derived from the condensation reaction of two amino acid residues (see Figure 1.1). Cyclic pseudo peptides that contain imidazole units in their scaffold have not yet been isolated from nature, most likely as a result of the low natural abundance of diaminopropionic acid (Dap), formally the amine analogue of serine.[47-48] The natural cyclic pseudo peptides are produced by symbiotic cyanobacteria up to several percentage of the dry weight of the *ascidians*, and due to this rather high production it is assumed that the macrocycles complexes are involved in the *ascidian's* metabolism.[30, 49] Furthermore, as

they are most likely produced in order to coordinate copper(II) it seems reasonable that the copper(II) complexes of the cyclic peptides are also involved in the *ascidian's* metabolism.

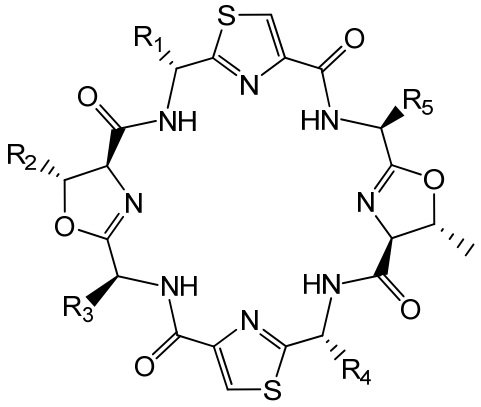

Patellamides	R_1	R_2	R_3	R_4	R_5
A	*D*-val	H	*L*-ile	*D*-val	*L*-ile
B	*D*-ala	Me	*L*-leu	*D*-phe	*L*-ile
C	*D*-ala	Me	*L*-val	*D*-phe	*L*-ile
D	*D*-phe	Me	*L*-ile	*D*-ala	*L*-ile
E	*D*-val	Me	*L*-val	*D*-phe	*L*-ile
F	*D*-phe	H	*L*-val	*D*-val	*L*-val
G	*D*-phe	Me	*L*-ile	*D*-ala	*L*-leu
Ascidiacyclamide	*D*-val	Me	*L*-ile	*D*-val	*L*-ile

Figure 1.2. Scaffold of the natural cyclic pseudo octapeptides (left); substituents of the patellamides A-G and ascidiacyclamide (right).[41-46]

Besides the described cyclic pseudo octapeptides, *ascidians* were also found to contain smaller macrocycles. Various cyclic pseudo hexapeptides could be isolated from the marine genus *lissoclinum bistratum*, found on the Great Barrier Reef (Northeast Australia). The structures of bistratamide A and B have been reported by Watters *et al.* in 1989 (see Figure 1.3).[42]

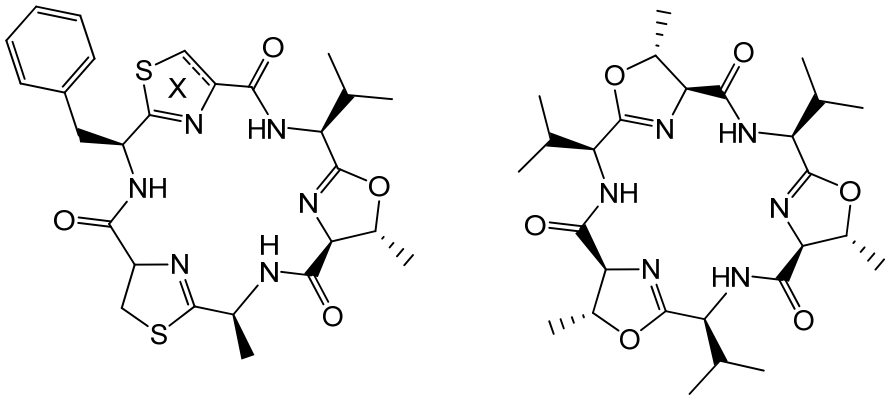

bistratamide A, X = thiazoline
bistratamide B, X = thiazole

$\mathbf{H_3L^{wa}}$

Figure 1.3. Natural cyclic pseudo hexapeptides isolated from *lissoclinum bistratum* (bistratamide A and B; left) and *westiellopsis prolifica* (westiellamide, $\mathbf{H_3L^{wa}}$, right).[42, 50-51]

Three years later, in 1992, the same group reported the isolation and structure of a C_3-symmetric cyclo tris-oxazoline from a marine organism, while at the same time, Prinsep *et al.* isolated an identical substance from the terrestrial cyano bacterium *westiellopsis prolifica* and named it westiellamide (see Figure 1.3).[50-51] As most of the previous work focused on the pharmaceutical application of the maritime metabolites, their actual coordination chemistry is hardly known.[1-11]

The synthesis of a variety of natural as well as modified cyclic pseudo peptides can be found in the literature.[22, 39, 52-55] Besides the naturally occurring heterocycles, imidazoles and oxazoles are incorporated into the macrocycle. Depending on the complexity of the desired macrocycle, they are either synthesized via cyclo oligomerization or cyclo dimerisation of the respective building blocks (see Chapter 2).

1.3. Structural Features of Cyclic Pseudo Peptides

In order to understand and investigate the copper(II) coordination chemistry of cyclic pseudo peptides, one has to be aware of their structural features. Studies of the conformations of azole-based marine cyclic peptides, both in solution and in the solid state, have provided valuable insights into the factors which may affect the reactivities and the biology of these unique secondary metabolites.[9, 43, 56-63]

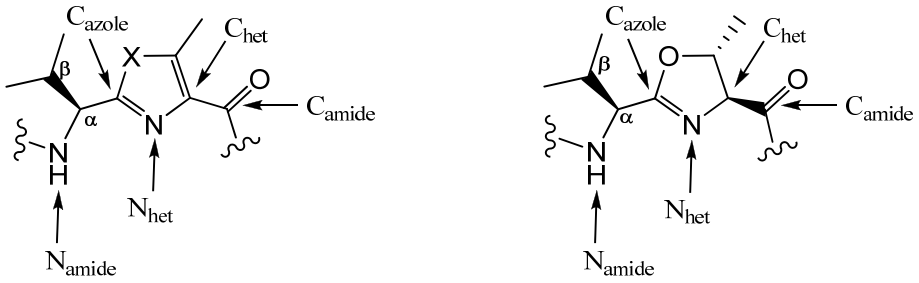

Figure 1.4. Nomenclature of the heterocyclic building blocks of the macrocycles.

The structure of cyclic pseudo peptides and their analogues is dependent on the amino acid residues that connect the heterocycles, on the absolute configuration (R^* vs. S^*) of the

amino acids, and on the incorporated heterocycles. The macrocycles adopt a relatively rigid structure, as the macrocyclic ring closure fixes the position of five ring atoms (C_α-C_{azole}-N_{het}-C_{het}-C_{amide}; see Figure 1.4 for nomenclature) and the incorporation of unsaturated heterocycles reduces the flexibility of the macrocycle as the planarity of the heterocycle is enhanced to the vicinal peptide group.[64-65]

Usually, all protons of the peptide NH groups point towards the center of the ring and the peptide carbonyl functions towards the outside of the macrocycle. In the case of an identical configuration (*e.g.* $\mathbf{H_3L^{wa}}$, all-*S**) of the amino acid that connect the heterocycles in the macrocycle, all amino acid residues face the same side of the molecule and adopt axial positions. The incorporation of oxazole or oxazoline units results in azole moieties of the macrocycle that are almost coplanar, whereas in the case of the thiazole or imidazole containing peptides, the heterocyclic moieties of the macrocycle have a cone-like structure (see Chapter 4.1.1).[65] The dihedral angle χ [N_{amide}-C_α-C_{azole}-X] can be taken to express the extent of deviation from planarity ($\chi = 180°$ in case of planarity). Haberhauer *et al.* showed that the adopted angle χ is dependent on the azole system and on the size of the amino acid side chains.[64] They calculated the change in energy of a reference system induced by a change of χ. A plot of the calculated energies is given in Figure 1.5.

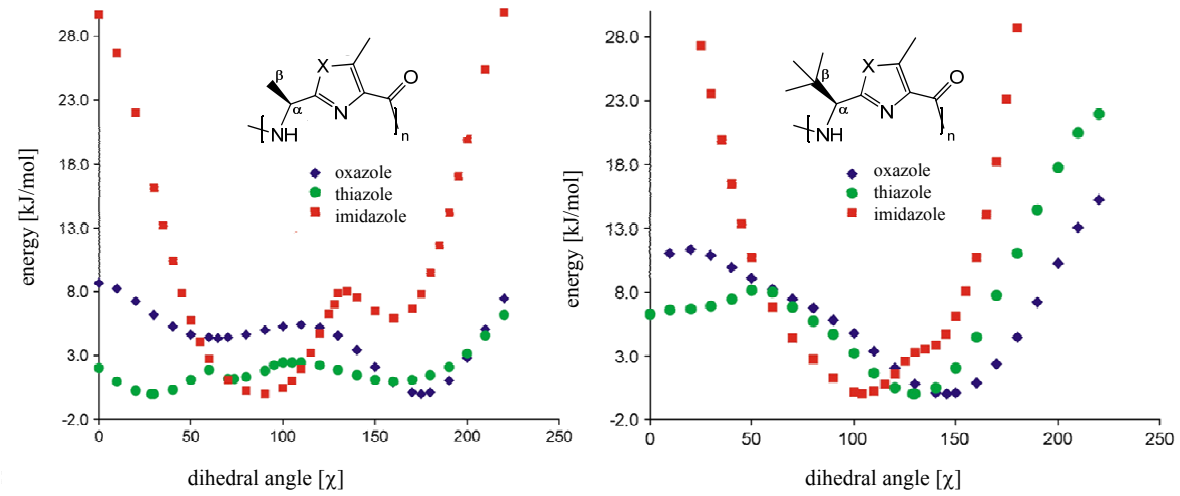

Figure 1.5. DFT-calculated (G03, B3LYP/6-31g**) energy profiles of the oxazole- , thiazole- and imidazole- reference systems, respectively, in relation to the dihedral angle χ.[64-65]

The energy profile reflects the flexibility of the distinct reference systems and also reveals the reason for the different conformations of the macrocycles. The imidazole and oxazole reference systems with a small side chain (Figure 1.5, left) show two minima in the

region of 0-200°; the minima of the imidazole system are at 90° and 150° and those of the oxazole system at 60° and 170°. The small thiazole reference system, on the other hand, has three energetically similar minima at 30°, 80° and 160° respectively, suggesting that thiazole containing macrocycles are slightly more flexible. The energy profiles change remarkably upon replacement of the methyl groups by the sterically more demanding *tert*-butyl groups (Figure 1.5, right). As a consequence of the large side groups, the rotation around the dihedral angle χ has a higher activation barrier, and in combination with electronic effects the energy profile changes remarkably, especially in the region of 120°–200°. Each profile has a single minimum now in the range of 100°-150°. The distinctive minima are 149° for the oxazole-, 129° for the thiazole- and 104° for the imidazole *tert*-butyl reference system. The computed preference of the azole systems for different dihedral angles corresponds to what was found in the X-ray structures of the respective cyclic pseudo hexapeptides (see Chapter 3). The reason for this difference is mainly of electronic origin: the $\pi(C_{azole}\text{-}N_{het})$-orbital of an imidazole ring is high in energy and, accordingly, preferably interacts with the $\sigma^*(C_\alpha\text{-}N_{amide})$-orbital. The optimum interaction between these two orbitals is at an angle of 90°, where the $\sigma^*(C_\alpha\text{-}N_{amide})$-orbital is oriented parallel to the $\pi(C_{azole}\text{-}N_{het})$-orbital. In contrast, the $\pi^*(C_{azole}\text{-}N_{het})$-orbital of an oxazole ring is of low energy and therefore preferably interacts with the energetically high $\sigma(C_\alpha\text{–}C_\beta)$- and $\sigma(C_\alpha\text{–}H_\alpha)$-orbitals. This interaction has its optimum at an angle χ of 180°.[64]

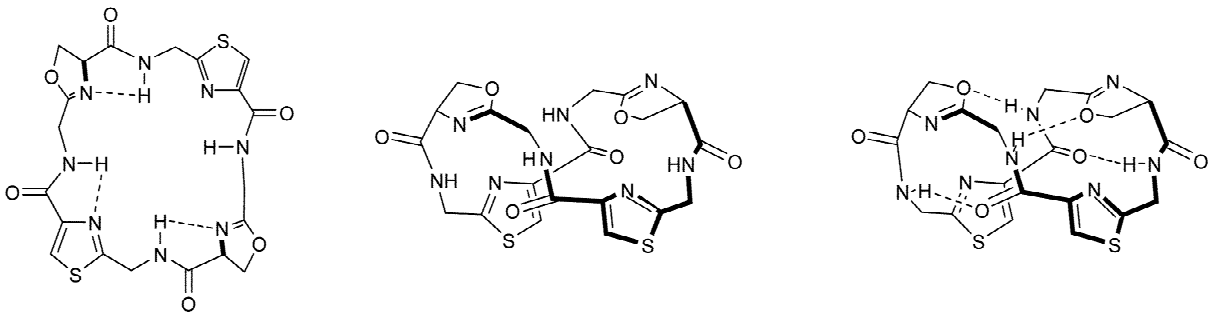

A B (solution) C (solid state)

square conformation figure of eight

Figure 1.6. Adopted conformations (square and figure of eight) of ascidiacyclamide and the patellamides in solution and the solid state.[26, 59, 66]

The majority of the cyclic pseudo hexapeptides reported to date are built up from standard *L*-amino acids, resulting in all-*S** configured amino acid linkers. In contrast, the patellamides A-G and ascidiacyclamide are built up from *D*- and *L*-amino acids and exhibit an

alternating stereochemistry in the linkers. The cyclic pseudo hexapeptides adopt a C_3-symmetrical conformation in solution and solid state.[64, 67] The lower symmetry caused by the configurational difference in the linker of cyclic pseudo octapeptides enables them to adopt different conformations in solution and the solid state (see Figure 1.6).[26, 59, 66] In the solid state the formation of a intramolecular hydrogen bond network can be observed that presumably is no longer present in solution.[26]

An early X-ray crystal structure determination of the C_2-symmetric ascidiacyclamide, reported by Ishida et *al.*, in 1988, showed that it adopts a "square" (also sometimes referred to as "saddle-shaped") conformation, *i.e.* **A** in Figure 1.6, in the solid state with its thiazole and oxazoline rings occupying the corners of a rectangle.[58, 61, 66, 68-69] Patellamide A has a similar rectangular shape in the solid state, but, by contrast, the X-ray analysis of patellamide D (see Figure 1.7) shows that it adopts a "twisted figure of eight" conformation (see Figure 1.6, **C**), stabilized by intramolecular hydrogen-bonds and by π-stacking of its thiazole rings.[59-60, 69-70] Ishida *et al.* have suggested that the different solid state conformations found in patellamides A and D are related to the degree of asymmetry in patellamide D.[59]

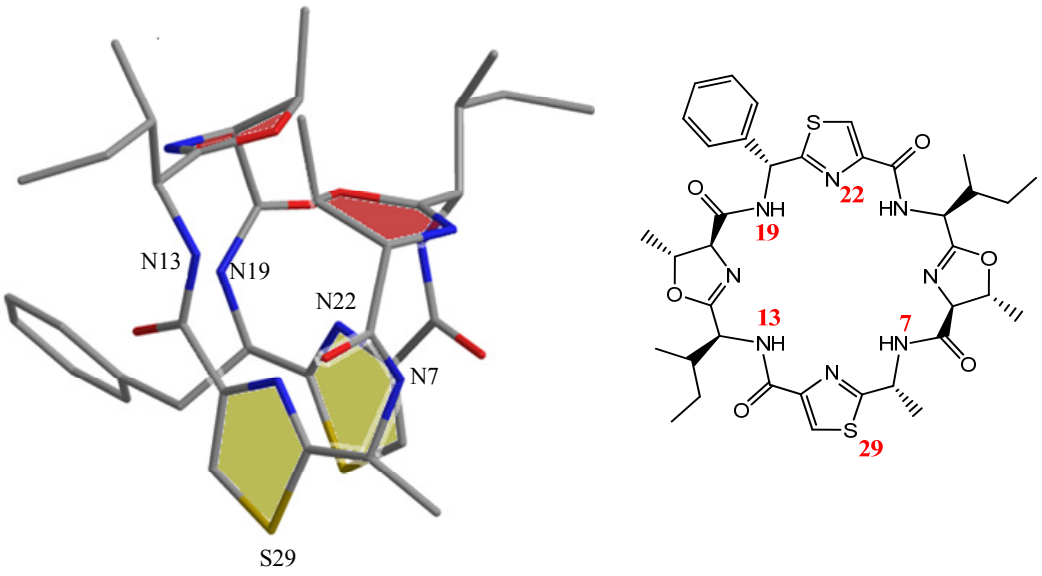

Figure 1.7. X-ray (left) and chemical structure of patellamide D (right).[43] (nitrogen = blue, oxygen = red, carbon = grey, sulfur = yellow, hydrogen atoms and solvent molecules are omitted for clarity).

They conclude that the square conformation in patellamide A (and ascidiacyclamide), is able to resist, to a degree, the transition to the twisted figure-of-eight conformation, since this would lead to deformation of its preferred C_2-symmetric structure. In agreement with this assumption, the solution conformations (measured in chloroform) of the related non-

C_2-symmetric patellamides B and C have similar twisted figure-of-eight-like backbone conformations, albeit without intramolecular hydrogen-bonding (see Figure 1.6, **B**).

1.4. Metal Coordination to Cyclic Pseudo Peptides

The previously mentioned high copper(II) concentration in *ascidians* together with the structural similarity of the cyclic pseudo peptides to aza-crown ethers and porphyrins suggests that the peptides are tailor made for association and binding to metal ions.[26] The interaction of patellamides and ascidiacyclamide with metal ions, was first studied by Hawkins *et al.*[71-73] In 1988, they reported the circular dichroism of the mono- and dinuclear copper(II) complexes of patellamide D.[74-75] Later on, in 1994, they reported the carbonato-bridged dinuclear copper(II) complex of ascidiacyclamide (Figure 1.8), where two copper(II) ions are bridged by a carbonate anion and embedded in the saddle-shaped ascidiacyclamide macrocycle.[73-74] The copper(II) ions are coordinated to three nitrogen donors, two of heterocyclic origin and the third originates from a deprotonated amide. The coordination sphere of copper(II) is completed by two water molecules. The reported affinity of the ascidiacyclamide–copper(II) complex for carbonate is of special interest as it suggests that these metal peptide conjugates could be involved in the activation and transport of CO_2 *in vivo* for specific biochemical processes.[71] In this perspective the cyclic pseudo peptides are also of environmental interest.

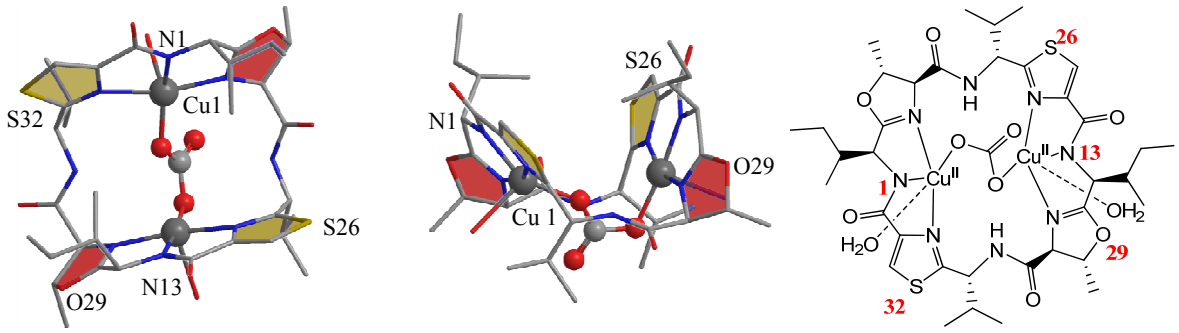

Figure 1.8. X-ray structure of the carbonato-bridged dinuclear copper(II) complex of ascidiacyclamide. Top view (left), side view (middle) and chemical structure (right).[71] (Color code: carbon = grey, sulfur = yellow, nitrogen = blue, oxygen = red).

The ongoing climate change debate demands the discovery and investigation of new methods and technologies that are capable to fixate and hydrolyze atmospheric CO_2.[76-77] CO_2 fixation and hydrolysis usually occur at neutral to slightly basic conditions, although some metal complexes have been reported to hydrolyze atmospheric CO_2 under acidic conditions.[78-79] The hydrolysis of CO_2 in general takes place in an intramolecular reaction and, therefore, the formation of intermolecular carbonato-bridged complexes is rare.[80-81] Dinuclear zinc(II) complexes that catalytically hydrolyze CO_2 via a nucleophilic attack of coordinated water or hydroxide have been studied in detail.[82-88] However, although copper(II) complexes are known that react with CO_2 to respective carbonato-bridged complexes and also some that are able to catalyze the hydration of CO_2, they have not been investigated in detail.[79, 89-92]

At the same time that Hawkins *et al.* studied the interaction of copper(II) with ascidiacyclamide and patellamides, Wipf *et al.* described the synthesis and X-ray structure of a silver complex of the C_3-symmetric cyclic peptide westiellamide (see Chapter 3).[53, 93] These studies provided the first clear evidence for the binding of *lissoclinum* peptides to metal ions and provided the impetus for further investigations in this area.

These investigations revealed that although patellamides A, B and E easily bind to zinc(II) and copper(II), they show no affinity for binding to other metals, such as magnesium(II) and calcium(II).[62, 94-95] All studied cyclic pseudo octapeptides bind up to two metal ions, copper(II) and zinc(II), respectively, having binding constants in the range of 2×10^4 to 2×10^5 for the first binding domain and 20 to 230 for the second binding site.[95] The CD spectra of the patellamide–metal conjugates are consistent with a square conformation of the cyclic pseudopeptide's backbone. Jaspars *et al.* found that patellamide C showed a higher affinity for copper(II) ions than patellamide A and assigned this feature to the ability of patellamide C to readily change its conformation from figure-of-eight to square.[26] Complexation of the second copper(II) ion then occurs without further change in conformation, suggesting a cooperative effect of the macrocycles, *i.e.* the coordination of the first metal ion preorganizes the macrocycle for the coordination of the second. These findings provide strong evidence for copper(II) as the biological relevant metal.

In order to probe the importance of oxazoline rings in patellamides for metal chelation in more detail, Comba *et al.* synthesized analogues of patellamide A, where the oxazoline rings have been hydrolyzed, resulting in cyclic pseudo octapeptides that only contain two heterocycles in their macrocycles. Their studies showed, that these macrocycles are also preorgan-

ized for the complexation of copper(II) ions.[96-97] Further studies by van den Brenk *et al.* showed that hydrolyzed patellamide A coordinates potassium, see Figure 1.9.[97] As a consequence of the presence of hydrolyzed oxazolines, the macrocycle is larger now and more flexible. In the X-ray structure, the potassium(I) ion is coordinated to two thiazole-nitrogen atoms and two amide oxygen atoms in a octahedral coordination environment, where the coordination sphere is completed by the oxygen atoms of two perchlorate ions.

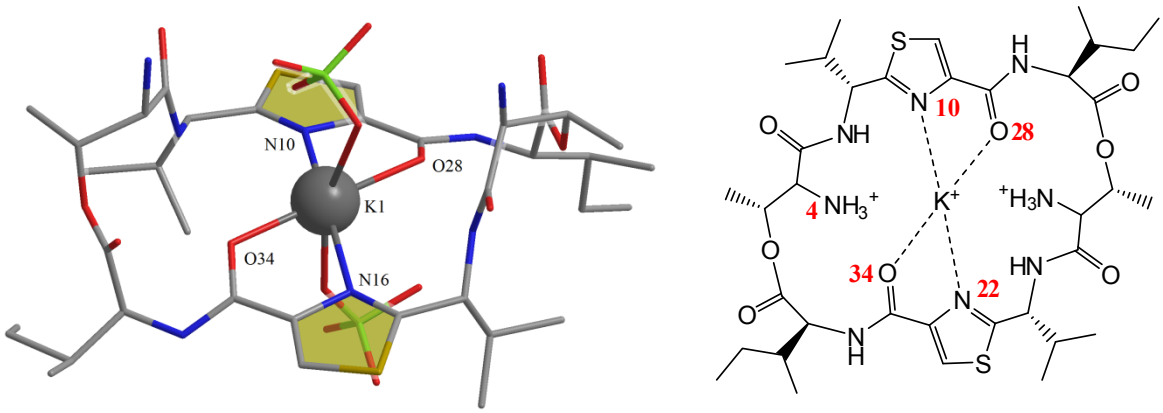

Figure 1.9. X-ray (left) and chemical structure (right) of the potassium(I) complex of hydrolyzed ascidiacyclamide.[97]

1.5. Synthetic Routes to Cyclic Pseudo Peptides

The general synthesis used to construct macrocyclic pseudo peptides consists of two parts. Firstly, the heterocyclic building blocks (see Figure 1.4, for an example of a building block), consisting of an amino acid linker and a heterocycle, are synthesized and are secondly cyclo-oligomerized to form the desired macrocyclic pseudo peptide. When oxazolines, which are very sensitive towards hydrolysis, are present in the pseudo peptides, the oxazoline forming ring closure is performed as one of the last synthetic steps, either after the macrocycle is already formed or in the preceding step.[98-100] Symmetrical pseudo peptides can also be built from mono- or dimeric building blocks in a one pot reaction, while asymmetric macrocycles require the synthesis of a linear peptide sequence with a subsequent intramolecular ring closure.[101] The syntheses of ascidiacyclamide and the patellamides A-C were already reported in the mid 1980's by Hamada *et al.*[56-57, 98] As an alternative to reactions in solution,

solid phase reactions were developed, which are well suited to the synthesis of asymmetric macrocycles.[62, 96-97]

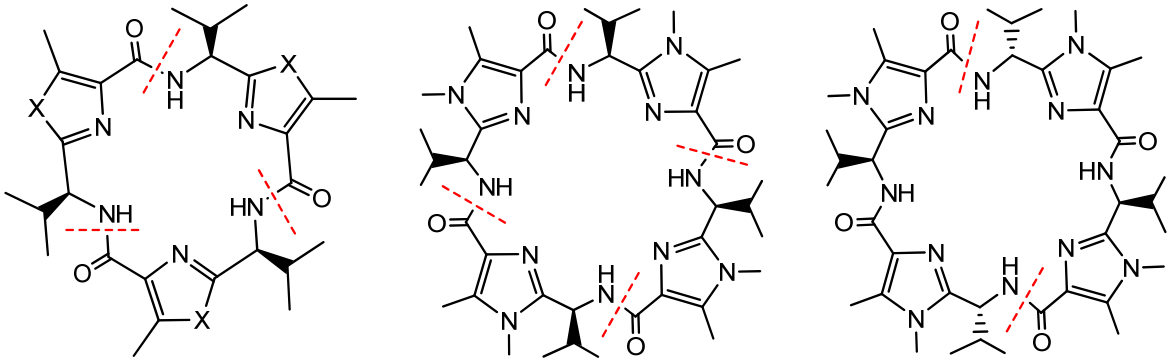

H_3L^1, X = NMe
H_3L^2, X = O
H_3L^3, X = S

H_4L^4

H_4L^{rs}

Figure 1.10. Molecular structures of the cyclic pseudo hexapeptides **H_3L^{1-3}** and octapeptides **H_4L^4** and **H_4L^{rs}** and their retrosynthetic disassembling into monomeric or dimeric building blocks.

Recently the one-pot syntheses of macrocyclic pseudo peptides have been intensively studied and improved by Haberhauer *et al.*[52-53, 65, 102] The C_3-symmetric westiellamide and its analogues are usually synthesized in a cyclo-oligomerisation reaction from the enantiomerically pure azole building blocks. C_4-symmetric pseudo octapeptides are either derived via cyclo-oligomerization of the respective monomeric azole unit (analogous to the synthesis of westiellamide and its analogues) or by cyclodimerisation of two coupled azole units. Although cyclo-dimerisation enhances the yields, it also elongates the synthesis by four time consuming steps. The retrosynthetic disassembling into mono- and diazole units, respectively, is depicted in Figure 1.10. A detailed description of the syntheses can be found in the experimental section (Chapter 5).

1.6. Aim

Important questions that are related to the marine organisms and their metabolites are: why do *ascidians* and other marine organisms produce these complicated molecules? Are they relevant for the *ascidian's* metabolism? And if so – what is their actual function? Is it "just" metal ion complexation and transport in the organisms or do the metal complexes themselves have a metabolic role? A point of interest is the mode of interaction of copper(II) with the macrocycles and from where the differences between the synthetic and natural cyclic pseudo peptides arise. The role of the heterocyclic moieties as well as the influences of the stereochemistry of the amino acid linkers and their correlation to the coordinating properties of a pseudo peptide are of special interest.

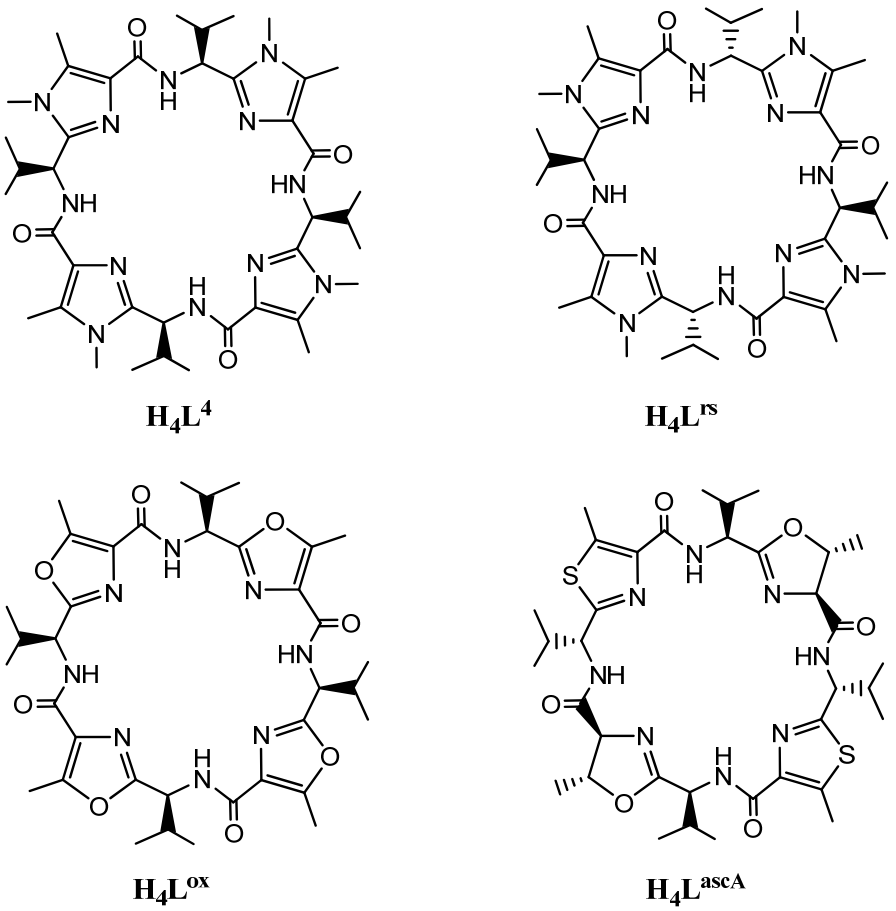

Figure 1.11. Chemical structure of the studied cyclo pseudo octapeptides $\mathbf{H_4L^4}$, $\mathbf{H_4L^{rs}}$, $\mathbf{H_4L^{ox}}$, and $\mathbf{H_4L^{ascA}}$.

Recent experiments showed that the dinuclear copper(II) complexes of patellamide analogues are able to react with atmospheric CO_2 and hydrolyze it to form bridged carbonato complexes, similar to the natural pseudo peptide ascidiacyclamide.[103] Initial experiments indicated that this process might be catalytic.

The main focus of this work is the investigation of the copper(II) coordination chemistry of the cyclic pseudo octapeptides $\mathbf{H_4L^4}$, $\mathbf{H_4L^{rs}}$, $\mathbf{H_4L^{ox}}$, and $\mathbf{H_4L^{ascA}}$ (see Figure 1.11). The stereocenters of the connecting amino acids in the natural cyclic pseudo octapeptides have an alternating R^*- and S^*- configuration and the incorporated macrocycles are oxazolines and thiazoles. By variation of the incorporated heterocycles, *e.g.* $\mathbf{H_4L^4}$ *vs* $\mathbf{H_4L^{ox}}$, and of the stereochemistry in the linkers ($\mathbf{H_4L^4}$ *vs* $\mathbf{H_4L^{rs}}$), the studied macrocycles gradually approach the molecular design of the natural macrocycles patellamide A-G and ascidiacyclamide. This enables the investigation of the influence of the heterocycle and of the stereochemistry of the amino acids on the formation of the copper(II) complexes and on the reaction of dinuclear copper(II) complexes with atmospheric CO_2. Thus, it is expected to gain a more sophisticated knowledge and new insight into a possible metabolic role of the copper(II) complexes of these interesting molecules.

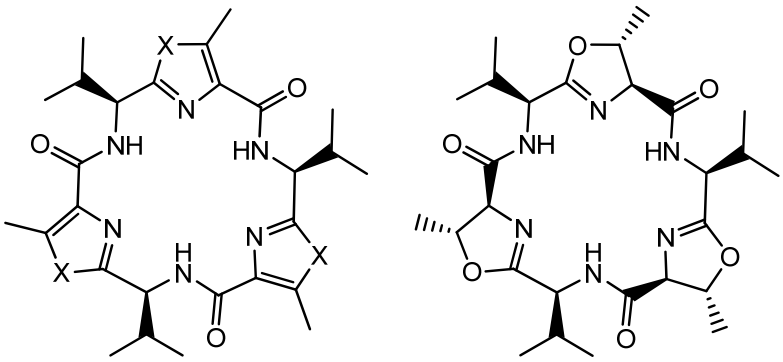

$\mathbf{H_3L^1}$, X = NMe
$\mathbf{H_3L^2}$, X = O
$\mathbf{H_3L^3}$, X = S

$\mathbf{H_3L^{wa}}$

Figure 1.12. Chemical structure of the studied cyclic pseudo hexapeptides $\mathbf{H_3L^{1-3}}$ and the natural cyclic pseudo hexapeptide westiellamide $\mathbf{H_3L^{wa}}$.

Besides the investigation of the copper(II) coordination chemistry of cyclic pseudo octapeptides also cyclic pseudo hexapeptides have been studied. The smaller macrocycles

give rise to a different coordination chemistry. The cyclic pseudo hexapeptides $\mathbf{H_3L^{1\text{-}3}}$, synthetic analogues of the natural pseudo peptide westiellamide $\mathbf{H_3L^{wa}}$ (see Figure 1.12) have been studied previously.[103] For a better understanding of their coordination chemistry, the complexation constants of the mono- and dinuclear will be measured by isothermal titration calorimetry (ITC). The emphasis in this work will be put on the calculation of the EPR parameters of the mononuclear copper(II) complexes of $\mathbf{H_3L^{1\text{-}3}}$ and $\mathbf{H_3L^{wa}}$. The performed benchmark calculations will be used to find a combination of functional and basis set that reproduces the EPR parameters correctly. The thus identified combination can then be applied to dinuclear complexes and new complexes, helping to gain structural informations.

2. Syntheses of Cyclic Pseudo Peptides

2.1. Synthesis of H_3L^1 and H_4L^4

A detailed description of all syntheses is given in the experimental section (Chapter 5). The cyclic pseudo octapeptides $\mathbf{H_4L^4}$ and $\mathbf{H_3L^1}$, have precedence in the literature and were synthesized according to the published procedures. They are synthesized in a cyclo-oligomerization reaction from the monomeric imidazole building block **6** (Scheme 2.1), and the tri- and tetrameric products can be separated by column chromatography.[39]

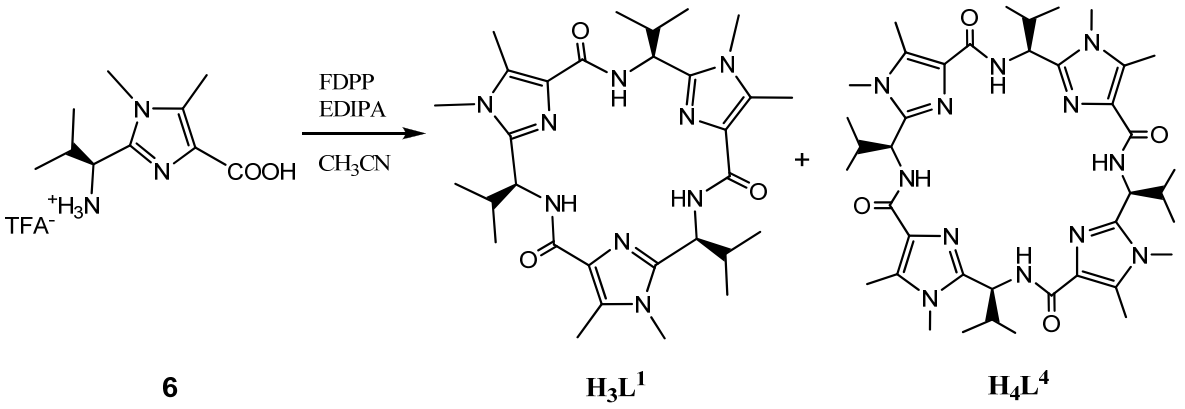

6 $\mathbf{H_3L^1}$ $\mathbf{H_4L^4}$

Scheme 2.1. Synthesis of $\mathbf{H_3L^1}$ and $\mathbf{H_4L^4}$.

Variation of the dilution of the reaction mixture allowed the ratio of $\mathbf{H_3L^1}$/$\mathbf{H_4L^4}$ to be altered, at low dilution the percentage of $\mathbf{H_4L^4}$ increases. The synthesis of the monomeric imidazole building block **6** is known from the literature and was prepared from methyl aceto acetate in six steps (see Scheme 2.2).[39] The first step was the reaction of methyl aceto acetate with sodium nitrate in glacial acetic acid to give the oxime **1**, that was obtained in 88% yield. It was important to repeatedly wash the diethyl ether solution of the product with a saturated bicarbonate solution, in order to obtain the oxime **1** in high purity and enable its crystallization. In the second step, the oxime **1** was reduced with a 3 M solution of HCl in ethanol under a hydrogen atmosphere, using 5 % palladium on charcoal as catalyst. The temperature sensitive, white ammonium chloride salt **2** was obtained in high yields (85%) and was purified by repeated washing with cold dichloromethane. In the third step the ammonium chloride salt **2** was coupled to Boc-protected *L*-valine, using isobutyl chloroformate and

NMM as coupling agents, giving the Boc-protected dipeptide **3** in 75% yield. The imidazole ring was then formed by reaction of the Boc-protected *L*-valine-dipeptide **3** with acetic acid and an 8 M methanol solution of methylamine in xylene. The doubly protected monomeric methyl-imidazole building block **4** was thus obtained in moderate yields of 53%. Subsequent saponification with NaOH and deprotection of the amine with TFA, respectively, gave the desired monomer, **6**, in two quantitative steps.

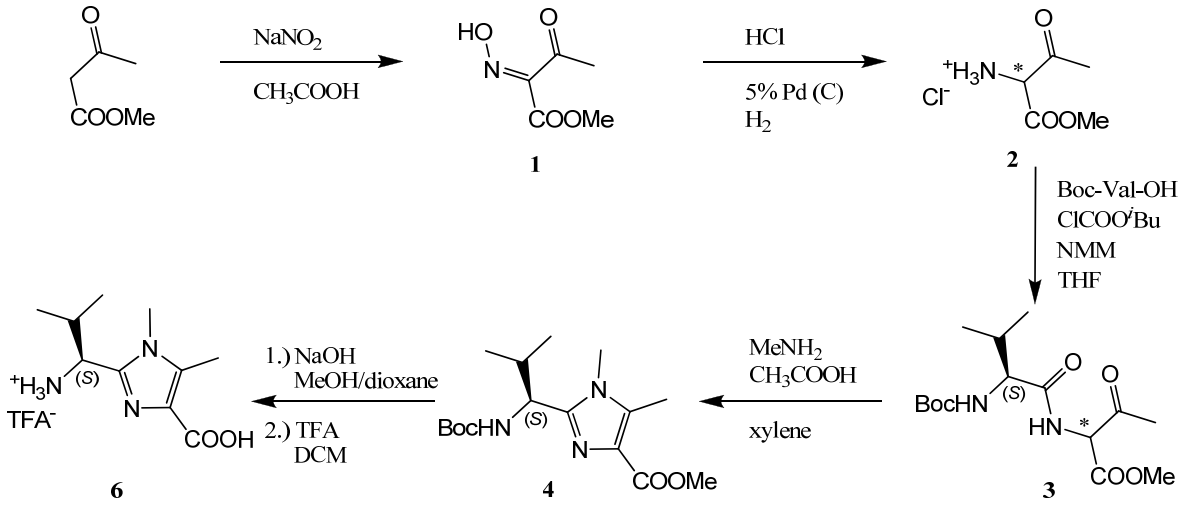

Scheme 2.2. Synthesis of the monomeric building block **6**.

2.2. Synthesis of $H_4L^{4\text{-bn}}$

As a result of its C_2-symmetry, $\mathbf{H_4L^{4\text{-bn}}}$ cannot be synthesized in a one-pot reaction from monomeric building blocks. Instead, it was synthesized in a dimerisation reaction from the bis-imidazole building block **15** (see Scheme 2.3). The chosen reaction conditions, analogous to the known literature coupling of monomeric building blocks, gave the cyclic pseudo octapeptide $\mathbf{H_4L^{4\text{-bn}}}$, using FDPP as a coupling agent, EDIPA as base and acetonitrile as solvent (Scheme 2.3).[39, 52] The reaction was monitored by TLC and found to be complete after six days. $\mathbf{H_4L^{4\text{-bn}}}$ was obtained in moderate yields of 48% after purification by flash chromatography. Suitable crystals for X-ray diffraction were obtained from $\mathbf{H_4L^{4\text{-bn}}}$ (see Chapter 4).

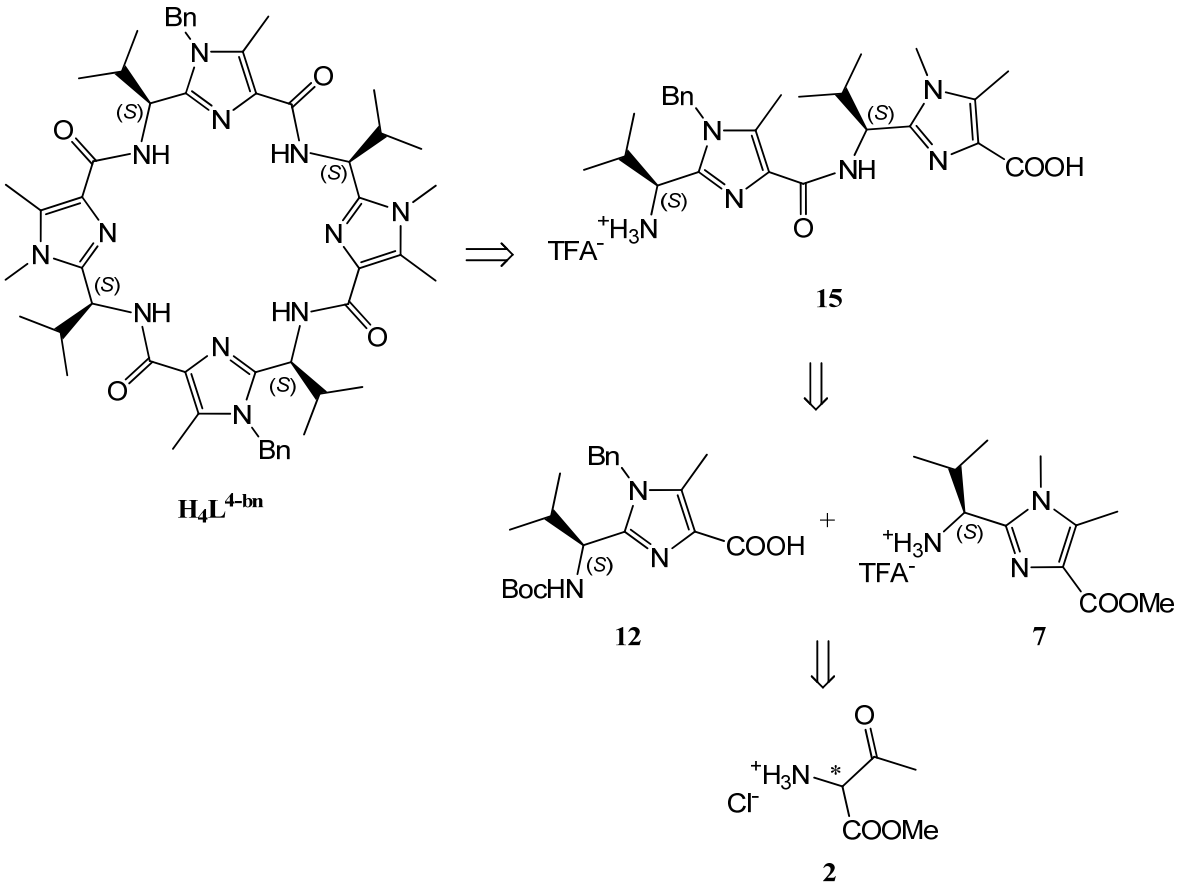

Scheme 2.3. Retrosynthetic disassembling of $\mathbf{H_4L^{4-bn}}$.

The bis-imidazole building block **15** was constructed in a reaction sequence from the monomeric benzyl and methyl imidazole building blocks **7** and **12**, respectively. Firstly the building block **7** and **12** were coupled, using FDPP as coupling agent and EDIPA as base. The doubly protected bis-imidazole building block **13** was thus obtained in 60% yield. It was subsequently deprotected to quantitatively yield the bis-imidazole building block **15** (see Scheme 2.4). Both building blocks **7** and **12** are known compounds and can be synthesized from the ammonium chloride salt **2** in moderate yields.[52, 104]

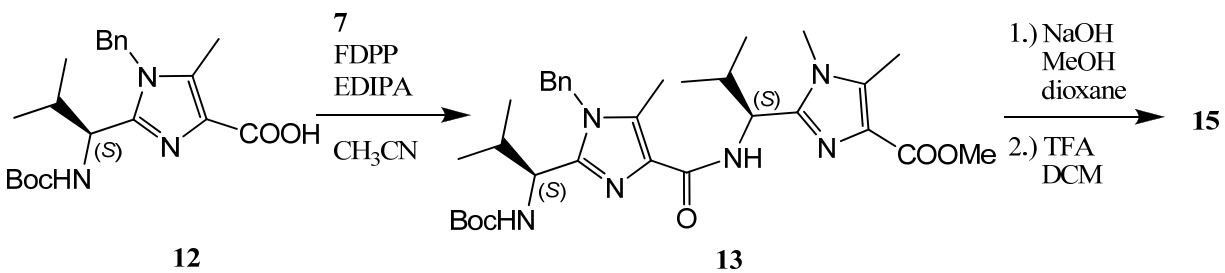

Scheme 2.4. Synthesis of the bis-imidazole building block **15**.

The synthesis of the monomeric imidazole building block **7** is straight forward and nearly identical to the synthesis of the imidazole building block **6**. Only the acid function was not saponificated.

The synthesis of the benzyl imidazole building block **12** is more complicated and involves a series of deprotection and reprotection steps (see Scheme 2.5). It is available from the ammonium chloride salt **2** in a five step synthesis. In the first reaction step, the ammonium chloride salt **2** was coupled with Cbz-protected *L*-valine to the Cbz-protected dipeptide **8** in moderate yields of (46%). The reaction conditions were identical to those of the synthesis of the Boc-protected dipeptide **3**. In the second reaction step, the Boc-protected dipeptide **8** was reacted with 8 M ammonia in ethanol and trifluoro acetic acid in xylene to give the doubly protected monomeric imidazole building block **9**, that can be obtained in moderate yields (50%). Subsequently the Cbz group was changed to the Boc group by the reaction with di-*tert*-butyl dicarbonate giving the Boc-protected imidazole building block **10** in 88% yield. In the following reaction step building block **10** was reacted with benzylbromide and sodium hydride in DMF to give the Boc-protected benzyl-imidazole building block **11** in high yield (95%), which was then quantitatively converted to the monomeric benzyl-imidazole building block **12** by saponification.

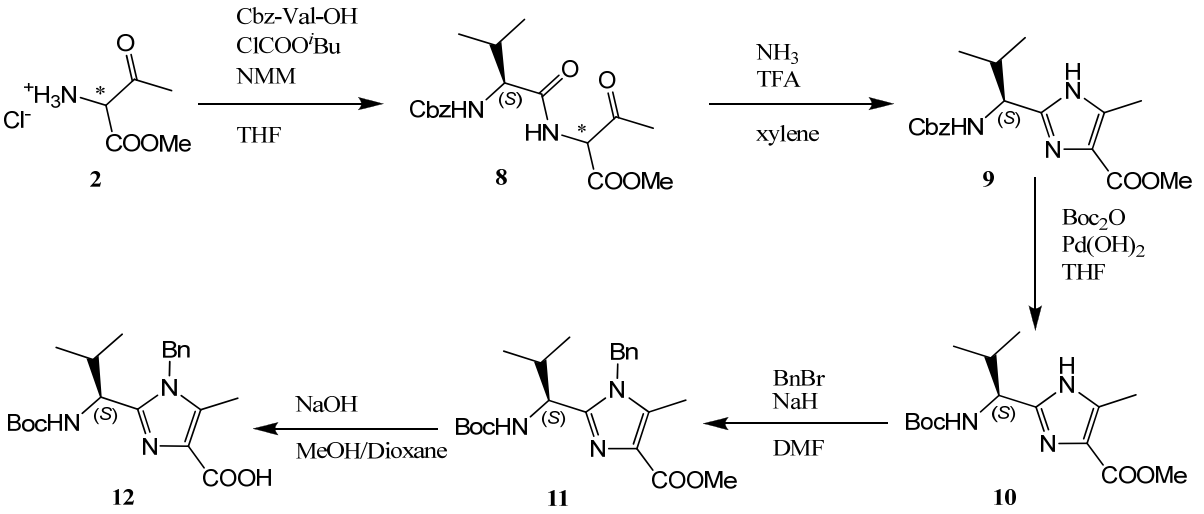

Scheme 2.5. Synthesis of the monomeric benzyl-imidazole building block **12**.

2.3. Synthesis of H_4L^{rs}

H_4L^{rs} was prepared from the bis-imidazole building block **21** in an analogous manner to the literature procedures for the dimerization of bis-heterocyclic building blocks to cyclic pseudo octapeptides (see Scheme 2.6). [39, 52]

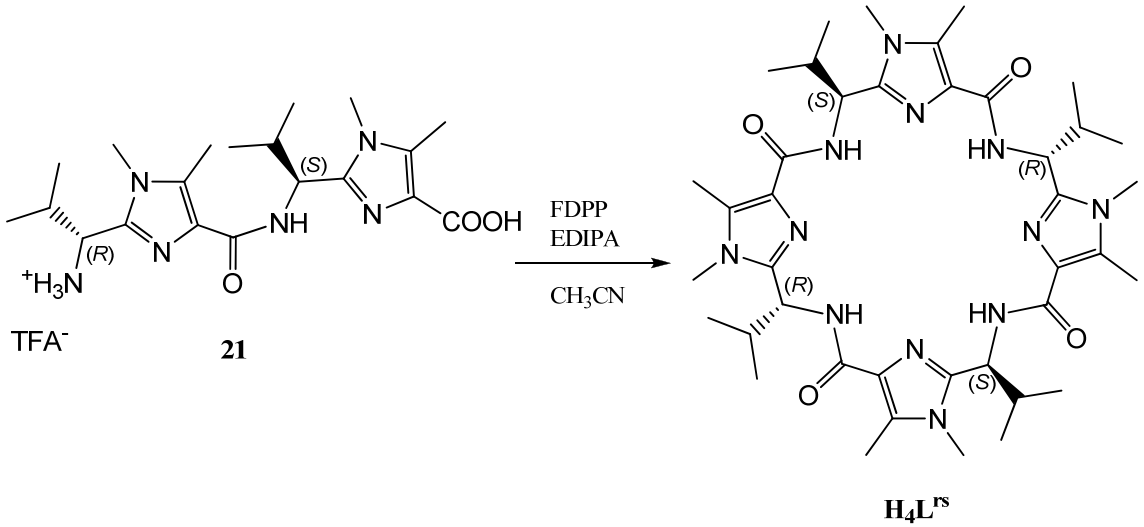

Scheme 2.6. Synthesis of H_4L^{rs}.

The reaction was performed at room temperature, and a complete conversion of the starting material was achieved after three days. The crude cyclic pseudo octapeptide H_4L^{rs} was then purfied by flash column chromatography and obtained in moderate yields of 51%. The bis-imidazole building block **21** was synthesized by analogy to the synthesis of the bis-imidazole building block **15**.

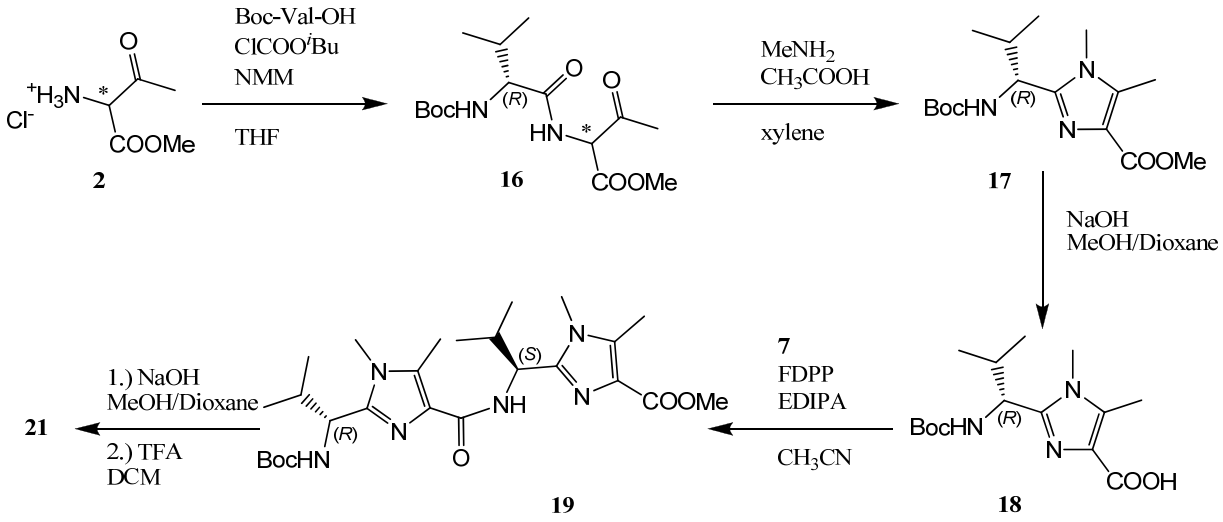

Scheme 2.7. Synthesis of the bis-imidazole building block **21**.

The ammonium chloride salt **2** was converted to the *D*-valine dipeptide **16** via reaction with Boc-protected *D*-valine in THF, using NMM and isobutyl chloroformate as coupling agents. The dipeptide **16** was obtained in yields of 87%. In the next reaction step the imidazole ring was formed by reaction of the dipeptide **16** with methylamine and acetic acid in xylene. The doubly protected monomeric methyl-imidazole building block **17** was obtained in moderate yields of 51%. After the quantitative saponification, the acid **18** was coupled to the monomeric methyl-imidazole building block **7** to yield the doubly protected bis-imidazole building block **19** in 68% yield. This was then quantitatively converted to the bis-imidazole building block **21** by a reaction sequence of saponification and deprotection with TFA (see Scheme 2.7).

2.4. Synthesis of H_4L^{ascA}

H_4L^{ascA} was synthesized from the thiazole-oxazoline building block **31**, according to a known procedure (see Scheme 2.8).[103] As a consequence of the easy hydrolysis of the oxazoline rings, acidic conditions have to be avoided throughout the synthesis. In a one-pot reaction, the thiazole-oxazoline building block **31** was first deprotected by stirring for one hour in methanol under a hydrogen atmosphere, using 10% palladium on charcoal as catalyst. After the removal of the catalyst and evaporation of the solvent, the crude product was dissolved in

acetonitrile and used without further purification in the next step. Reaction with FDPP and EDIPA gave the cyclic pseudo octapeptide $\mathbf{H_4L^{ascA}}$ in poor yields of 30%.

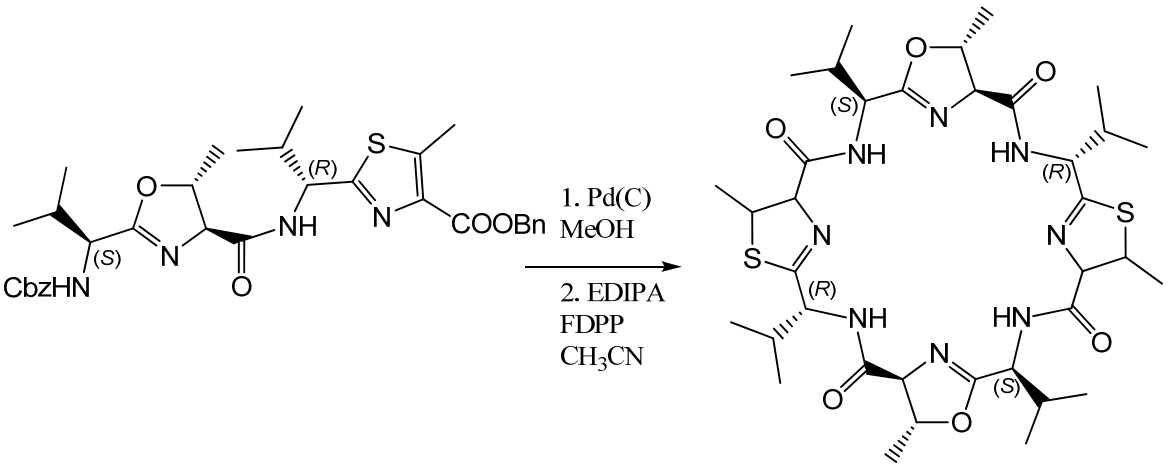

31 $\mathbf{H_4L^{ascA}}$

Scheme 2.8. Synthesis of $\mathbf{H_4L^{ascA}}$.

The thiazole-oxazoline building block **31** was obtained in 56% yield from the monomeric oxazoline and thiazole building blocks **26** and **30** (see Scheme 2.11) by a coupling reaction using FDPP and EDIPA in acetonitrile (Scheme 2.9).

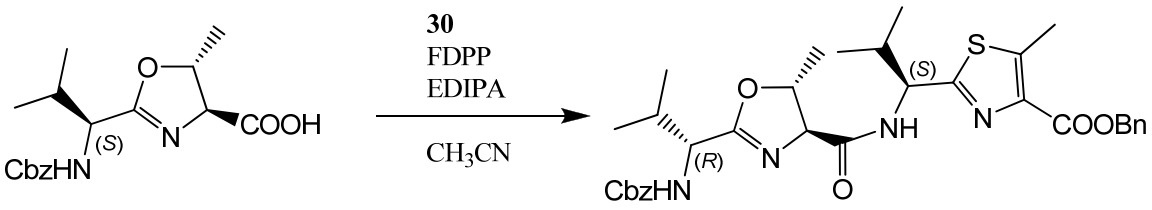

26 **31**

Scheme 2.9. Synthesis of the thiazole-oxazoline building block **31**.

The monomeric oxazoline building block **26** was synthesized in a five-step synthesis, starting from *L*-threonine methyl ester, that in the first step was coupled with Boc-protected *L*-valine to the dipeptide **22**, using isobutyl chloroformate and NMM as coupling agents. In the next step, the oxazoline ring was formed, using *Burgess' Reagent* in dry THF, giving the monomeric building block **23** in 68% yield. However, the stereochemistry at the oxazoline does not match the desired one. Therefore, the oxazoline ring was opened using methanolic hydrochloric acid (80% yield) and subsequently closed again, with the desired stereo-

chemistry under equivalent reaction conditions as for the formation of **23**. The doubly protected monomeric building block **25** was obtained in 80% yield. Saponification of the acid function, using sodium hydroxide in a methanol dioxane mixture quantitatively yielded the oxazoline building block **26**.

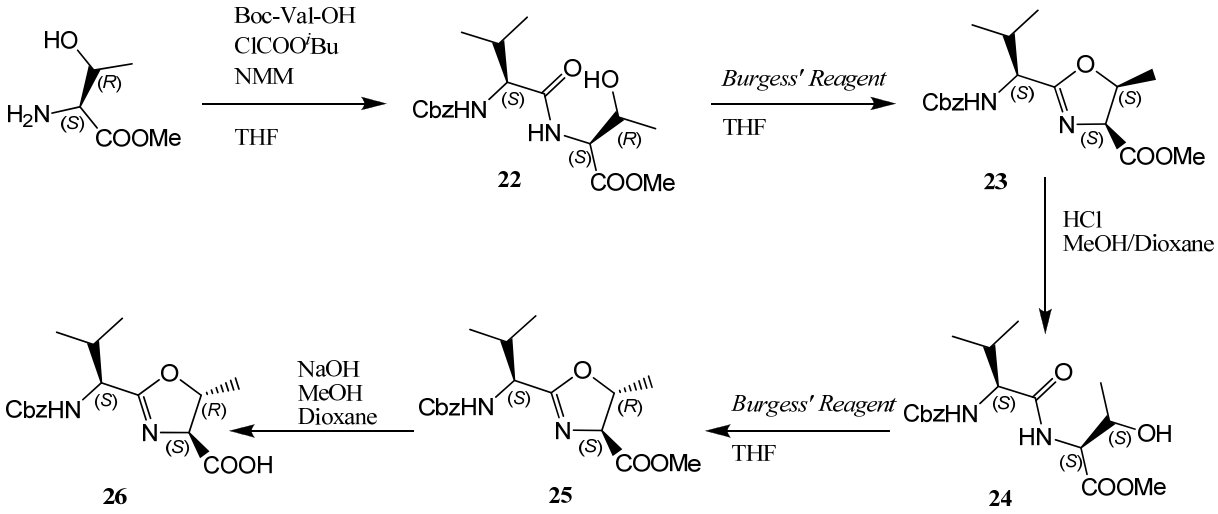

Scheme 2.10. Synthesis of the monomeric oxazoline building block **26**.

The thiazole building block **30** was derived from the Boc-protected *D*-valine dipeptide **16** in a four step synthesis. Initially the thiazole ring was formed in 72% yield, using *Lawesson's Reagent* in THF. Subsequently, the ester functionality was quantitatively hydrolyzed to the thiazole acid **28**, which was then converted to the benzyl protected thiazole building block **29** in 60% yield. In the last reaction step the amine function was deprotected to quantitatively yield the thiazole building block **30** (Scheme 2.11).

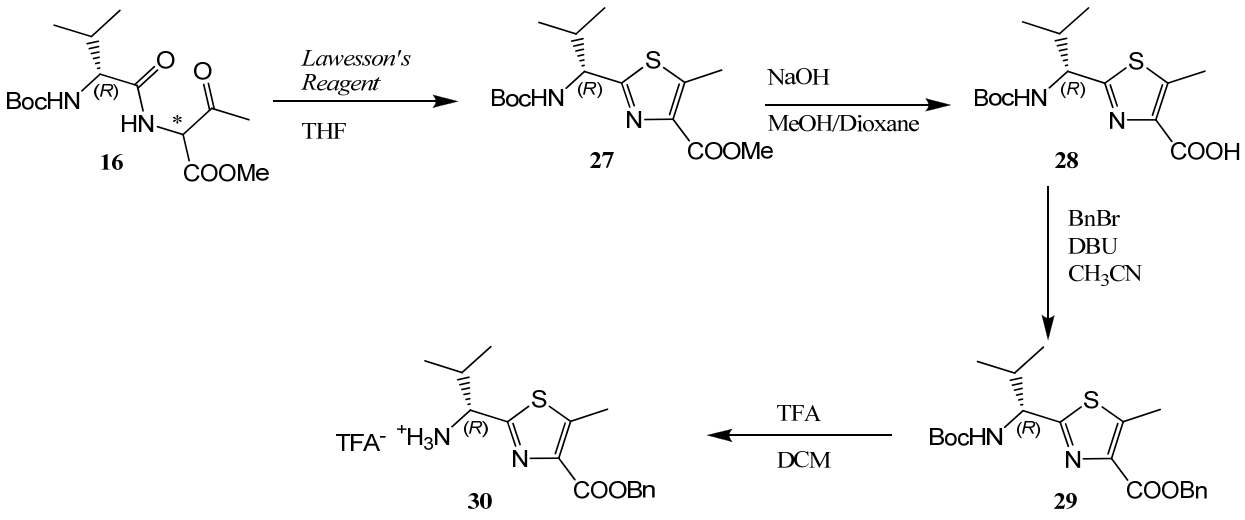

Scheme 2.11. Synthesis of the thiazole building block **30**.

3. Copper(II) Complexes of the Cyclic Pseudo Hexapeptides H_3L^{1-3}

3.1. Introduction

Westiellamide, a cyclic pseudo hexapeptide, that can be isolated from the marine genus *lissoclinum bistratum* and from the terrestrial genus *westiellopsis prolifica*, is known to accumulate in leukemia cells and found to inhibit cytokinesis.[105] Initial studies on the metal complexation of westiellamide were performed by Wipf *et al*., who reported an unusual Ag_4 cluster complex formed with westiellamide.[93] In this cluster three of the silver(I) ions are disposed in a pseudo trigonal arrangement about Ag1 and are sandwiched between two westiellamide, $\mathbf{H_3L^{wa}}$, macrocycles (see Figure 3.1). The central silver ion Ag1 is coordinated in a distorted octahedral arrangement by the carbonyl oxygen atoms of the two westiellamide molecules.

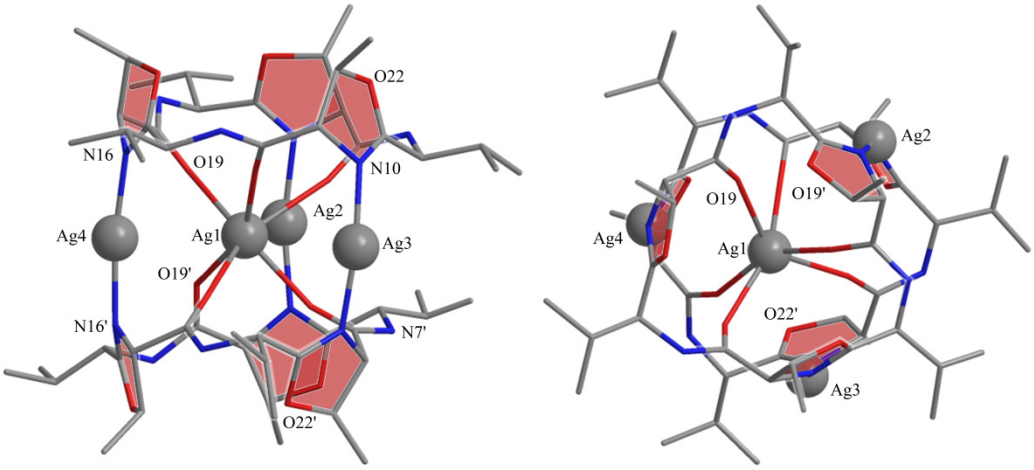

Figure 3.1. X-ray structure of the Ag_4 cluster of westiellamide.[93]

In solution and the solid state, the metal free macrocycle $\mathbf{H_3L^{wa}}$ adopts a highly symmetric configuration (see Figure 3.3), where the heterocyclic nitrogens and the amide hydrogen atoms point towards the inside of the macrocycle, while the isopropyl residues face to the same side of the macrocycle. This conformation, however, is strongly distorted in the silver cluster. In order to coordinate to the central silver(I) ion Ag1, the carbonyl groups of westiellamide are rotated towards the inside of the ring and simultaneously rotate the amide nitrogens.

As a result the amide nitrogen and hydrogen atoms now point towards the outside of the macrocycle. Apart from the interaction with silver(I), Wipf *et al.* only observed weak interactions between westiellamide and other metal ions such as sodium (I), copper(I), iron(II), iron(III), mercury(II), gold(II), and zinc(II).[93]

Van den Brenk found evidence for a strong interaction of copper(II) with $\mathbf{H_3L^{wa}}$.[106] Further studies on the copper(II) interaction of $\mathbf{H_3L^{wa}}$ and a series of its synthetic analogues $\mathbf{H_3L^{1-3}}$ (see Figure 3.2) by Comba *et al.*, revealed that after addition of base all cyclic pseudo hexapeptides readily form stable mono- and dinuclear copper(II) complexes.[107] In these complexes each copper(II) is coordinated by three nitrogen atoms of the macrocycle and its coordination sphere is completed by one or two solvent molecule. In the mononuclear complexes two of the coordinating nitrogen atoms originate from incorporated azole rings and one from the connecting amide bond, forming the N_{het}-N_{amide}-N_{het} binding motif. A coordination in a N_{amide}-N_{het}-N_{amide} motif is also possible, yet in the mononuclear complexes a strong preference for the coordination in the N_{het}-N_{amide}-N_{het} binding motif can be observed, while in the dinuclear copper(II) complexes the copper(II) centers have to be bound to both binding sites. In order to complex copper(II), the amide nitrogen of the binding site needs to be deprotonated. This deprotonation is metal ion assisted and takes place at relatively low pH values. The protons that are released upon coordination of copper(II) acidify the solution, and thus addition of base is mandatory in order to achieve complete complexation. The fact that seawater is slightly basic (pH ~8) supports the notion that cyclic peptides are likely involved in metal ion coordination and transport and potentially have a metabolic role.

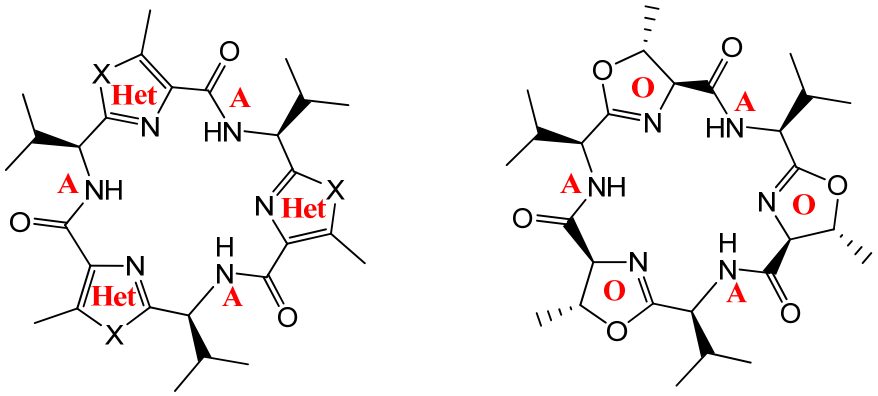

$\mathbf{H_3L^1}$, X = NMe
$\mathbf{H_3L^2}$, X = O
$\mathbf{H_3L^3}$, X = S

$\mathbf{H_3L^{wa}}$

Figure 3.2. Binding sites in $\mathbf{H_3L^{1-3}}$ and $\mathbf{H_3L^{wa}}$. Het = heterocyclic-, A = amide-, O = oxazoline nitrogen.

Due to the similarities in shape and size of the macrocycles, $\mathbf{H_3L^{1-3}}$ are possible model systems for westiellamide. Their differences in electronics, *e.g.* basicity of the heterocycles (pK_a values: pK_a (5-methyl-imidazole) = 7, pK_a (5-methyl-oxazole) = 1.29, pK_a (5-methyl-thiazole) = 2.8, pK_a (oxazoline) = 4.8) allows a detailed investigation of the heterocycles influence on the copper(II) complex stabilities.[108] This might reveal new ideas about the metabolic role of westiellamide and cyclic peptides in general.

$\mathbf{H_3L^{1-3}}$ and $\mathbf{H_3L^{wa}}$ have a common backbone, derived from *L*-valine amino acid residues, and differ solely in their heterocyclic donor groups. Plots of their X-ray structures are shown in Figure 3.3.[64] Importantly, the difference in the heterocycles results in a subtle difference of the shape of the four macrocycles as the single bonds of the oxazoline rings of westiellamide $\mathbf{H_3L^{wa}}$ enlarge the flexibility of the macrocycle.

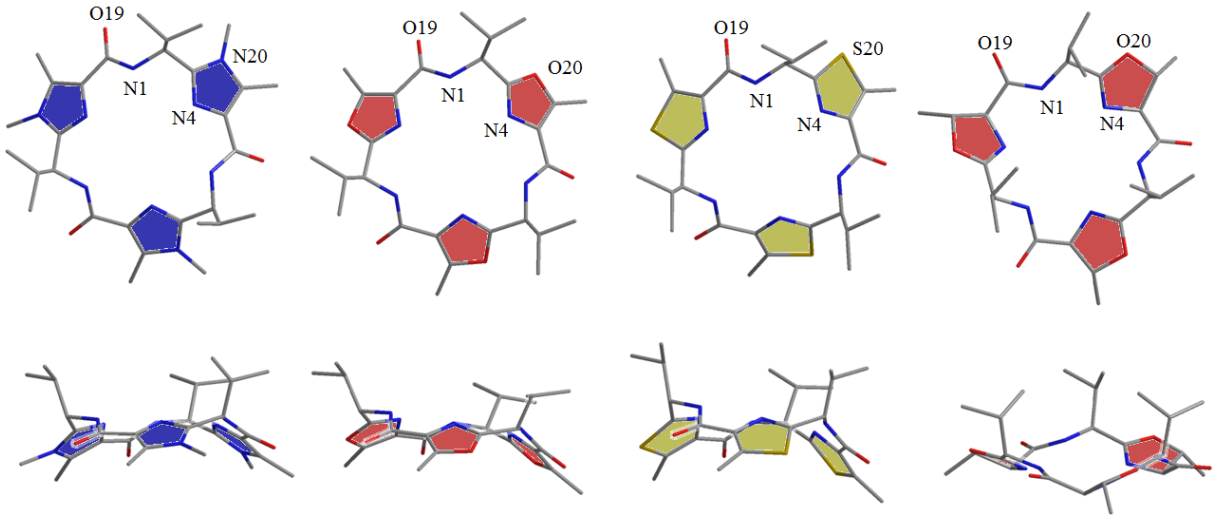

Figure 3.3. Top (top) and side view (bottom) of the X-ray structures of $\mathbf{H_3L^{1-3}}$ and $\mathbf{H_3L^{wa}}$. From left to right: $\mathbf{H_3L^1}$, $\mathbf{H_3L^2}$, $\mathbf{H_3L^3}$, and $\mathbf{H_3L^{wa}}$.

In the mononuclear complexes copper(II) is exclusively bound in the N_{het}-N_{amide}-N_{het} binding motif. In the dinuclear copper(II) complexes, however, the second copper(II) has to be bound to the less favored N_{amide}-N_{het}-N_{amide} motif. The dinuclear copper(II) complexes are methoxide or methanol bridged and it is assumed that methoxide or methanol is needed as an anchor to coordinate the second copper(II).[107]

3.2. Results and Discussion

3.2.1 General Remarks

The copper(II) coordination chemistry of $\mathbf{H_3L^{1-3}}$ was studied by means of ESI-MS spectrometry, isothermal titration microcalorimetry (ITC), EPR, NMR, MCD, and UV-vis spectroscopy. Due to the low solubility of the macrocycles in aqueous solution, methanol was used as a solvent. All experiments were performed under aerobic conditions. Upon coordination of each copper(II) at least one amide nitrogen is deprotonated, therefore the number of amide protons present in the macrocycles is added to the ligand abbreviations ($\mathbf{H_3L^3}$, $\mathbf{H_2L^3}$, etc). The complexation equilibria were further studied by computational methods. So far no suitable crystals for X-Ray single crystal structure determination could be obtained from the copper(II) complexes.

3.2.2 Determination of the Stability Constants of the Copper(II) Complexes of $\mathbf{H_3L^{1-3}}$

Isothermal titration calorimetry (ITC) is a sensitive and versatile technique, widely used to obtain thermodynamic data of biochemical processes at constant temperature. In an ITC experiment the heat released or absorbed upon binding of a host to a guest is measured and it is thereby possible to obtain all binding parameters of a host-guest interaction in a single experiment, *i.e.* the enthalpy $\Delta H°$, entropy $\Delta S°$, reaction stoichiometry N, and the binding constant K.[109-113] In a typical isothermal titration microcalorimetry experiment, one reactant, A, is titrated into a sample solution containing the other reactant B. After each addition of a known amount of A, the heat released or absorbed is monitored by the calorimeter. The thermodynamic analysis allows the quantitative characterization of the energetics of the processes associated with the binding reaction. The analysis of the calorimetric data is based on standard fitting procedures with known computational approaches.[109, 114-115]

The ITC experiments were performed under conditions, where the formation of either exclusively mono- or dinuclear copper(II) species was expected.[107] The mononuclear copper(II) complexes of $\mathbf{H_3L^{1-3}}$ were investigated in methanolic solutions containing the macrocycle and triethylamine in a 1:1 ratio, and the dinuclear copper(II) complexes were investigated at a macrocycle to base ratio of 1:3. For the formation of the mononuclear copper(II) complexes $[\mathbf{H_2L^{1-3}}Cu^{II}(solvent)_n]^+$ (n = 1,2) the equilibria described in Eq. 3.1 and Eq. 3.2 were considered. Eq. 3.3 - Eq. 3.6 have been considered, for the formation of the dinuclear copper(II) complexes $[\mathbf{L^{1-3}}Cu^{II}_2]^+$.

$$Cu^{II} + [\,H_2L^{1-3}\,]^- \leftrightharpoons [H_2L^{1-3}Cu^{II}\,]^+ \qquad \text{Eq. 3.1}$$

$$K = \frac{[H_2L^{1-3}Cu^{II}\,]^+}{[Cu^{II}]\,[H_2L^{1-3}]^+} \qquad \text{Eq. 3.2}$$

$$Cu^{II} + [L^{1-3}\,]^{3-} \leftrightharpoons [L^{1-3}Cu^{II}\,]^- \qquad \text{Eq. 3.3}$$

$$Cu^{II} + [L^{1-3}Cu^{II}\,]^- \leftrightharpoons [L^{1-3}Cu^{II}_2\,]^+ \qquad \text{Eq. 3.4}$$

$$K_1 = \frac{[L^{1-3}\,Cu^{II}]^+}{[Cu^{II}]\,[L^{1-3}\,]^{3-}} \qquad \text{Eq. 3.5}$$

$$K_2 = \frac{[L^{1-3}Cu^{II}_2\,]^+}{[Cu^{II}]\,[L^{1-3}Cu^{II}\,]^-} \qquad \text{Eq. 3.6}$$

The parameters derived from the analysis are listed in Table 3.1 (see Appendix B for original data). The values are in the expected range for copper(II) binding constants to peptides and heterocyclic nitrogens, which generally are in a range of log*K* = 5-8.[116-118] The calculated stoichiometric parameter *N* indicates a diverse coordination chemistry of the cyclic peptides at low base concentrations. The stability constants and coordination chemistry at low base concentrations of the imidazole and thiazole macrocycles $\mathbf{H_3L^1}$ and $\mathbf{H_3L^3}$ are identical within experimental accuracy (log*K* = 5.77 (13) for $[\mathbf{H_2L^1}Cu^{II}]^+$ and 5.74 (6) for $[\mathbf{H_2L^3}Cu^{II}]^+$), however, the values derived for the oxazole-based ligand $\mathbf{H_3L^2}$ differ remarkably.

Table 3.1. Best Fit Parameter of the ITC data obtained for the mono- and dinuclear copper(II) complexes (e.s.d.'s given in parentheses). Reaction conditions: methanol (μ = 0.1 M (n-Bu_4N)(ClO_4)), T = 25°C, c(**H_3L^{1-3}**) = 0.1 mM, base (A: c(NEt_3) = 0.1 mM, B: c(NEt_3) = 0.3 mM).

A	**$[H_2L^1Cu^{II}(MeOH)]^+$**	**$[(H_3L^2)_2Cu^{II}(MeOH)_n]^+$**	**$[H_2L^3Cu^{II}(MeOH)]^+$**
N [a]	0.962 (21)	0.439 (27)	0.725 (11)
K [b]	5.85 x 10^5 (170)	2.41 x 10^5 (80)	5.60 x 10^5 (81)
Log$K$	5.77 (0.13)	5.38 (0.14)	5.74 (6)
$\Delta H°$ [kJ/mol]	22.0 (12)	-40.1 (38)	21.0 (7)
$\Delta S°$ [J/(mol K)]	184	-40	181
B.	**$[L^1Cu^{II}_2(\mu\text{-MeOH})]^+$**	**$[L^2Cu^{II}_2(\mu\text{-MeOH})]^+$**	**$[L^3Cu^{II}_2(\mu\text{-MeOH})]^+$**
K_1 [b]	2.03 x 10^5 (22)	3.31 x 10^5 (83)	1.97 x 10^5 (19)
LogK_1	5.31 (5)	5.51 (0.11)	5.29 (4)
$\Delta H°_1$ [kJ/mol]	9.0 (7)	-113.4 (101)	-4.4(13)
$\Delta S°_1$ [J/(mol K)]	132	-274	86
K_2 [b]	0.67 x 10^5 (0.07)	4.14 x 10^5 (0.99)	0.50x 10^5 (6)
LogK_2	4.83 (5)	5.61 (0.1)	4.69 (5)
$\Delta H°_2$ [kJ/mol]	42.6 (5)	72.1 (99)	51.2 (9)
$\Delta S°_2$ [J/mol K]	236	350	262

a) computed $Cu^{II}/(HL^n)^-$ ratio of the complex formed in solution, b) complex formation constant.

The stoichiometric factor N indicates that, for **H_3L^2** there is an unexpected formation of a **H_3L^2**/copper(II) 2:1 complex, while the other two cyclic pseudo peptides form the expected **$H_3L^{1,3}$**/copper(II) 1:1 complexes. This complex not only has a different stoichiometry but also differs from the other macrocycles in terms of formation entropy and enthalpy. The formation of the mononuclear copper(II) complexes of **H_3L^1** and **H_3L^3** is endotherm and thus entropy driven ($\Delta S° \sim 180$ J/mol, $\Delta H° \sim 22$kJ/mol), while the formation of the **H_3L^2**/copper(II) 2 :1 complex is exotherm ($\Delta H°$ = -40kJ/mol), thus enthalpy driven. It is expected that the different stoichiometry of the complexes is reflected in the formation entropy and most likely also a different coordination mode is present in the complexes. In NMR experiments it could be shown that in the 2:1 complex copper(II) is coordinated by the amide oxygen atoms of the macrocycle instead of the nitrogen atoms of the binding site (see Section 3.2.3). In the mononuclear copper(II) complexes of **H_3L^1** and **H_3L^3** copper(II) is bound to the N_{het}-N_{amide}-N_{het} binding motif and the positive formation enthalpies indicate that copper(II) is stronger coordinated to the solvent (methanol) than to the binding site of the cyclic pseudo peptide.

However, upon coordination of copper(II) to the cyclic peptide, coordinated solvent molecules are dissociated and the entropy of the system significantly enlarges. The deviation from the expected stoichiometry in the coordination of copper(II) to $\mathbf{H_3L^3}$, N = 0.75 instead of 1, is presumably a result of the lower nucleophilicity of the thiazole heterocycles in combination with a less favorable ligand conformation (see Table 3.2), that leads to an incomplete complex formation under the conditions of the performed experiments.

As expected from previous experiments, at high base concentrations all three macrocycles form dinuclear $\mathbf{H_3L^{1-3}}$/copper(II) 1:2 complexes.[107] While at low base concentrations no $\mathbf{H_3L^2}$/copper(II) 1:1 complex is observed (see stoichiometry *N* above), with higher base concentrations (starting from 1.3 equivalents of base), the formation of a $\mathbf{H_3L^2}$/copper(II) 1:1 complex could be detected (ITC, ESI and EPR experiments). Higher base concentrations lead to a higher degree of deprotonation in the cyclic pseudo hexapeptide $\mathbf{H_3L^2}$ and the deprotonated (preorganized) N_{het}-N_{amide}-N_{het} binding motif enables the formation of the mononuclear complex. From the ITC experiments it can be concluded that at three equivalents of base the deprotonated cyclic pseudo peptides first form the mononuclear copper(II) complexes and subsequently the dinuclear copper(II) complexes. $\mathbf{H_3L^2}$ is the only cyclic pseudo peptide that exhibits a cooperative effect, *i.e.* $K_2 > K_1$ (see Table 3.1). The parameters of the first complexation step, at high base concentrations, in solutions of $[\mathbf{L^1}]^{3-}$ and $[\mathbf{L^3}]^{3-}$ (K_1, $\Delta H°_1$, $\Delta S°_1$) are very similar to those obtained with lower base concentrations. Small differences in the values are expected due to the different degree of protonation of the ligands. For the second complexation step, the thermodynamics of the three ligands are very similar to each other. Remarkably $\mathbf{H_3L^2}$ forms the most stable dinuclear complexes ($\log K_2$ ($\mathbf{H_3L^2}$) = 5.61 *vs* $\log K_2$ ($\mathbf{H_3L^1}$) = 4.83 *vs* $\log K_2$ ($\mathbf{H_3L^3}$) = 4.69), although it is the macrocycle with the least basic heterocycles.

The issues described above must have their origin in subtle structural and electronic effects. DFT (density functional theory) calculations with Gaussian 03[119] were performed to investigate the energetic changes in the macrocyclic backbone upon coordination to one and two copper(II) ions. Overlay plots of the X-ray structures (see Figure 3.3) of the metal-free ligands $\mathbf{H_3L^{1-3}}$ with the corresponding DFT-optimized structures (G03, B3LYP/6-31g*) of the mononuclear copper(II) complexes $[\mathbf{H_2L^{1-3}}Cu^{II}(MeOH)]^+$ (see Figure 3.5) reveal that upon copper(II) coordination, all macrocycles maintain a conformation close to that of the metal-free ligand. However, the calculation of the relative energies of the particular macrocyclic conformations shows that there are remarkable differences in terms of the energy change.

Table 3.2. Relative single point energies [kJ/mol] of the macrocyclic ligand backbone of the mono- and dinuclear copper(II) complexes of $\mathbf{H_3L^{1-3}}$, compared to the energy of the metal-free ligand (X-ray coordinates, calculated at the B3LYP/6-31g* level).

energy [kJ/mol]	$\mathbf{H_3L^1}$	$\mathbf{H_3L^2}$	$\mathbf{H_3L^3}$
X-ray structure	0	0	0
mononuclear copper(II) complexes $[\mathbf{H_2L}Cu^{II}(MeOH)]^+$	63.3	68.7	77.8
dinuclear copper(II) complexes $[\mathbf{L}Cu_2^{II}(MeOH)]^{2+}$	82.5	75.8	93.4

The energies of the ligand conformations were calculated by taking a fully optimized DFT structure of the mono- or dinuclear copper(II) complexes (see Figure 3.4 for the calculated structures of $\mathbf{H_3L^1}$ and Appendix C for those of $\mathbf{H_3L^{2,3}}$ and $\mathbf{H_3L^{wa}}$), removing the copper(II) ion(s) and coligands, resaturating the ligand with hydrogen atoms, where required, and reoptimizing the position of the added hydrogen atoms. A single point calculation was then performed on the macrocyclic conformation.

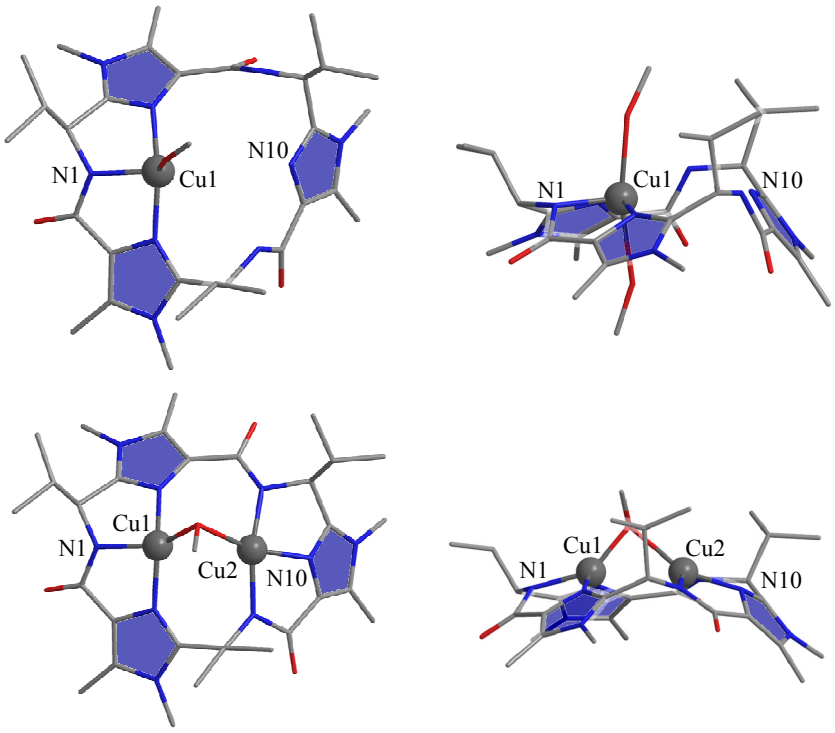

Figure 3.4. DFT calculated (G03, B3LYP/6-31g*) structures of the mono- and dinuclear copper(II) complexes of $\mathbf{H_3L^1}$.

The relative energies listed in Table 3.2 indicate that coordination of the first copper(II) ion and formation of the mononuclear copper(II) complex (for $\mathbf{H_3L^2}$ only observable at high base concentrations), considerably distorts the macrocyclic backbone and that the steric strain is similar for all three ligands. Conversely, the energy needed for the conformational change in the macrocycle going from a mono- to a dinuclear complex is much smaller. While $\mathbf{H_3L^2}$ requires a relatively small energy of 7.1 kJ/mol for the reorganization of the macrocyclic backbone conformation, the reorganization energy that is needed for the change of the macrocyclic backbones of $\mathbf{H_3L^1}$ and $\mathbf{H_3L^3}$ is two to three times as large (15.6 kJ/mol for $\mathbf{H_3L^3}$ and 19.5 kJ/mol for $\mathbf{H_3L^1}$). The differences in energies are most the reason for the high stability of the dinuclear copper(II) complexes of $\mathbf{H_3L^2}$, at high base concentrations, in spite of the inherently less basicity of the oxazoles, which is responsible for the formation of the unusual $\mathbf{H_3L^2}$/copper(II) 2:1 complex at low base concentrations. This 2:1 complex is the reason for the observed negative formation entropy of $[(\mathbf{H_3L^2})_2Cu^{II}]^{2+}$, observed at low base concentrations, in contrast to the positive formation entropies of the $[\mathbf{H_2L^1}Cu^{II}(solvent)_2]^+$ and $[\mathbf{H_2L^3}Cu^{II}(solvent)_2]^+$.

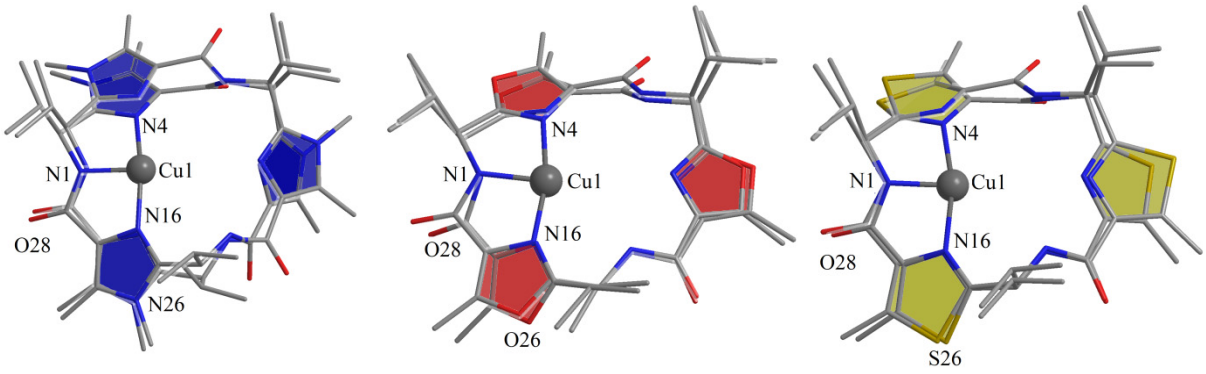

Figure 3.5. Overlay plots (top view) of the X-ray structures of $\mathbf{H_3L^{1-3}}$ with the DFT geometry optimized structures (G03, B3LYP/6-31g*) of the corresponding mononuclear copper(II) complexes $[\mathbf{H_2L^{1-3}}Cu^{II}(MeOH)_2]^+$ (hydrogen atoms and co-ligands omitted for clarity, carbon = grey, nitrogen = blue, oxygen = red). Left to right: $\mathbf{H_3L^1}$, $\mathbf{H_3L^2}$ and $\mathbf{H_3L^3}$.

3.2.3 UV-vis and NMR spectroscopy of H_3L^2/copper(II)/base equilibria

The unusual copper(II) coordination chemistry of $\mathbf{H_3L^2}$ compared to $\mathbf{H_3L^1}$, $\mathbf{H_3L^3}$, and $\mathbf{H_3L^{wa}}$ was investigated in more detail by UV-vis and NMR experiments. A detailed UV-vis investigation of $\mathbf{H_3L^1}$ has been performed previously.[107] UV-vis titrations were performed at 20°C in quartz cuvettes with a path length of 1 cm. After each titration step the well mixed solution was allowed to equilibrate for 5 minutes before the spectrum was measured. 1 mL of a $\mathbf{H_3L^2}$ solution ($c(\mathbf{H_3L^2}) = 2$mM) was titrated with a copper(II) triflate solution ($c(Cu(Otf)_2) = 40$mM) in 5 µL (0.1eq) steps.

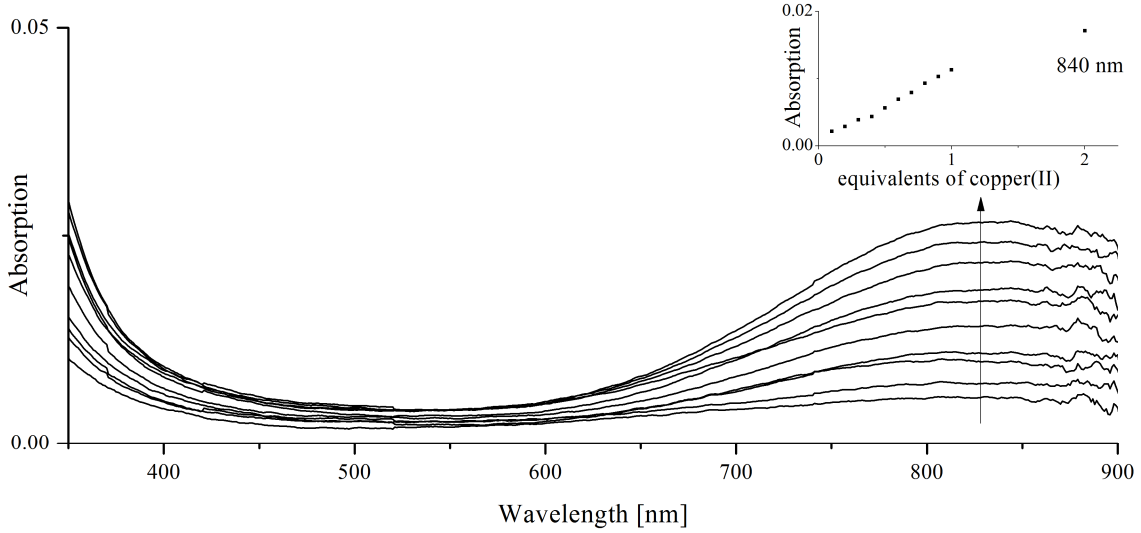

Figure 3.6. UV-vis spectra of the titration of $\mathbf{H_3L^2}$ ($c = 2$mM, methanol) with 0-2 eq copper(II) in 0.1 eq (0-1 eq) and 1 eq (1-2 eq) steps.

UV-vis spectra of the titration of copper(II) to a solution of $\mathbf{H_3L^2}$ are shown in Figure 3.6. Addition of up to two equivalents of copper(II)triflate to a solution of $\mathbf{H_3L^2}$ leads to the formation of an absorption band at 840 nm that approximately linearly increases with the copper(II) concentration. Upon binding of copper(II) to the N_{het}-N_{amide}-N_{het} binding motif a hypsochrome shift is expected as nitrogen ligands cause a higher ligand field than oxygen ligands. The fact that the absorption band does not shift supports the assumption that in the absence of base no coordination in the N_{het}-N_{amide}-N_{het} binding mode occurs, but rather copper(II) remains coordinated by a set of oxygen atoms. In combination with the ITC data, that in presence of one equivalent of base predict a $\mathbf{H_3L^2}$/copper(II) 2:1 complex, this suggests

that copper(II) is not coordinated in the N_{het}-N_{amide}-N_{het} binding side, but rather coordinated to the carbonyl oxygens of $\mathbf{H_3L^2}$ in a probably similar fashion to the central silver in the Ag_4 cluster of westiellamide, reported by Wipf *et al*. (see Figure 3.1). The absence of copper(II) coordinated to the N_{het}-N_{amide}-N_{het} motif could also be supported by the ESI-MS and EPR experiments.

In contrast to $\mathbf{H_3L^2}$ the time-dependant spectra of a $\mathbf{H_3L^1}$/copper(II) 1:2 solution in absence of base shows a shift of the absorption maximum from 840 to 771 nm consistent with the coordination of copper(II) in the N_{het}-N_{amide}-N_{het} binding motif of the macrocycle (see Figure 3.7).

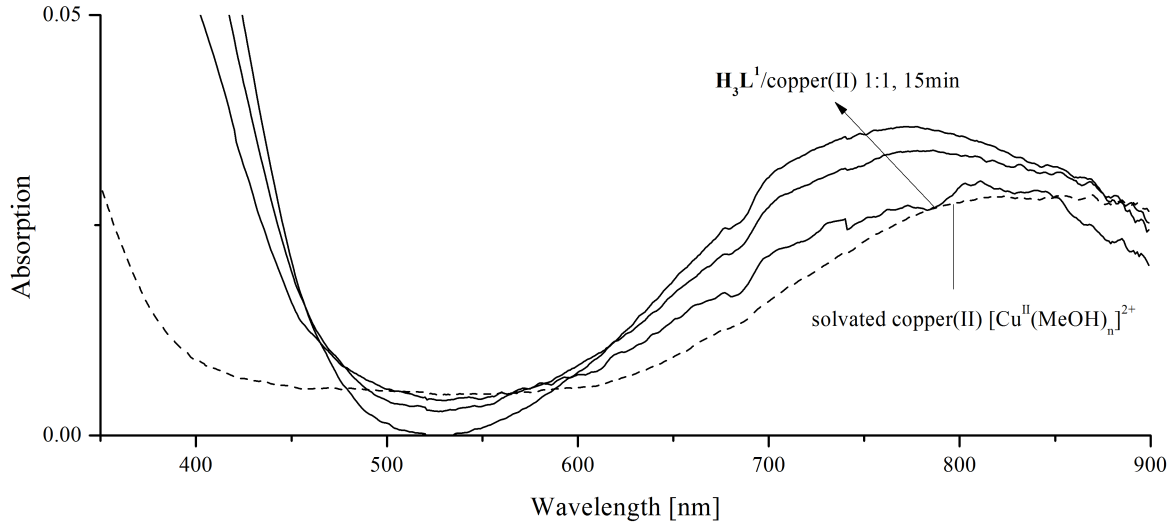

Figure 3.7. UV-vis spectra of solvated copper(II) (dotted line) and time-dependent spectra (15 min) of $\mathbf{H_3L^1}$/copper(II) 1:1.

^{13}C-NMR proved to be a useful tool to probe the coordination of copper(II) by the carbonyl oxygens of $\mathbf{H_3L^2}$. Paramagnetic ions, such as copper(II), coordinated to an organic ligand shorten the relaxation time of nearby nuclei and therefore broaden the corresponding NMR signals. Consecutive addition of $Cu(CF_3SO_3)_2$ to a solution of $\mathbf{H_3L^2}$ (MeOH-d_4, 10 mM) gradually broadens the ^{13}C-resonance of the amide carbon atom, assigned to the resonance observed at 162 ppm (see Figure 3.8).

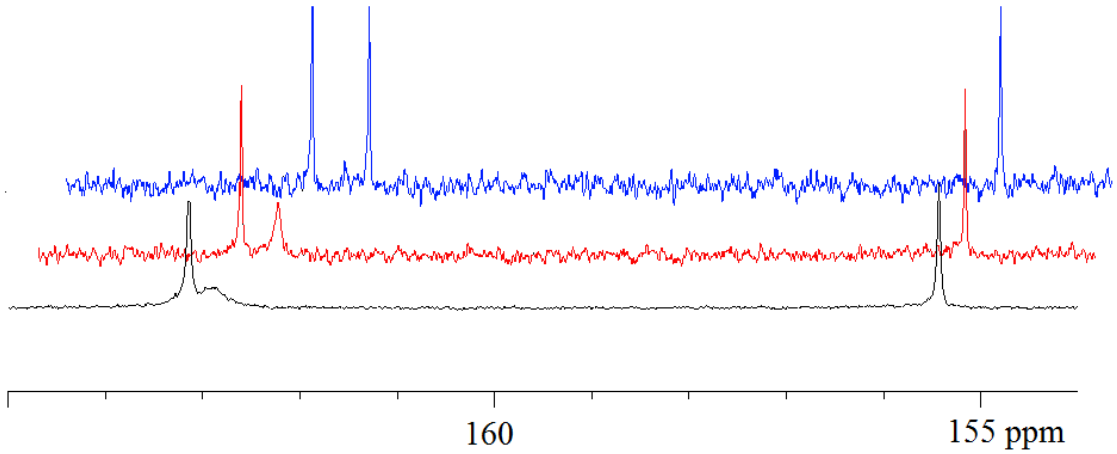

Figure 3.8. Section of interest of the ^{13}C-NMR spectra of $\mathbf{H_3L^2}$ in MeOH-d_4 (50 MHz, 10 mM) with varying amounts of Cu^{II}. 0 eq copper(II) (blue, back); 0.2 eq copper(II) (red, middle); 0.5 eq copper(II) (black, front); δ = 155.41 ($\underline{C}_{im}CH_3$); 162.79 ($\underline{C}_{amide}$); 163.19 ($N_{im}\underline{C}_{im}$) ppm (see Figure 1.4 for used abbreviations).

After addition of 0.5 equivalents of copper(II) to the solution, the resonance of the amide carbon atom is broadened to an extent where it is hardly detectable. Because all other resonances of $\mathbf{H_3L^2}$ are not affected, copper(II) must interact with the corresponding carbonyl oxygen atom. The NMR spectra of imidazole-containing macrocycles, which are known to exclusively form complexes where copper(II) is coordinated in the N_{het}-N_{amide}-N_{het} cleft, do not show this behavior. Therefore it is concluded that in the $\mathbf{H_3L^2}$/copper(II) 2:1 complex, identified from the ITC experiments, the copper(II) is coordinated by at least one carbonyl group of each $\mathbf{H_3L^2}$ macrocycle.[103, 107]

3.2.4 EPR Experiments and DFT Calculation of EPR Parameters

EPR experiments are commonly used to gain insight into the coordination geometry of complexes that contain a paramagnetic metal center. In the case of dinuclear complexes they also provide information about the exchange coupling constant *J* and the zero field splitting. In order to extract the structural and electronic informations the spectra need to be simulated. While the simulation of mononuclear complexes is generally straight forward, that of dinuclear complexes is often complicated. The DFT calculation of the EPR tensors of a given

complex can help simulate the experimentally obtained spectra, however, it is known that the accurate prediction of the EPR tensors of metal complexes is challenging.[120-121]

$$H = \sum_{i=x,y,z} (\underline{B}_i \cdot g_i \cdot \underline{S}_i + \underline{S}_i \cdot A_i(^{63.65}Cu) \cdot \underline{I}_i(^{63.65}Cu) - g_n \beta_n \underline{B}_i \cdot \underline{I}_i) + \sum_{j=1}^{3,4} (\underline{S}_i \cdot A_i(^{14.15}N) \cdot \underline{I}_i(^{14.15}N) - g_n \beta_n \underline{B}_i \cdot \underline{I}_i) \quad \text{Eq. 3.7}$$

Table 3.3. Anisotropic spin Hamiltonian parameters of the mononuclear copper(II) complexes $[\mathbf{H_2L^1}Cu^{II}(MeOH)_2]^+$, $[\mathbf{H_2L^2}Cu^{II}(MeOH)_2]^+$, $[\mathbf{H_2L^3}Cu^{II}(MeOH)_2]^+$, and $[\mathbf{H_2L^{wa}}Cu^{II}(MeOH)]^+$.[107], a), b)

	$[\mathbf{H_2L^1}Cu^{II}]^+$	$[\mathbf{H_2L^2}Cu^{II}]^+$	$[\mathbf{H_2L^3}Cu^{II}]^+$	$[\mathbf{H_2L^{wa}}Cu^{II}]^+$
g_x	2.088	2.083	2.082	2.083
g_y	2.051	2.034	2.037	2.051
g_z	2.278	2.279	2.263	2.267
A_x (Cu)	17.0	17.3	15.7	14.0
A_y (Cu)	15.4	17.2	19.9	16.2
A_z (Cu)	153.4	153.0	150.0	175
A_x (N_{het})	14.5	15.7	14.3	12.4
A_y (N_{het})	7.1	7.1	7.0	6.2
A_z (N_{het})	9.0	9.0	9.0	10.4
A_x (N) – N_{amide} (+ N_{het}) c)	13.2	13.4	11.5	16.5
A_y (N) – N_{amide} (+ N_{het}) c)	15.2	14.1	15.7	12.7
A_z (N) – N_{amide} (+ N_{het}) c)	9.5	9.5	9.5	13.4

a) A in 10^{-4} cm^{-1}; b) the simulated spectra included two magnetically equivalent heterocyclic nitrogen nuclei; c) for $[\mathbf{H_2L^{wa}}Cu^{II}]^+$.

The experimental EPR parameters (see Table 3.3)[107] of the mononuclear copper(II) complexes of $\mathbf{H_3L^{1-3}}$ and $\mathbf{H_3L^{wa}}$ are known and have been simulated previously with the program packages XSophe-Sophe-XeprView[122] (version 1.1.4) and Molecular Sophe[123] (version 2.0.91), using Eq. 3.7.[124-126] So far, the EPR spectra of the dinuclear copper(II) complexes of $\mathbf{H_3L^{1-3}}$ and $\mathbf{H_3L^{wa}}$ could not be simulated in good agreement with the experiment. Given that the EPR tensors of the dinuclear copper(II) complexes of a cyclic pseudo peptide could be reproduced by a DFT calculation, a correct simulation might be obtained and

provide structural informations. To ensure that the derived EPR tensors from the DFT calculation are accurate, benchmark calculations, using the program packages ORCA 2.6[120] and MAG-ReSpect 1.2[127] were performed on the mononuclear copper(II) complexes of **H_3L^{1-3}** and **H_3L^{wa}**. The benchmark calculations were performed on fully DFT optimized structures (G03, B3LYP/6-31g*) of the respective complexes.

The computed *g* tensors of the mononuclear copper(II) complex of **H_3L^1**, derived from DFT calculations with various combinations of functionals and basis sets are shown in Table 3.4 (see Appendix D for the calculated values of the mononuclear copper(II) complex of **H_3L^2**, **H_3L^3** and **H_3L^{wa}**).

Table 3.4. Calculated and experimental *g* tensors of the mononuclear copper(II) complex of **H_3L^1**. Calculated with program packages MAG-ReSpect and ORCA. The dependence of the *g* factors on the functional is reflected in the large deviation of the calculated values. The most accurate predicted parameters are denoted in bold. A visualization is given in Figure 3.9

	Experimental *g* values		
Functional / Basis set[#)]	g_x = 2.088	g_y = 2.051	g_z = 2.278
PBE / SVP	2.027	2.039	2.105
PBE / 6-311g*	2.026	2.036	2.101
TPSS / 6-311g*	2.026	2.035	2.097
TPSS / 6-311g* [a)] TZVP [b, c)]	2.029	2.040	2.104
B3PW / 6-311g*	2.041	2.052	2.148
B3PW / 6-311g* [a)] TZVP [b, c)]	2.046	2.059	2.163
B3LYP / 6-311g* [a)] Wachters [c)]	2.043	2.055	2.155
B3LYP / 6-311g*	2.040	**2.051**	2.146
B1LYP / SVP	2.046	2.059	2.163
B1LYP / SVP [a)] Wachters [c)]	2.047	2.061	2.171
B38LYP / IGLO-II [a)] Wachters [c)]	2.071	2.084	2.248
B40LYP / IGLO-II [a)] Wachters [c)]	2.074	2.088	2.259
B40LYP / IGLO-III [a)] Wachters [c)]	2.072	2.085	2.254
BHLYP / IGLO-II [a)] Wachters [c)]	2.085	2.100	2.304
BHLYP / EPR-II [a)] Wachters [c)]	2.084	2.099	2.303
BHLYP / IGLO-II [a)] TZVP [b)] Wachters [c)]	**2.090**	2.100	2.310
BHLYP / IGLO-II [a)] Wachters [c)] SOC	2.100	2.080	2.306
MAG-ReSpect (BHandHLYP / TZVP)	2.093	2.076	**2.278**

a) C, H, N, O; b) first coordination sphere; c) Cu; [#])see text for references.

The influence of the amount of exact exchange in the functional on the calculated *g* tensors was probed by using pure GGA functionals and functionals with various amounts of exact exchange B3LYP (25% HF) *vs* B1LYP (20% HF) as well as modified BXLYP functionals, where X corresponds to the percentage of exact exchange. The functionals: PBE,[128-129] B3PW,[130-133] TPSS,[134] B3LYP,[130, 135-136] B1LYP,[137] B38LYP, B40LYP, BHLYP, and BHandHLYP in combination with the basis sets SVP,[138] TZV,[136] TZVP,[136] 6-31g*,[139] 6-311g*,[139] IGLO-II,[140] IGLO-III,[140] EPR-II,[141] and Wachters[142] have been used in the benchmark calculations (see Table 3.4).

It was not possible to predict all *g* values with the same accuracy. The general underestimation of the *g* shift (especially $g_{\|}$) has been attributed to a combination of too covalent bonding and the prediction of a too large d-orbital splitting and hybrid functionals like B3LYP are certainly to be preferred.[120] However, elevated levels of HF exchange are problematic since they lead to strong spin contamination.[143]

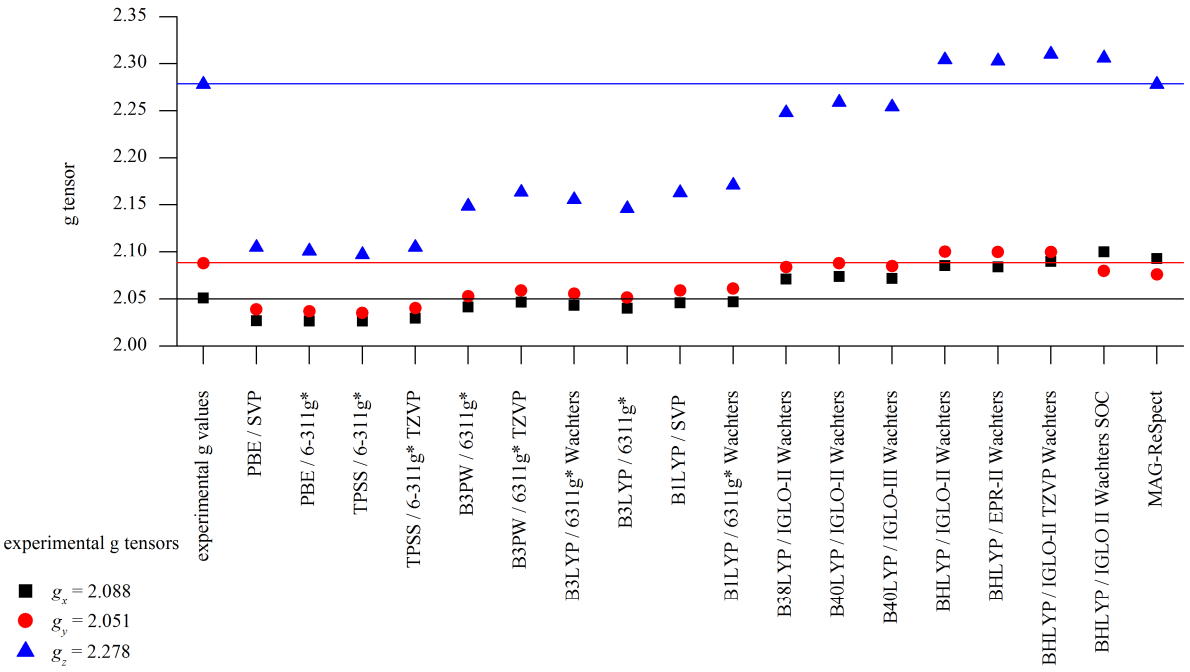

Figure 3.9. Calculated and experimental *g* tensors of $\mathbf{H_3L^1}$, calculated with various combinations of functionals and basis sets with the program packages ORCA and MAG-ReSpect. The experimental values are depicted as horizontal lines.

It was found that increasing the amount of exact exchange to at least 38% is mandatory to obtain $g_{\|}$ tensors in a reasonable range (see Figure 3.9). The best agreement of $g_{\|}$ and g_y with the experimentally derived values is obtained applying the B40LYP functional. Although in

most of the cases the *g* tensors are overestimated by the BHLYP functional (50% HF exchange), this was used for further investigations. BHLYP is a well established functionnal, and its various dependencies are well understood. Manually changing the amount of exact exchange might have some unforeseen influence on the calculation, and thus the application of an established functional was considered reasonable. The MAG-ReSpect calculated *g* tensors of $[\mathbf{H_2L^1}Cu^{II}(\mu\text{-OMe})]^+$ are so far those that agree best with the experimental findings, especially $g_{\|}$ is predicted in excellent agreement with the experiment.

Table 3.5. Calculated (MAG-ReSpect and ORCA) *A* tensors [10^{-4} cm^{-1}] of the mononuclear copper(II) complex of $\mathbf{H_3L^1}$ $[\mathbf{H_2L^1}Cu^{II}(HOMe)]^+$. A visualization of these data is given in Figure 3.10. Most accurate calculated parameters are depicted in bold.

	Experimental *A* tensors [10^{-4} cm^{-1}]		
Functional / Basis set *)	$A_x = 15$	$A_y = 17$	$A_z = 153$
PBE / SVP	49	63	131
PBE / 6-311g*	61	73	122
TPSS / 6-311g*	61	76	129
TPSS / 6-311g* a) TZVP b)	93	110	111
B3PW / 6-311g*	63	79	161
B3PW / 6-311g* a) TZVP b)	94	111	146
B3LYP / 6311g* a) Wachters c)	3	**19**	252
B3LYP / 6311g*	65	81	**153**
B1LYP / SVP	47	66	182
B1LYP / 6311g* a) Wachters c)	67	84	168
B38LYP / IGLO-II a) Wachters c)	10	30	290
B40LYP / IGLO-II a) Wachters c)	9	30	295
B40LYP / IGLO-III a) Wachters c)	11	29	294
BHLYP / IGLO-II a) Wachters c)	10	33	312
BHLYP / EPR-II a) Wachters c)	10	34	312
BHLYP / IGLO-II a) TZVP b Wachters c))	10	33	312
BHLYP / IGLO-II a) Wachters c) SOC	**13**	31	175
MAG-ReSpect	21	5	133

a) C, H, N, O; b) first coordination sphere; c) Cu; *)see text for references.

The *g* and *A* tensors have different dependencies on functional and basis set. While the *g* tensors strongly depend on the applied functional, the *A* tensors are hardly effected by the

functional yet strongly change with the basis set and therefore one needs to offset the accurate prediction of $g_{\|}$ values for the accurate prediction of $A_{\|}$ and $A\perp$. The most reasonable results for A and g tensors are obtained with the BHLYP functional (50% HF exchange) and a combination of the IGLO-II (C, H, N, O and S) and Wachters (Cu) basis sets. The good agreement with the experimental findings that was obtained with MAG-ReSpect for the g tensors could, unfortunately, not be reproduced for the A tensors of $[\mathbf{H_2L^1}Cu^{II}(HOMe)_2]^+$ nor for any of the EPR tensors of the mononuclear copper(II) complexes of $\mathbf{H_3L^2}$, $\mathbf{H_3L^3}$, and $\mathbf{H_3L^{wa}}$ $[\mathbf{H_2L^{2,3,wa}}Cu^{II}(HOMe)_2]^+$ (see Appendix D). Considering the higher computational costs of the MAG-ReSpect calculation and the comparable accuracy of MAG-ReSpect and ORCA calculations, it was decided to use ORCA for the benchmark tests.

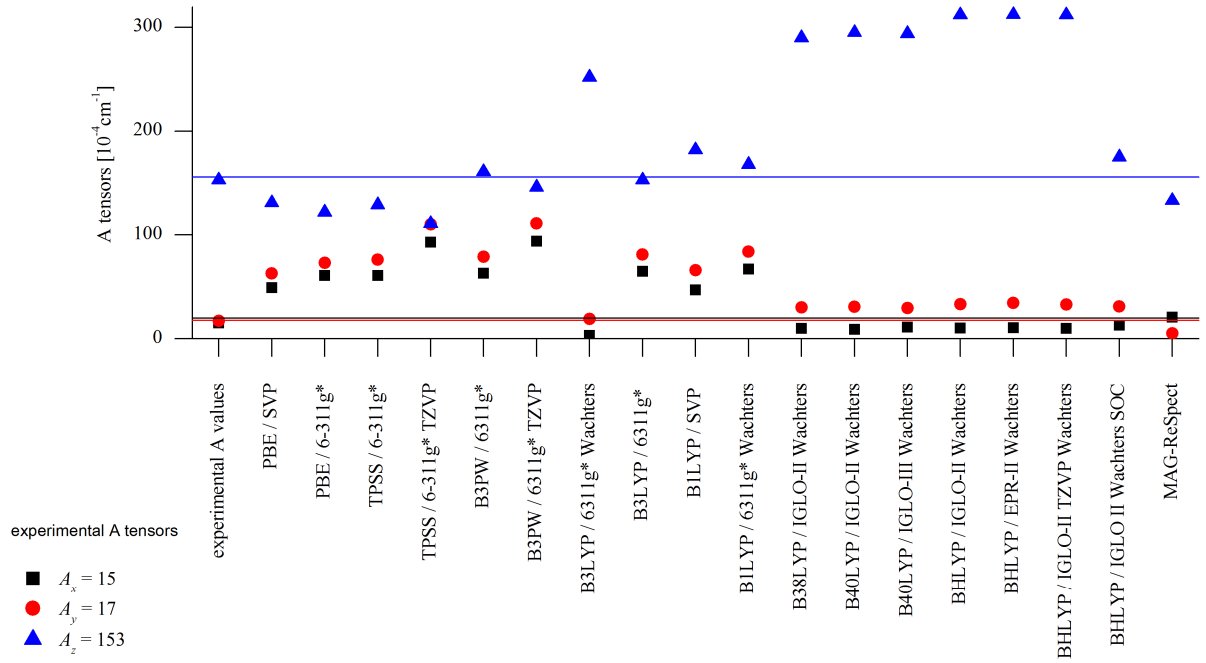

Figure 3.10. Calculated and experimental A tensors [$10^{-4}cm^{-1}$] of $\mathbf{H_3L^1}$ (taken from Table 3.5). The experimental values are represented as horizontal lines.

The EPR-II basis set of Barone is commonly applied in A tensor calculations.[144] However, for the investigated copper(II) complexes of $\mathbf{H_3L^{1-3}}$ and $\mathbf{H_3L^{wa}}$, it was found that the basis set limit is reached at the IGLO-II level (see Figure 3.10), IGLO-III as well as EPR-II basically provided identical results to those of IGLO-II. Analyzing the data it emerges that a basis set with a flexible core region is important as otherwise the $A_{\|}$ values are in good agreement with the experiment but the $A\perp$ values are strongly overestimated, *e.g.* TZVP and 6-31g*. Applying Wachters basis set to copper significantly improves the calculation,

reproducing the observed trend that $A\perp$ is significantly smaller than $A_{||}$, yet $A_{||}$ is overestimated by a factor of about two.[142] This massive overestimation is caused by the neglection of the spin orbit coupling (SOC) of copper(II) and the results are substantially improved when the spin orbit coupling is included. The calculated *A* tensors and their dependence on the applied basis sets is depicted in Figure 3.10.

The calculation of the *g* and *A* tensors of the mononuclear copper(II) complexes of $\mathbf{H_3L^{1-3}}$ and $\mathbf{H_3L^{wa}}$ was found to be challenging and to significantly differ from the experimentally derived values. Considering that the calculation of EPR parameters of transition metals, and copper(II) in particular is considered as demanding, the obtained results are acceptable. However, given that no combination of functional and basis set was found to reproduce the *g* and *A* tensors of all complexes accurately the calculation of the EPR tensors of the dinuclear copper(II) complexes is not expected to reveal reliable results. From the performed calculations it can be concluded the spin orbit coupling is an important contribution for the accurate computation of the parameters. Additionally, the incorporation of at least 40% HF exchange leads to $g_{||}$ tensors that are in a reasonable range, though the amount of HF exchange should not exceed 50% in order not to overestimate $g_{||}$. For the accurate prediction of the *A* tensors the Wachters basis set proved to be very useful. Considering that the *g* and *A* tensors are also dependent on the structure of a complex one has to be sure that the geometry of the complex used to calculate the EPR parameters is identical to the one measured in the experiments. The obtained results from the calculations have to be considered with care as a significant deviation from the experiment can occur.

As mentioned above the DFT calculation of the *g* and *A* tensors of the dinuclear copper(II) complexes of $\mathbf{H_3L^{1-3}}$ and $\mathbf{H_3L^{wa}}$ were not expected to provide further insight into the electronic structure of these complexes. However, it is known, that the isotropic exchange coupling *J*, *i.e.* the interaction of an unpaired electron at metal center (1) with the unpaired electron at metal center (2), of dinuclear transition metal complexes can be calculated relatively accurately.[145-148] Thus, in order to gain insight into the electronics of the dinuclear complexes, the *J* coupling of the dinuclear copper(II) complexes of $\mathbf{H_3L^{1-3}}$ and $\mathbf{H_3L^{wa}}$ was calculated using the program package ORCA (version 2.6) and a combination of the B3LYP functional and the 6-31g* (C, H, N, O, S) and TZVP (Cu, first coordination sphere) basis sets.

The magnetic properties of dinuclear transition metal complexes may be described with the *Heisenberg-Dirac-van Vleck* spin Hamiltonian, given in Eq. 3.8.[145-148]

$$H = -2J_{12}S_1 \cdot S_2 \qquad \text{Eq. 3.8}$$

The broken-symmetry approach, given in Eq. 3.9 (E^{BS} = energy of the broken symmetry state (BS); E^{HS} = energy of the high spin state (HS); $\langle S \rangle^2$ = spin expectation value of HS or BS state) is known to be well adapted for complexes with weak as well as complexes with strong orbital overlap and was used for the DFT based calculation of the exchange coupling constants.[149-151] In the broken symmetry formalism one tries to obtain a wave function that breaks spatial and spin symmetry. This can be done by an unrestricted calculation (for low spin open-shell molecular systems) in which the α and β densities are allowed to be localized on different atomic centers.

$$J_{12} = \frac{E^{BS} - E^{HS}}{\langle S \rangle_{HS}^2 - \langle S \rangle_{BS}^2} \qquad \text{Eq. 3.9}$$

The *J* coupling constants of the dinuclear complexes could not be extracted from the performed experiments as J > hν. However, the fact, that it is possible to obtain EPR data at 77 K for the dinuclear copper(II) complexes of $\mathbf{H_3L^2}$, $\mathbf{H_3L^3}$, and $\mathbf{H_3L^{wa}}$ is a strong indication for their ferromagnetic coupling, while the fact that the dinuclear copper(II) complex of $\mathbf{H_3L^1}$ is EPR silent at 77 K suggest that the copper(II) centers are antiferromagnetically coupled. The calculated *J* couplings of the dinuclear complexes of $\mathbf{H_3L^{1-3}}$ and $\mathbf{H_3L^{wa}}$ are consistent with the EPR experiments. The copper(II) centers in $\mathbf{H_3L^1}$ are antiferromagnetically coupled, while $\mathbf{H_3L^2}$, $\mathbf{H_3L^3}$, and $\mathbf{H_3L^{wa}}$ are ferromagnetically coupled (see Table 3.6). The *J* coupling depends on the structure of the complex, especially the relative orientation of the copper(II) centers. From the accurate prediction of the *J* coupling it can be concluded, that the DFT calculated geometries of the complexes are close or identical to the actual structures in solution. The deviation of the *J* coupling constants is a result of the slightly different relative orientation of the copper(II) centers in the respective complexes.

Table 3.6. DFT-calculated *J* values of the dinuclear copper(II) complexes of $\mathbf{H_3L^{1-3}}$ and $\mathbf{H_3L^{wa}}$. Experimental *J* values could not be extracted from the performed experiments. Computational detail: ORCA, version 2.6; B3LYP/6-31g*(C, H, N, O, S)/TZVP(Cu, first coordination sphere).

	$\mathbf{H_3L^1}$	$\mathbf{H_3L^2}$	$\mathbf{H_3L^3}$	$\mathbf{H_3L^{wa}}$
Calculated *J* coupling	-147 cm^{-1}	76 cm^{-1}	31 cm^{-1}	179 cm^{-1}

While for the formation of the mononuclear copper(II) complexes of cyclic pseudo hexapeptides, $\mathbf{H_3L^2}$ was found to exhibit a different coordination chemistry, the calculated *J* coupling constants and recorded EPR spectra at 77 K suggest that in case of the dinuclear copper(II) complexes $\mathbf{H_3L^1}$ differs from the other macrocycles. The *J* coupling of a dinuclear metal complex can either be extracted from a variable temperature EPR measurement or from an MCD experiment and thus, the copper(II) coordination chemistry of $\mathbf{H_3L^1}$ was further investigated by MCD.

3.2.5 MCD Spectroscopy of the Copper(II) Complexes of H_3L^1

An MCD experiment provides simultaneous information about the ground and excited states of the investigated substance.[152-153] A spectrum can be observed when circularly polarized light is propagated through a sample positioned within a strong magnetic field parallel to the direction of propagation and, in order for the MCD spectrum to be detected, an absorbance difference of the substance between left circularly polarized and right circularly polarized light is required.[154]

The general equation that describes the MCD signal is given in Eq. 3.10 (γ = constant; B = magnetic flux density; k = Boltzman constant; μ_B = Bohr magneton; f(E) = line shape function; T = temperature; d = path length; c = concentration; E = hν, energy of the incident radiation).[152-156] A, B and C are characteristic terms that depend on the electronic and geometric structure of the molecule under investigation. Each molecule with degenerate excited states exhibits an A term with a derivative band shape. While the B term has an absorption like band shape and arises when the applied field causes a mixing of the ground state or an excited state with an intermediate state. The C term is caused by degenerate ground states, and

therefore only present in paramagnetic species. It is the only temperature dependent term, dominating the spectra at low temperatures and identifies paramagnetic species.

$$\frac{\Delta\varepsilon}{E} = \frac{\varepsilon_{LCP} - \varepsilon_{RCP}}{E} = \gamma\mu_B B\left[\left(-\frac{\partial f(E)}{\partial E}\right)\bar{A}_1 + \left(\bar{B}_0 + \frac{\bar{C}_0}{kT}\right)f(E)\right] \qquad \text{Eq. 3.10}$$

The MCD spectra of the monomeric copper(II) complex $[\mathbf{H_2L^1}Cu^{II}(MeOH)]^+$ are in good agreement with the experimental findings from the EPR, UV-vis, and CD experiments.[103, 107] These predict a monomeric copper(II) complex bound to the N_{het}-N_{amide}-N_{het} binding motif, with a square pyramidal coordination environment of the copper(II) center. The variable temperature (VT) MCD spectrum of the monomeric copper(II) complex $[\mathbf{H_2L^1}Cu^{II}(MeOH)]^+$ is depicted in Figure 3.11. The strong temperature dependence of the signals is result of a large C term that arises from the paramagnetic copper(II) center. The MCD saturation curve of the absorption at 700 nm and its fit (red) is shown in the right corner of Figure 3.11. It was fitted assuming $g_{||} = 2.283$ and an xy polarized transition. This is in agreement with the simulated EPR data (see Table 3.3, $g_{||} = 2.278$).

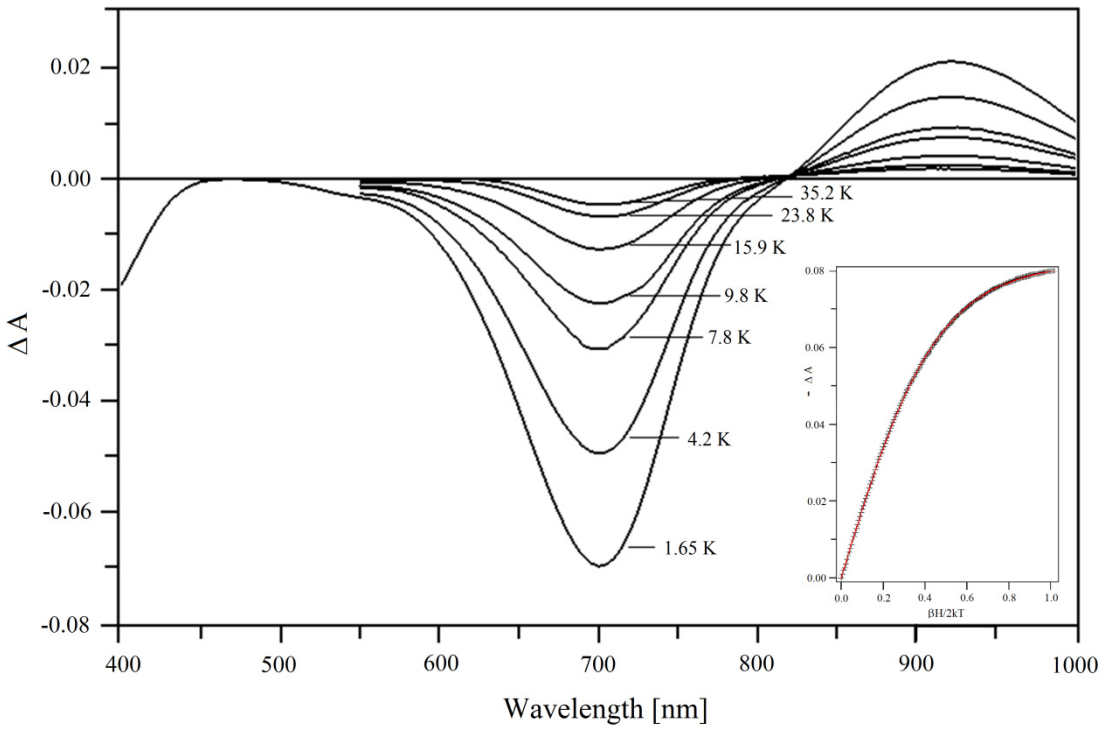

Figure 3.11. VT MCD spectra of the mononuclear copper(II) complex of $\mathbf{H_3L^1}$, $[\mathbf{H_2L^1}Cu^{II}(MeOH)]^+$ measured at 5 T in methanol/glycerol 1:1, $c(\mathbf{H_3L^1}) = 30$ mM, and experimental (black bars) and simulated (red line) saturation curve (inlay) at $\lambda = 700$ nm.

The dinuclear copper(II) complex, used for the MCD spectra is assumed to be methoxide bridged, *i.e.* $[\mathbf{H_1L^1}Cu^{II}_2(\mu\text{-OMe})]^{2+}$, however, this is in contrast to the observed EPR data (see Figure 3.12). While the EPR measurements predict an antiferromagnetically coupled species, *e.g.* EPR silent at 77 K, the MCD data are consistent with a ferromagnetically or weakly anti-ferromagnetically coupled species (nested VTVH curves) and it should be possible to obtain an EPR spectrum at 77 K. The possibility that the recorded MCD spectrum arises from an impurity of monomeric copper(II) complex $[\mathbf{H_2L^1}Cu^{II}]^+$ in the sample can be excluded for several reasons. The signal, that was recorded for the dimeric complex is strong and the absorption values (ΔA) are similar to those of the monomeric species, while a signal arising from an impurity is expected to have considerably smaller absorption values. Furthermore, the spectra of the mono- and the dinuclear species are significantly different. The monomeric copper(II) complex $[\mathbf{H_2L^1}Cu^{II}]^+$ has a negative absorption band at 700 nm and a positive absorption at 940 nm, whereas the dinuclear copper(II) complex of $\mathbf{H_3L^1}$ exhibits two negative absorption bands at 550 and 660 nm (see Figure 3.12). Moreover, the variable temperature variable field (VTVH) curves of the dinuclear copper(II) complex, measured at 660 nm are nested, which is a strong indication for a ferromagnetically coupled species (see Figure 3.13).

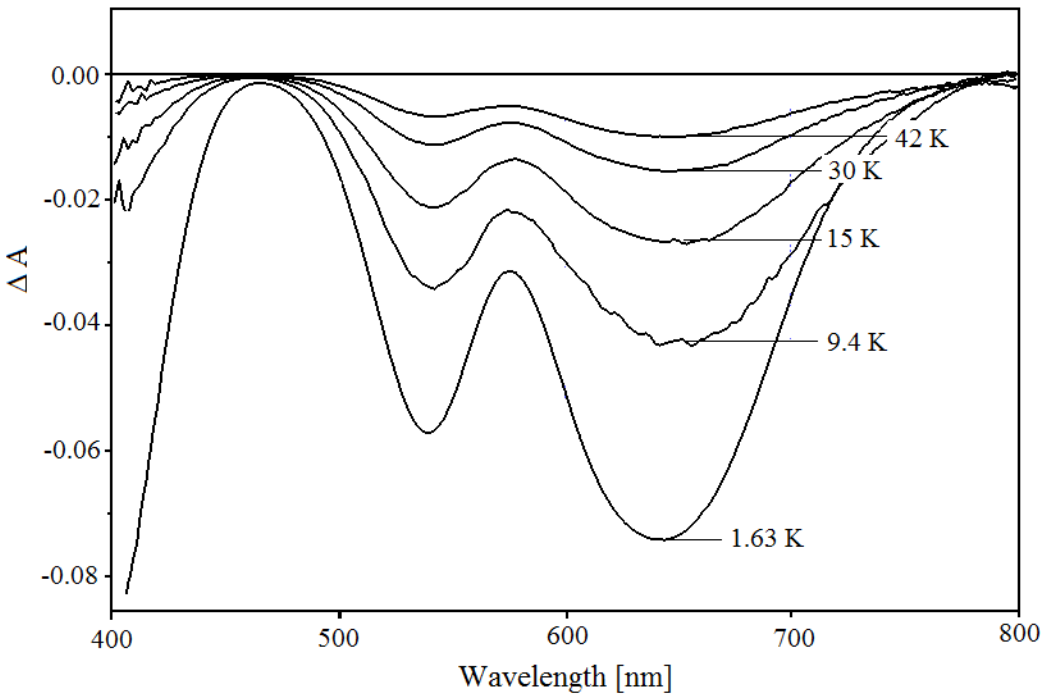

Figure 3.12. VT MCD spectra, measured at 5T in methanol/glycerol 1:1 ($c(\mathbf{H_3L^1})$ = 30 mM), of the dinuclear copper(II) complex of $\mathbf{H_3L^1}$ $[\mathbf{H_2L^1}Cu^{II}(MeOH)]^+$.

The reason for the discrepancy between the MCD and EPR results was found to be due to slightly different experimental conditions. In the MCD experiments, glycerol was added to the methanol solutions, in order to get a high resolution. It was then found that in the presence of glycerol the bridging methanol is replaced by glycerol and the macrocycle adopts a different conformation, in which the copper(II) centers now are ferromagnetically coupled.

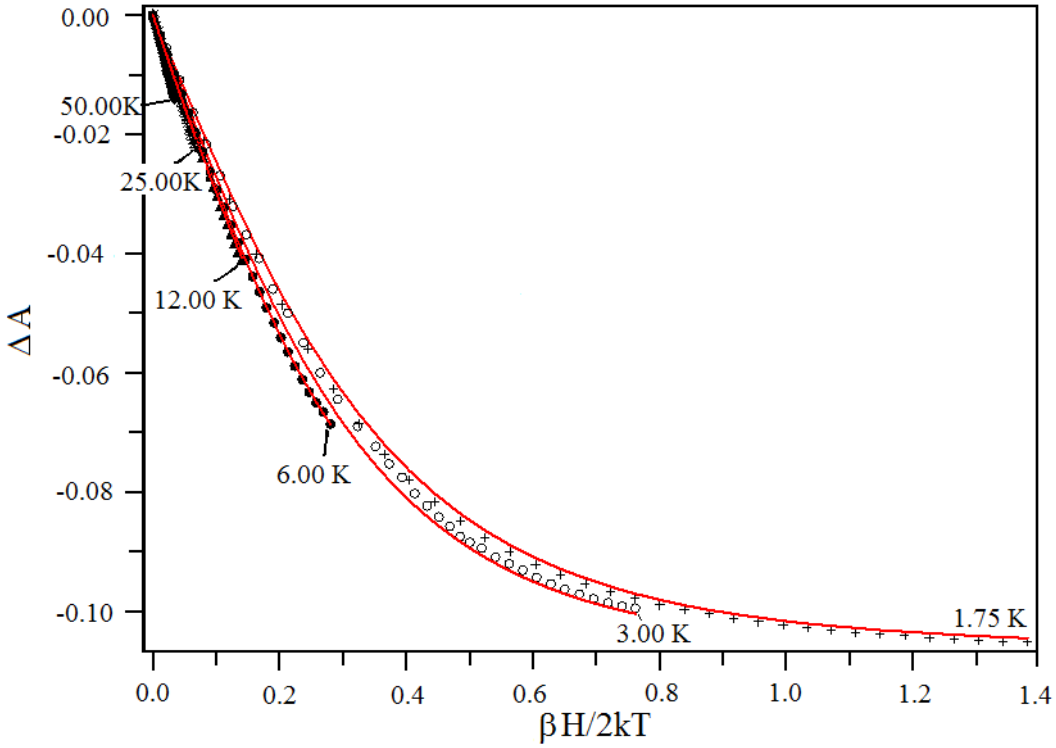

Figure 3.13. VTVH curves (black = experimental, red = fit; λ = 660 nm; T = 1.75 K – 50 K; methanol/glycerol 1:1) of the dinuclear copper(II) complex of $\mathbf{H_3L^1}$ (*c* = 30 mM), *i.e.* $[\mathbf{H_1L^1}Cu^{II}_2(\mu\text{-}OHCH(CH_2OH)_2)]^{2+}$ measured at 7 Tesla.

From the experimental splitting of the VTVH curves of the dinuclear copper(II) complex the *g* tensor as well as the *J* coupling and D and E values can be derived via a fitting of the nested VTVH curves. The VTVH data has been analyzed using the formalism developed by Neese and Solomon, using Eq. 3.11.[152] For a particular coupled spin system S_1 and S_2, the MCD magnetization curves are calculated as:

$$\frac{\Delta A}{E} = -\frac{1}{4\pi S}\int_0^{\pi}\int_0^{2\pi}\sum_i N_i\,(1 < S_{xli} > M_{yz1}^{eff} + m < S_{Yli} > M_{xz1}^{eff} + n < S_{zli} > M_{yx1}^{eff} +$$

$$l < S_{x2i} > M_{yz2}^{eff} + m < S_{y2i} > M_{xz2}^{eff} + n < S_{z2i} > M_{yz2}^{eff})\sin\theta d\theta d\varphi \qquad \text{Eq. 3.11}$$

where N_i are the Boltzmann populations of the energy levels; $<S_{xli}>$ is the expectation value of the spin operator S_{x1} for spin 1 in level i; and *l*, *m*, *n* specifies the direction of the magnetic field with respect to a molecular fixed axis system, and the integration is carried out numerically over all orientations. The M_{xy}^{eff}, M_{xz}^{eff}, M_{yz}^{eff} are the effective transition dipole moment products for transitions centered on either the S_1 or S_2 metal. For a transition allowed in x and y polarization, one expects $M_{xy}^{eff} \gg M_{xz}^{eff} \sim M_{yz}^{eff}$. The population factors N_i and the spin expectation values are calculated from the energies and wavefunctions, respectively, of the spin-Hamiltonian for the coupled system, given in Eq. 3.12.

$$H_{Spin} = -2J_{12}S_1 \cdot S_2 + H_s(S_1) + H_s(S_2) \qquad \text{Eq. 3.12}$$

The best fit of the experimental data is shown in Figure 3.13. It assumes two ferromagnetically coupled copper(II) centers with a small *J* value (0.4 cm^{-1}) and a small zero field splitting (D = 0.68). The *g* tensors assumed for this fit are $g_x = g_y$ =2.05 and g_z = 2.254. The data can also be fitted to an isolated S = ½ system, *e.g.* a monomeric impurity, or an antiferromagnetically coupled dinuclear copper(II) species (see Appendix E). However, in order to obtain an acceptable fit $g_{||}$ value had to be set to unreasonable values of 2.856 (monomer) and 3.41 (dimer). Therefore, it can be concluded, that a ferromagnetically coupled dinuclear copper(II) species gives rise to the MCD spectra.

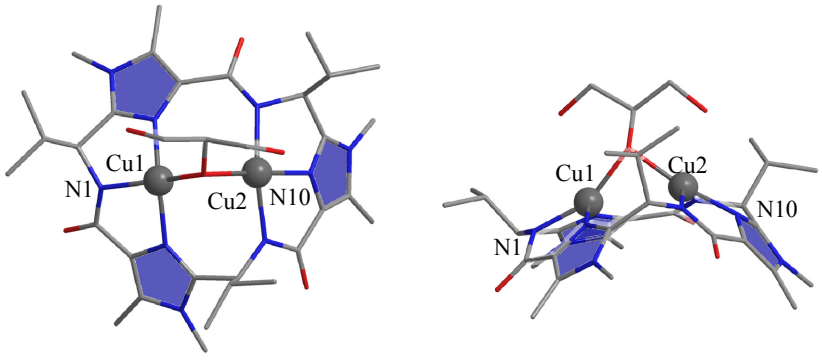

Figure 3.14. DFT calculated structure (G03, B3LYP/6-31g*/TZVP) of the glycerol bridged dinuclear copper(II) complex of $\mathbf{H_3L^1}$.

The assumed ferromagnetically coupled dinuclear glycerol bridged complex of $\mathbf{H_3L^1}$, $[\mathbf{H_1L^1}Cu^{II}_2(\mu\text{-}OHCH(CH_2OH)_2]^{2+}$ was optimized with DFT methods (B3LYP/6-31g* (C, H, N, O)/TZVP(Cu); see Figure 3.14) and the coupling constant *J* was calculated for the structure thus obtained. The calculated value of *J* is -18 cm^{-1}. The calculation does not reproduce the experimentally derived *J* value, yet can be considered as within in accuracy. The measured MCD spectra are those of an exchange coupled glycerol bridged complex. To verify its existence an EPR measurement of the dinuclear copper(II) complex $[\mathbf{H_1L^1}Cu^{II}_2(\mu\text{-}MeOH)]^+$ dissolved methanol/glycerol was recorded (see Figure 3.15).

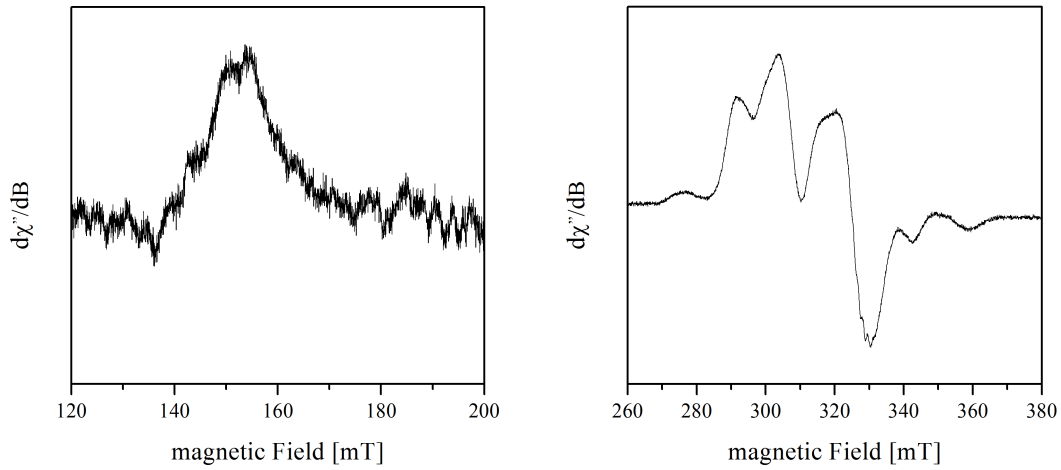

Figure 3.15. Experimental X-Band EPR spectra of the glycerol bridged dinuclear copper(II) complex $[\mathbf{H_1L^1}Cu^{II}_2(\mu\text{-}OHCH(CH_2OH)_2]^{2+}$, $c(\mathbf{H_3L^1})$ = 15 mM, methanol/glycerol 1:1, ν = 9.434401 GHz, T = 50 K. Formally forbidden $\Delta m_s = \pm 2$ (left) and allowed $\Delta m_s = \pm 1$ transitions (right).

The EPR spectrum arises from a dipole-dipole coupled dinuclear copper(II) species, with allowed transitions ($\Delta m_s = \pm 1$) and formally forbidden ($\Delta m_s = \pm 2$) EPR transitions around 300 and 160 mT, respectively (see Figure 3.15). When the temperature is decreased to 10 K, a saturation of the EPR transitions is observed, which is consistent with a small exchange coupling, predicted by the MCD measurements. The influence of glycerol on the dinuclear copper(II) complexes of $\mathbf{H_3L^2}$, $\mathbf{H_3L^3}$ and $\mathbf{H_3L^{wa}}$ has not been measured yet.

3.3 Summary and Outlook

The investigation of the cyclic pseudo hexapeptides $\mathbf{H_3L^{1-3}}$, models of the natural pseudo peptide westiellamide $\mathbf{H_3L^{wa}}$ revealed interesting differences in their coordination chemistry.

At low base concentrations $\mathbf{H_3L^{wa}}$, $\mathbf{H_3L^{1}}$, and $\mathbf{H_3L^{3}}$ exclusively form mononuclear complexes. However, the incorporation of oxazole rings substantially alters the coordination chemistry of the pseudo peptides: at low base concentrations $\mathbf{H_3L^{2}}$ coordinates copper(II) in an interesting and new coordination mode, where instead of a "normal" coordination in the N_{het}-N_{amide}-N_{het} binding site copper(II) is coordinated from the outside of the macrocycle by the oxygen atoms of the peptide bonds, thus forming a $\mathbf{H_3L^{2}}$/copper(II) 2:1 complex. This coordination mode was verified by EPR and NMR spectroscopy and is reminiscent of the unusual Ag_4-cluster that was reported by Wipf *et al.* for westiellamide.[93]

At high base concentrations all macrocycles show the formation of dinuclear methanol bridged copper(II) complexes. Most interestingly $\mathbf{H_3L^{2}}$, the ligand with the least basic heterocycles (oxazoles) is the only pseudo hexapeptide that has a cooperative effect. The imidazole pseudo hexapeptide $\mathbf{H_3L^{1}}$, on the other hand, is the only macrocycle that was found to form an antiferromagnetically coupled dinuclear copper(II) complex. This difference in coordination chemistry was reflected in the DFT calculations of the exchange coupling constants of the dinuclear complexes. The divergent behavior of $\mathbf{H_3L^{1}}$ was found to be the result of a slightly different orientation of the copper(II) planes within the complex of $\mathbf{H_3L^{1}}$ compared to the dinuclear complexes of $\mathbf{H_3L^{2}}$ and $\mathbf{H_3L^{3}}$. Addition of glycerol replaces the bridging methanol in the dinuclear complex of $\mathbf{H_3L^{1}}$ and leads to a reorganization of the complex, resulting in a weakly coupled species that was investigated by DFT, EPR, and MCD experiments.

The calculation of the EPR properties of the mononuclear copper(II) complexes of $\mathbf{H_3L^{1-3}}$ and $\mathbf{H_3L^{wa}}$ was found to be challenging. It was aimed to find a generally applicable combination of functional and basis set that provides good results, both for the calculated *g* and *A* tensors. Acceptable results were obtained with the BHLYP functional in combination with the basis sets 6-31g* (C, H, N, S, O), TZVP (first coordination sphere), and Wachters (Cu). However, a substantial deviation of the A_z (Cu^{II}) tensor from the experimental derived values has to be accepted. It cannot be predicted whether A_z is over or underestimated by the calculations the prediction of EPR tensors by DFT methods and it is concluded that the

prediction of copper(II) EPR tensors with DFT methods is too inaccurate to provide meaningful results for the investigation of unknown complexes of cyclic pseudo peptides.

The performed experiments provided new insights into the various factors that influence the copper(II) coordination chemistry of cyclic pseudo hexapeptides, yet the question of the metabolic role of westiellamide remains. The performed experiments did not provide any evidence for a reaction of the dinuclear copper(II) complexes with atmospheric CO_2, as found for the cyclic pseudo octapeptides (see Chapter 4). Most likely the cyclic pseudo hexapeptides have a different role in the metabolism of the *ascidians* than the cyclic pseudo octapeptides.

4 Cyclic Pseudo Octapeptides

4.1 Introduction and General Remarks

Recent findings reinforce the involvement of the dinuclear copper(II) complexes of patell-amides and ascidiacyclamide in CO_2 fixation and as yet it is unclear whether this is a catalytic reaction or not.[103] To investigate the impact of structural features for CO_2 hydrolysis and subsequent formation of carbonato-bridged complexes a variety of cyclic pseudo octapeptides (**H_4L^4**, **$H_4L^{4\text{-bn}}$**, **H_4L^{rs}**, **$H_4L^{ox,}$** and **H_4L^{ascA}**) was synthesized and studied (see Figure 4.1). Their molecular structure gradually approaches the configuration and composition of the natural pseudo octapeptides (see Figure 1.2, page 4).

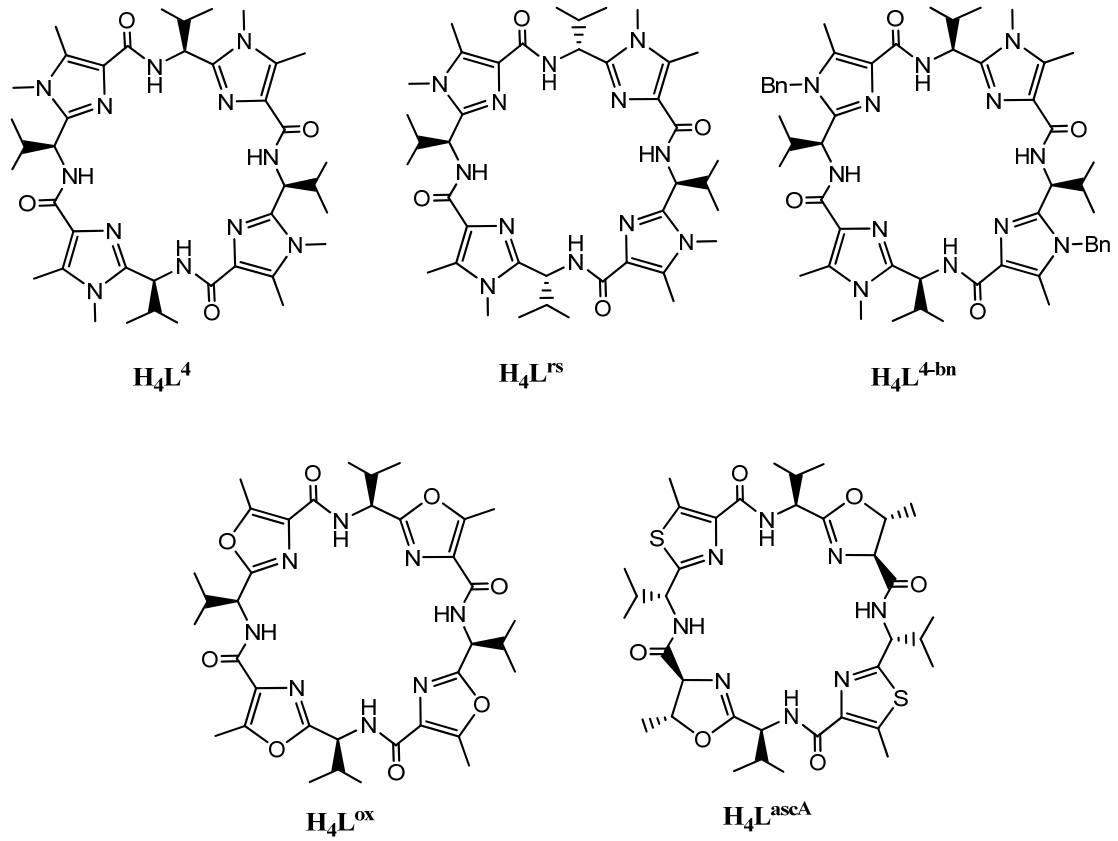

Figure 4.1. Chemical structure of the studied macrocycles **H_4L^4**, **H_4L^{rs}**, **$H_4L^{4\text{-bn}}$**, **H_4L^{ox}**, and **H_4L^{ascA}**.

From the simple model systems with C_4-symmetry and all S^*-configured amino acid linkers, *e.g.* **H_4L^4**, the gradual exchange of the linkers and the heterocycles leads to C_2-symmetric macrocycles, *e.g.* **H_4L^{rs}**, and thus enables the investigation of the influence of

the linker and the incorporated heterocycle on the copper(II) coordination chemistry of a cyclic pseudo octapeptide.

The copper(II) coordination chemistry of the cyclic pseudo octapeptides $\mathbf{H_4L^4}$, $\mathbf{H_4L^{rs}}$, $\mathbf{H_4L^{ox}}$, and $\mathbf{H_4L^{ascA}}$ was studied by a variety of spectroscopic methods in combination with computational methods (ESI-MS, CD, UV-vis, and EPR spectroscopy as well as DFT and molecular mechanics calculations). The cyclic peptides are poorly soluble in water. Therefore all experiments were performed in methanol. Unless stated otherwise freshly prepared methanolic solutions with variable ratios of cyclic pseudo octapeptide/copper(II)triflate/base ((*n*-Bu_4N)(OMe)) were used for the experiments. The concentration of the pseudo octapeptides was 1.25 mM in case of the spectroscopic and 1.25 μM in case of the MS experiments. The ESI-MS experiments in methanolic solutions were used to gain initial insight into the copper(II) coordination chemistry. The observed signals were assigned to the potential copper(II)-macrocycle complexes, and the solution equilibria were then investigated by UV-vis and CD spectroscopy. Those deemed interesting were, further studied by EPR spectroscopy and computational methods (DFT and MM calculations). Suitable crystals for X-ray crystallography could be obtained from the cyclic pseudo octapeptides $\mathbf{H_4L^{rs}}$ and $\mathbf{H_4L^{4\text{-}bn}}$ and from a dinuclear copper(II) complex of $\mathbf{H_4L^{rs}}$ (see Appendix F for crystallographic information). The structural features and differences of cyclic pseudo octapeptides are discussed in Section 4.1.1. Their copper(II) coordination chemistry is discussed in detail in the following sections of this Chapter.

4.1.1 Structural Features of Cyclic Pseudo Octapeptides

The cyclic pseudo octapeptides include four heterocycles in their macrocycle and are thus, unlike the cyclic pseudo hexapeptides discussed in Chapter 3, able to bind two copper(II) ions in the preferred N_{het}-N_{amide}-N_{het} binding motif (see Section 3.1). In the complexes the copper(II) centers are coordinated to trans-disposed binding sites.

While the C_4-symmetric macrocycles with all S^*-configured linkers, *e.g.* $\mathbf{H_4L^4}$, have four identical N_{het}-N_{amide}-N_{het} binding sites (see Figure 4.2, left), and therefore two identical di-nuclear copper(II) complexes with identical copper(II) sites. The alteration of the stereo-chemistry of the linkers, *e.g.* $\mathbf{H_4L^{rs}}$, leads to two enantiomeric binding sites in the mono- and dinuclear copper(II) complexes. Depending on the configuration of the linker, copper(II) can either be coordinated to a N_{het}-$N_{\textit{R}\text{-amide}}$-$N_{het}$ or a N_{het}-$N_{\textit{S}\text{-amide}}$-$N_{het}$ binding site (see Figure 4.2, right). In the dinuclear copper(II) complexes both copper(II) ions are either coordinated by a N_{het}-$N_{\textit{R}\text{-amide}}$-$N_{het}$ or a N_{het}-$N_{\textit{S}\text{-amide}}$-$N_{het}$ binding site forming enantiomeric complexes. The alternating stereochemistry of $\mathbf{H_4L^{rs}}$ is identical to the molecular design of the natural metabolites patellamide A-G and ascidiacyclamide. As a consequence of the incorporated oxazoline rings with additional stereocenters leads the coordination of copper(II) in the N_{het}-$N_{\textit{R}\text{-amide}}$-$N_{het}$ or the N_{het}-$N_{\textit{S}\text{-amide}}$-$N_{het}$ binding site of the natural cyclic pseudo peptides not to the formation of enantiomers but diasteromers.

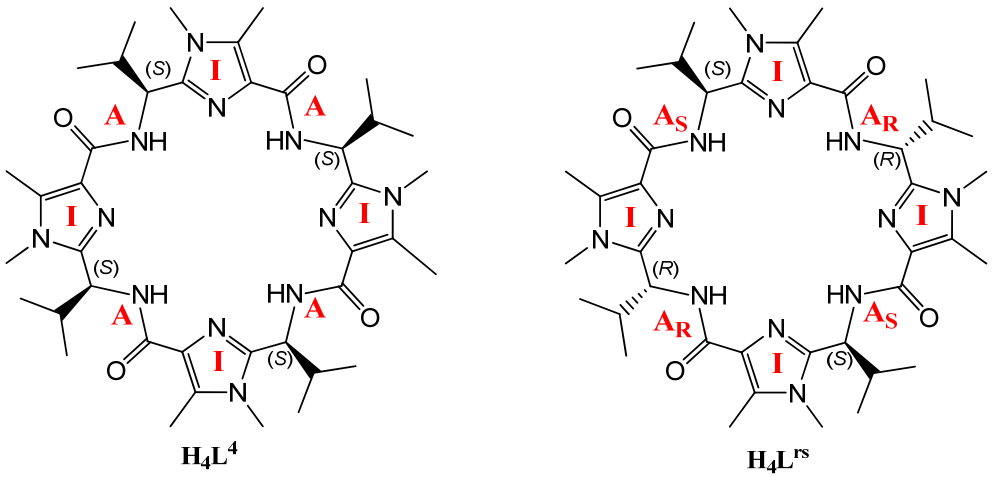

Figure 4.2. Binding motifs of the cyclic pseudo octapeptides $\mathbf{H_4L^4}$ and $\mathbf{H_4L^{rs}}$. I = imidazole-, A = amide-, $A_{S,R}$ = amide nitrogen at S^*/R^*-configured linker.

The conformation that is adopted by a cyclic pseudo peptide in solution and in the solid state is dependent on various factors: the stereochemistry of the amino acid linker, the incorporated azole moieties, the potential existence of sterically demanding residues, and the molecule's symmetry (see Chapter 1.3).

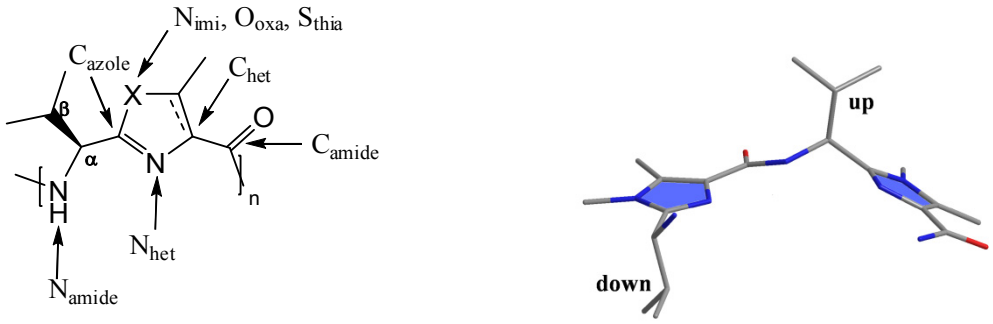

Figure 4.3. Abbreviations for the heterocyclic moiety of cyclic pseudo peptides (left) and definition of the up- and downside of the macrocycles (right).

To simplify the description of the cyclic pseudo peptides one can define an "up" and a "down" side of their ring system: looking at the amino acid linker (C_{amide}-N_{amide}-C_{α}-C_{azole}) from the inside of a pseudo peptide's macrocycle in such a way that the amide bond is located on the left hand side, all atoms that are above the linker-plane are defined as up, while all those that are below are assigned as down (see Figure 4.3, right).

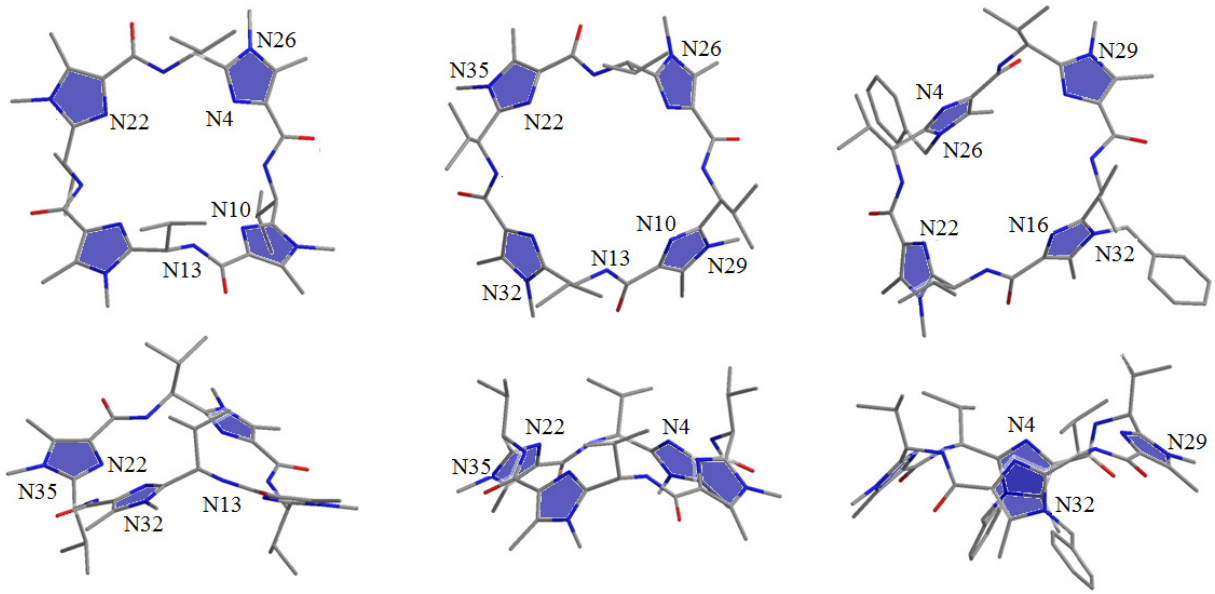

Figure 4.4. Top (top) and side view (bottom) of the X-ray structures of $\mathbf{H_4L^{rs}}$, $\mathbf{H_4L^4}$, and $\mathbf{H_4L^{4\text{-}bn}}$.

The dependency of the adopted conformation on the stereochemistry of the amino acid linker and on sterical demanding residues can be seen by comparing the X-ray structures of $\mathbf{H_4L^4}$, $\mathbf{H_4L^{rs}}$, and $\mathbf{H_4L^{4\text{-}bn}}$ (see Figure 4.4 for a comparison of their X-ray structures and Figure 4.5 for the ORTEP plots of $\mathbf{H_4L^{4\text{-}bn}}$ and $\mathbf{H_4L^{rs}}$). The pseudo peptides only differ slightly from each other with respect to their chemical structure. They all consist of four imidazole heterocycles connected via valine linkers, and the only differences are the configuration at C_α and the substituents at the imidazole nitrogen atoms N_{imi} (see Figure 4.3, left for abbreviations). From NMR studies and X-ray crystallography it is known that in solution and the solid state, the pseudo peptides $\mathbf{H_4L^4}$, $\mathbf{H_4L^{rs}}$, and $\mathbf{H_4L^{4\text{-}bn}}$ adopt the square conformation (see Chapter 1.3, page 7 for definition of the conformations), as expected for C_2- and C_4-symmetric pseudo octapeptides. However, there are remarkable differences in the orientation of the imidazole units and the valine side chains. As a result of the large benzyl residues at the imidazole rings in $\mathbf{H_4L^{4\text{-}bn}}$, these are rotated in the solid state structure and the benzyl substituted imidazole rings are nearly collinear, while the methyl substituted imidazole rings are turned towards the outside of the ring system. In contrast the trans-disposed imidazole rings in $\mathbf{H_4L^4}$ and $\mathbf{H_4L^{rs}}$ are twisted with respect to each another with angles of 78° and 54°, respectively. The parallel orientation of the imidazole rings in $\mathbf{H_4L^{4\text{-}bn}}$ is reflected in the distance of the outer imidazole nitrogens N_{imi}. This distance is small for the parallel imidazole rings, and increases with the degree of rotation of the imidazole ring towards to outside of the macrocycle (see Table 4.1). While in $\mathbf{H_4L^4}$ all trans-disposed imidazole nitrogens N_{imi} have a distance of ~10.4 Å the distance of the benzyl substituted N_{imi} atoms shrinks to 7.88 Å in $\mathbf{H_4L^{4\text{-}bn}}$. In solution, however, the NMR data (see Chapter 5.2.2, page 160) indicate, that the benzyl substituted imidazole rings are no longer parallel but instead adopt a conformation similar to the X-ray structure of $\mathbf{H_4L^4}$ and this is also reproduced by the DFT-calculated structures. This indicates that the twist of the substituted imidazole rings is mainly caused by crystal packing effects and, indeed a π–stacking between the benzyl rings of different $\mathbf{H_4L^{4\text{-}bn}}$ molecules can be observed in the crystal lattice. This induces the rotation of the substituted imidazole rings. These findings indicate that the influence of large substituents at N_{imi} is primarily present in the solid phase.

Table 4.1. Selected angles and distances (e.s.d.'s are given in parantheses) of the X-ray and the DFT optimized structures of $\mathbf{H_4L^4}$, $\mathbf{H_4L^{rs}}$, $\mathbf{H_4L^{ox}}$, and $\mathbf{H_4L^{4\text{-}bn}}$.

	$\mathbf{H_4L^4}$		$\mathbf{H_4L^{rs}}$		$\mathbf{H_4L^{4\text{-}bn}}$		$\mathbf{H_4L^{ox}}$ [102]
	X-ray	DFT [a]	X-ray	DFT [a]	X-ray	DFT [a]	X-ray
θ [H-N_{amide}-C_α-H] [b, c]	178, 160	all 160	-165[*], 165	-162[*], 162	-136[*], 176	-153[*], -156	158/168
χ [N_{amide}–C_α–C_{azole}–N_{imi}]	120, 102	all 102	-133[*], 133	-126[*], 126	94[*], 124	-98[*], 104	79/187
α [N4-N10-N16-N22] [d]	4	0	20	20	8	1	3
β [N/O35–N22–N10–N/O29], [N/O26–N4–N16–N/O32] [d]	93, 49	71	-160, 160	-145, 145	79, 53[*]	69,70	133/68
γ [N26-N29-N32-N35] [d] γ [O26-O29-O32-O35] [d]	9	0	-18	-21	20	2	8
ρ (angle between binding sites)	161	161	78	78	170/160	172/168	129/66
d (N_{amide}-N_{amide}) consecutive	5.398(4), 5.623(4)	all 5.60	all 5.3637(6)	all 5.25	5.4183(6), 5.868(1)	5.58, 5.66	5.265(5)/5.891(5)
d (N_{amide}-N_{amide}) trans-disposed	7.951(4), 7.560(4)	all 7.93	all 7.189(1)	all 6.59	8.2250(8)[*], 7.854(1)	7.81[*], 8.00	6.918(5)/8.293(5)
d (N_{het}-N_{het}) consecutive	5.139(3), 5.346(4)	all 5.28	all 4.9633(7)	all 4.71	5.1809(9), 5.4497(6)	5.34, 5.25	4.585(5)/5.446(5)
d (N_{het}-N_{het}) trans-disposed	7.620(3), 7.196(3)	7.48	all 6.9027(8)	6.56	7.0801(7)[*], 7.904(2)	7.41[*], 7.56	7.592(5)/6.606(5)
d (N_{imi}-N_{imi}) trans-disposed d(O_{oxa}-O_{oxa})	10.464(4), 10.306(4)	10.16	11.079(1)	10.67	7.8848(7)[*], 11.403(2)	9.78[*], 10.24	8.859(5)/11.875(5)
d (N_{imi}-N_{imi}) consecutive d(O_{oxa}-O_{oxa})	7.123(4), 7.607(3)	all 7.18	all 7.929(1)	7.68	6.9043(7), 7.166(1)	all 7.08	6.770(5)/8.026(5)

Units: d [Å], angles [°] a) TURBOMOLE, B3LYP/6-31g*; b) analysis of the ^{1}H-NMR data provided the following angles: $\mathbf{H_4L^4}$, $\mathbf{H_4L^{ox}}$ = 155°<| θ |<165°; $\mathbf{H_4L^{rs}}$ = 140°<| θ |<165°; $\mathbf{H_4L^{4\text{-}bn}}$ = 135°<| θ |<155° and 145°<| θ |<180°; c) see Figure 4.3 for used abbreviations d) see Figure 4.4, Figure 4.5, and Figure 4.7 for atom numbers [*]) at benzyl-imidazole/*R*[*]-configured C_α.

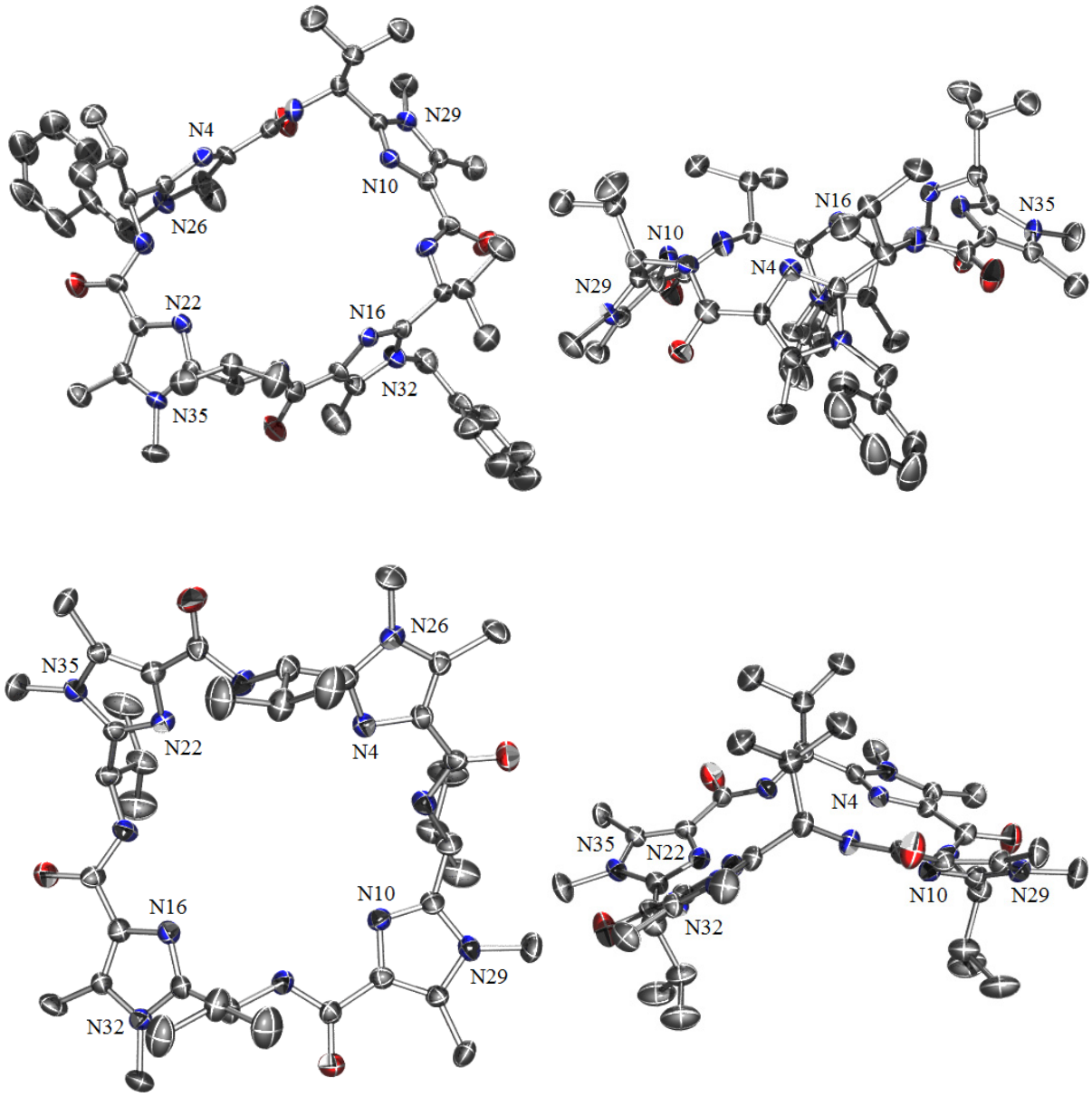

Figure 4.5. ORTEP plots: Top (left) and side view (right) of the X-ray structures of $\mathbf{H_4L^{4\text{-}bn}}$ (top) and $\mathbf{H_4L^{rs}}$ (bottom). Ellipsoids are drawn at 50% probability (hydrogen atoms and solvent molecules are omitted for clarity, carbon = grey, nitrogen = blue, oxygen = red, see Appendix F for crystallographic information).

In comparison to $\mathbf{H_4L^4}$ and $\mathbf{H_4L^{4\text{-}bn}}$, two of the stereocenters in $\mathbf{H_4L^{rs}}$ are inverted. This rather minor modification has a considerable influence on the shape of the macrocycle (for selected angles and distances see Table 4.1). $\mathbf{H_4L^4}$ and $\mathbf{H_4L^{4\text{-}bn}}$ adopt a cone like structure, where all valine residues are oriented on the up side and the substituents at N_{imi} are oriented downwards (see Figure 4.4 bottom). Apart from the distance of trans-disposed N_{imi} atoms, the cone like shape of the macrocycles is also reflected in the dihedral angle β, between the nitrogen atoms (N_{het}-N_{imi}-N_{imi}-N_{het}) of trans-disposed imidazole rings N4-N10-N16-N22 (see

Table 4.1, Figure 4.4). The geometry optimized structures of $\mathbf{H_4L^4}$ and $\mathbf{H_4L^{4\text{-}bn}}$ have identical values of β (70°), while in $\mathbf{H_4L^{rs}}$ a strikingly different angle of 145° is adopted. The configurational modification of two C_α–carbon atoms in $\mathbf{H_4L^{rs}}$ induces a change of the macrocycle's shape from a cone to a zig-zag like structure, resulting in valine residues that have alternating orientations on the up and down side (see Figure 4.4, bottom and Figure 4.5, bottom) and this also influences the diameter of the macrocycle (see Table 4.1). While trans-disposed N_{amide} atoms in $\mathbf{H_4L^4}$ and $\mathbf{H_4L^{4\text{-}bn}}$ are roughly 8 Å apart (e.s.d. = 0.004 Å), their distance shrinks to 7.189(1) Å in the X-ray and further down to 6.5 Å in the fully optimized DFT structure of $\mathbf{H_4L^{rs}}$ thereby changing the degree of planarity of the inner heterocyclic N_{het} and amide nitrogen atoms N_{amide} (see Figure 4.6, bottom). Their deviation from perfect planarity in $\mathbf{H_4L^4}$ is marginal, two of the heterocyclic nitrogens N_{het} are 0.09 Å distant from the plane that is spanned by the inner nitrogens and two of the amide nitrogens, N_{amide}, are 0.33 Å apart and insignificantly enlarges in $\mathbf{H_4L^{4\text{-}bn}}$: 0.17 Å distance for two heterocyclic nitrogens N_{het} and 0.33 Å for two N_{amide} atoms. Yet, within the experimental error they can be considered as coplanar and this could be verified by DFT calculations and is also visible in the dihedral angle α of the inner imidazole nitrogen atoms of 0° for $\mathbf{H_4L^4}$ and 1° for $\mathbf{H_4L^{4\text{-}bn}}$ (see Table 4.1).

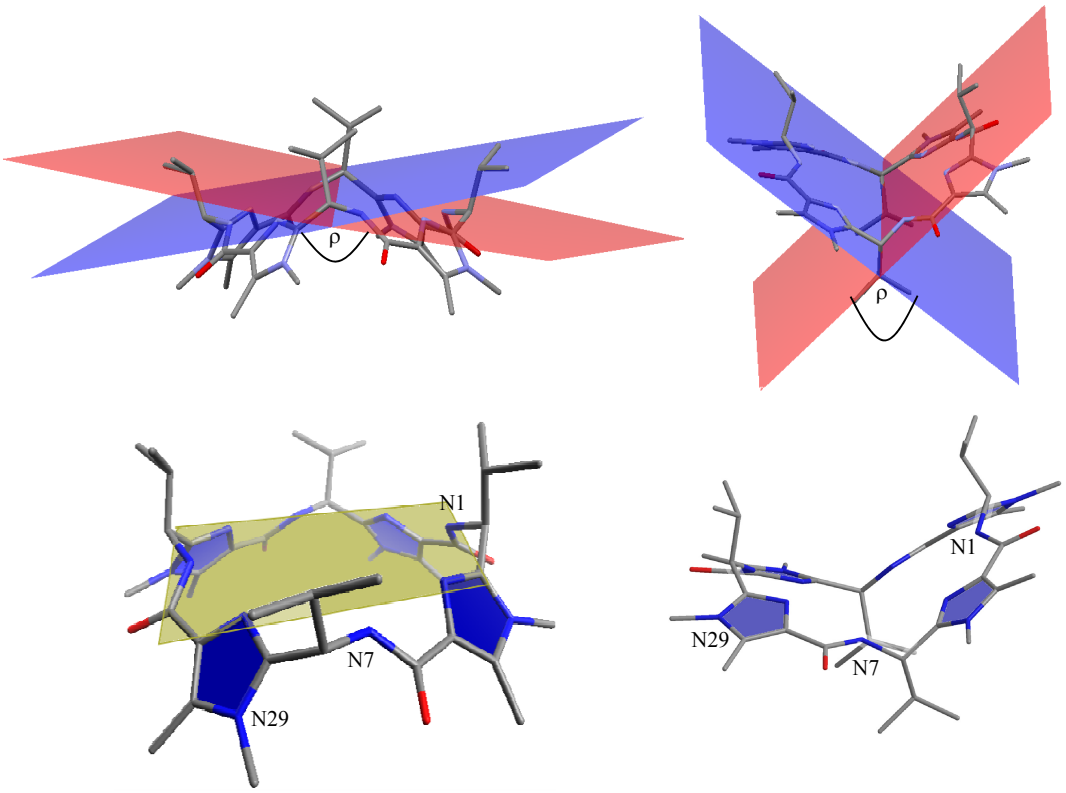

Figure 4.6. Structural parameters of $\mathbf{H_4L^4}$ (left) and $\mathbf{H_4L^{rs}}$ (right). Planes spanned by the coordinating nitrogen atoms N_{het}-N_{amide}-N_{het} of the respective binding sites, depicted in blue and red (top); folding of the macrocycles and the plane spanned by the inner nitrogen atoms N_{het} and N_{amide} of $\mathbf{H_4L^4}$ (bottom).

$\mathbf{H_4L^{rs}}$, however, has a conformation that precludes coplanar inner nitrogen atoms. The zig-zag folding makes it impossible to span a plane that includes all nitrogen atoms, or all imidazole/amide nitrogen atoms, *e.g.* the dihedral angle between the nitrogen atoms is 20°. The zig-zag structure of $\mathbf{H_4L^{rs}}$ is closer to the conformation of the natural cyclic pseudo octapeptide ascidiacyclamide than the cone like structures of $\mathbf{H_4L^4}$ and $\mathbf{H_4L^{4\text{-}bn}}$.

The differences of the macrocycles can also be visualized comparing the planes of the binding sites in the molecules. When in each of the two trans-disposed binding sites a plane is constructed from the coordinating nitrogen atoms N_{het}-N_{amide}-N_{het}, the folding of the macrocycle is reflected in the angle ρ between the planes (see Table 4.1 and Figure 4.6, top). Trans-disposed binding sites of $\mathbf{H_4L^4}$ include an angle of 160°, this angle is remarkably smaller in $\mathbf{H_4L^{rs}}$ (78°). It is expected that the orientations of the binding sites influence the copper(II) coordination chemistry, *e.g.* stability of complexes, preorganization for complexes, and magnetic properties of the dinuclear complexes. However, it is not known so far which characteristics influence the coordination chemistry the most.

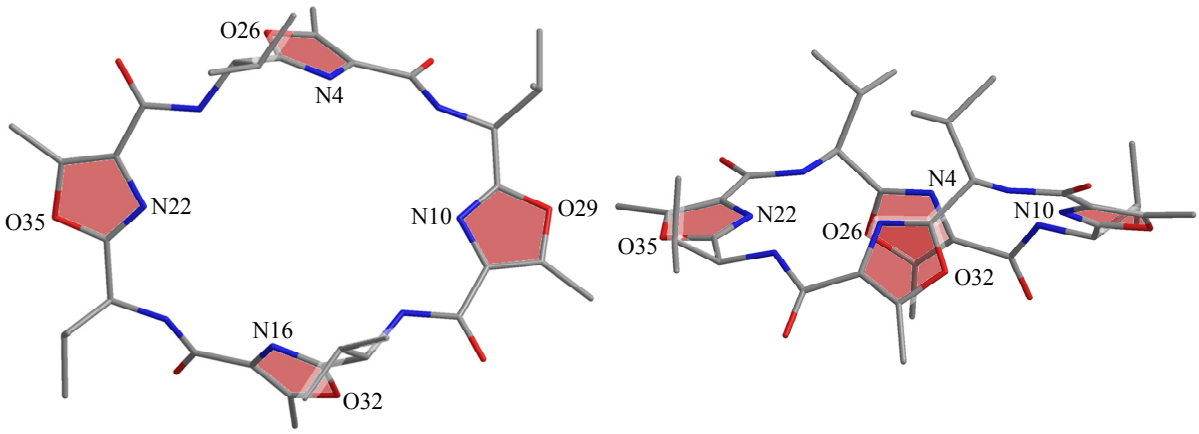

Figure 4.7. Top (left) and side view (right) of the X-ray structure of $\mathbf{H_4L^{ox}}$.[102]

Apart from the influence of the configuration of C_α and large substituents at the heterocyclic rings the adopted conformation in the solid phase also strongly depends on the incorporated heterocycles. This effect can be seen when the X-ray structure of $\mathbf{H_4L^{ox}}$ is examined (see Table 4.1 for structural parameters).[102] It has all S^*-configured amino acid linkers (as $\mathbf{H_4L^4}$) and thus one would expect that in the solid phase it also adopts a cone like conformation. However, the adopted conformation remarkably differs: similar to the obtained structure of $\mathbf{H_4L^{4\text{-}bn}}$ two of the heterocyclic rings are parallel, while the other two rings are

rotated towards the outside of the macrocycle (see Figure 4.7). While in $\mathbf{H_4L^{4\text{-}bn}}$ crystal packing effects, such as π-stacking between the benzene rings are thought to be responsible for the adopted conformation, it is assumed that the effect is of electronic nature in case of $\mathbf{H_4L^{ox}}$ and expected to be related to the preferred dihedral angle χ that strongly depends on the heterocycle (see Section 1.3, Figure 1.5). However, NMR studies suggest that in solution $\mathbf{H_4L^{ox}}$ adopts a C_4-symmetric structure and thus these effects seem to be restricted to the solid phase.[102]

4.2 Copper(II) Coordination Chemistry of H_4L^4

4.2.1 Complexation Equilibria and Spectroscopy

The C_4-symmetric macrocycle $\mathbf{H_4L^4}$ is a simple model system for natural cyclic pseudo octapeptides. It consists of four methylimidazole units connected via *L*-valine linkers. The complexation equilibria of $\mathbf{H_4L^4}$, shown in Figure 4.8, were previously derived from a combination of ESI-MS, UV-vis, CD, and EPR spectroscopy.[103] The UV-vis, CD and EPR spectra are of particular interest, as the differences between the macrocycles studied are reflected in their spectra. The copper(II) complexation equilibria of $\mathbf{H_4L^4}$ are briefly described below and can be found in detail elsewhere.[103] In contrast to the previously reported formation of a μ-oxo-bridged dinuclear copper(II) complex, it is assumed that the addition of four equivalents of base leads to the formation of a dihydroxo complex (see Figure 4.8). This assumption is based on the distance of the copper(II) ions that is predicted from the simulation of the EPR spectra (4.5 Å, see Table 4.3) in combination with the computed DFT structures of the dihydroxo- and μ-oxo complexes (see Section 4.2.3).

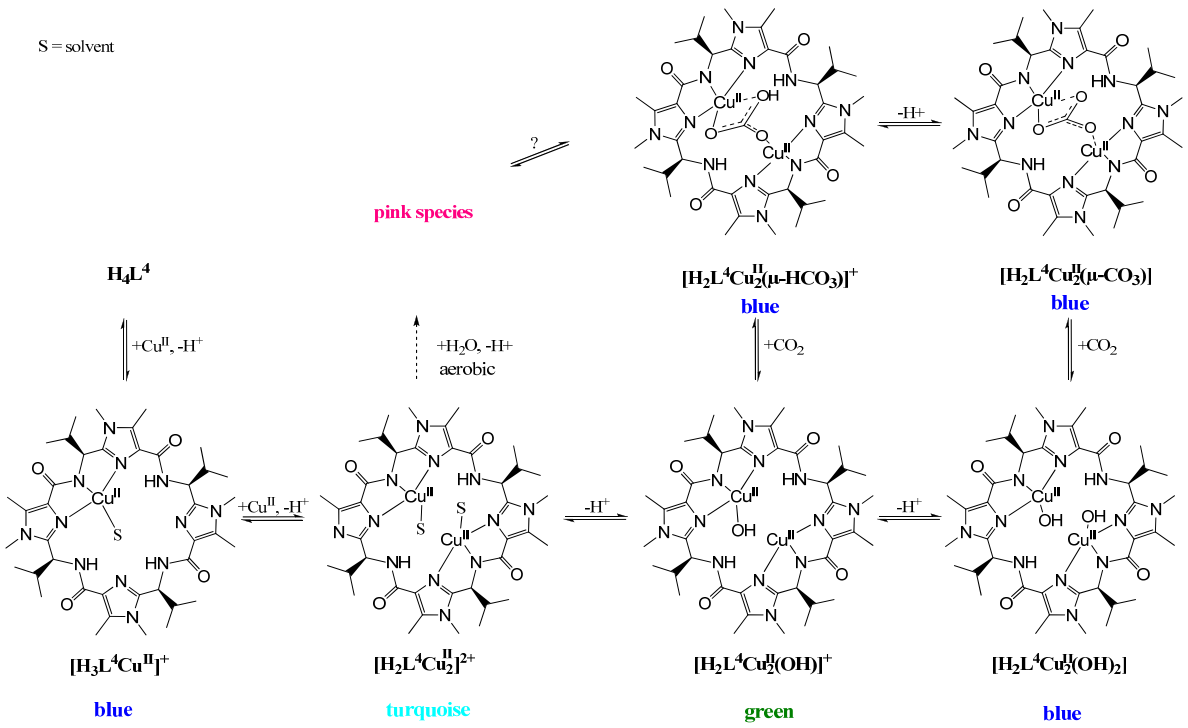

Figure 4.8. Complexation equilibria of $\mathbf{H_4L^4}$ with copper(II) and base (solvent = methanol).

The coordination of copper(II) to $\mathbf{H_4L^4}$ is accompanied by a series of color changes. The blue mononuclear copper(II) complex $[\mathbf{H_3L^4}Cu^{II}]^+$ is converted to the turquoise dinuclear copper(II) complex $[\mathbf{H_2L^4}Cu^{II}_2]^{2+}$ upon addition of copper(II) and two equivalents of base. Addition of further base shifts the complexation equilibrium to the green hydroxo complex $[\mathbf{H_2L^4}Cu^{II}_2(OH)]^+$ (at three equivalents of base) and further to the blue dihydroxo complex $[\mathbf{H_2L^4}Cu^{II}_2(OH)_2]$ (at four equivalents of base). The latter two complexes were found to react with CO_2 from air to form the dark blue (bi)carbonato-bridged dinuclear complexes, $[\mathbf{H_2L^4}Cu^{II}_2(\mu\text{-}HCO_3)]^+$ and $[\mathbf{H_2L^4}Cu^{II}_2(\mu\text{-}CO_3)]$, respectively. One important aim of this study was to determine whether this reaction is catalytic or not.

In the mono- and dinuclear copper(II) complexes the chirality of the cyclic pseudo peptides induces an asymmetry at the copper(II) centers that can be observed by CD spectroscopy. Remarkably, the formation of mono- and dinuclear copper(II) complexes can even be observed in absence of base (see Figure 4.9 for CD and UV-vis spectra). The CD spectra show a negative Cotton effect at 639 nm and a positive Cotton effect at 483 nm that increase with the copper(II) concentration. Their separation by isosbestic points indicates an equilibrium involving two species. In the UV-vis spectra addition of copper(II) to a $\mathbf{H_4L^4}$ solution leads to the formation of a d-d absorption band at 674 nm. Compared to solvated copper $[Cu^{II}(MeOH)_n]^{2+}$ (λ_{max} = 840 nm) this band is shifted to lower wavelength as a result of the coordination of copper(II) to one of the binding sites of $\mathbf{H_4L^4}$.

All the CD and UV-vis bands of a $\mathbf{H_4L^4}$/copper(II) 1:2 solution linearly intensify upon addition of up to two equivalents of base (see Figure 4.9). From the performed ESI-MS and EPR experiments it is known that the mononuclear copper(II) complex is formed first and subsequently converted to the dinuclear complex.[103] Neither the absorption bands in the UV-vis, nor the Cotton effects in the CD spectra are shifted during the titration and this is consistent with an identical coordination geometry at the copper(II) centers of the mono- and the dinuclear copper(II) complexes of $\mathbf{H_4L^4}$, $[\mathbf{H_3L^4}Cu^{II}]^+$ and $[\mathbf{H_2L^4}Cu^{II}_2]^{2+}$, respectively, expected from the molecular design of the macrocycle (see Chapter 4.1).

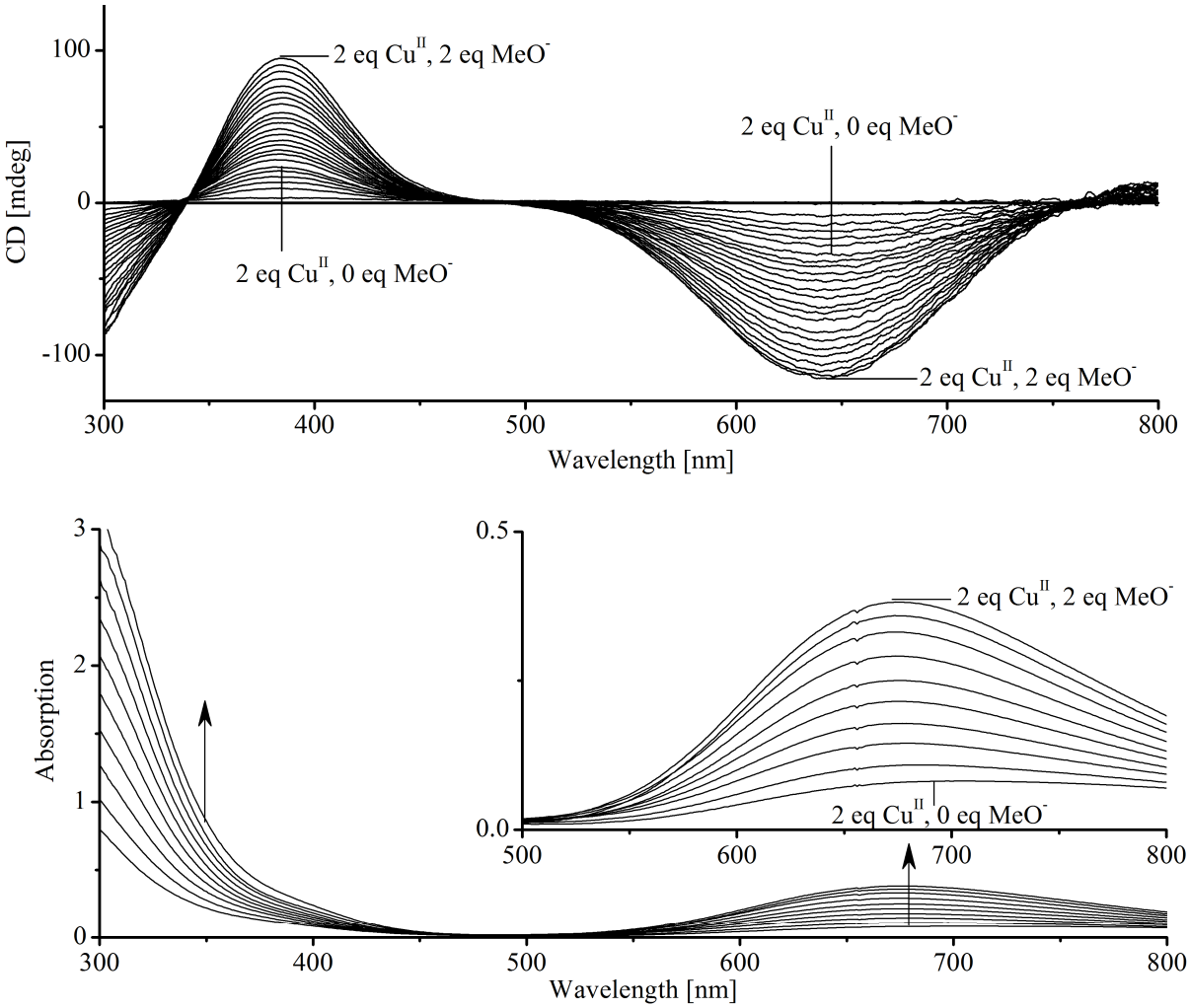

Figure 4.9. CD spectra (top) of the titration of 0-2 eq of Cu^{II}, in 0.1 eq steps, to a $\mathbf{H_4L^4}$ solution (c = 1.25 mM, methanol), and subsequent titration of 0-2 eq of base (MeO^-), in 0.1 eq steps, to a $\mathbf{H_4L^4}$/copper(II) 1:2 solution. UV-vis spectra (bottom) of the titration of 0-2 eq of base (MeO^-), in 0.2 eq steps, to a $\mathbf{H_4L^4}$/copper(II) 1:2 solution.

The linear increase in intensity of the absorption bands in the UV-vis and CD spectra ends after the addition of two equivalents of base. The UV-vis spectra show a shift of the absorption band from 674 (ε = 370 $M^{-1}cm^{-1}$) to 722 nm (ε = 210 $M^{-1}cm^{-1}$) presumably a result of the coordination of hydroxide to one of the copper(II) centers (see Figure 4.10). The isosbestic points at 320 and 535 nm are consistent with an equilibrium between the two dinuclear species $[\mathbf{H_2L^4}Cu_2^{II}]^{2+}$ and $[\mathbf{H_2L^4}Cu_2^{II}(OH)]^{+}$. The change of the coordinated ligand influences the asymmetry at the copper(II) centers and consequently changes the CD spectra. The CD spectra now exhibit two isosbestic points, at 716 and 502 nm (see Figure 4.10) and change to a greater extent than the UV-vis spectra. The positive Cotton effect at 383 nm is slightly shifted to 388 nm and increased in intensity. The negative Cotton effect of the dinuclear copper(II) complex $[\mathbf{H_2L^4}Cu_2^{II}]^{2+}$ at 638 nm diminishes and at three equivalents of

base a relatively broad negative Cotton effect (550–800 nm) with a maximum at 660 nm can be observed.

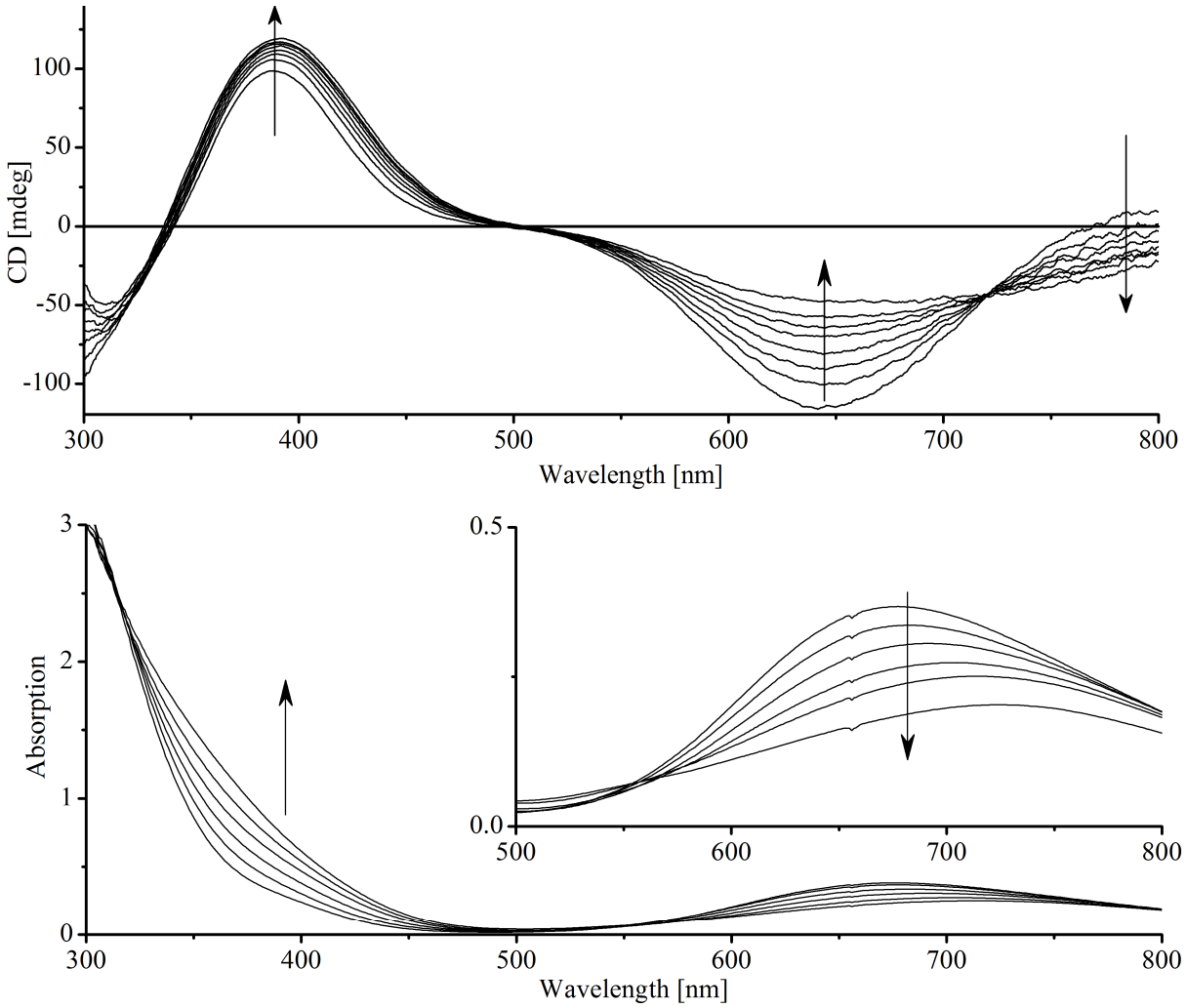

Figure 4.10. CD (top) and UV-vis spectra (bottom) of the titration of 2-3 eq of base (MeO^-), in 0.2 eq steps, to a $\mathbf{H_4L^4}$/copper(II) (1:2) solution ($c(\mathbf{H_4L^4})$ = 1.25 mM, methanol).

Addition of a fourth equivalent of base ((*n*-Bu_4N)(OMe)) induces a further change in the CD and UV-vis spectra. The CD spectra are indicative of another structural rearrangement upon the formation of the dihydroxo complex [$\mathbf{H_2L^4}Cu^{II}_2(OH)_2$] (see Figure 4.11) as the Cotton effect at 388 nm is shifted to 365 nm and slightly decreased in intensity. A new negative Cotton effect at 729 nm develops while the effect at ~660 nm decreases. The absorption band in the UV-vis spectrum is shifted to 657 nm. This band in the UV-vis spectra is presumably a superposition of the dihydroxo complex and already formed carbonato complex.

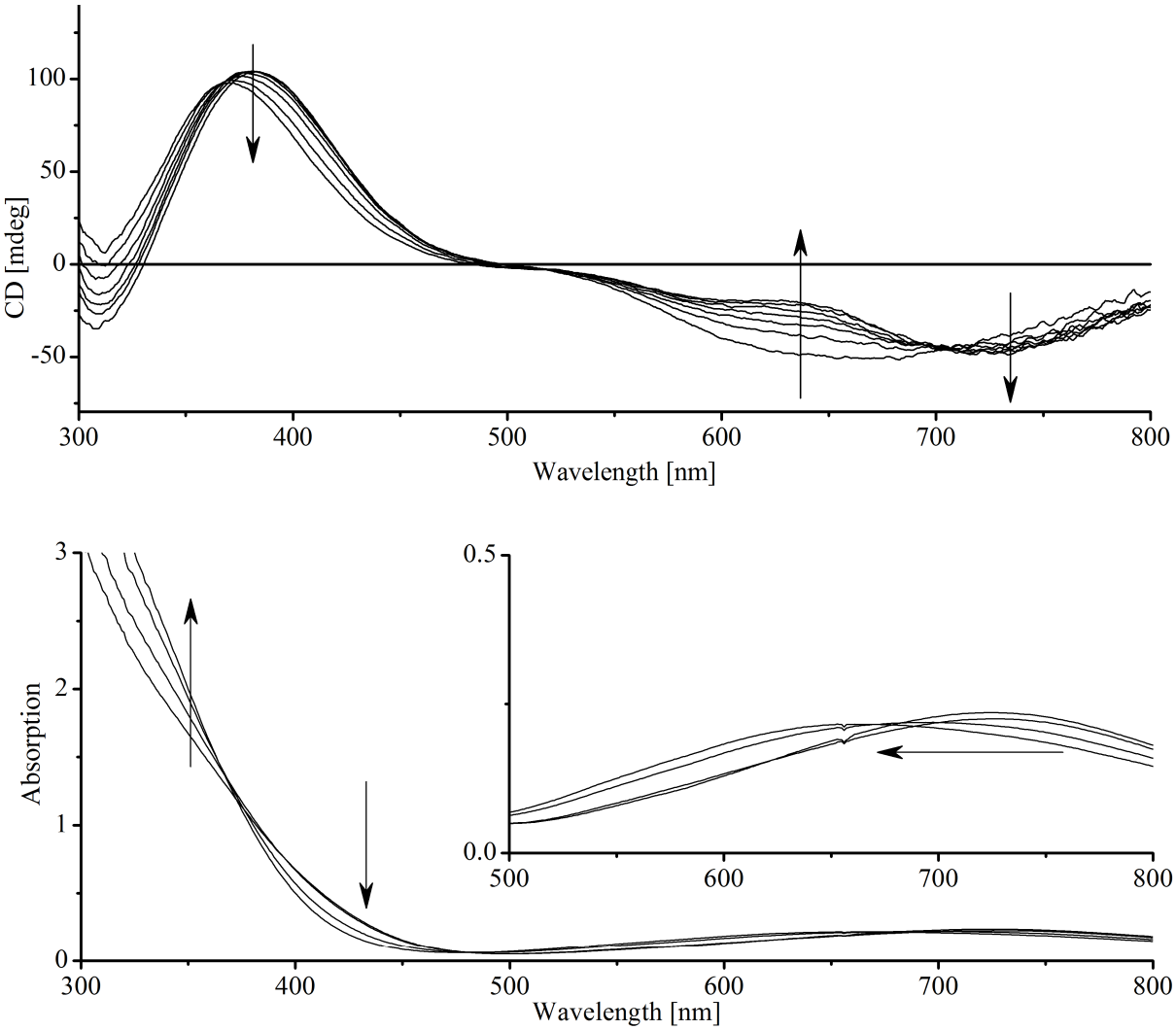

Figure 4.11. CD (top) and UV-vis (bottom) spectra of the titration of 3-4 eq of base (MeO^-), in 0.2 eq steps, to a solution of $\mathbf{H_4L^4}$/copper(II) 1:2 ($c(\mathbf{H_4L^4})$ = 1.25 mM, methanol).

The dinuclear copper(II) complexes (hydroxo and dihydroxo) that are present in solutions that contain four or more equivalents of base react with atmospheric CO_2 and show a time-dependent complete conversion to the carbonato complex [$\mathbf{H_2L^4}Cu^{II}_2(\mu\text{-}CO_3)$] (assigned from ESI-MS experiments) that can be followed spectroscopically in the CD and UV-vis spectra. The conversion is accompanied by a shift to lower wavelength (722 to 657 nm) in the UV-vis spectra and a change of the CD spectra (see Figure 4.12). The positive Cotton effect at 365 nm is increased in intensity and slightly shifted to 355 nm. At 705 nm a new negative and at 511 and 603 nm two new positive Cotton effects develop. The positive Cotton effects are assigned to the carbonato species [$\mathbf{H_2L^4}Cu^{II}_2(\mu\text{-}CO_3)$], identified by ESI-MS experiments. When the experiments are performed under anaerobic/CO_2 free conditions the formation of carbonato-bridged species cannot be observed (ESI-MS, EPR, UV-vis, and CD spectra). The

CD, UV-vis, and EPR spectra do not change within days, suggesting the formation of stable complexes.

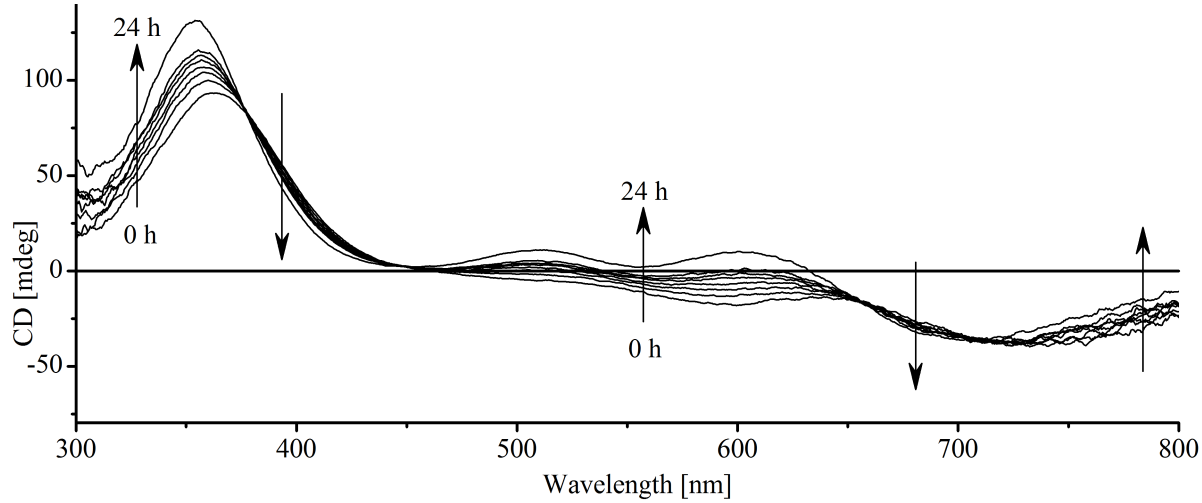

Figure 4.12. CD spectra of the time-dependent (0-24 h) conversion of the dihydroxo complex [$\mathbf{H_2L^4}Cu_2^{II}(OH)_2$] to the carbonato complex [$\mathbf{H_2L^4}Cu_2^{II}(\mu\text{-}CO_3)$], ($c(\mathbf{H_4L^4})$ = 1.25 mM, methanol).

4.2.2 CO_2 Fixation by the Dinuclear Copper(II) Complexes of H_4L^4

The observed conversion of CO_2 to carbonate and the formation of carbonato complexes was further studied by a variety of methods. Experiments with labeled water ($^{18}OH_2$) and carbon dioxide ($^{13}CO_2$) were performed, and the incorporation of both isotopes was followed by high resolution ESI mass spectrometry. The molecular formula and the experimental and calculated masses of representative dinuclear copper(II) complexes of $\mathbf{H_4L^4}$ are shown in Table 4.2. The neutral carbonato complex [$\mathbf{H_2L^4}Cu_2^{II}(\mu\text{-}CO_3)$] could be detected in the positive mode as the sodium and tetrabutylammonium adducts. Addition of ^{18}O labeled water to a solution containing $\mathbf{H_4L^4}$/copper(II)/base in a ratio of 1:2:2 or 1:2:3 causes a shift of the signal of the hydroxo complex [$\mathbf{H_2L^4}Cu_2^{II}(OH)]^+$ from *m/z* 913.3315 to *m/z* 915.3363 ([$\mathbf{H_2L^4}Cu_2^{II}(^{18}OH)]^+$). The exchange of the coordinated hydroxide in the hydroxo complex [$\mathbf{H_2L^4}Cu_2^{II}(^{16/18}OH)]^+$ with ^{18}OH or ^{16}OH, respectively, is fast and can be observed within minutes.

When an $^{18}OH_2$ containing solution is exposed to air, the ESI-MS signals of the bicarbonato- and carbonato-bridged species [$\mathbf{H_2L^4}Cu_2^{II}(\mu\text{-}HCO_3)]^+$ and [$\mathbf{H_2L^4}Cu_2^{II}(\mu\text{-}CO_3)$], respec-

tively, are shifted by two mass units indicating that the hydroxo complex is involved in the fixation of CO_2. The exposition of a hydroxo or dihydroxo complex solution to a ^{13}C labeled carbon dioxide atmosphere leads to the incorporation of ^{13}C into the (bi)carbonato complexes and a shift of the signals of the bicarbonato and carbonato complexes by one mass unit to *m/z* 958.3274 and *m/z* 980.3072, respectively can be observed (see Table 4.2). The incorporation of ^{13}C is reversible, *e.g.* exposure of a ^{13}C-labeled carbonato complex [$\mathbf{H_2L^4}Cu^{II}_2(\mu\text{-}^{13}CO_3)$] solution to air leads to a slow (~60 min) conversion into the unlabeled complex [$\mathbf{H_2L^4}Cu^{II}_2(\mu\text{-}CO_3)$] and vice versa.

Table 4.2. Observed dinuclear high resolution ESI-MS copper(II) complexes of $\mathbf{H_4L^4}$, their molecular formula and experimental and calculated exact masses.

species	molecular formula	experimental	calculated
$[\mathbf{H_2L^4}Cu^{II}_2(OH)]^+$	$C_{40}H_{59}Cu_2N_{12}O_5^+$	913.3315	913.3318
$[\mathbf{H_2L^4}Cu^{II}_2(\mu\text{-}HCO_3)]^+$	$C_{41}H_{59}Cu_2N_{12}O_7^+$	957.3214	957.3216
$[\mathbf{H_2L^4}Cu^{II}_2(\mu\text{-}CO_3)Na]^+$	$C_{41}H_{58}Cu_2N_{12}O_7Na^+$	979.3045	979.3036
$[\mathbf{H_2L^4}Cu^{II}_2(\mu\text{-}CO_3)n\text{-}Bu_4N]^+$	$C_{57}H_{94}Cu_2N_{13}O_7^+$	1198.5988	1198.5986
$[\mathbf{H_2L^4}Cu^{II}_2(^{18}OH)]^+$	$C_{40}H_{59}Cu_2N_{12}O_4{}^{18}O^+$	915.3363	915.3360
$[\mathbf{H_2L^4}Cu^{II}_2(\mu\text{-}HCO_2{}^{18}O)]^+$	$C_{41}H_{59}Cu_2N_{12}O_6{}^{18}O^+$	959.3264	959.3259
$[\mathbf{H_2L^4}Cu^{II}_2(\mu\text{-}CO_2{}^{18}O)Na]^+$	$C_{41}H_{58}Cu_2N_{12}O_6{}^{18}ONa^+$	981.3086	981.3078
$[\mathbf{H_2L^4}Cu^{II}_2(\mu\text{-}H^{13}CO_3)]^+$	$^{13}CC_{40}H_{59}Cu_2N_{12}O_7^+$	958.3274	958.3250
$[\mathbf{H_2L^4}Cu^{II}_2(\mu\text{-}^{13}CO_3)Na]^+$	$^{13}CC_{40}H_{58}Cu_2N_{12}O_7Na^+$	980.3072	980.3069

The interconversion of the labeled and non-labeled carbonato complexes in presence of $^{12/13}CO_2$ seems to be slower than the exchange of the labeled hydroxide. First indications of the conversion, *i.e.* different isotope pattern in the exact mass spectrum, were observed after 30 minutes. A change of the isotope pattern of the coordinated hydroxide, on the other hand, could be observed within minutes.

The formation of carbonato-bridged complexes was further investigated by addition of $(NH_4)_2CO_3$ to a solution of the dinuclear copper(II) complex $[\mathbf{H_2L^4}Cu^{II}_2]^{2+}$. It was found that addition of ammonium carbonate to a solution of the dinuclear copper(II) complex $[\mathbf{H_2L^4}Cu^{II}_2]^{2+}$ or the hydroxo complex $[\mathbf{H_2L^4}Cu^{II}_2(OH)]^+$ readily leads to the formation of

(bi)carbonato complexes. When naturally abundant carbonate is added to a solution of a ^{13}C labeled carbonato complex a slow exchange can be observed that is not completed within 24 hours. These findings support a moderately stable carbonato complex, where carbonate can be exchanged.

The findings that the carbonato complex is moderately stable and the reversibility of the reaction, *e.g.* labeled carbonate can be exchanged by unlabeled, indicate that this reaction might be catalytic. When an excess (> 6eq) of barium perchlorate is added to solutions of the carbonato complex [$\mathbf{H_2L^4}Cu^{II}_2(\mu\text{-}CO_3)$], barium carbonate precipitates and the UV-vis and CD spectra of the solution are now identical to those of the hydroxo complex. After addition of one or two equivalents of base and exposure to air these solutions convert back to the carbonato complex. Consequently, we tested the catalytic activity of the hydroxo complex towards CO_2 hydrolysis applying the stopped flow indicator method, first reported by Gibbons *et al.*[84, 157] It was found that the hydroxo and dihydroxo complexes of $\mathbf{H_4L^4}$ do not show any significant catalytic activity. Nevertheless, the ready capture and release of CO_2 from the complexes and thus reversibility of the reaction, implies that the metabolic role of cyclic pseudo octapeptides might be related to CO_2 capture and carbonate transport in the *ascidian's* organism.

When the reversibility of the formation of the carbonato complexes was tested, by passing argon through a (bi)carbonato complex solution to remove CO_2 from the equilibrium, an unusual pink species was discovered. It was found that the formation of the pink species can also be followed by CD spectroscopy when a solution of the carbonato complex, *i.e.* [$\mathbf{H_2L^4}Cu^{II}_2(\mu\text{-}CO_3)$], is exposed to air (see Figure 4.13). The initial CD spectrum of the carbonato complex [$\mathbf{H_2L^4}Cu^{II}_2(\mu\text{-}CO_3)$] exhibits two negative Cotton effects at 723 and 541 nm and two positive Cotton effect at 366 and 605 nm. In the course of the reaction, the negative Cotton effect at 723 nm is shifted to 715 nm and increases in intensity, while the negative effect at 541 nm vanishes and instead, a positive Cotton effect at 536 nm develops. The positive cotton effect at 366 nm also increases in intensity over time and is shifted to 358 nm and at 611 nm a new negative cotton effect develops. From the isosbestic points at 451 and 583 nm it emerges that the carbonato complex is converted into a new complex – the observed pink species. The recorded CD spectra suggest that the previously assigned CD spectrum of the carbonato-bridged species with positive Cotton effects at 511 and 603 nm (see Figure 4.12) is actually a superposition of the CD spectra of the carbonato-bridged (pos.

Cotton effect at 605 nm and neg. Cotton effect at 541 nm) and the pink complex (pos. Cotton effect at 536 nm and neg. Cotton effect at 715 nm).

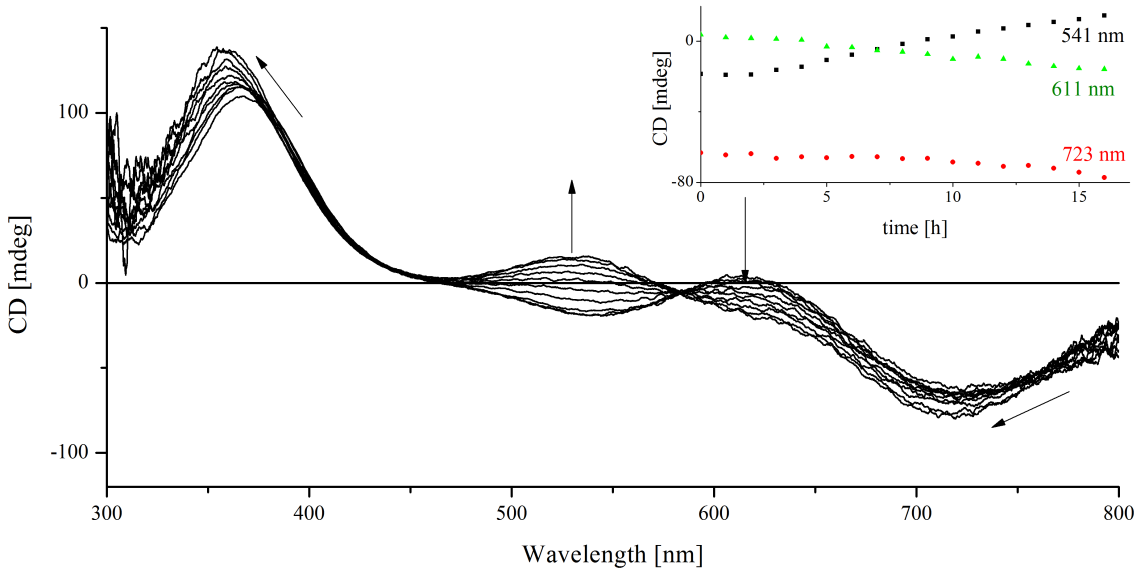

Figure 4.13. Time-dependent CD spectra (0-16h) of a [$\mathbf{H_2L^4}Cu_2^{II}(\mu\text{-}CO_3)$] solution ($c$ = 1.25 mM, methanol) that, upon exposition to air, converts to the pink species. Time dependent increase and decrease of the respective Cotton effects (inlay).

Given that at least 5% water is present in the methanol solution it was found that the pink species can also be created by addition of four or more equivalents of a strong base (MeO^-) under aerobic conditions to the dinuclear copper(II) complex [$\mathbf{H_2L^4}Cu_2^{II}$]$^{2+}$ (see Figure 4.8). Solutions of the pink species do not show any signals of note in the ESI-MS spectra, suggestive of a neutral or manifold negatively (high base concentration) charged species. It is known from the CD, UV-vis, and EPR spectra that both copper(II) ions are still coordinated, otherwise a decrease of the Cotton effects in the CD spectra should be observable, as "free" copper(II) does not exhibit CD spectroscopic features. Furthermore, the EPR spectra do not show any signals that are attributable to "free" copper, instead solutions of the pink species are EPR silent at 77 K, although two equivalents of copper(II) are present in solution. This points to a dinuclear, strongly ferromagnetically coupled species, identified by the ability to record NMR spectra at room temperature. The NMR spectra display the same set of signals as the free cyclic pseudo peptide $\mathbf{H_4L^4}$ (see Appendix G). An EPR at helium temperature, showing a set of signals attributable to a strongly coupled species, verified the pink species as a dinuclear copper(II) species (see Appendix G). To date the exact composition of the pink species could not be determined. From the interconversion of the carbonato to the pink species in combination with the observation that the pink species is only formed in presence

of water, at high base concentrations, and under aerobic conditions, it is assumed that the carbonato complex has to be built first and subsequently converted to the pink species. The strong ferromagnetic coupling indicates the presence of a bridging ligand, for example μ-oxo, though the presence of this ligand has yet to be confirmed.

4.2.3 Computational and EPR Spectroscopic Investigation of the Copper(II) Complexes of H_4L^4

Suitable crystals for X-ray crystallography could not be obtained from any copper(II) complex of **H_4L^4**. Therefore, the structural information about the complexes had to be obtained from computational and spectroscopic methods. From the EPR spectrum of a dipole-dipole coupled dinuclear complex the *g* and *A* tensors of the metal centers can be extracted and from strongly coupled complexes the coupling constant *J* can be obtained. In both cases the relative orientation of the copper(II) centers can be extracted. As the interactions of the metal centers are, among others, dependent on their distance, the simulation of EPR spectra can be used for structure determination. Another frequently used tool for structure determination are computational methods, *e.g.* geometry optimization by DFT (density functional theory). However, the simulation of an EPR spectrum may not have one unique solution and one cannot be sure whether the structure derived from the DFT calculation is a local or the global energy minimum. Therefore, a combination of EPR spectra simulation and structure optimization is used to determine the structure of the investigated compounds. The putative complexes of the complexation equilibria depicted in Figure 4.8 were prepared in situ and EPR spectra of the respective solutions were measured. The simulations of the spectra in combination with DFT calculations were used to gain structural information about the various species.

The analysis of the calculated structures of the mono- and dinuclear copper(II) complexes of **H_4L^4** revealed that, upon coordination of copper(II) to the binding site, the macrocycle is locked into a particular conformation. The distances of copper(II) to the nitrogen atoms of the binding sites are nearly identical in all complexes (see Table 4.4): the copper-N_{het} distances vary from 2.02 to 2.13 Å and the Cu-N_{amide} distances are somewhat smaller and in the range

of 1.89 to 1.97 Å; the copper-copper distance in the complexes varies from 3.5 Å (μ-oxo) to 5.4 Å (carbonato, see Table 4.4).

The EPR spectra of the dinuclear copper(II) complexes of **H_4L^4** were simulated with the program package Molecular Sophe,[123] using the spin Hamiltonian described in Eq. 3.7. In an automated procedure the spin Hamiltonians of the copper(II) centers were optimized and fitted simultaneously to the spectra of the allowed ($\Delta m_S = \pm 1$) and forbidden ($\Delta m_S = \pm 2$) transitions. As result of the optimization algorithm it is possible that derived *g* and *A* tensors of the respective copper(II) centers differ significantly (*e.g.* for $[\mathbf{H_2L^4}Cu_2^{II}]^{2+}$ g_z(Cu1) = 2.376 and g_z(Cu2) = 2.163) as a result of the optimization to a local minimum. From a structural point of view it is unlikely that the coordination geometry of the two sites differs much and the obtained parameters cannot be used for a structural discussion. The distance of the copper(II) centers is reflected in the distance of the perpendicular peaks (~290 to 340 mT); these are accurately reproduced by the simulations of the spectra (see Figure 4.13) and are the following discussion focuses on the derived distances from DFT calculations and EPR simulations.

The spectra and their preliminary simulations are depicted in Figure 4.14. The derived parameters from the simulations are given in Table 4.3. The simulated EPR data of the dinuclear copper(II) complex $[\mathbf{H_2L^4}Cu_2^{II}]^{2+}$ are in good agreement with the DFT calculated structure. From the DFT calculations, a Cu^{II}-Cu^{II} distance of 5.35 Å was derived and the simulation of the EPR spectrum predict a distance of 5.22 Å. In the DFT calculated structure both copper(II) ions have a distorted square pyramidal coordination geometry with minor alterations. This is reflected in the simulated *A* tensors of the complex that are slightly different to each other, yet consistent with a square pyramidal coordination environment ($A_\perp < A_\parallel$, $g_\perp < g_\parallel$) of the complex (see Table 4.3). However, one has to keep in mind, that the derived structural parameters from the EPR simulation are not reliable.

From the combination of the EPR and DFT data it is assumed that in the hydroxo complex the hydroxide is most likely bound in a terminal fashion, although, a good agreement between calculated structure and EPR predicted structure could not be obtained so far. The EPR simulations predict a distance of 4.47 Å for the copper(II) centers. While from the DFT calculations of the hydroxo-bridged and terminal hydroxo complex distances of 3.97 and 5.02 Å were derived (see Table 4.4 and Figure 4.15, left).

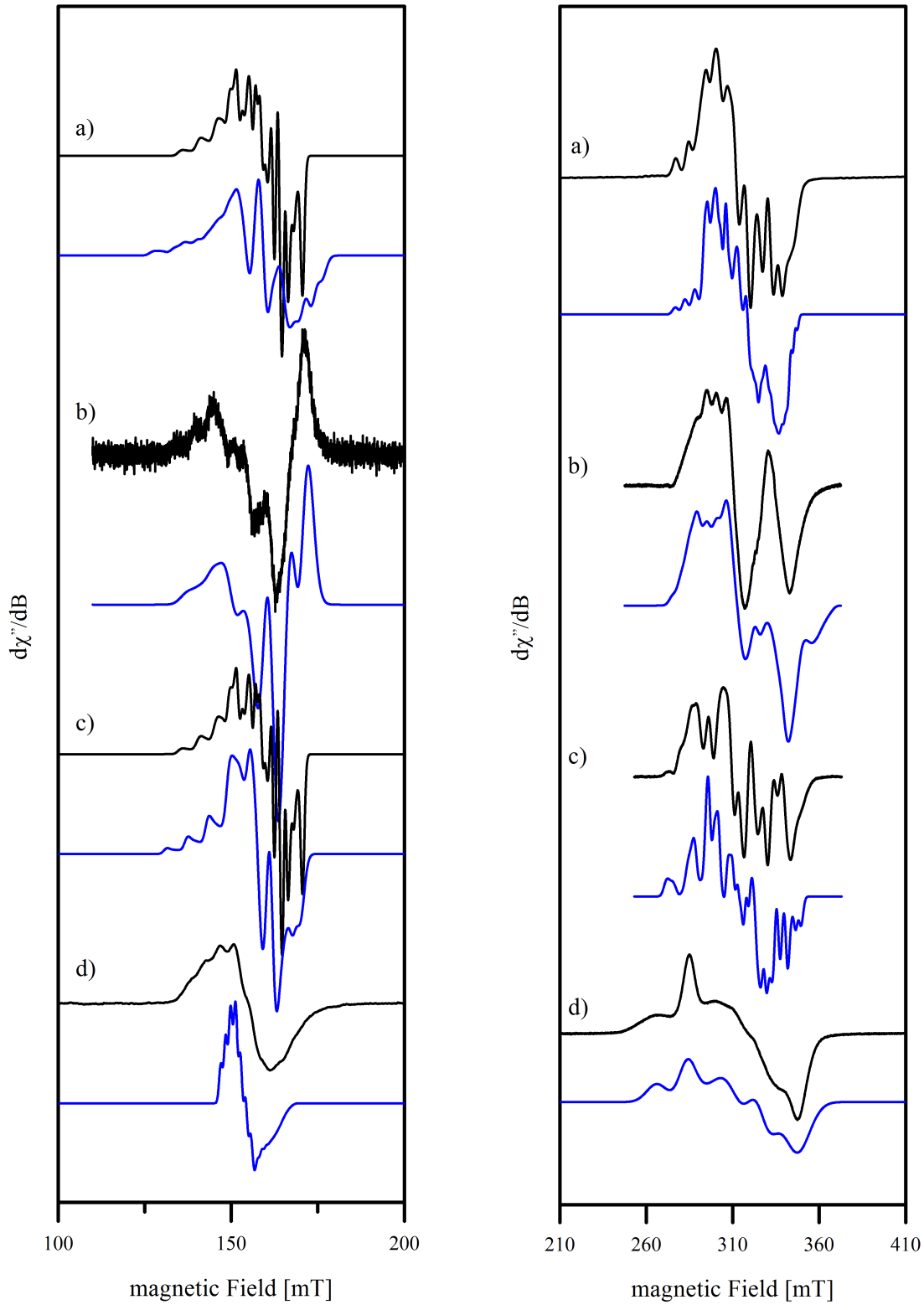

Figure 4.14. Experimental (black) and simulated (blue, dotted) EPR spectra of the dinuclear copper(II) complexes of $\mathbf{H_4L^4}$ and of the carbonato-bridged complex of ascidiacyclamide (turquoise), methanol, T = 50 K, formally forbidden $\Delta m_S = \pm 2$ (left) and allowed $\Delta m_S = \pm 1$ transitions (right): **a)** $[\mathbf{H_2L^4}Cu_2^{II}]^{2+}$ ν = 9.3752 GHz; **b)** $[\mathbf{H_2L^4}Cu_2^{II}(OH)]^{+}$ ν = 9.3748 GHz; **c)** $[\mathbf{H_2L^4}Cu_2^{II}(OH)_2]$ ν = 9.3736 GHz; **d)** $[\mathbf{H_2L^4}Cu_2^{II}(\mu\text{-}CO_3)]$ ν = 9.3769 GHz

Table 4.3. Anisoptropic EPR spin Hamiltonian parameters of the dinuclear copper(II) complexes of $\mathbf{H_4L^4}$ (see Appendix H for line width parameters and angles).

Parameters **Cu 1 /Cu 2**	$[\mathbf{H_2L^4}Cu_2^{II}]^{2+}$		$[\mathbf{H_2L^4}Cu_2^{II}(OH)]^{+}$		$[\mathbf{H_2L^4}Cu_2^{II}(OH)_2]$		$[\mathbf{H_2L^4}Cu_2^{II}(CO_3)]$	
g_x	2.050	2.08	2.086	2.052	2.064	2.064	2.022	2.021
g_y	2.090	2.10	2.073	2.075	2.109	2.1077	2.192	2.191
g_z	2.200	2.15	2.176	2.175	2.192	2.192	2.192	2.193
A_x	20	30	42	29	5	68	46	9
A_y	30	50	54	80	123	12	46	48
A_z	155	140	48	160	130	134	111	93
$J^{a)}$	-20		-20		-20		-20	
d (Cu-Cu)	5.22		4.47		4.53		4.23	

Units: d [Å], A [$10^{-4}cm^{-1}$], J [cm^{-1}]; a) $H = J\,S_1 \cdot S_2$.

It was found that the geometry and the copper-copper distance in the DFT calculated structures strongly depends on the number of coligands (such as methanol, water) that are co-ordinated to the copper(II) centers (see Table 4.4 for selected distances). A bridging hydroxide was only obtained when no or two coligands were present at the copper(II) centers. With more than two water molecules as coligands or with methanol molecules as coligands, the structure always converted to a terminal hydroxo complex. Thus, it is assumed that in solution a terminal hydroxo complex is formed (see in Figure 4.15, left). In the bridged complex, the oxygen of the hydroxide is equidistant to both copper(II) ions (2.0 Å) and the adopted symmetry is high.

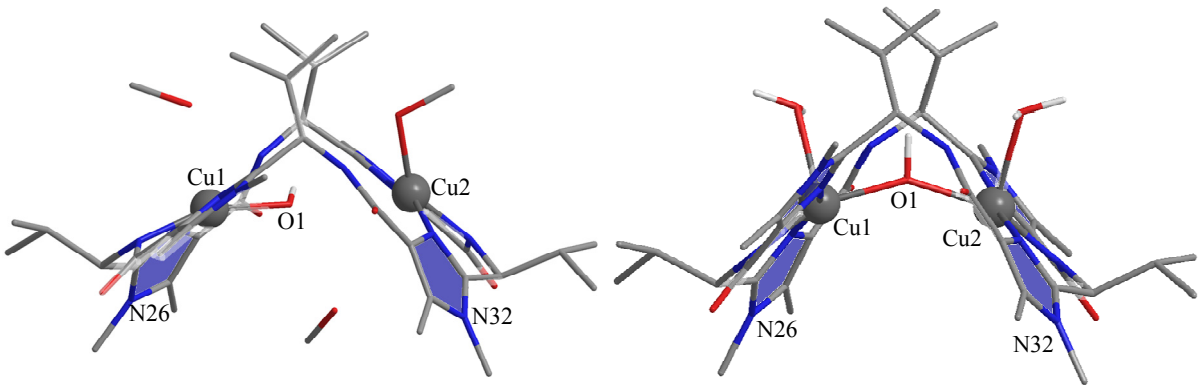

Figure 4.15. Side views of the DFT calculated structures of the terminal hydroxo (left) and hydroxo-bridged (right) complex of $\mathbf{H_4L^4}$.

Table 4.4. Structural parameters of the dinuclear copper(II) complexes of $\mathbf{H_4L^4}$ derived from DFT calculations and from the simulation of the EPR spectra.

	Cu1/2-N_{het}	Cu1/2-N_{amide}	Cu1/2-N_{het}	Cu1-Cu2	Cu1-Cu2 (EPR)	N_{het}-N_{het} consecutive	N_{amide}-N_{amide} trans-disposed	Cu1/2-O1	∠ [Cu1-O1-Cu2]
$\mathbf{H_4L^4}$	-	-	-	-	-	5.28	7.93	-	-
$[\mathbf{H_2L^4}Cu_2^{II}(MeOH)_4]^{2+}$	2.02	1.90	2.05	5.35	5.22	4.11*)/5.91	9.14*)/5.70	-	-
$[\mathbf{H_2L^4}Cu_2^{II}(\mu\text{-}OH)(H_2O)_2]^{+}$	2.07	1.92	2.13	3.97		4.1*)/4.8	7.2*)/5.5	2.0	147
$[\mathbf{H_2L^4}Cu_2^{II}(\mu\text{-}OH)(MeOH)_2]^{+}$	2.03	1.93	2.04	5.47	4.47	4.01*)/5.64	9.14*)/5.65	3.82	115
$[\mathbf{H_2L^4}Cu_2^{II}(OH)(H_2O)_3]^{+}$	2.10	1.95	2.05	5.26		4.06*)/5.60	9.09/5.64	1.90/3.51	164
$[\mathbf{H_2L^4}Cu_2^{II}(OH)(MeOH)_3]^{+}$	2.07	1.95	2.04	5.02		4.1*)/5.6	9.08*)/5.5	1.93	163
$[\mathbf{H_2L^4}Cu_2^{II}(\mu\text{-}O)(H_2O)_2]$	2.05	1.97	2.12	3.53		4.1*)/4.6	7.03*)/5.27	1.87	140
$[\mathbf{H_2L^4}Cu_2^{II}(OH)_2(MeOH)_2]$	2.06	1.93	2.14/2.23	5.31	4.53	4.0*)/5.9	9.02*)/5.8	1.92	-
$[\mathbf{H_2L^4}Cu_2^{II}(OH)_2(MeOH)_2]$ a)	2.13	1.96	2.16	5.43		4.2*)/5.7	8.83*)/5.9	1.92	-
$[\mathbf{H_2L^4}Cu_2^{II}(\mu\text{-}CO_3H)(H_2O)_2]^{+}$	2.03	1.89	2.07/2.24	5.40	-	4.20*)/5.87	9.13*)/5.87	-	-
$[\mathbf{H_2L^4}Cu_2^{II}(\mu\text{-}CO_3)(H_2O)_2]$	2.05	1.94	2.22/2.84	5.11	4.23	4.27*)/5.88	8.88*)/6.24	-	-

Units: d [Å], ∠ [°]; a) alternative conformation, both OH groups on top side (see Appendix I for visualization); *) at copper(II) bound site.

Similar considerations led to the assumption that rather a dihydroxo than a μ-oxo complex is formed in solutions with four equivalents of base.[103] The predicted copper-copper distance from the EPR simulation is neither consistent with the calculated distance in a μ-oxo nor with that in a dihydroxo complex (see Table 4.4). Both distances are approximately one angstrom apart from the distance predicted by the EPR spectra simulation.

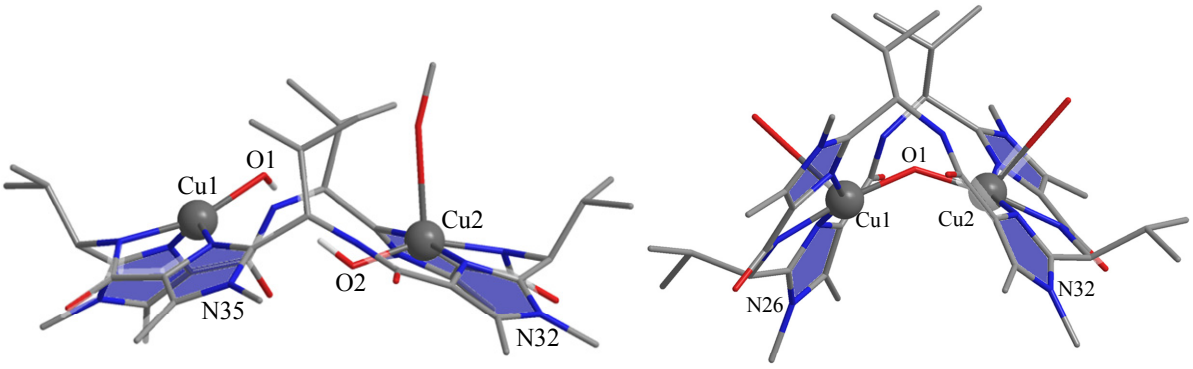

Figure 4.16. DFT calculated structures of the dihydroxo (left) and the μ-oxo complex (right) of $\mathbf{H_4L^4}$.

Two conformations of the dihydroxo complex were derived from the calculations. In the first conformation (see Figure 4.16 left) one hydroxide is on the up side and the other hydroxide faces the down side of the macrocycle. In the second conformation both hydroxide molecules are on the up side (see Appendix I). With respect to the conformation of the macrocycle and the copper(II) copper(II) distance the structures are alike (see Table 4.4). There is a small variation in the copper-copper distance of 0.12 Å (5.31 Å (up/down) *vs.* 5.43 Å (both up)) and thus in the distance of the N_{amide} atoms of the binding site. When these structures are compared to the structure of the μ-oxo complex it can be seen that the conformation adopted by the macrocycle is substantially different. This is reflected in the distance of the coordinating N_{amide} atoms. In the dihydroxo complex they are 9.08 Å apart while their distance in the μ-oxo complex is only 7.03 Å. From the experiments it is known that the complex at four equivalents of base is readily formed. Considering the steric strain that it put on the system by the formation of a μ-oxo complex it emerges that a dihydroxo complex has to be present in the solutions. Whether an up/down or a up/up configuration of the hydroxides in the dihydroxo complex is adopted cannot be distinguished.

A large deviation between calculated and EPR derived structure was also found for the carbonato-bridged complex [$\mathbf{H_2L^4}Cu^{II}_2(\mu\text{-}CO_3)$]. The overall shape of the EPR spectra of the carbonato-bridged complex of $\mathbf{H_4L^4}$ and the carbonato-bridged complex of ascidiacyclamide

is alike, indicating a similar coordination geometry.[71] However, the *g* and *A* tensors of the copper(II) centers are quite different (see Table 4.5) and this suggests that the adopted structures and potentially also the coordination mode of carbonate is different, but might also arise from different electronics caused by the oxazoline and thiazole heterocycles. The different conformations of the macrocycles can be seen by comparing the DFT calculated structure of the carbonato complex of **H_4L^4** to the X-ray structure of the carbonato complex of ascidiacyclamide (see Figure 4.17).

Table 4.5. Anisoptropic EPR spin Hamiltonian parameters of the carbonato-bridged complexes of **H_4L^4** and ascidiacyclamide.[71]

	$g_\perp$	$g_\parallel$	$A_\perp$ [a)]	$A_\parallel$ [a)]	Cu1-Cu2[)]
$[\mathbf{H_2L^4}Cu_2^{II}(\mu\text{-}CO_3)]$	2.02/2.19	2.19	45/28	111/93	4.23
$[\mathbf{H_2L^{asc}}Cu_2^{II}(\mu\text{-}CO_3)]$ [*)]	2.10	2.31	70	111	3.9

Units: A [10^{-4} cm^{-1}]; distance in Å; *) two equivalent copper(II) atoms.[71]

One has to keep in mind that the calculated carbonato complex might not be the global minimum. While ascidiacyclamide adopts a conformation where trans-disposed amino acid residues face towards one another, the distance between the trans-disposed isopropyl residues in **H_4L^4** is large. In addition, the orientation of the heterocycles with respect to each other is strikingly different in the two complexes. While the imidazole rings in **H_4L^4** adopt the known cone like structure where all N_{het} face the up side and all N_{imi} face the down side the folding of ascidiacyclamide causes the N_{het} atoms to be oriented in the plane of the binding site or slightly towards the downside. The oxygen and sulfur atoms that correspond to the N_{imi} atoms of **H_4L^4** face different directions and are either located in the plane of the binding site or on the up side.

The combination of the DFT calculations and EPR simulations did not yet provide a satisfying answer about the geometry of the complexes. As DFT calculations of dicopper(II) complexes of cyclic pseudo peptides are quite time consuming and an investigation of different conformations is only possible at high computational cost, molecular mechanics (MM) calculations were used for a further insight into the conformations that might be adopted by a cyclic pseudo peptides.

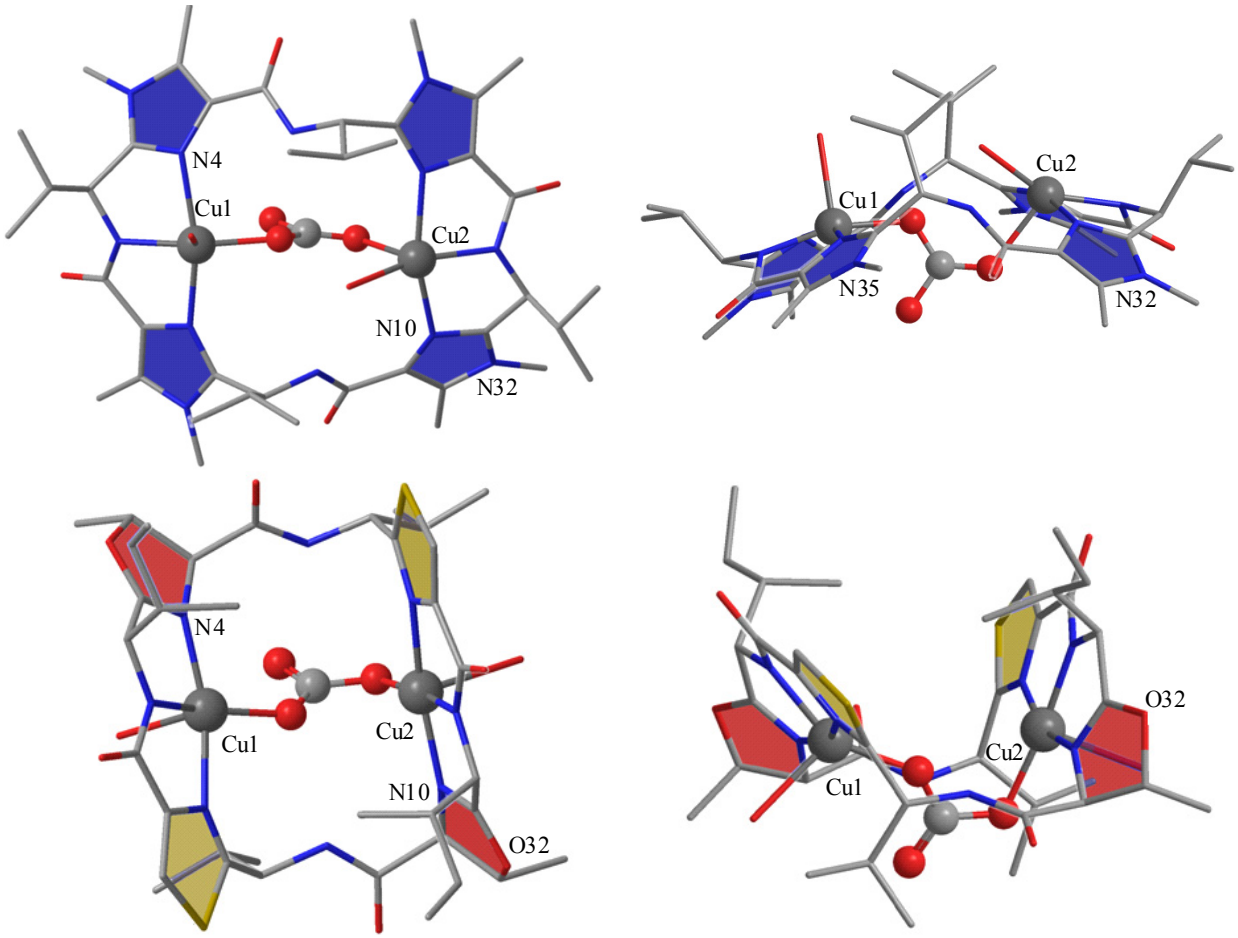

Figure 4.17. Top (left) and side view (right)of the DFT calculated (G03, B3LYP/6-31g*) structure of the carbonato-bridged complex of $\mathbf{H_4L^4}$ [$\mathbf{H_2L^4}Cu_2^{II}(\mu\text{-}CO_3)$] (top) and of the X-ray structure of the carbonato-bridged copper(II) complex of ascidiacyclamide [$\mathbf{H_2L^{asc}}Cu_2^{II}(\mu\text{-}CO_3)$] (bottom).

4.2.4 Molecular Mechanics Investigation of $[\mathbf{H_2L^4}Cu_2^{II}(H_2O)_4]^{2+}$ and $[\mathbf{H_2L^4}Cu_2^{II}(\mu\text{-}CO_3)]$

DFT calculations, where different coordination modes of the bridging carbonate were chosen as starting points all converged to the structure shown above (see Figure 4.17). Thus, the DFT calculations suggest that a coordination mode of carbonate that shortens the copper(II)-copper(II) distance can be excluded. The possible conformations that can be adopted from the dinuclear copper(II) complex of $\mathbf{H_4L^4}$ [$\mathbf{H_2L^4}Cu_2^{II}(H_2O)_4]^{2+}$ were investigated by means of MM and DFT calculations.

Table 4.6. Structural parameters of the conformations of $[\mathbf{H_2L^4}Cu_2^{II}(H_2O)_4]^{2+}$ calculated with molecular mechanics and DFT-methods, respectively.

	U-shape		**V-shape**		**3up-1down**		**2up-2down**		$\mathbf{[H_2L^4Cu_2(H_2O)_3]^{2+}}$ **V-shape**
	MM *vs* DFT* (2 H_2O dissociated)		**MM *vs* DFT* (1 H_2O dissociated)**		**MM *vs* DFT***		**MM *vs* DFT* (2 H_2O dissociated)**		**DFT***
Cu1-Cu2	3.63	5.64	5.56	5.83	5.59	5.63	5.60	5.30	5.4Å
d ($N_{amide}N_{amide}$) coordinated	4.09	8.17	8.95	9.03	9.22	7.51	8.82	8.95	7,9Å
d ($N_{amide}N_{amide}$) non coordinated	4.99	5.43	5.74	5.86	5.79	6.70	6.38	6.73	6.3Å
∠ [N_{het}-C_{alpha} N_{het}]	58/59	98/98	99/107	105/102	113/114	113/114[a)]	101/102	105/108	92°/100°
∠ [N_{het} C_{alpha} $N_{im(cu)}$]	68	71/71	67/67	67/73	67/76	72/72	67	72	70/76
ρ angle between binding sites	9	-	126		2	124	3	85	

Units: d [Å], ∠ [°]; a) at flipped C_α; *) Jaguar 6.5[158] B3LYP/LACVP[159].

The calculations were performed using the program package Maestro[160] and a modified Amber force field.[161-162] No electrostatic interactions or partial charges were considered. For the conformational search, a 100 ps molecular dynamics (MD) simulation was performed at a range of different temperatures (300 K to 800 K). The MD simulation of the dinuclear copper(II) complex $[\mathbf{H_2L^4}Cu^{II}_2(H_2O)_4]^{2+}$, followed by a multiple minimization of the obtained structures revealed four different conformers: u-shape, v-shape, 3up-1down, and 2up-2down (see Figure 4.18).

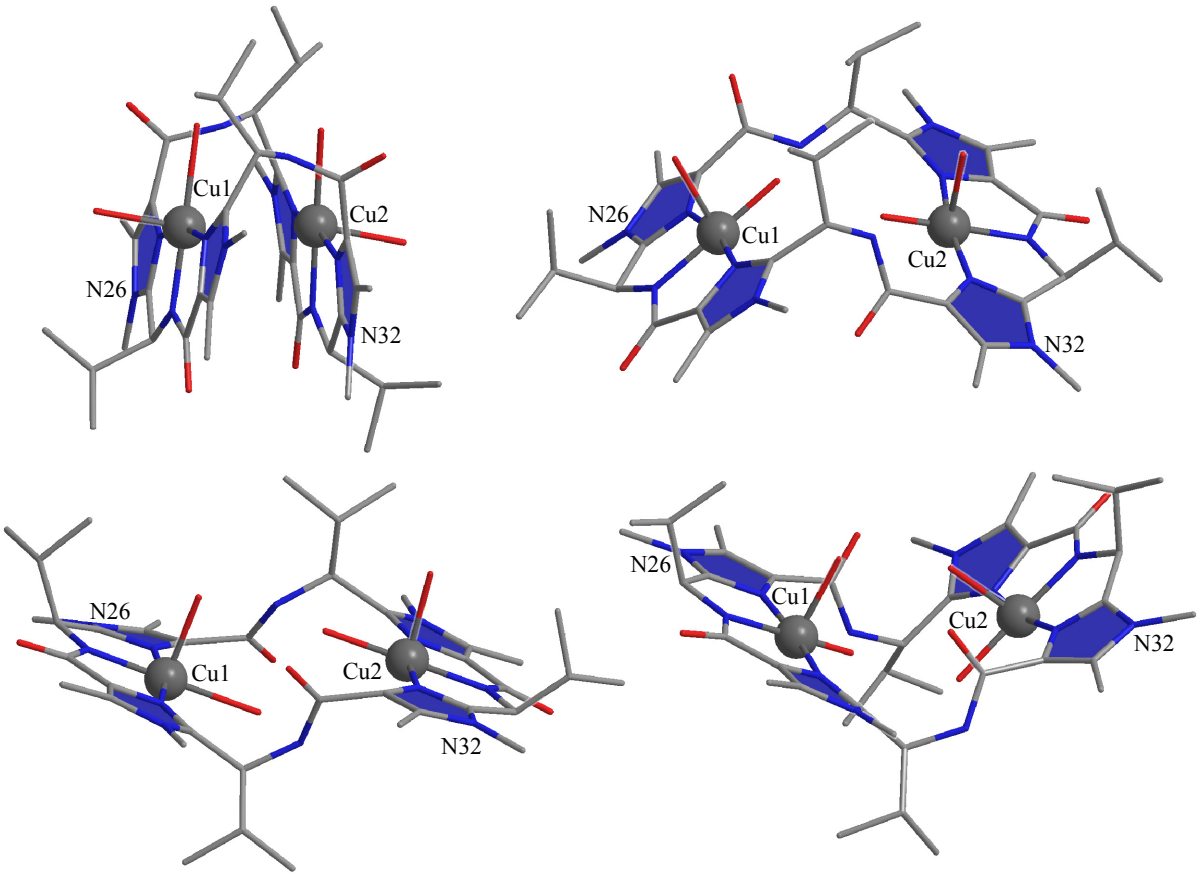

Figure 4.18. Conformations of $[\mathbf{H_2L^4}Cu^{II}_2(H_2O)_4]^{2+}$. U-shape (top left), v-shape (top right), 3up-1down (bottom left) and 2up-2down (bottom right).

The nomenclature of the conformers of $[\mathbf{H_2L^4}Cu^{II}_2(H_2O)_4]^{2+}$ refers to the shape of the macrocyclic backbone (u-shape and v-shape) and to the orientation of the valine residues on different sides of the macrocyle (3up-1down and 2up-2down), respectively. In the u- and the v-shaped structures (top left and top right structures in Figure 4.18) the orientation of the valine residues is equivalent to that of the X-ray structure of $\mathbf{H_4L^4}$ (see Figure 4.4).

The considerable difference in folding of the predicted conformations is caused by a variation of the dihedral angle ω of the C_{azole}-C_α-N_{amide}-C_{amide} bonds in the valine linkers that are not part of the binding sites. The angle ω changes from 90° and 92° in the u-shape form to 42° and 172° in the v-shaped conformation. The 3up-1down and 2up-2down conformations even show a further modification along these bonds and as a consequence of the rotation of the C_α-N_{amide} and the amide bond, the valine residues are flipped from the up to the down side of the ring. However, it is worth noting that this flip does not alter the stereochemistry at C_α. Nevertheless, the orientation of the valine residues in the 2up-2down conformation is very similar to the orientation of the amino acid residues in ascidiacyclamide and $\mathbf{H_4L^{rs}}$, although the stereochemistry at C_α in these macrocycles is different. The different conformations seem to solely be a result of the flexibility of the non-coordinated linkers.

The conformations of the dinuclear copper(II) complex $[\mathbf{H_2L^4}Cu^{II}_2(H_2O)_4]^{2+}$, obtained from the MD simulations were further investigated in order to determine how much energy is needed to change the folding of the cyclic peptides, and whether these conformations are also accessible in the metal free cyclic pseudo octapeptide. Therefore, the metal free conformations v-shape, u-shape, 3up1down, and 2up2down were DFT-optimized and a frequency analysis was performed on the macrocyclic conformation thus obtained (see Figure 4.19). Interestingly, the u-shape conformation, although closer to the conformation of the natural cyclic pseudo peptide ascidiacyclamide, could not be optimized to a minimum, but instead relaxed back to the v-shape conformation, which was also present in the X-ray structure of $\mathbf{H_4L^4}$. This emphasizes the influence of the configuration at C_α on the adopted conformation of the macrocycle. The v-shaped structure is lowest in energy and the 3up-1down and 2up-2down conformations are 56 and 116 kJ/mol, respectively, higher in energy indicating an energy increase of ~60 kJ/mol per flipped isopropyl residue.

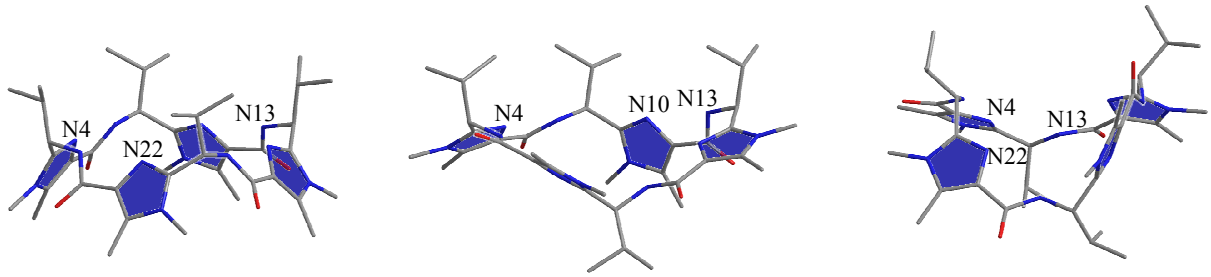

Figure 4.19. Structures of the DFT optimized metal free conformations of $\mathbf{H_4L^4}$. From left to right: v-shape, 3up-1down and 2up-2down conformation.

It is known that the electronic interactions between the $\pi/\pi*$ (C_{azole}-N_{het})-orbital of the heterocycles and the $\sigma*/\sigma$ orbital of the linker substantially influence the adopted conformation of the macrocycles (see Chapter 1.3). In the structures, obtained from the MD simulations the dihedral angles χ in the linkers are not always at their global minimum (see Chapter 1.3, Figure 1.5). Hence, the structures obtained from the MM calculations were reoptimized by DFT methods. Upon DFT optimization of the conformations, the amide bonds are rotated in a way, that the oxygen atoms face towards the outside and are now at their energetical minimum. Futhermore, it was found that the MM calculations predict the imidazole rings of the binding site to be too planar, *e.g.* they are nearly coplanar with the plane of the binding site itself, whereas the DFT calculations show that in general at least one heterocyclic ring is twisted. A summary of selected distances and angles of the molecular mechanics and the DFT calculations is given in Table 4.6.

The observed reorganization of the metal free u-shape structure to the v-shape conformer was also observed in case of the dinuclear copper(II) complex $[\mathbf{H_2L^4}Cu^{II}_2(H_2O)_4]^{2+}$. This reorganization is not unexpected as the conformation of the linker derived from the MD simulations puts substantial strain on the system. From the structural investigation of patellamides it is known that the inclusion of a solvent sphere can be crucial to stabilize different conformations.[75] Nevertheless DFT calculations applying a solvation model (Gaussian 09,[163] PCM[164]) provided identical structures and distances to those derived from the gas phase calculations suggesting that the u-shape conformation is not important for the coordination chemistry of $\mathbf{H_4L^4}$ in solution.

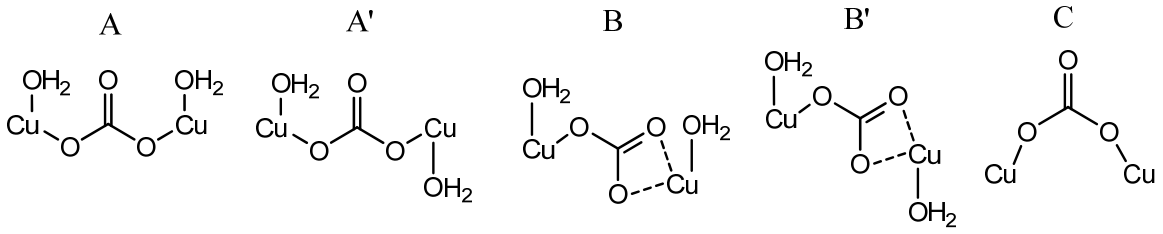

Figure 4.20. Coordination modes of the bridging carbonate ion considered in the MD simulations.

However, as the u-shaped conformation was found to have the closest copper-copper distance (3.6 Å) to the one derived from the simulation of the EPR spectrum of the carbonato complex $[\mathbf{H_2L^4}Cu^{II}_2(\mu\text{-}CO_3)]$ so far, this structure was chosen as a starting point for the further

investigation of the carbonato complexes, given that it might provide insight into a conformation with the desired copper-copper distance of ~ 4.2 Å.

To test the influence of the bridging carbonate ion on the possible conformations, the derived conformations from the molecular dynamics simulations of the dinuclear copper complex $[\mathbf{H_2L^4}Cu_2^{II}]^{2+}$ were manually bridged by a carbonate ion and subsequently a conformational search was performed. Three different coordination modes of the carbonate ion were considered (A, B, and C, see Figure 4.20). For the bridging modes A and B, two different orientations of the water coligands were investigated (A' and B').

Table 4.7. Coordination modes and respective copper-copper distances for the different conformations of $\mathbf{H_4L^4}$, optimized with DFT methods (Jaguar 6.5, B3LYP/LACVP)

	A	**A'**	**B**	**B'**	**C**
U-shape	No stable conformation found				
V-shape	5.20	-	4.95	-	Not converged
3up-1down	-	-	5.30	5.30	
2up-2down	5.18	5.18	5.22	4.91	

According to the MD simulations, the different conformations of the cyclic pseudo peptides prefer different carbonate coordination modes. A summary of the observed conformations for the different binding modes is given in Table 4.7. The u-shape conformation did not converge to a minimum with any of the considered bridging modes, but it was found to reorganize to the v-shape conformer. This behavior has also been observed for the dinuclear copper(II) complex where the u-shape conformation could not be converged to a minimum (see Table 4.6). It seems that the u-shape conformer is not important for the coordination chemistry of $\mathbf{H_4L^4}$ and probably just an artifact of the parameterization of the force field.

Coordination mode C, where the carbonate is not located in the plane of the copper(II) centers, could not be converged to a minimum with any of the conformations. Therefore, it is assumed that the bridging mode of carbonate is either A or B. The question, why the derived distances from the EPR experiment and the DFT calculations are so different remains. Although various conformations were tested it was not possible to obtain a structure where the copper(II) centers are as close as predicted from the EPR experiment. So far the smallest

copper-copper distance (4.91 Å) is obtained for the 2up-2down conformation with a B' bridging mode. Within the computational accuracy this distance can be considered as equal to the distance of 4.95 Å obtained from the v-shape configuration with a B bridging mode. Considering the high rotation barrier for a flip of the isopropyl residues (see Chapter 4.2.4) it is likely that the v-shape conformation is the only conformation present in solution.

The presented results show that, although highly simplified, $\mathbf{H_4L^4}$ is a useful model system for the natural occurring cyclic pseudo octapeptides. It is, as its natural analoga, highly preorganized, shows a cooperative effect and reacts with atmospheric CO_2 to the respective carbonato-bridged species. However, it is not expected that the conformation adopted by the copper(II) complexes of $\mathbf{H_4L^4}$ is identical to that of the natural peptides, as these are more flexible as a result of an alternating stereochemistry in the linkers and the incorporation of oxazoline rings. Furthermore, the formation of a pink species was observed, which could not yet be fully characterized. The pink species is known to be strongly ferromagnetically coupled. Such a species has not been reported for the natural cyclic peptides, but it is possible that it has not been observed. One advantage of $\mathbf{H_4L^4}$ is its, compared to the natural peptides, easy synthesis and availability.

4.3 Copper(II) Coordination Chemistry of H_4L^{rs}

4.3.1 ESI-MS Experiments

The alternating configuration of the C_α carbon atoms in $\mathbf{H_4L^{rs}}$ is identical to the configuration in the patellamides and ascidiacyclamide and should enable the investigation of the influence of the linkers' stereochemistry. In contrast to the *C*$_4$-symmetrical macrocycle $\mathbf{H_4L^4}$, $\mathbf{H_4L^{rs}}$ has two enantiomeric binding sites. Copper(II) can either be coordinated to a N_{het}-$N_{S\text{-amide}}$-N_{het} or a N_{het}-$N_{R\text{-amide}}$-N_{het} binding site (see Figure 4.21 and Section 4.1.1 for a structural discussion). The experimental findings, especially the absence of Cotton effects in the CD spectra (see Section 4.3.2) suggest that neither of the binding sites is favored. This is verified by a racemic crystal of the hydroxo-bridged cation $[\mathbf{H_2L^{rs}}Cu^{II}_2(\mu\text{-OH})(H_2O)_2]^+$ (see Section 4.3.4). The DFT calculations of the two conformers of the monomeric copper(II) complex $[\mathbf{H_3L^{rs}}Cu^{II}(H_2O)_2]^{2+}$, where copper(II) is bound to the different binding modes, suggest that the coordination of copper(II) in the N_{het}-$N_{S\text{-amide}}$-N_{het} motif is favored by 6 kJ/mol, *i.e.* within in the accuracy of the DFT method the structures can be considered as degenerate.

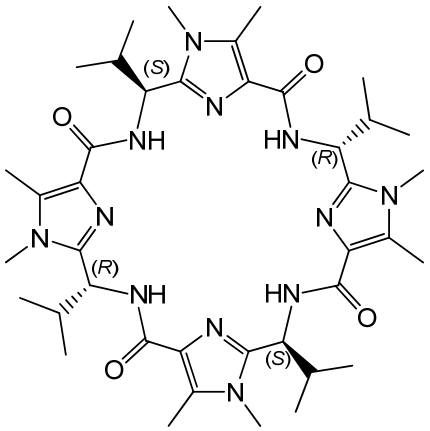

$\mathbf{H_4L^{rs}}$

Figure 4.21. Chemical structure of $\mathbf{H_4L^{rs}}$.

The performed ESI-MS experiments revealed that the copper(II) coordination chemistry of $\mathbf{H_4L^{rs}}$ differs from the one of $\mathbf{H_4L^4}$. The ESI-MS spectra of the *C*$_4$-symmetric pseudo octapeptide $\mathbf{H_4L^4}$ (see Section 4.2) with varying equivalents of copper(II) and base have concise peaks, that are consistent with the successive interconversion of the initial

mononuclear complex $[\mathbf{H_3L^4}Cu^{II}]^+$ to the dinuclear and then to bridged dinuclear copper(II) complexes. Addition of four equivalents of base to a $\mathbf{H_4L^4}$/copper(II) (1:2) solution leads to the formation of the neutral dihydroxo complex $[\mathbf{H_2L^4}Cu^{II}_2(OH)_2]$ (not detectible in ESI-MS experiments) and solutions of $\mathbf{H_4L^4}$ with a macrocycle/copper(II)/base ratio of 1:2:3 or higher show a time-dependent conversion of the (di)hydroxo species to the carbonato-bridged species $[\mathbf{H_2L^4}Cu^{II}_2(\mu\text{-}CO_3)]$ (see complexation equilibria of $\mathbf{H_4L^4}$ in Figure 4.8). The copper(II) coordination chemistry of $\mathbf{H_4L^{rs}}$ is different. A summary of representative species, present in methanolic solutions of different ratios of $\mathbf{H_4L^{rs}}$/copper(II)/base is given in Table 4.8.

Table 4.8. Observed high resolution ESI-MS signals of the mono- and dinuclear copper(II) complexes of $\mathbf{H_4L^{rs}}$, their molecular formula, experimental and calculated exact masses.

species	molecular formula	experimental	calculated
$[\mathbf{H_5L^{rs}}]^+$	$C_{40}H_{61}N_{12}O_4^+$	773.4936	773.4932
$[\mathbf{H_4L^{rs}}Na]^+$	$C_{40}H_{60}N_{12}O_4Na^+$	795.4757	795.4752
$[\mathbf{H_3L^{rs}}Cu^{II}]^+$	$C_{40}H_{59}CuN_{12}O_4^+$	834.4081	834.4073
$[\mathbf{H_3L^{rs}}Cu^{II}(H_2O)]^+$	$C_{40}H_{61}CuN_{12}O_5^+$	852.4189	852.4178
$[\mathbf{H_2L^{rs}}Cu^{II}(H_2O)Na]^+$	$C_{40}H_{60}CuN_{12}O_5Na^+$	874.4010	874.3997
$[\mathbf{H_2L^{rs}}Cu^{II}_2(OH)]^+$	$C_{40}H_{59}Cu_2N_{12}O_5^+$	913.3315	913.3318

The analysis of the ESI-MS signals from the copper(II) complexes of $\mathbf{H_4L^{rs}}$ indicates that this macrocycle has a higher preference or preorganization for the formation of a dinuclear hydroxo complex $[\mathbf{H_2L^{rs}}Cu^{II}_2(OH)]^+$ than $\mathbf{H_4L^4}$:

Signals assigned to the dinuclear hydroxo complex $[\mathbf{H_2L^{rs}}Cu^{II}_2(OH)]^+$ at *m/z* 913.3318 could even be observed in the absence of base at a macrocycle/copper(II) ratio of 1:1. In the absence of base, when the copper(II) concentration is increased above one equivalent, a decrease of the signal intensity of the hydroxo complex $[\mathbf{H_2L^{rs}}Cu^{II}_2(OH)]^+$ can be observed while that intensity of the mononuclear complex $[\mathbf{H_3L^{rs}}Cu^{II}]^+$ at *m/z* 834.4081 increases. At a first glance this seems to contradict the idea that the dinuclear copper(II) complexes of $\mathbf{H_4L^{rs}}$ are preferred over the mononuclear. Nevertheless, one has to keep in mind that for each

coordinated copper(II) in the N_{het}-N_{amide}-N_{het} binding site one amide nitrogen is deprotonated and accordingly a proton released. This proton is subsequently able to protonate a free $\mathbf{H_4L^{rs}}$ molecule or a copper(II) complex, changing the equilibrium and withdrawing the protonated macrocycle's ability to coordinate copper(II). The fact that addition of base immediately increases the amount of dinuclear hydroxo complex $[\mathbf{H_2L^{rs}}Cu^{II}_2(OH)]^+$ present in solution reflects the preference of $\mathbf{H_4L^{rs}}$ for the formation of dinuclear copper(II) complexes. At a $\mathbf{H_4L^{rs}}$/copper(II)/base ratio of 1:2:3 the dominant signal was assigned to the hydroxo complex $[\mathbf{H_2L^{rs}}Cu^{II}_2(OH)]^+$ (*m/z* 913.3318) and the spectra were unaffected by addition of further base.

The disappearance of signals, due to the formation of a neutral species as well as a time-dependent conversion of the hydroxo complex $[\mathbf{H_2L^{rs}}Cu^{II}_2(OH)]^+$ to a carbonato-bridged complex, could not be observed for $\mathbf{H_4L^{rs}}$. A further difference to the coordination chemistry of $\mathbf{H_4L^4}$ is that the addition of carbonate to the copper(II) complex solutions of $\mathbf{H_4L^{rs}}$ does not lead to the formation of carbonato-bridged complexes. Instead, the added carbonate acts as a base and the obtained spectra are comparable to those measured at higher base concentrations. From these experiments the following complexation equilibrium is assumed (see Figure 4.22).

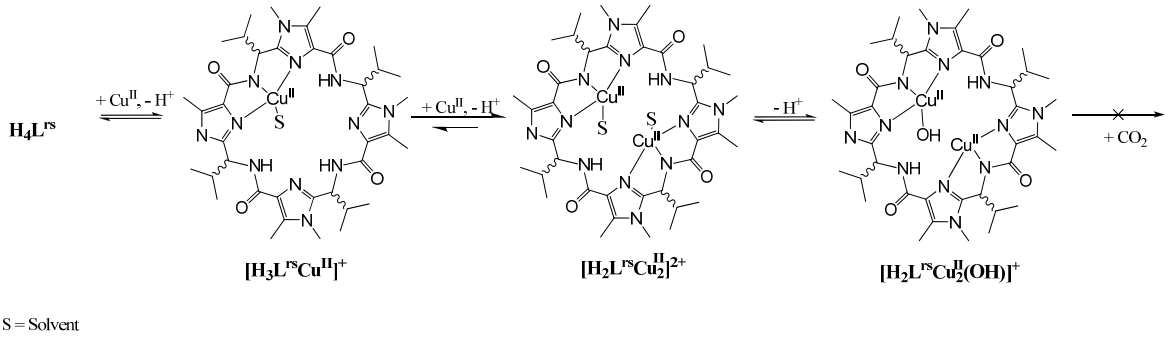

Figure 4.22. Assumed copper(II) complexation equilibria of $\mathbf{H_4L^{rs}}$ (solvent = methanol).

Addition of copper(II) to a solution of $\mathbf{H_4L^{rs}}$ leads to the formation of the mononuclear copper(II) complex $[\mathbf{H_3L^{rs}}Cu^{II}]^+$ that immediately is converted to the dinuclear copper(II) complex $[\mathbf{H_2L^{rs}}Cu^{II}_2]^{2+}$. However, the formation of the complexes releases protons that acidify the solution and thus, in absence of base an equilibrium between the mono- and the dinuclear complex is observed. A complete conversion to the dinuclear complex can only be observed when the released protons are absorbed by added base. Addition of three equivalents of base shifts the equilibrium to the hydroxo complex $[\mathbf{H_2L^{rs}}Cu^{II}_2(OH)]^+$. A reaction of the the di-

nuclear complexes with atmospheric CO_2 or the formation of a carbonato complex upon addition of carbonate to the solutions could not be observed.

4.3.2 Spectroscopic Investigation of H_4L^{rs}

In contrast to the copper(II) complexes of $\mathbf{H_4L^4}$, the analogous copper(II) complexes of $\mathbf{H_4L^{rs}}$ do not exhibit any CD-spectroscopic features of note as the Cotton effects of enantiomeric compounds have reverse signs and thus are cancelled when the two forms of the complex are formed with similar probability (see Figure 4.29 for the DFT calculated structures of the two enantiomers of the mononuclear complex). UV-vis spectroscopy, however, is insensitive to chirality and provides further insight into the copper(II) coordination chemistry of $\mathbf{H_4L^{rs}}$.

In a first titration series, up to two equivalents of copper(II) were added to a solution of $\mathbf{H_4L^{rs}}$ in steps of 0.4 eq (see Figure 4.23 top). A broad d-d-absorption band arises at ~700 nm that linearly increases in intensity with the copper(II) concentration and exhibits a minor shift throughout the titration from 690 nm in the first spectrum to 712 nm in the last spectrum. The small shift of the band is presumably the result of the different ratios of $[\mathbf{H_2L^{rs}}Cu^{II}_2]^{2+}$ to solvated copper $[Cu^{II}(MeOH)_n]^{2+}$ in solution. The observed band consequently can be assigned to a combination of the absorption band of the dinuclear copper(II) complex $[\mathbf{H_2L^{rs}}Cu^{II}_2]^{2+}$ (λ_{max} = 685 nm, comparable to λ_{max} = 674 nm of $[\mathbf{H_2L^4}Cu^{II}_2]^{2+}$ (see Figure 4.9)) and solvated copper(II) $[Cu^{II}(MeOH)_n]^{+}$ with an absorption maximum at 840 nm. From the analysis of the ESI-MS spectra (see Table 4.8), it is known that at low concentrations of copper(II) a nearly complete formation of the dinuclear complex can be observed. On the other hand, an increase of the copper(II) concentration leads to an enhanced formation of the mononuclear complex $[\mathbf{H_3L^{rs}}Cu^{II}]^{+}$ and solvated copper(II) in solution, which consequently shifts the absorption band to a higher wavelength. The UV-vis experiments emphasize the high stability of the dinuclear complexes of $\mathbf{H_4L^{rs}}$.

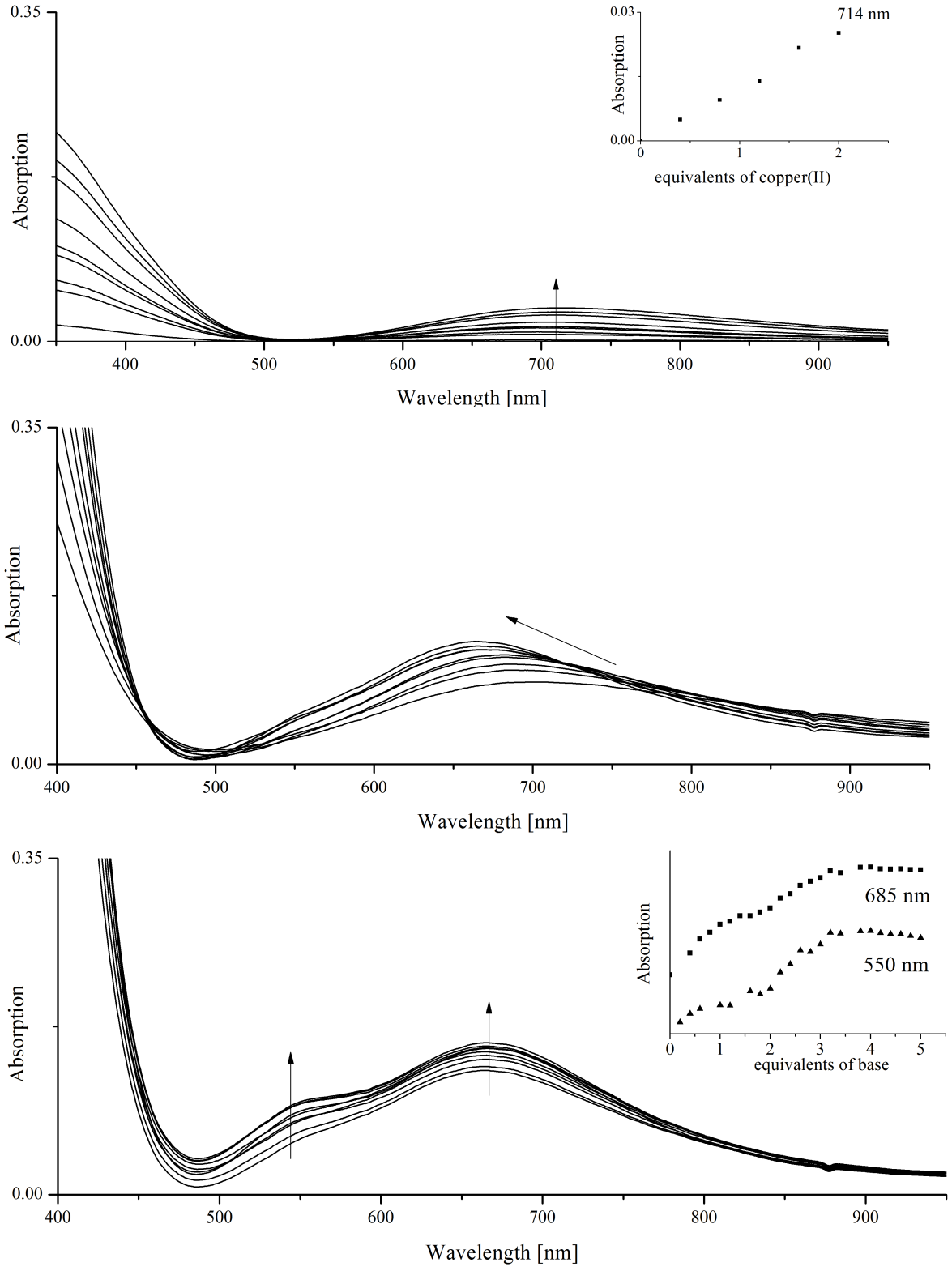

Figure 4.23. UV-vis spectra in methanol ($c(\mathbf{H_4L^{rs}})$ = 1.25mM, base: (n-Bu_4N)(OMe)): titration of 0-2 eq of Cu^{II}, in 0.2 eq steps, to a solution of $\mathbf{H_4L^{rs}}$ (top), titration of 0–2 eq of base, in 0.2 eq steps, to a $\mathbf{H_4L^{rs}}$/copper(II) 1:2 solution (middle), and titration of 2-5 eq of base, in 0.2 eq steps, to a $\mathbf{H_4L^{rs}}$/copper(II) 1:2 solution (bottom).

Subsequent to the addition of copper(II) to a $\mathbf{H_4L^{rs}}$ solution, base (*n*-Bu_4)(OMe) was added stepwise to the $\mathbf{H_4L^{rs}}$/copper(II) 1:2 solution. Addition of up to two equivalents of base (Figure 4.23, middle) induces a shift from 714 ($\varepsilon = 27\ M^{-1}cm^{-1}$) to 685 nm ($\varepsilon = 109\ M^{-1}cm^{-1}$) and an increase of the absorption band, consistent with the formation of the dinuclear copper(II) complex $[\mathbf{H_2L^{rs}}Cu_2^{II}]^{2+}$. Upon addition of 2–3 equivalents of base a shoulder at 550 nm emerges ($\varepsilon = 81\ M^{-1}cm^{-1}$). In agreement with the analysis of the ESI-MS data the spectra are invariant upon addition of more than three equivalents of base.

The intensities of the absorption bands at 685 and 550 nm have an inflection point at the addition of two equivalents of base. While the absorption band at 685 nm strongly increases upon the addition of up to two equivalents of base and only slightly upon addition of the third equivalent of base, the effect on the absorption band at 550 nm is inverse (Figure 4.23, bottom). This suggests that the dinuclear copper(II) complex $[\mathbf{H_2L^{rs}}Cu_2^{II}]^{2+}$ with an absorption maximum at 685 nm is formed first and subsequently converted into the hydroxo species $[\mathbf{H_2L^{rs}}Cu_2^{II}(OH)]^{+}$. The ongoing increase of the d-d-absorption at 685 nm from 2-3 equivalents of base is caused by its overlap with the absorption band at 550 nm.

The intensity of the whole spectrum marginally decreases during the addition of 4-5 equivalents of base, caused by a bluish precipitate, most likely copper(II) methoxide or hydroxide, that is formed at base concentrations above four equivalents and removes copper(II) from the solution. The addition of carbonate to $\mathbf{H_4L^{rs}}$/copper(II) 1:2 solutions shifts the UV-vis spectrum to a spectrum identical to that recorded at higher base concentrations. It might be that $\mathbf{H_4L^{rs}}$ is not flexible enough to form carbonato-bridged complexes.

4.3.3 EPR Experiments

EPR measurements of solutions with varying ratios of $\mathbf{H_4L^{rs}}$/copper(II)/base were performed and it emerged that the copper(II) complexation equilibrium of $\mathbf{H_4L^{rs}}$ depicted in Figure 4.22 is more complex than anticipated. The EPR spectra of the mono- and especially the dinuclear copper(II) complexes of $\mathbf{H_4L^{rs}}$ were found to have interesting features.

In comparison to the spectrum of solvated copper (Figure 4.24 a), a new set of signals between 260 and 340 mT arises in the EPR spectra at a $\mathbf{H_4L^{rs}}$/copper(II)/base ratio of 1:2:1

(Figure 4.24 b). When a second equivalent of base is added the signals of solvated copper(II) disappear and the spectrum exclusively consists of the set of signals that was previously observed at lower base concentrations in addition to the signals of solvated copper(II) (Figure 4.24 b) and usually would be assigned to a mononuclear copper(II) complex of **H_4L^{rs}**.

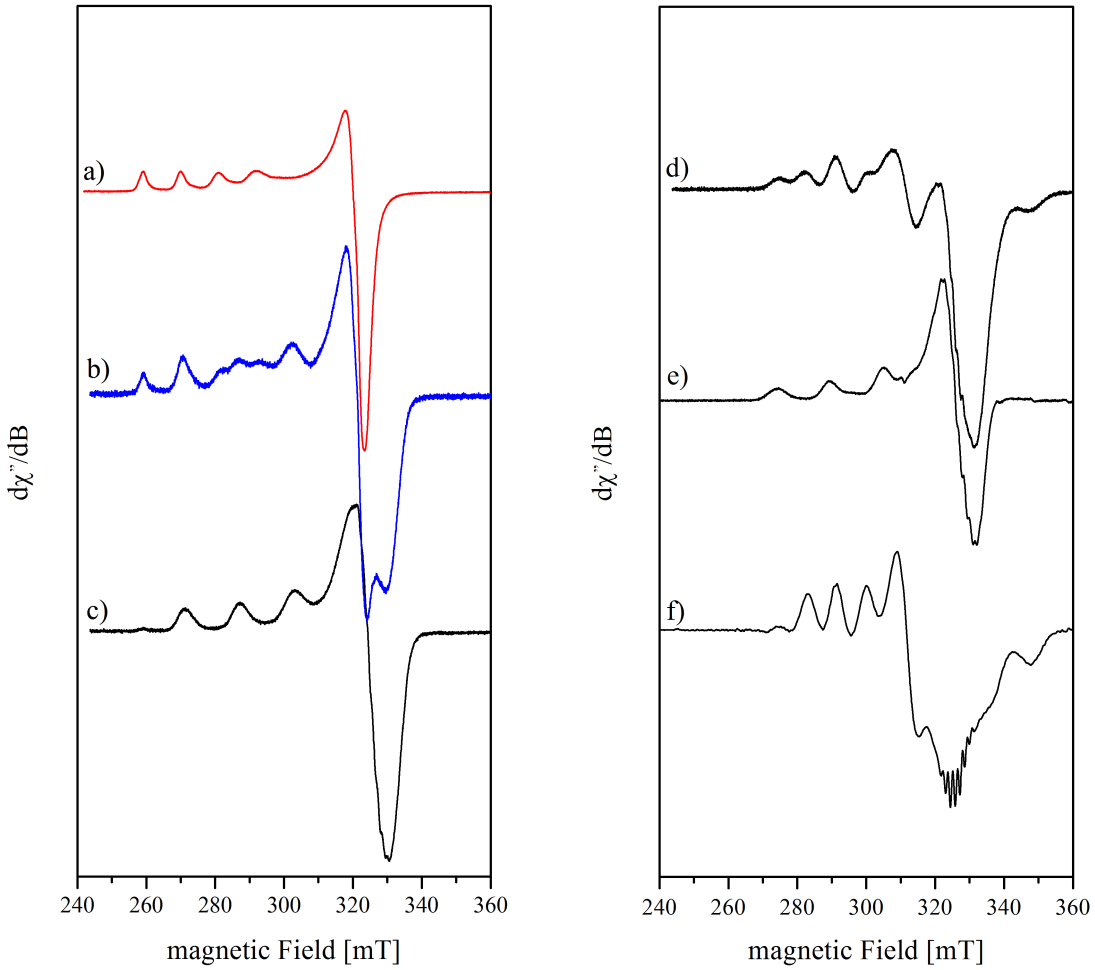

Figure 4.24. Experimental X-Band EPR spectra in methanol, *c*(**H_4L^{rs}**) = 1.25mM: **a)** solvated Cu^{II} $[Cu^{II}(MeOH)_n]^{2+}$, T = 145 K, ν = 9.427799 GHz; **b)** **H_4L^{rs}**/copper(II)/MeO^- 1:2:1, T = 10 K, ν = 9.377228 GHz; **c)** **H_4L^{rs}**/copper(II)/MeO^- 1:2:2, T = 4.5 K, ν = 9.375067 GHz; **d)** **H_4L^{rs}**/copper(II)/MeO^- 1:2:3, T = 50 K, ν = 9.377548 GHz; **e)** pure "monomer" species present in *d)* derived from spectra subtraction of the spectrum with three equivalents of base from the spectrum with four equivalents of base (see Figure 4.26 for 1:2:4 spectrum) **f)** dimeric species present in *d)*, derived from spectra subtraction.

Considering that two equivalents of copper(II) are present in solution and that the spin Hamiltonian parameters of coordinated and solvated copper(II) are significantly different (see Table 4.9, *e.g.* $g_{\|}$ = 2.42 (solvated) *vs* 2.25 (complexed)) these signals have to be due to a

dinuclear copper(II) complex of $\mathbf{H_4L^{rs}}$. In combination with the ESI-MS and UV-vis spectra this spectrum can be assigned to the dinuclear copper(II) complex $[\mathbf{H_2L^{rs}}Cu_2^{II}(H_2O)]^{2+}$. In general the EPR spectrum of a randomly oriented mononuclear copper(II) complex consist of a set of four peaks in the parallel region of the spectrum and one in the perpendicular region, caused by the interaction of the nuclear spin of copper(II) ($I = {}^3/_2$) with the spin of the unpaired electron ($S = {}^1/_2$). The interaction of the copper(II) centers in dinuclear complexes on the other hand gives rise to a set of seven signals, which often overlap, resulting in complicated spectra. The expected seven signals were not observed in the EPR spectra of the dinuclear copper(II) complexes of $\mathbf{H_4L^{rs}}$, $[\mathbf{H_2L^{rs}}Cu_2^{II}(H_2O)]^{2+}$ and $[\mathbf{H_2L^{rs}}Cu_2^{II}(OH)]^{+}$, respectively, (see Figure 4.24 c and e), where only four signals were seen. The spectra were recorded at a $\mathbf{H_4L^{rs}}$/copper(II)/MeO^- ratio of 1:2:2 and 1:2:3.

On behalf of their EPR spectrum the mono- and the dinuclear copper(II) complexes of $\mathbf{H_4L^{rs}}$ are not distinguishable: the signals that arise at a $\mathbf{H_4L^{rs}}$/copper(II)/base concentration of 1:2:1 are a mixture of mono- and dinuclear complexes are identical to those at a 1:2:2 ratio and it emerges that the coordination environment of copper(II) in the mono- and in the dinuclear complexes is identical. In order for the detection of a pseudo mononuclear spectrum the dipole-dipole interaction of the copper(II) centers in the dinuclear water and hydroxo complex has to be cancelled. From the EPR spectrum it arises that copper(II) has a square pyramidal coordination environment in the mono- and in the dinuclear copper(II) complexes and this could be reproduced by the DFT calculated structures of the mononuclear and bridged dinuclear complexes (see Section 4.3.4). The observation of a dinuclear complex exhibiting essentially mononuclear EPR features is known in literature.[75] The dipole-dipole interaction between the two copper(II) centers is cancelled, when the orientation of their *g* and *A* tensors is twisted with respect to each other by Euler angles of $\alpha = 54.7°$ and $\beta = 37.5°$. They are said to be set up in a magic angle.

In accordance with the initially proposed complexation equilibrium derived from ESI-MS and UV-vis data(see Figure 4.22), the EPR spectra change upon addition of a third equivalent of base (see Figure 4.24 d). The recorded spectrum now consists of a mixture of a dinuclear copper(II) complex and a new “mononuclear” complex. Again the “mononuclear” features can be assigned to a dinuclear copper(II) complex of $\mathbf{H_4L^{rs}}$, *i.e.* $[\mathbf{H_2L^{rs}}Cu_2^{II}(OH)]^{+}$. As in case of the water complex, this complex is also expected to have a square pyramidal coordination environment at the copper(II) centers (see Figure 4.31). The formally forbidden $\Delta m_S = \pm 2$ transitions at half field, usually a good indicator for the presence of dinuclear complexes

could not be recorded for the dinuclear complexes $[\mathbf{H_2L^{rs}}Cu^{II}_2(H_2O)]^{2+}$ and $[\mathbf{H_2L^{rs}}Cu^{II}_2(OH)]^{+}$. They are expected to be too low in intensity. Being formally forbidden, the transition probability of the $\Delta m_S = \pm 2$ transitions is already one order of magnitude lower than that of the allowed $\Delta m_S = \pm 1$ transitions. The magic angle set up of the dinuclear complexes $[\mathbf{H_2L^{rs}}Cu^{II}_2(H_2O)]^{2+}$ and $[\mathbf{H_2L^{rs}}Cu^{II}_2(\mu\text{-OH})]^{+}$ reduces the already low signal intensity by a further order of magnitude.

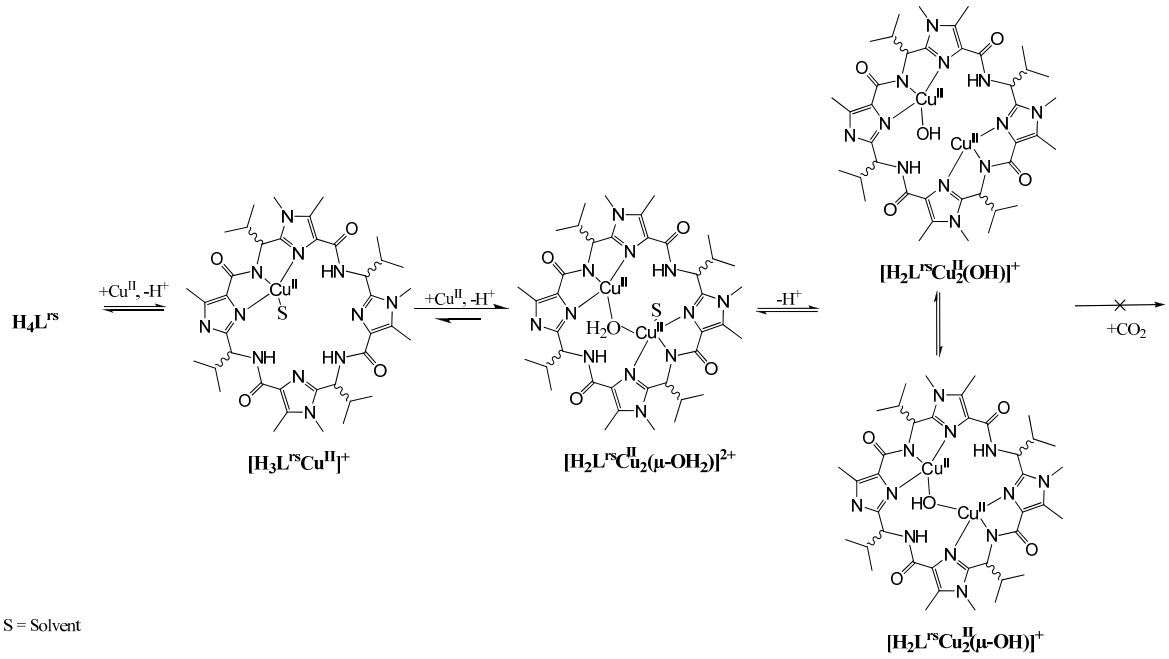

Figure 4.25. Assumed copper(II) complexation equilibria of $\mathbf{H_4L^{rs}}$ (solvent = methanol).

Considering these and the findings from the ESI-MS and UV-vis experiments, as well as those of the DFT calculations (see Section 4.3.4) the complexation equilibria depicted in Figure 4.25 are proposed. The dinuclear copper(II) complex that is formed at low base concentrations is bridged by a water molecule $[\mathbf{H_2L^{rs}}Cu^{II}_2(H_2O)]^{2+}$ and as a result of the bridge, the copper(II) centers are oriented in a magic angle, which leads to a pseudo mononuclear copper(II) EPR spectrum. When a third equivalent of base is added, two isomeric hydroxo complexes $[\mathbf{H_2L^{rs}}Cu^{II}_2(\mu\text{-OH})]^{+}$ and $[\mathbf{H_2L^{rs}}Cu^{II}_2(OH)]^{+}$, respectively, are formed that give rise to the set of signals depicted in Figure 4.24 d. While the copper(II) centers in the hydroxo-bridged isomer are still oriented at a magic angle, thus resulting in a pseudo mononuclear EPR spectrum, the change from a bridging to a terminal hydroxide causes a conformational reorientation in the pseudo octapeptide which now exhibits a dinuclear EPR spectrum (see Figure 4.24 f). The respective spectra of the isomeric hydroxo complexes $[\mathbf{H_2L^{rs}}Cu^{II}_2(\mu\text{-OH})]^{+}$

and $[\mathbf{H_2L^{rs}}Cu^{II}_2(OH)]^+$ (see Figure 4.24 e and f), could be obtained by spectral subtraction of the EPR spectra measured at four and at three equivalents of base. The DFT geometry optimizations of the hydroxo-bridged and water bridged complexes revealed a square pyramidal coordination sphere of the copper(II) centers in both complexes, with a small difference among the complexes that gives rise to the different *g* and *A* tensors of the complexes (see Table 4.9).

Table 4.9. Anisotropic spin Hamiltonian parameters of solvated copper(II) $[Cu^{II}(MeOH)_n]^{2+}$ [165] and of the dinuclear bridged copper(II) complexes of $\mathbf{H_4L^{rs}}$: $[\mathbf{H_2L^{rs}}Cu^{II}_2(\mu\text{-}H_2O)]^{2+}$ and $[\mathbf{H_2L^{rs}}Cu^{II}_2(\mu\text{-}OH)]^+$.

	$[Cu^{II}(MeOH)_n]^{2+}$	$[\mathbf{H_2L^{rs}}Cu^{II}_2(H_2O)]^{2+}$	$[\mathbf{H_2L^{rs}}Cu^{II}_2(\mu\text{-}OH)]^+$
g_x	2.084	2.0719	2.0503
g_y	2.084	2.0456	2.0539
g_z	2.428	2.258	2.2600
A_x (^{63}Cu)	15	4.019	12.6896
A_y (^{63}Cu)	15	4.423	9.2275
A_z (^{63}Cu)	108	166.878	161.641
A_x (^{14}N) – N_{het} *)	-	8.0751	6.9792
A_y (^{14}N) – N_{het} *)	-	11.629	9.0013
A_z (^{14}N) – N_{het} *)	-	10.500	10.000
A_x (^{14}N) – N_{amide}	-	15.455	13.369
A_y (^{14}N) – N_{amide}	-	13.078	12.849
A_z (^{14}N) – N_{amide}	-	13.500	12.000

*) simulated spectra of $\mathbf{H_4L^{rs}}$ included two magnetically identical heterocyclic nitrogen nuclei.

Addition of four and up to nine equivalents of base results in minor modifications of the EPR spectra, caused by a slightly different ratio of the hydroxo complex isomers (see Figure 4.26 a-c for the spectra with three, four, and five equivalents of base, respectively). As expected and observed in the previous experiments carbonate ions that are added to $\mathbf{H_4L^{rs}}$/copper(II) 1:2 solutions, do not appear to interact with the complex, nor lead to the formation of carbonato-bridged complexes. Thus, considering the so far performed experiments, it is possible to exclude the existence of a stable carbonato complex of $\mathbf{H_4L^{rs}}$, *i.e.* $[\mathbf{H_2L^{rs}}Cu^{II}_2(\mu\text{-}CO_3)]$.

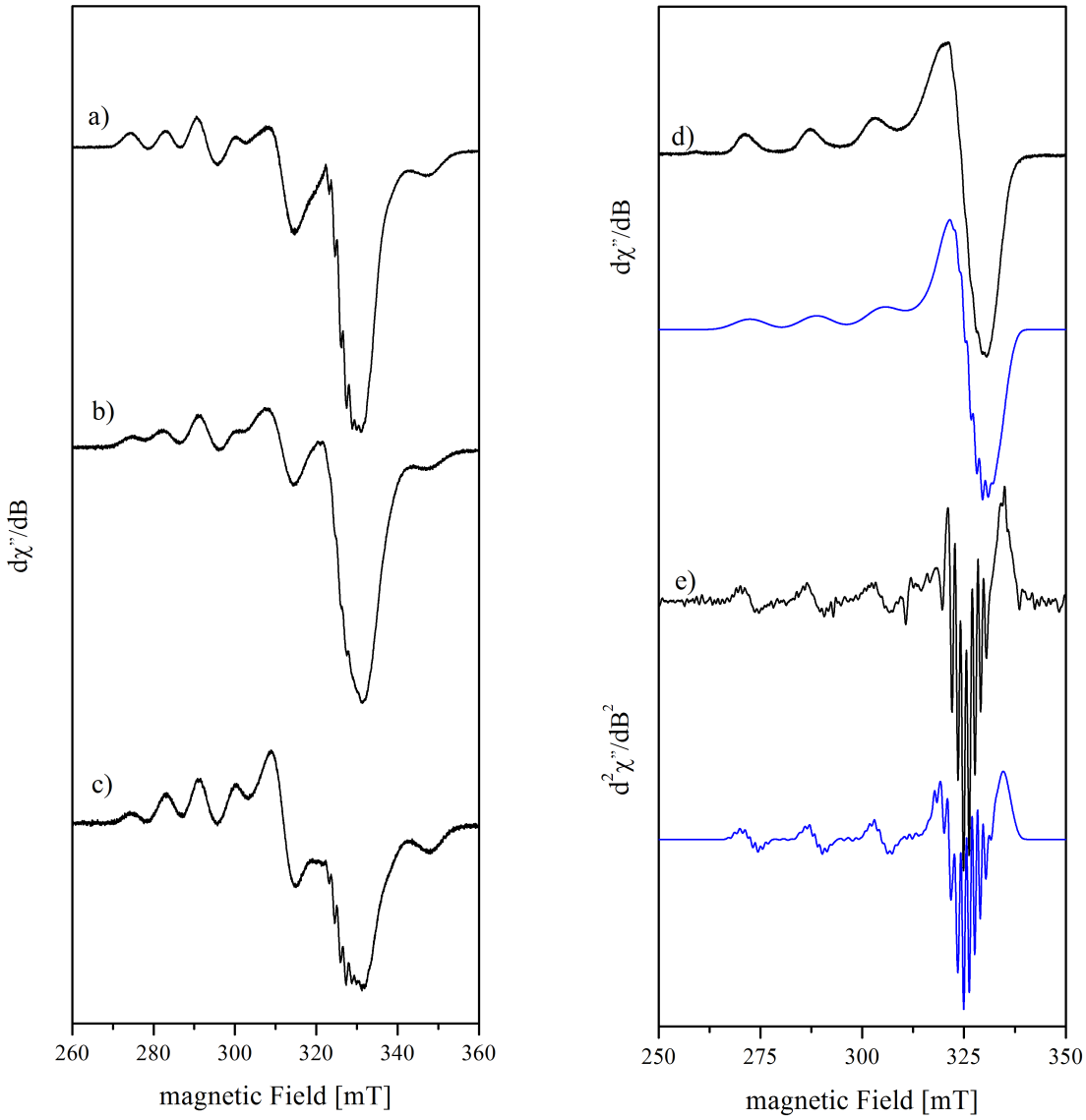

Figure 4.26. Experimental (black) and simulated (blue) X-Band EPR spectra in methanol, $c(\mathbf{H_4L^{rs}}) = 1.25$ mM: **a)** $\mathbf{H_4L^{rs}}$/copper(II)/MeO^- 1:2:3, T = 50 K, ν = 9.377548 GHz; **b)** $\mathbf{H_4L^{rs}}$/copper(II)/MeO^- 1:2:4, T = 5 K, ν = 9.376811 GHz; **c)** $\mathbf{H_4L^{rs}}$/copper(II)/MeO^- 1:2:5, T = 5 K, ν = 9.376811 GHz; **d)** $[\mathbf{H_2L^{rs}}Cu^{II}_2(\mu\text{-}H_2O)]^{2+}$, $\mathbf{H_4L^{rs}}$/copper(II)/MeO^- 1:2:2; T = 4.5 K, ν = 9.375067 GHz **e)** second derivative of the spectrum of $[\mathbf{H_2L^{rs}}Cu^{II}_2(\mu\text{-}H_2O)]^{2+}$.

The experimental first derivative EPR spectrum of the water bridged dinuclear complex $[\mathbf{H_2L^{rs}}Cu^{II}_2(\mu\text{-}H_2O)]^{2+}$ and its simulation are shown in Figure 4.26 d. After differentiation, *Fourier*- and *Savitzky-Golay* filtering, the second derivative of the EPR spectra could be obtained, where the superhyperfine coupling A ($^{14,15}N$) of the coordinated nitrogen atoms is resolved. The second derivative spectrum and its simulation are shown in Figure 4.26 e. The spectra were simulated with the program package X-Sophe-Sophe-XeprView, based on the

Spin-Hamilton Operator shown in Eq. 3.7.[122] Two magnetically equivalent heterocyclic nitrogen nuclei and one amide nitrogen nucleus were assumed in the simulation in order to correctly reproduce the observed hyperfine coupling. The EPR spectrum is suggestive of a square pyramidal coordination sphere of both copper centers.

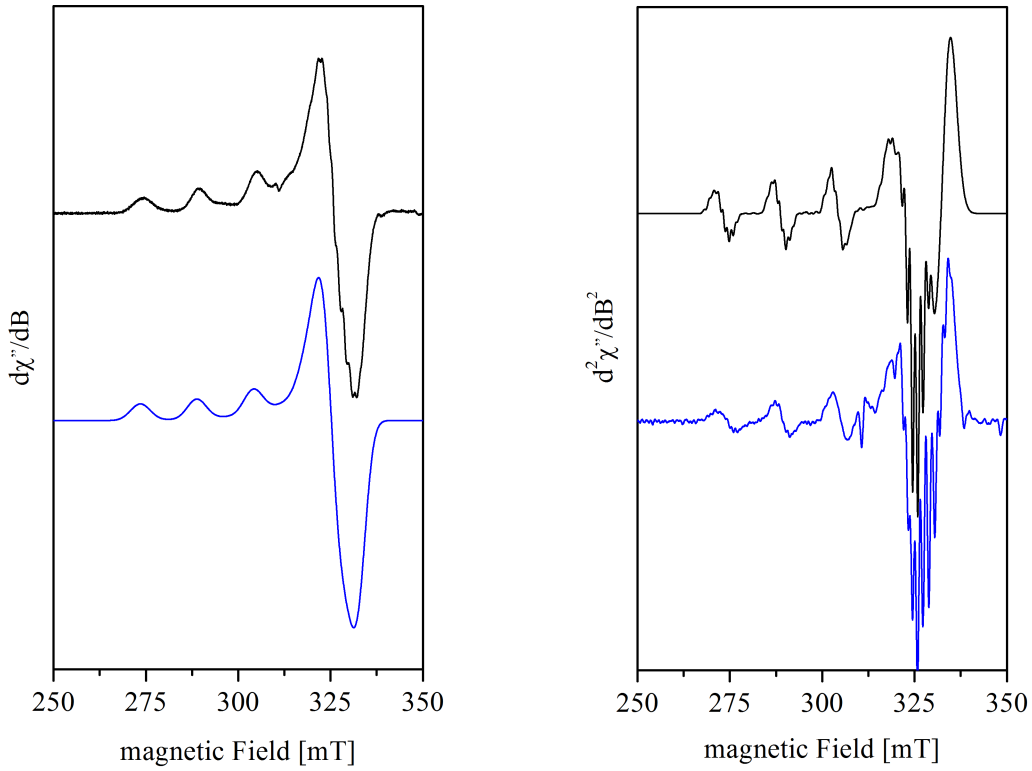

Figure 4.27. Experimental (black) and simulated (blue) first (left) and second derivative (right) X-Band EPR spectra in methanol of the bridged hydroxo complex $[\mathbf{H_2L^{rs}}Cu^{II}_2(\mu\text{-OH})]^+$, derived from spectra subtraction; T = 50 K, $c(\mathbf{H_4L^{rs}})$ = 1.25 mM, ν = 9.375402 GHz.

The experimental first and second derivative EPR spectra of the bridged hydroxo complex $[\mathbf{H_2L^{rs}}Cu^{II}_2(\mu\text{-OH})]^+$, that was derived from spectra subtraction (see Figure 4.24 e) together with their simulated spectra are shown in Figure 4.27. The simulation confirmed the slightly different coordination sphere of the copper(II) centers in the dinuclear bridged complexes $[\mathbf{H_2L^{rs}}Cu^{II}_2(\mu\text{-}H_2O)]^{2+}$ and $[\mathbf{H_2L^{rs}}Cu^{II}_2(\mu\text{-OH})]^+$. The spin Hamiltonian parameters are listed in Table 4.9. The parameters were fitted with the least mean square method to the experimental spectrum and show excellent agreement with the experimental spectra with a RMS of 0.04. The g_x and A_z tensors of the hydroxo complex $[\mathbf{H_2L^{rs}}Cu^{II}_2(\mu\text{-OH})]^+$ are slightly smaller than those of the dinuclear complex $[\mathbf{H_2L^{rs}}Cu^{II}_2(\mu\text{-}H_2O)]^{2+}$. Yet, in a structural sense it is not expected that there are large differences between the complexes, as the copper(II)

centers still have to be set up in an magic angle and the differences are thought to be caused by the deprotonation of the bridging water and hence formation of a hydroxide bridged complex.

The simulated spin Hamiltonian parameters of the bridged complexes are suggestive of a distorted square pyramidal coordination sphere. They are in a similar range as the spin Hamiltonian parameters reported for the mononuclear copper(II) complexes of $\mathbf{H_3L^{1-3}}$ (see Table 3.3) and $\mathbf{H_4L^4}$ ($g\perp = 2.09,\ 2.05$; $g_{||} = 2.26$; $A\perp = 14,\ 15$; $A_{||} = 169$).[103] The distorted square pyramidal coordination sphere of copper(II) ions in μ-OH_n (n = 1,2) bridged dinuclear copper(II) complexes of $\mathbf{H_4L^{rs}}$ can also be observed in the X-ray structure of the dinuclear copper(II) complex $[\mathbf{H_2L^{rs}}Cu^{II}_2(\mu\text{-}OH)(H_2O)_2]^+$ and in the DFT calculated structures (see Section 4.3.4).

A satisfactory simulation of the non-bridged hydroxo complex $[\mathbf{H_2L^{rs}}Cu^{II}_2(OH)]^+$ has yet to be obtained. The simulations to date suggest a copper(II)-copper(II) distance in the range of 4.6 Å, this distance is longer than the distance in the bridged complexes.

4.3.4 DFT Calculations and X-Ray Crystallography

In order to rationalize the experimental observations, the structures of $\mathbf{H_4L^{rs}}$ and its mono- and dinuclear copper(II) complexes were geometry optimized using DFT methods. The calculations were performed in gas phase and solution, using the program packages Gaussian 03,[119] Gaussian 09,[163] and Turbomole.[166] Geometry optimizations were performed using the B3LYP functional and the 6-31g* (C, H, N, O) and TZVP (Cu) basis sets.[130, 135-136, 139] Subsequent to the geometry optimization a frequency analysis was performed in order to confirm the structures as a minimum on the potential surface.

Bearing in mind the similarity of $\mathbf{H_4L^{rs}}$ and $\mathbf{H_4L^4}$ it is surprising that in none of the experiments with $\mathbf{H_4L^{rs}}$ the formation of carbonato complexes could be observed. It is likely that this is a result of the different folding of the macrocycles that strongly influences the orientation of the amino acid residues. An alternating up and down conformation, as adopted in $\mathbf{H_4L^{rs}}$, might inhibit the formation of a carbonato complex for steric reasons. This might explain why in the natural cyclic pseudo octapeptides oxazoline rings are incorporated as they

enlarge the flexibility that might be needed to form carbonato-bridged complexes. The DFT calculation of two possible conformations of the metal free macrocycle of $\mathbf{H_4L^{rs}}$ revealed that the conformation that is equivalent to the one adopted by $\mathbf{H_4L^4}$ is 62 kJ/mol higher in energy than the one adopted in the X-ray of $\mathbf{H_4L^{rs}}$, emphasizing the preferred adoption of one conformer (see Figure 4.28). The high energy difference of flipped conformers has also been observed and calculated for the conformations of $\mathbf{H_4L^4}$ (see Figure 4.19, page 84). In addition to the already quite high energy difference it is likely that the flip of the isopropyl residue is accompanied by a high rotation barrier and therefore it appears that a conformation similar to that of $\mathbf{H_4L^4}$ cannot be adopted by $\mathbf{H_4L^{rs}}$.

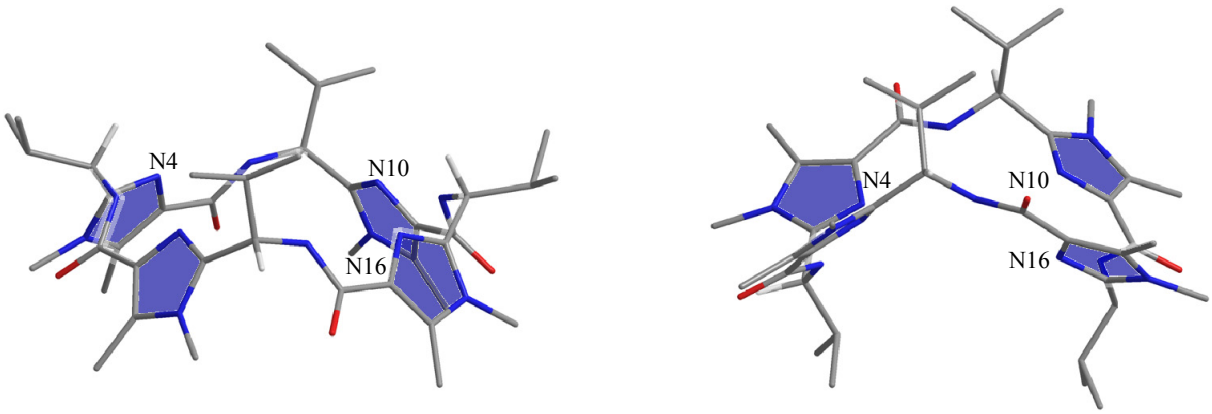

Figure 4.28. DFT calculated conformations of $\mathbf{H_4L^{rs}}$: conformation equivalent to the one adopted by $\mathbf{H_4L^4}$ in the X-ray structure (left) and conformation of the X-ray structure of $\mathbf{H_4L^{rs}}$ (right).

The influence of a solvation model (PCM,[164] methanol) on the optimized geometry of the copper(II) complexes of $\mathbf{H_4L^{rs}}$ was tested with the mononuclear copper(II) complex $[\mathbf{H_3L^{rs}}Cu^{II}(H_2O)_2]^+$ and found to be insignificant (see Appendix I). As mentioned in the introduction of this Chapter, $\mathbf{H_4L^{rs}}$ has two different binding sites. Copper(II) can either bind to the N_{het}-$N_{\textit{R}\text{-amide}}$-$N_{het}$ $[\mathbf{H_3L^{rs}}Cu^{II}_r(H_2O)_2]^+$ or the N_{het}-$N_{\textit{S}\text{-amide}}$-$N_{het}$ $[\mathbf{H_3L^{rs}}Cu^{II}_s(H_2O)_2]^+$ binding site. The inexistence of Cotton bands was a strong indication that in the solutions are racemic, suggesting that the two complexes are energetically identical. In the calculated mononuclear copper(II) complexes, the coordination sphere of copper(II) was completed by two water molecules and, as assumed from the EPR spectra they were found to have a distorted square pyramidal coordination sphere. The equatorial positions are occupied by two imidazole nitrogens N_{het}, one amide nitrogen N_{amide}, and one oxygen of a coordinated water molecule. The water molecule that occupies the apical position has a longer Cu1-O2 distance

(2.29 Å) than the water coordinated in the equatorial plane (Cu1-O1 = 2.04 Å). This water molecule hardly changes its position upon formation of the dinuclear complex, suggesting that the water molecule is used as an anchor to form the dinuclear complexes. This might also explain the observed preference for the formation of dinuclear complexes.

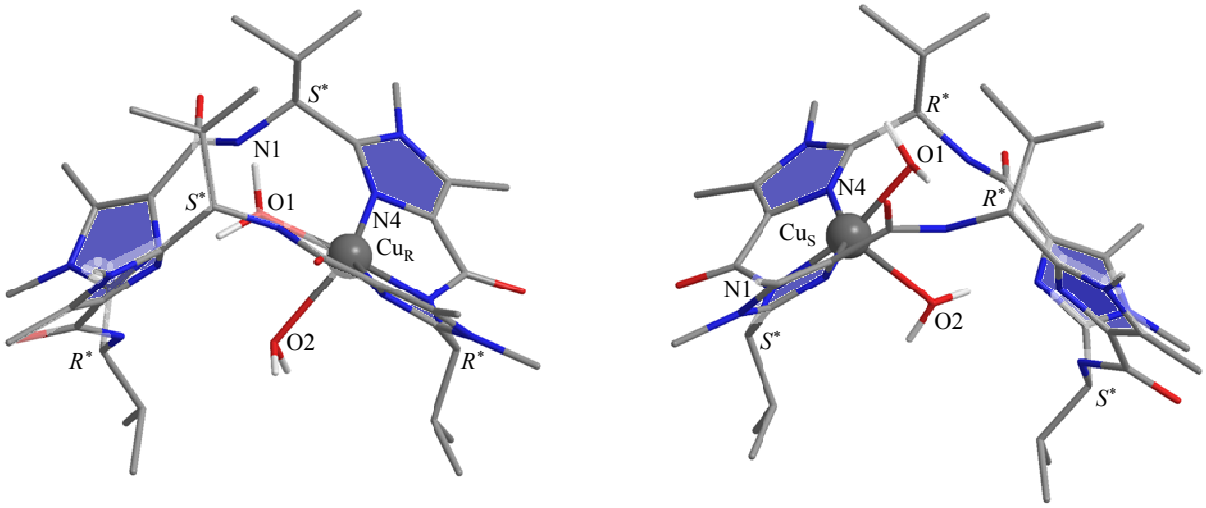

Figure 4.29. Top views of the enantiomers $[\mathbf{H_3L^{rs}}Cu^{II}_r(H_2O)_2]^+$ (left) and $[\mathbf{H_3L^{rs}}Cu^{II}_s(H_2O)_2]^+$ (right).

When the structures of the two possible monomeric complexes are compared, their enantiomeric character emerges (see Figure 4.29, Table 4.10). The intramolecular distances and angles in the two enantiomeric complexes are nearly identical, *e.g.* the largest deviation between the complexes is found to be the distance of the trans-disposed N_{het} atoms (0.3 Å). The small variations in the adopted conformations might be the reason for the calculated small energy difference of 6 kJ/mol.

Table 4.10. Selected angles and distances (e.s.d.'s are given in parentheses) of the DFT [a] optimized structures of the copper(II) complexes of $\mathbf{H_4L^{rs}}$, of the X-ray structure of the hydroxo-bridged complex of $\mathbf{H_4L^{rs}}$ $[\mathbf{H_2L^{rs}}Cu^{II}_2(\mu\text{-}OH)(H_2O)_2]^+$, and for comparison the DFT calculated structure of the hydroxo-bridged complex of $\mathbf{H_4L^4}$ $[\mathbf{H_2L^4}Cu^{II}_2(\mu\text{-}OH)]^+$.

	$[\mathbf{H_3L^{rs}}Cu^{II}(H_2O)_2]^+$ [a]			$\mathbf{H_4L^4}$	$\mathbf{H_4L^{rs}}$		**X-ray**
	at S^*-configured N_{amide}	at R^*-configured N_{amide}	$[\mathbf{H_2L^{rs}}Cu^{II}_2(\mu\text{-}OH)]^+$ [a]	$[\mathbf{H_2L^4}Cu^{II}_2(\mu\text{-}OH)]^+$ [a]	$[\mathbf{H_2L^{rs}}Cu^{II}_2(\mu\text{-}H_2O)]^+$ [a]	$[\mathbf{H_2L^{rs}}Cu^{II}_2(\mu\text{-}H_2O)]^{2+}$	$[\mathbf{H_2L^{rs}}Cu^{II}_2(\mu\text{-}OH)(H_2O)_2]^+$
α [N4-N10-N16-N22] [c]	22	31	-27	28	28	28	-40
β [N35–N22–N10–N29], [N26–N4–N16–N32] [c]	11/11	-15/13	0/-14	10/6	111/37	111/37	96/22
∠ (Cu1-O1-Cu2)	-	-	137	148	133	145	140
ρ (angle between binding sites)	61	61	71	86	77		77
N_{amide}-N_{amide} consecutive	5.19/5.33/ 5.00/5.26	5.22/5.18/ 5.44/4.89	5.15/5.19/ 5.19/5.12	5.05/5.19/ 5.06/5.19	5.15/5.18/ 5.15/5.18	5.15/5.18/ 5.15/5.18	5.087(1)/5.1549(1)
N_{amide}-N_{amide} trans-disposed	6.43/5.88	5.94/6.25	6.88/5.56	6.99/5.61	7.26/5.04	7.26/5.04	5.547(1)/6.753(1)*)
N_{het}-N_{het} consecutive	4.13/4.67/ 4.50/4.76	4.68/4.14/ 4.43/4.48	4.13/5.01/ 4.05/4.90	4.15/4.67/4.15/4.67	3.90/4.97/ 3.90/4.97	3.90/4.97/ 3.90/4.97	4.6238(8)/3.999(1)*)
N_{het}-N_{het} trans-disposed	6.04/6.47	5.89/6.13	6.34/6.19	5.88/6.25	5.85/6.30	5.85/6.30	6.076(2)/5.458(1)
Cu1-Cu2	-	-	3.76	3.97	4.89	4.00	3.6290 (7)
Cu1-O1/Cu2-O1	2.04	2.11	2.00/2.03	2.06/2.06	2.01	2.09/2.09	1.93/1.93
Cu1-O2/Cu2-O2	2.29	2.28	2.4/-	2.35/-	-	-	2.51/-
Cu1-O3/Cu2-O3	-	-	-/2.35	-/2.35	-	-	-/-
Cu^{II} coordination sphere	dis. sq pyr	dis. sq pyr	dis. sq pyr	dis. sq planar	dis. sq pyr	dis. sq pyr	dis. sq pyr

Units: d [Å] ∠ [°] a) G09, B3LYP/6-31g* (C,H,N,O)/TZVP (Cu); b) see Figure 4.3 for used abbreviations; c) see Figure 4.4 for atom numbers; *) at R^*-configured C_α, at copper bound site.

The coordination of the first copper(II) ion lowers the macrocycle's high symmetry and induces a bending that can be nicely visualized by an examination of the angle ρ between the planes of the binding sites (see Section 4.1.1 for definition of ρ and Figure 4.6 for a visualization). In the metal-free cyclic pseudo octapeptide the binding sites include an angle of 77° that decreases to 61° upon coordination of copper(II) in one of the binding sites. In the dinuclear copper(II) complexes, both copper(II) ions are either bound in an N_{het}-$N_{\textit{R}\text{-amide}}$-$N_{het}$ or in an N_{het}-$N_{\textit{S}\text{-amide}}$-$N_{het}$ binding site. This coordination mode leads to the formation of racemic complexes, which was confirmed by the absence of Cotton effects in the CD spectra. It is known from the experiments, and from the calculations of the monomeric complexes, that none of the binding sites is favored and therefore it was chosen to solely study the dinuclear copper(II) complexes, with copper(II) bound in the N_{het}-$N_{\textit{S}\text{-amide}}$-$N_{het}$ binding sites.

The coordination of a second copper(II) ion increases the angle ρ between the binding sites back to 76°, nearly the same angle as found in the free cyclic pseudo peptide. In the bridged complexes, both copper(II) ions have a square pyramidal coordination sphere, where the equatorial planes are spanned by the nitrogen atoms of the binding site (N_{het}-N_{amide}-N_{het}) and one additional oxygen atom. In the hydroxo complex $[\mathbf{H_2L^{rs}}Cu^{II}_2(\mu\text{-OH})]^+$ shown on the right hand side in Figure 4.30, the equatorial plane of both copper(II) ions is completed by the oxygen atom of the bridging hydroxide anion, emphasizing the similarity of the two binding sites that is visible in the EPR spectra of the bridged complexes. The overlay plots of the X-ray structure of $\mathbf{H_4L^{rs}}$ with the calculated mono- and dinuclear copper(II) complexes reveal, that although the planes of the binding sites are nearly identical in the dinuclear copper(II) complex and the X-ray structure, there is a substantial difference in the overall structure. When electronic effects are considered, *e.g.* by calculating the energetic change that is needed in the macrocycle's backbone to adopt the conformation of the mono- or the dinuclear complex, it emerges that the dinuclear copper(II) complexes are energetically favored. The conformation adopted by the dinuclear complexes is 25 kJ/mol lower in energy than the conformation calculated for the mononuclear copper(II) complexes (Table 4.11).

Table 4.11. Relative single point energies [kJ/mol] of the macrocyclic ligand backbone of the mono- and dinuclear copper(II) complexes of $\mathbf{H_4L^{rs}}$, compared to the energy of the metal-free cyclic pseudo peptide, calculated at the B3LYP/6-31g* level).

	$\mathbf{H_4L^{rs}}$ **X-ray (opt)**	$\mathbf{[H_3L^{rs}Cu^{II}]^+}$	$\mathbf{[H_2L^{rs}Cu^{II}_2(\mu\text{-OH})(H_2O)_2]^+}$
Energy [kJ/mol]	0	60	35

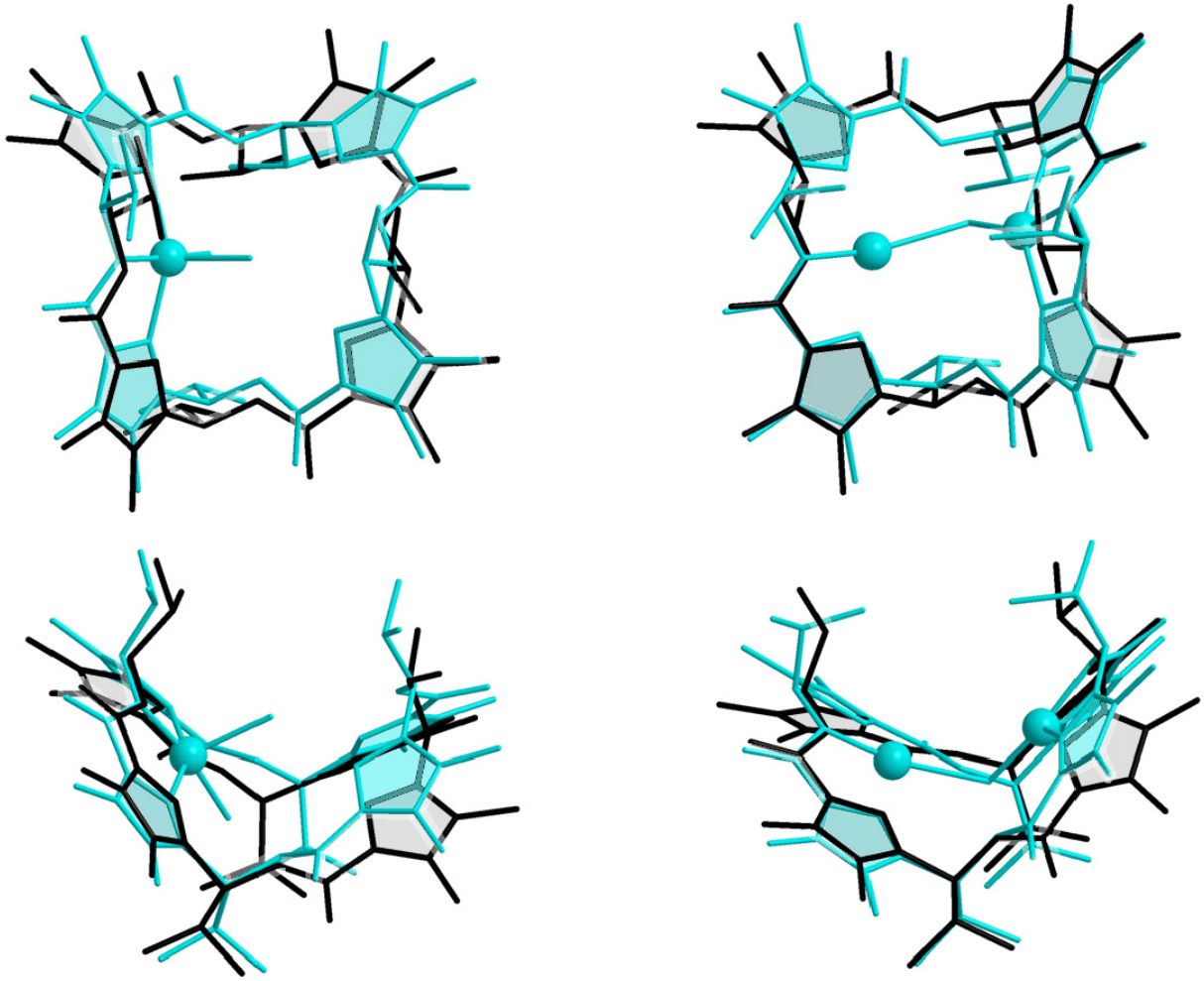

Figure 4.30. Top (top) and side views (bottom) of overlay plots of the X-ray structure of $\mathbf{H_4L^{rs}}$ with its computed (G09, B3LYP/6-31g*/TZVP) mono- (left) and dinuclear copper(II) complexes (right). $[\mathbf{H_3L^{rs}}Cu_s^{II}]^+$ (turquoise, right), $\mathbf{H_4L^{rs}}$ (black) and $[\mathbf{H_2L^{rs}}Cu_2^{II}(\mu\text{-OH})]^+$ (turquoise, right).

From the EPR experiments the existence of both a hydroxo-bridged and terminal hydroxo complex was concluded. In the so far performed DFT calculations a terminal hydroxo complex could not be obtained, but instead always converted to the bridging hydroxide. Probably the used functional and basis set prohibit the formation of a terminal hydroxo complex or the dinuclear complex that is seen in the EPR spectra at three equivalents of base arises from a species that could not be characterized yet.

Suitable crystals for single crystal X-ray structure determination were obtained for the dinuclear copper(II) cation $[\mathbf{H_2L^{rs}}Cu_2^{II}(\mu\text{-OH})(H_2O)_2]^+$. It is a racemic crystal that contains two dinuclear copper(II) complexes in the unit cell, a further proof of the equality of both binding sites. An ORTEP plot of the X-ray structure of $[\mathbf{H_2L^{rs}}Cu_2^{II}(\mu\text{-OH})(H_2O)_2]^+$ is shown in Figure 4.31. The structure is nearly identical to that derived from the DFT calculations (see Table 4.10). Of particular interest is the short copper(II)-copper(II) distance of 3.63 Å, that

might be a reason for the inability to prepare carbonato complexes. However, the copper(II)-copper(II) distance in the X-ray structure of the carbonato-bridged complex of ascidiacyclamide is also very short (3.9Å). Thus, the short distance of the copper(II) ions cannot be the only reason for the inexistence of carbonato-bridged species and other effects have to be considered.

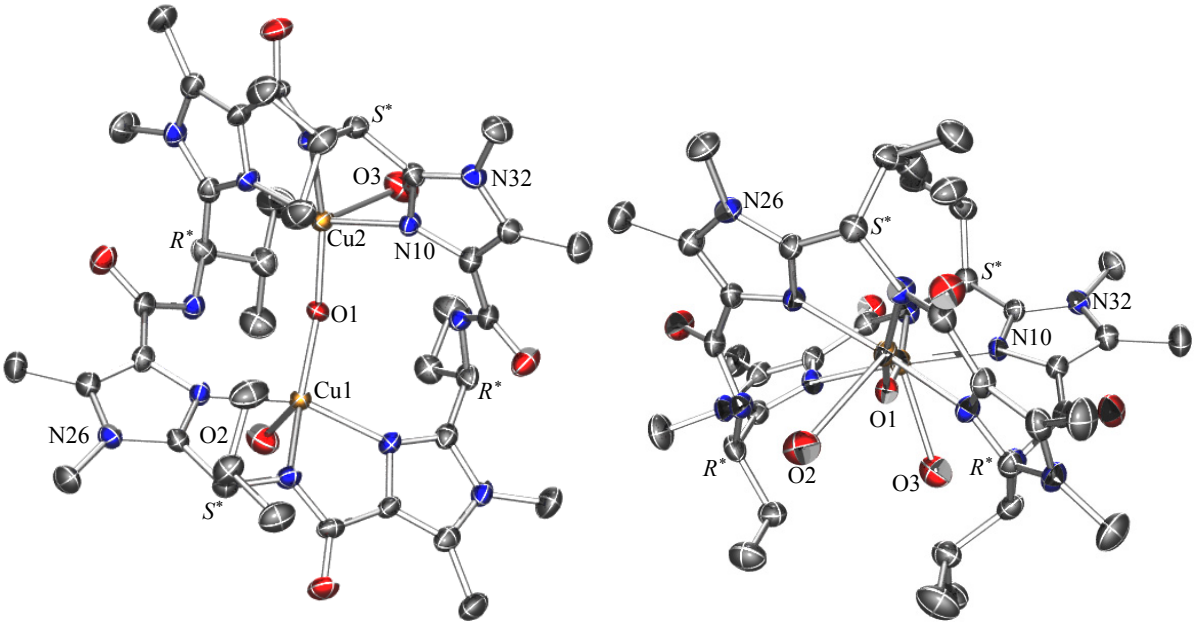

Figure 4.31. ORTEP plot of the *S** enantiomer of the X-ray structure of the of hydroxo-bridged cation $[\mathbf{H_2L^{rs}}Cu_2^{II}(\mu\text{-OH})(H_2O)_2]^+$ top (left) and side view (right). Ellipsoids are drawn at 50% probability, hydrogen atoms and solvent molecules are omitted for clarity; C = grey, N = blue, O = red, Cu = yellow.

In the X-ray structure of $[\mathbf{H_2L^{rs}}Cu_2^{II}(\mu\text{-OH})(H_2O)_2]^+$ both copper(II) centers have a square pyramidal coordination polyhedron. The three nitrogen atoms of the binding site and the oxygen atom of the bridging hydroxide form the equatorial plane. The apical positions of both copper(II) ions are occupied by a water molecule at a distance of 2.51 Å. The twist of the copper(II) planes with respect to each other is visualized in Figure 4.32.

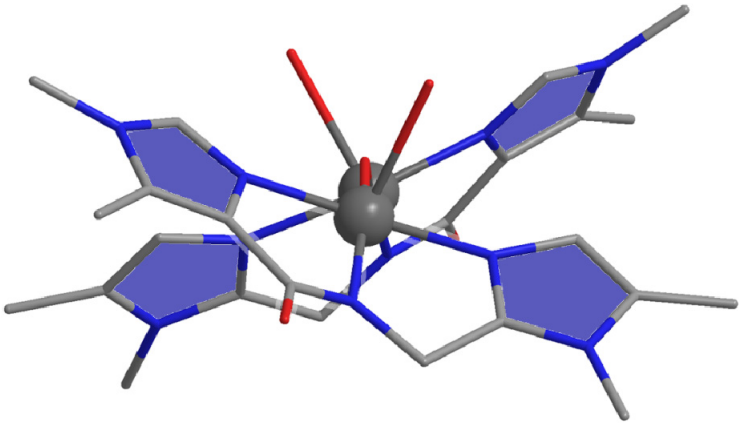

Figure 4.32. Orientation of the binding sites in $\mathbf{H_4L^{rs}}$, with respect to the copper(II) copper(II) vector.

It is expected that upon coordination of carbonate, the distance of the copper(II) centers enlarges. This would reduce the distance of trans-disposed isopropyl residues, thereby inducing steric strain in the macrocyclic backbone and thereby hampering the formation of a carbonato-bridged complex. This indicates that an alternating R^* and S^* configuration at C_α is inhibiting the formation of carbonato-bridged species. Yet, as mentioned above, ascidiacyclamide, that also exhibit an alternating configuration at C_α is found to readily react with atmospheric CO_2 to the carbonato-bridged complex. However, the incorporation of the less flexible imidazole rings in $\mathbf{H_4L^{rs}}$ seem to hamper the formation of carbonato bridged complexes.

Surprisingly $\mathbf{H_4L^{rs}}$ has a substantially different copper(II) coordination chemistry than $\mathbf{H_4L^4}$. It was expected that its chemistry is similar to that of $\mathbf{H_4L^4}$ and potentially closer to that of the natural cyclic peptides as a result of the alternating stereochemistry at C_α. Yet, it was found that $\mathbf{H_4L^{rs}}$ in incapable to react with CO_2 or carbonate and thus no formation of carbonato-bridged complexes could be observed. The reason seems to be the combination of imidazole heterocycles with an alternating R^* and S^* configuration. The imidazole rings induce a rigidity in the system and the alternating configuration induces steric strain that seems to hamper the reaction with CO_2. The dinuclear bridged complexes of $\mathbf{H_4L^{rs}}$ were found to be very interesting as due to their conformation, probably induced by the rigidity of the system, their copper(II) centers are set up in an magic angle and thus exhibit EPR

spectroscopic features of a mononuclear complex. This magic angle set up was found to be partly offset by the addition of more than three equivalents of base to the solutions. It was then possible to obtain the spectrum of a dinuclear coupled species that is thought to be a terminal hydroxo complex. **H_4L^{rs}** is an interesting cyclic pseudo peptide, however, it cannot be used as a model system for the natural cyclic peptides as the reaction of CO_2 seems to be important feature of these molecules. In future experiments the nature of the dinuclear coupled species shall be revealed and it might also be of interest to further investigate the seemingly high rigidity of the system.

4.4 Copper(II) Coordination Chemistry of H_4L^{ox}

4.4.1 ESI-MS Experiments

The ESI-MS experiments performed with the tetraoxazole cyclic pseudo peptide $\mathbf{H_4L^{ox}}$ (see Figure 4.33), provided spectra that contained a large number of doubly charged species and ions assigned to complexes with two pseudo peptide molecules per copper(II) present in the solutions, *i.e.* $[(\mathbf{H_4L^{ox}})_2Cu^{II}]^{2+}$. These observations suggest that the coordination chemistry of $\mathbf{H_4L^{ox}}$ is similar to that of the cyclic pseudo hexapeptide $\mathbf{H_3L^2}$ (see Chapter 3). Table 4.12 lists the species present in solutions of $\mathbf{H_4L^{ox}}$ found at varying ratios of $\mathbf{H_4L^{ox}}$/copper(II)/base.

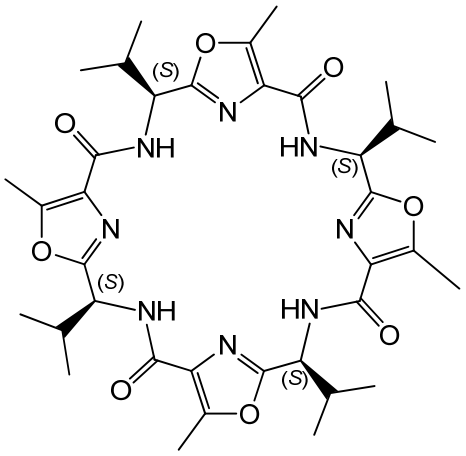

Figure 4.33. Chemical structure of $\mathbf{H_4L^{ox}}$.

The ESI-MS experiments revealed a mixture of different species in solution, indicative of a complicated complexation equilibrium. The $\mathbf{H_4L^{ox}}$/copper(II) 1:2 solutions with more than two equivalents of base give spectra that exhibit signals attributable to the dinuclear hydroxo complex $[\mathbf{H_2L^{ox}}Cu_2^{II}(OH)]^+$ *m/z* 861.2263 and a time-dependent conversion of this signal to the bicarbonato $[\mathbf{H_2L^{ox}}Cu_2^{II}(\mu\text{-}HCO_3)]^+$ *m/z* 905.2298 and carbonato-bridged complexes $[\mathbf{H_2L^{ox}}Cu_2^{II}(\mu\text{-}CO_3)]$ could be observed. Addition of carbonate to $\mathbf{H_4L^{ox}}$/copper(II) 1:2 solutions also leads to the formation of bicarbonato and carbonato-bridged copper(II) complexes, comparable to the observed coordination behavior of $\mathbf{H_4L^4}$.

Table 4.12. Molecular formula, experimental and calculated masses of the observed mono- and dinuclear copper(II) complexes of $\mathbf{H_4L^{ox}}$.

species	molecular formula	experimental	calculated
$[\mathbf{H_5L^{ox}}]^+$	$C_{36}H_{49}N_8O_8^+$	721.3676	721.3667
$[\mathbf{H_4L^{ox}}Na]^+$	$C_{36}H_{49}N_8NaO_8^+$	743.3518	743.3487
$\mathbf{[H_5L^{ox}}K]^+$	$C_{36}H_{49}N_8KO_8^+$	759.3328	759.3227
$[(\mathbf{H_4L^{ox}})_2Cu^{II}]^{2+}$	$C_{72}H_{96}CuN_{16}O_{16}^{2+}$	751.8307	1503.6475
$[\mathbf{H_4L^{ox}}Cu^{II}]^{2+}$	$C_{36}H_{48}CuN_8O_8^{2+}$	391.6450	783.2880
$[\mathbf{H_3L^{ox}}Cu^{II}]^+$	$C_{36}H_{47}CuN_8O_8^+$	782.3082	782.2807
$[\mathbf{H_2L^{ox}}Cu^{II}_2(OH)]^+$	$C_{36}H_{47}Cu_2N_8O_9^+$	861.2263	861.2052
$[\mathbf{H_2L^{ox}}Cu^{II}_2(HCO_3)]^+$	$C_{37}H_{47}Cu_2N_8O_{11}^+$	905.2298	905.1951
$[\mathbf{H_2L^{ox}}Cu^{II}_2(CO_3)Na]^+$	$C_{37}H_{46}Cu_2N_8NaO_{11}^+$	927.2243	927.1770
$[\mathbf{H_2L^{ox}}Cu^{II}_2(CO_3)K]^+$	$C_{37}H_{46}Cu_2KN_8O_{11}^+$	943.1859	943.1510

4.4.2 CD, UV-vis, and NMR Spectroscopy

The copper(II) complexes of $\mathbf{H_4L^{ox}}$ have a distinct circular dichroism in the visible region of the electromagnetic spectrum and the copper(II) coordination chemistry of $\mathbf{H_4L^{ox}}$ can thus nicely be followed using CD and UV-vis spectroscopy.

UV-vis spectra of the solutions obtained by titration of up to two equivalents of copper(II) to a $\mathbf{H_4L^{ox}}$ solution have an absorption maximum at 840 nm. This absorption band was assigned to solvated copper(II), or copper(II) coordinated by a set of oxygen donor atoms. The fact that the absorption linearly increases with the copper(II) concentration and is not shifted throughout the titration strongly suggests that there is no interaction of copper(II) with the macrocycle. The CD-spectra of this titration, however, exhibit a clear change in the range of 250 to 300 nm. This region of the spectrum is correlated to the chirality of the macrocycle and can therefore provide information about its conformation (see Figure 4.34). The change of the CD spectra supports the assumption that there is an interaction of $\mathbf{H_4L^{ox}}$ with copper(II) and it is likely that copper(II) is coordinated from the "outside" of the

macrocycle, *i.e.* by the oxygen atoms of the peptide bonds, analogous to $\mathbf{H_3L^2}$ (see Section 3.2.3).

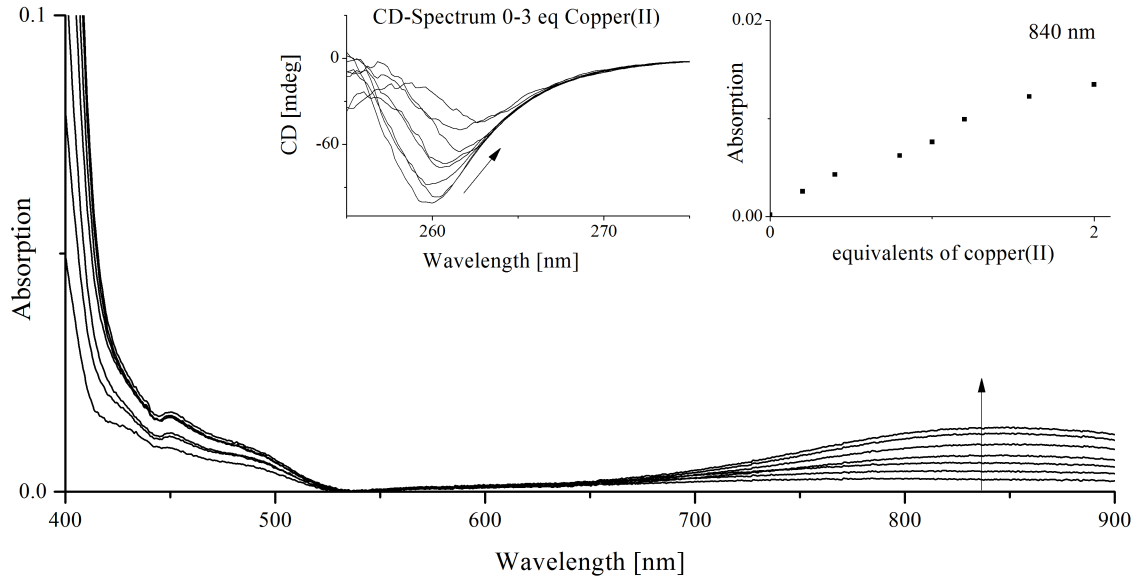

Figure 4.34. UV-vis and spectra of the titration of 0-2 eq of copper(II), in 0.2 eq steps, to a $\mathbf{H_4L^{ox}}$ solution, ($c(\mathbf{H_4L^{ox}})$ = 1.25 mM, methanol).

Even at high copper(II) concentrations, $\mathbf{H_4L^{ox}}$ solutions do not exhibit any CD spectroscopic features at wavelength higher than 300 nm, and thus an asymmetric copper(II) center can be excluded. The absence of asymmetry at the copper(II) centers is a further indicator that no coordination in the N_{het}-N_{amide}-N_{het} binding motif occurs, as this would introduce asymmetry and thus provide a CD signal. These findings further support the assumption that copper(II) is bound in an "outside coordination" mode.

The binding mode of copper(II) to $\mathbf{H_4L^{ox}}$ in absence of base was further investigated by means of ^{13}C-NMR spectroscopy. This method has provided useful insight into the copper(II) coordination chemistry of $\mathbf{H_3L^2}$ (see Chapter 3, page 38). As observed for the smaller tris-oxazole pseudo hexapeptide $\mathbf{H_3L^2}$, the addition of copper(II) gradually broadens the peak of the amide carbon C_{amide} at 164 ppm. At a $\mathbf{H_4L^{ox}}$/copper(II) ratio of 1:0.6 the signal of the C_{amide} resonance nearly vanished, which is highly suggestive of the unusual copper(II) coordination of $\mathbf{H_4L^{ox}}$ via the carbonyl oxygens (see Figure 4.35). This binding mode was further proved by EPR spectroscopy in acetonitrile (see Figure 4.40).

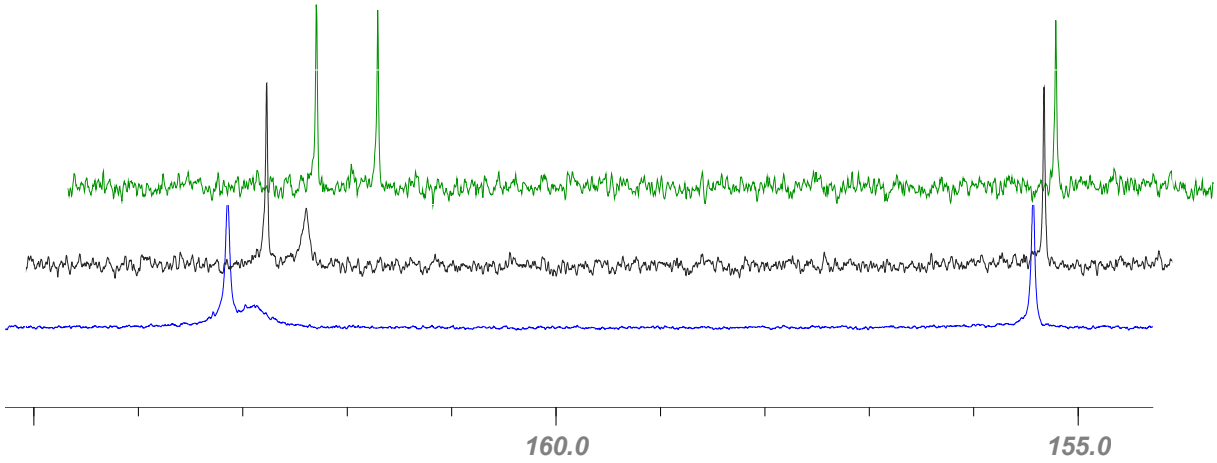

Figure 4.35. Section of interest of the ^{13}C-NMR spectra (MeOH-d_4, 50 MHz, 10 mM) of a titration of Cu^{II} to a $\mathbf{H_4L^{ox}}$ solution. 0 eq Cu^{II} (green, back); 0.3 eq Cu^{II} (black, middle); 0.6 eq Cu^{II} (blue, front). δ = 155.31 ($\underline{C}_{im}CH_3$); 163.99 ($\underline{C}_{amide}$); 164.24 ($N_{im}\underline{C}_{im}$) ppm.

Coordination of copper(II) in the N_{het}-N_{amide}-N_{het} binding motif is enabled upon addition of a strong base (methoxide) and can be followed spectroscopically. When base is added to a $\mathbf{H_4L^{ox}}$/copper(II) 1:2 solution, new bands in the visible region develop and increase in intensity up to a base concentration that corresponds to three equivalents. The absorption maximum is thereby shifted from 840 nm (solvated Cu^{II}) to 706 nm (see Figure 4.36, top). These findings can be interpreted by the formation of a dinuclear copper(II) complex. This is also reflected in the fact that the shift of the absorption band can be observed up to two equivalents of base and thereafter only an increase of the absorption band at 706 nm can be observed. In combination with the recorded ESI-MS data these findings are suggestive of the formation of a hydroxo-bridged complex, already at low base concentration. Considering the findings of the EPR experiments (see Section 4.4.3) it is likely that the absorption of the hydroxo complex is at lower wavelength and that the absorption band observed at three equivalents of base is a combination of the hydroxo complex and outside coordinated copper(II). This could also explain why the absorption maximum of the hydroxo complex of $\mathbf{H_4L^{ox}}$ has a higher wavelength than the hydroxo complexes of $\mathbf{H_4L^4}$ (λ_{max} = 674 nm) and $\mathbf{H_4L^{rs}}$ (λ_{max} = 685 nm). When more than three equivalents of base are added, the maximum of the absorption band is strongly shifted to lower wavelength (605 nm) and a shoulder at 525 nm emerges. The shift is completed after the addition of four equivalents of base, and thereafter, the observed bands slightly intensify. It is assumed that the change in the spectra is caused by the formation of the carbonato-bridged complex [$\mathbf{H_2L^{ox}}Cu^{II}_2(\mu\text{-}CO_3)$]. The shoulder

at 525 nm could not be assigned to a distinctive species yet. The formation of a dihydroxo species, as observed with $\mathbf{H_4L^4}$ (see Section 4.2) cannot be excluded.

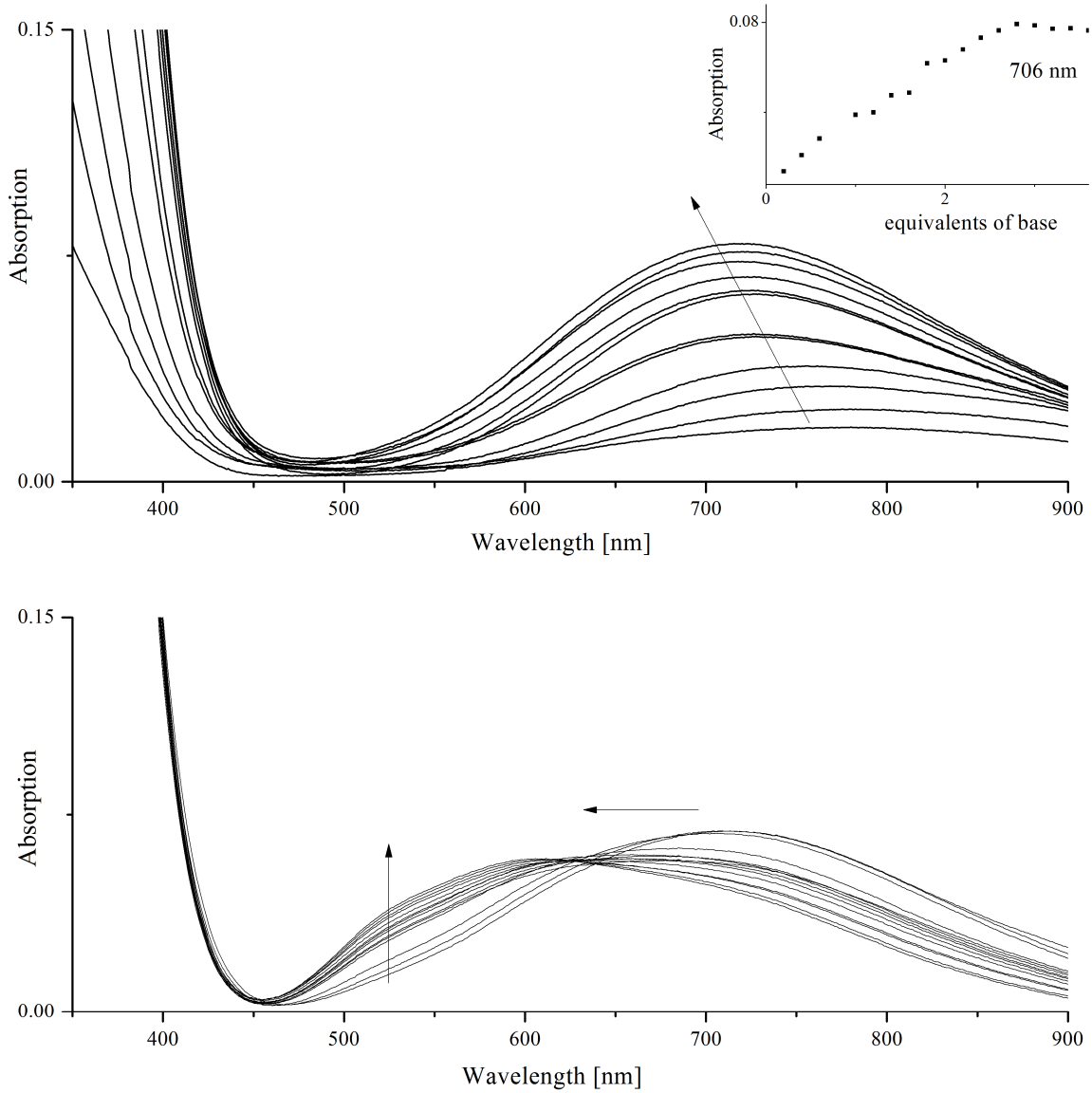

Figure 4.36. UV-vis spectra ($c(\mathbf{H_4L^{ox}})$ = 1.25mM, methanol). Titration of 0-2 eq of base (MeO^-), in 0.2 eq steps, to a $\mathbf{H_4L^{ox}}$/copper(II) 1:2 solution (top) and titration of 3-5 eq of base, in 0.2 eq steps, to a solution of $\mathbf{H_4L^{ox}}$/copper(II) 1:2 (bottom).

The observation of a CD signal is a clear indication of the development of asymmetry and, in case of the titration of copper(II) to a cyclic pseudo peptide, Cotton effects at wavelengths ≥ 400 nm are indicative of a coordination of copper(II) in the N_{het}-N_{amide}-N_{het} binding site. The CD spectra obtained by the titration of base (n-Bu_4N)(OMe) to a $\mathbf{H_4L^{ox}}$/copper(II) 1:2 solution show two positive Cotton effects at 372 and 647 nm and three

negative Cotton effects at 322, 548, and 790 nm that are separated by four isosbestic points at 341, 475, 583, and 692 nm (see Figure 4.37). The Cotton effects at wavelength ≤ 400 nm originate from the conformational change of the cyclic peptide that was induced by the binding of copper(II).

The accumulated CD spectra of a base titration to a **H_4L^{ox}**/copper(II) 1:2 solution are expected to exclusively show the asymmetry of the copper(II) centers in the dinuclear complex. Compared to the recorded CD spectra of the dinuclear copper(II) complexes of **H_4L^4** the Cotton effects are different (see Section 4.2.1). The dinuclear copper complex of **H_4L^4** has an intense negative Cotton effect at 639 nm, while the dinuclear copper(II) complexes of **H_4L^4** have a positive Cotton effect at 647 nm and an intense negative Cotton effect at 790 nm. This suggests a somewhat different coordination sphere in the complexes of the pseudo octapeptides.

Several observations were made that are suggestive of the coordination environment of the copper(II) ion not being affected by the addition of three equivalents of base. Firstly, the d-d band in the recorded UV-vis data does not shift but only intensifies, and this is mirrored in the CD spectra. However, the isosbestic point at 341 nm that was present in the spectra from the addition of the first two equivalents of base disappears and this indicates a modification of the macrocyclic peptide backbone.

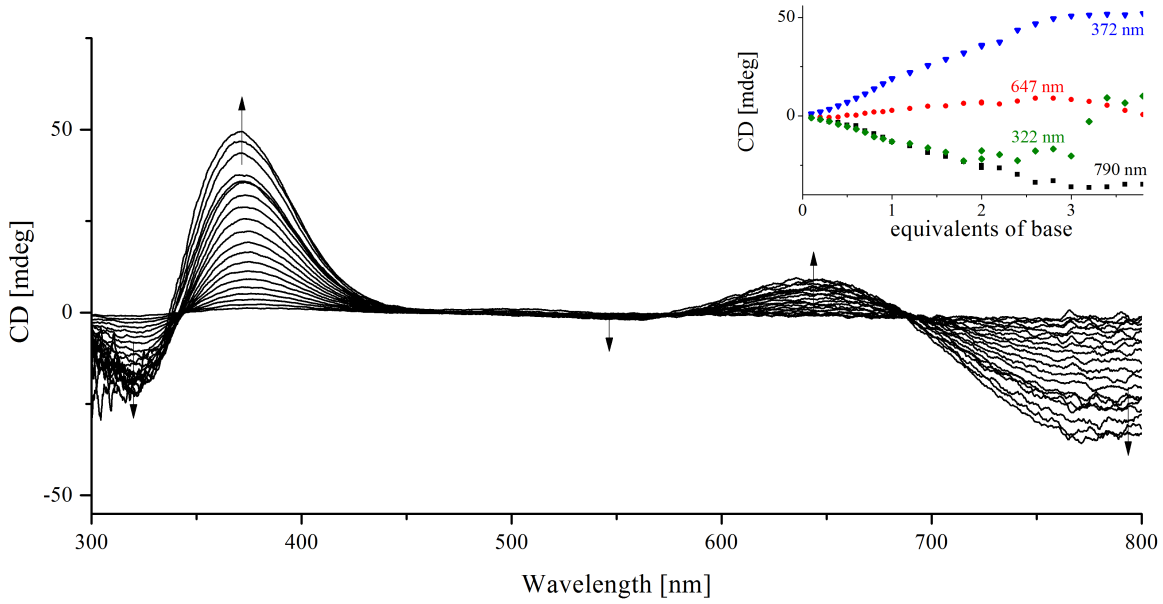

Figure 4.37. CD spectra of the titration of 0-3 eq of base (MeO^-), in 0.1 eq (0-1 eq) and 0.2 eq (1-3 eq) steps, to a **H_4L^{ox}**/copper(II) 1:2 solution (c(**H_4L^{ox}**) = 1.25 mM, methanol).

A substantial change can be observed in the CD spectra after the addition of a fourth equivalent of base (see Figure 4.38). The negative Cotton effect at 792 nm is shifted to a lower wavelength (752 nm) and the positive Cotton effects at 647 and 372 nm are shifted to 618 and 352 nm, respectively.

The spectrum now reminds of a combination of the carbonato complex of $\mathbf{H_4L^4}$ [$\mathbf{H_2L^4}Cu^{II}_2(\mu\text{-}CO_3)$] (pos. Cotton effect at 605 nm and neg. Cotton effects at 541 and 723 nm) and the pink species of $\mathbf{H_4L^4}$ (pos. Cotton effect at 536 nm and neg. Cotton effect at 715 nm, see Figure 4.13). The similarity of the spectra indicates similar coordination environments at the copper(II) centers. Thus, presumably the coordination environment in the carbonato-bridged complexes of $\mathbf{H_4L^4}$ and $\mathbf{H_4L^{ox}}$ is alike and possibly $\mathbf{H_4L^{ox}}$ also forms a species that is similar to the pink species of $\mathbf{H_4L^4}$. However, the formation of a pink species has not been observed for $\mathbf{H_4L^{ox}}$ and the positive Cotton effect at 618 nm could also result from traces of the hydroxo-bridged complex that are left in solution and hence give rise to the observed spectra.

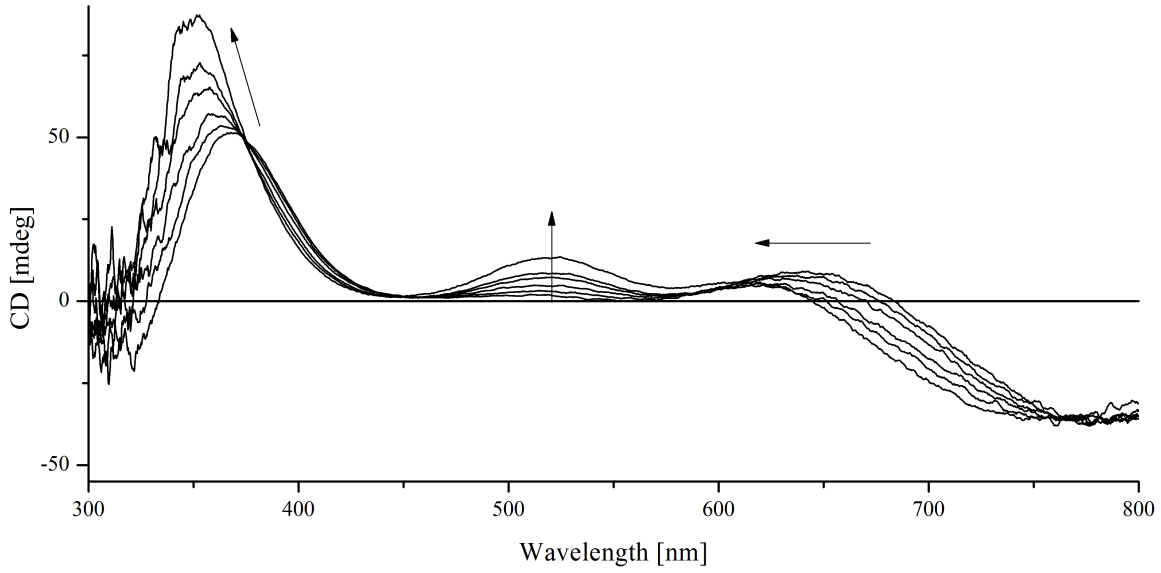

Figure 4.38. Titration of 3-4 eq of base (MeO^-), in 0.2 eq steps, to a $\mathbf{H_4L^{ox}}$/copper(II) 1:2 solution ($c(\mathbf{H_4L^{ox}})$ = 1.25 mM, methanol).

When more than four equivalents of base are added, no further change in the UV-vis or the CD spectra can be observed. The intensity of the CD spectra does intensify, but this is most likely due to the formation of carbonato-bridged complexes [$\mathbf{H_2L^{ox}}Cu^{II}_2(\mu\text{-}CO_3)$], as the experiments have not been performed anaerobically.

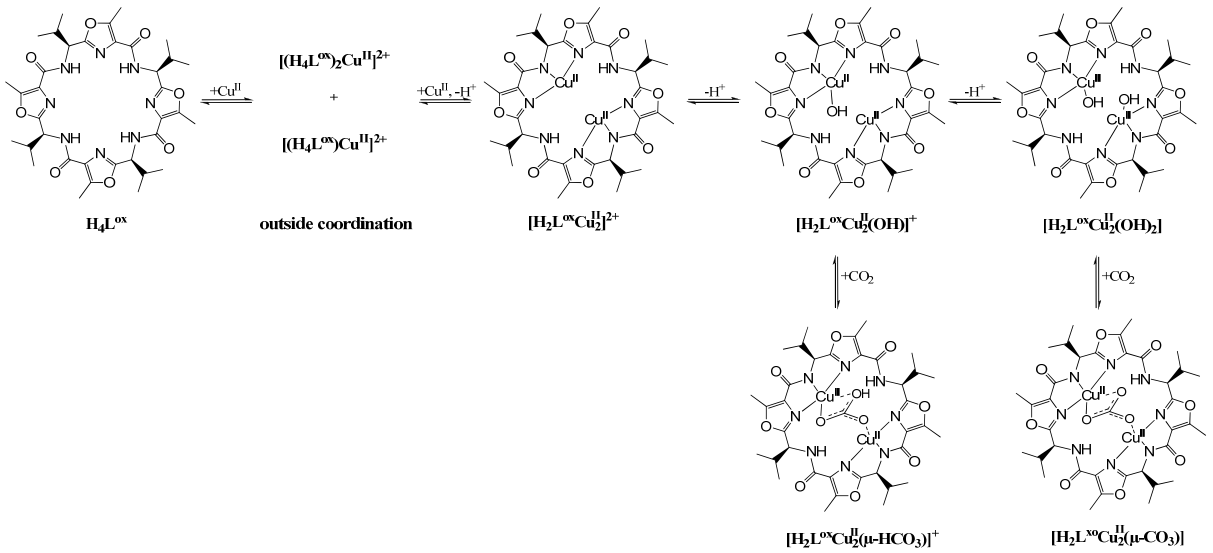

Figure 4.39. Assumed copper(II) complexation equilibria of $\mathbf{H_4L^{ox}}$.

From the performed experimental results the following equilibrium is concluded (see Figure 4.39): in a first complexation step, copper(II) is bound to the cyclic pseudo peptide from the outside, coordinated by the carbonyl oxygen atoms (see also coordination of $\mathbf{H_3L^2}$, Chapter 3). Addition of base then deprotonates the amide nitrogens and enables the coordination of copper(II) in the "normal" N_{het}-N_{amide}-N_{het} binding site of the cyclic pseudo peptide. The fact that the mononuclear complex $[\mathbf{H_3L^{ox}}Cu^{II}]^+$ could only be detected in traces, indicates preorganizational preference for dinuclear complexes and a cooperative effect. In presence of CO_2, a bridged carbonato complex $[\mathbf{H_2L^{ox}}Cu^{II}_2(\mu\text{-}CO_3)]$ was formed, similar to the one observed for $\mathbf{H_4L^4}$ $[\mathbf{H_2L^4}Cu^{II}_2(\mu\text{-}CO_3)]$.

4.4.3 EPR Experiments

To probe the putative complexation equilibria, the EPR spectra of representative solutions were measured. In contrast to $\mathbf{H_4L^{rs}}$, $\mathbf{H_4L^4}$, and the smaller cyclic pseudo hexapeptides $\mathbf{H_3L^{1\text{-}3}}$ and $\mathbf{H_3L^{wa}}$ the amount of mononuclear copper(II) complex formed was small. In the ESI-MS experiments traces of a mononuclear copper(II) complex $[\mathbf{H_3L^{ox}}Cu^{II}]^+$ could be detected. Careful subtraction of different dinuclear compounds provided a very weak signal attributable to a mononuclear copper(II) complex $[\mathbf{H_3L^{ox}}Cu^{II}]^+$ (see Figure 4.40 left). However, considering the low signal intensity both in the ESI-MS spectra and in the EPR spectra, it is assumed

that the mononuclear complex is not important in the copper(II) coordination chemistry of $\mathbf{H_4L^{ox}}$.

The signal of the mononuclear copper(II) complex $[\mathbf{H_3L^{ox}}Cu^{II}]^+$ that could be obtained from spectra subtraction and its simulation are shown in Figure 4.40. The spectrum was simulated with the program package X-Sophe-Sophe-XeprView[122] (version 1.1.4), using the spin Hamiltonian described in Eq. 3.7. Unfortunately, the spectrum has a very low resolution and it was not possible to extract the superhyperfine coupling constants to the remote nitrogen atoms. The spin Hamiltonian parameters are in the expected range ($g_{x,y,z}$ = 2.085, 2.065, 2.256; $A_{x,y,z}$ = 20, 20, 163 · 10^{-4} cm^{-1}) of a distorted square pyramidal copper(II) center coordinated in the N_{het}-N_{amide}-N_{het} binding motif of a cyclic pseudo peptide and are comparable to those of the mononuclear copper(II) complexes of $\mathbf{H_4L^4}$ ($g_{x,y,z}$ = 2.090, 2.050, 2.261; $A_{x,y,z}$ = 14, 15, 169 · 10^{-4} cm^{-1}) and of the dinuclear bridged complexes of $\mathbf{H_4L^{rs}}$ that have a "mononuclear" EPR spectrum as result of their magic angle set up (see Table 4.9). A summary of all measured and simulated mononuclear EPR spectra is given in Table 4.15, page 134.

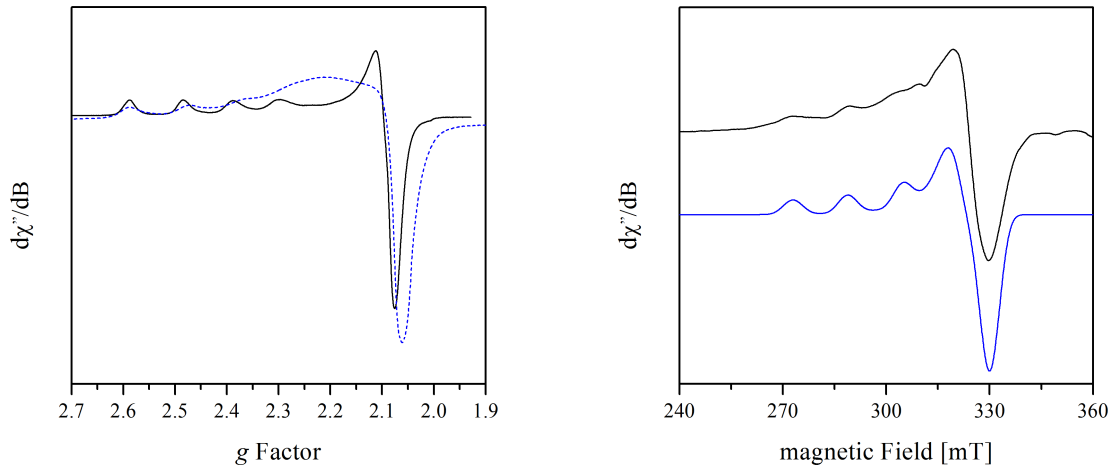

Figure 4.40. Experimental X-Band EPR spectra (*g*-space), acetonitrile, 50K of "free" copper(II) (black), ν = 9.445932 GHz and copper(II) coordinated to $\mathbf{H_4L^{ox}}$ from the "outside" (blue, dotted line), ν = 9.421455 GHz (left) and experimental (black) and simulated (blue) X-Band EPR spectrum of the mononuclear copper(II) complex $[\mathbf{H_3L^{ox}}Cu^{II}]^+$, derived from spectra subtraction (right).

In absence of base, the measured EPR spectra in methanol are identical to those of "free" copper(II), $[Cu^{II}(MeOH)_n]^{2+}$ (see Figure 4.41 a). As discussed in Section 3.2.4, it is not possible to distinguish between methanol solvated copper(II) and copper(II) that is bound in

an external fashion to the cyclic peptides in an EPR experiment. However, copper(II) that is dissolved in acetonitrile $[Cu^{II}(CH_3CN)_n]^{2+}$ has different *g* and *A* tensors than copper(II) that is coordinated to $\mathbf{H_4L^{ox}}$ in an outside fashion, as it is not coordinated by oxygen atoms. Indeed when the spectra of "free" copper(II) in acetonitrile are compared to those of a copper(II) solution that contains $\mathbf{H_4L^{ox}}$ a clear shift of the *g* factors can be observed. For a better comparability, the spectra were converted to the *g* space (see Figure 4.40). The low resolution of the acetonitrile spectrum that contains $\mathbf{H_4L^{ox}}$ was presumably caused by a bad glass. Furthermore it is likely that in solution there is an equilibrium between copper(II) coordinated by acetonitrile and copper(II) coordinated to $\mathbf{H_4L^{ox}}$ in an outside fashion and the overlapping spectra are expected to further decrease the resolution.

Addition of base, to methanolic $\mathbf{H_4L^{ox}}$ solutions, causes the coordination of copper(II) to the binding site of $\mathbf{H_4L^{ox}}$ and changes the EPR spectrum. However, in contrast to the other cyclic pseudo peptides, at two equivalents of base there is still a considerable amount of outside coordinated copper(II) present in solution (see Figure 4.41 b). This observation is suggestive of a high stability of the outside coordinated complex $[(\mathbf{H_4L^{ox}})_2Cu^{II}]^{2+}$ at moderate base concentrations, possibly in the range of the mononuclear complex $[\mathbf{H_3L^{ox}}Cu^{II}]^{+}$ or even higher. In absence of base it seems that the outside coordinated copper(II) complex has a higher stability than the mononuclear complex, as no coordination in the macrocycle could be seen, neither in the ESI-MS, nor in the UV-vis, CD or EPR spectra. The electronic influence of the incorporated heterocycles have been discussed in Section 1.3 and it is likely that this also influences the basicity of the amide protons what would subsequently influence the metal assisted deprotonation of the binding site. At higher base concentrations, the spectra seem to be a combination of outside coordinated copper(II) and dinuclear complex, indicating a strong complementary effect of the macrocycle and a decrease in stability of the outside coordinated complex. More likely than the decreased stability of the outside coordinated complex, however, is an increase of the stabilities of the N_{het}-N_{amide}-N_{het} binding site coordinated copper(II) complexes, as these are expected to strongly depend on the degree of deprotonation of the N_{amide} atom. As a result of the strong complementary effect the formation of the monomer complex could not be observed directly but only by spectra subtraction (see also Figure 4.40). Supportive of a high stability of the outside coordinated complex is the fact, that even at three equivalents of base, still minor amounts of outside coordinated copper(II) are observable in the spectra (see Figure 4.41 d). When four equivalents of base are present in solution a coordination via the outside cannot be observed anymore and the observed EPR spectra correspond to dinuclear copper(II) species (see Figure 4.41 e). Whether these spectra

show the hydroxo-bridged or possibly a dihydroxo species could not be determined yet. The addition of more than four equivalents of base does not lead to a further change in the spectra. They are equivalent to those recorded at a $\mathbf{H_4L^{ox}}$/copper/base ratio of 1:2:4 (see Figure 4.41 e and f).

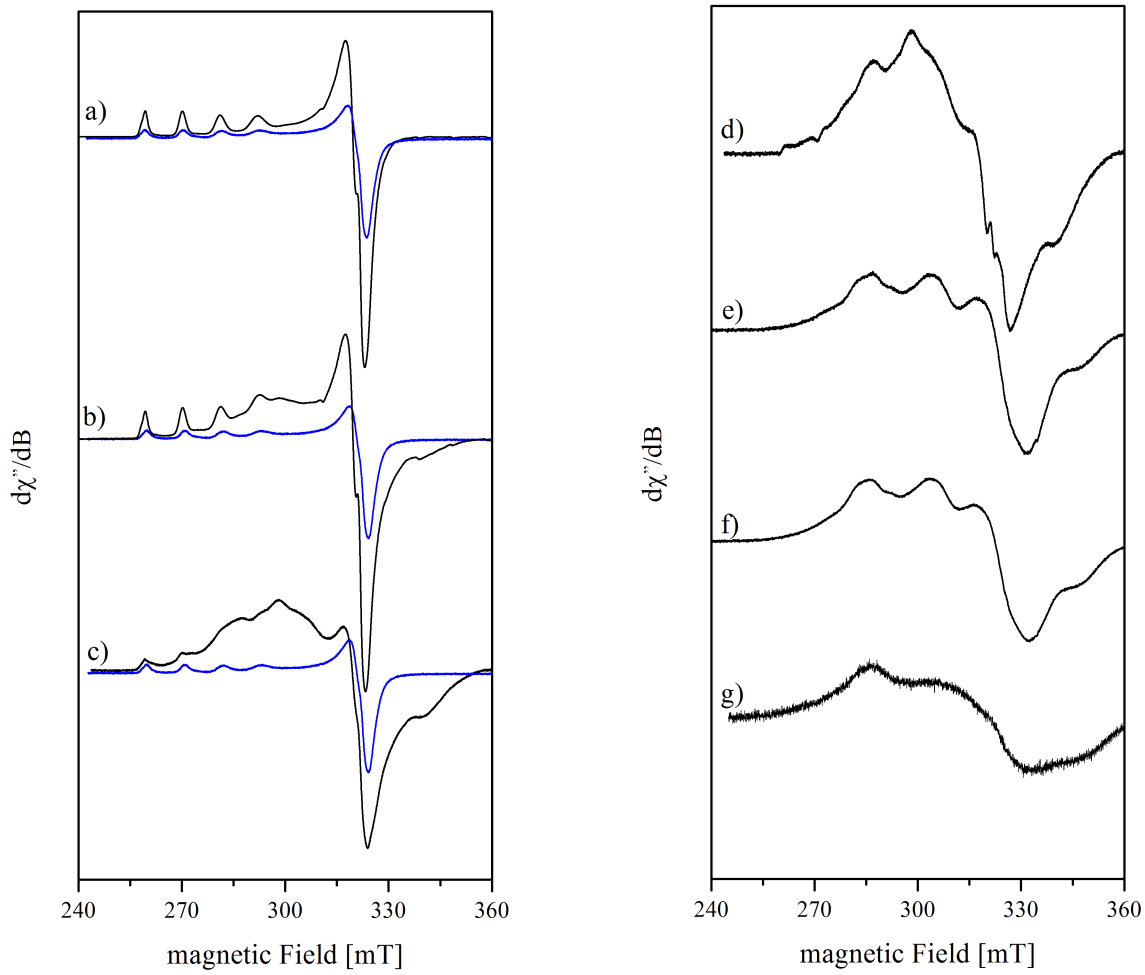

Figure 4.41. Experimental X-Band EPR spectra, methanol $c(\mathbf{H_4L^{ox}})$ = 1.25mM, T = 10 K, free Cu^{II} (blue, ν = 9.429674). **a)** $\mathbf{H_4L^{ox}}$/copper(II)/base 1:2:0, ν = 9.375956 GHz; **b)** $\mathbf{H_4L^{ox}}$/copper(II)/base 1:2:2, ν = 9.375771 GHz; **c)** $\mathbf{H_4L^{ox}}$/copper(II)/base 1:2:3, ν = 9.374496 GHz; **d)** $[\mathbf{H_2L^{ox}}Cu^{II}_2(OH)]^+$ obtained from spectra subtraction of free copper and *c)*; **e)** $\mathbf{H_4L^{ox}}$/copper(II)/base 1:2:4, ν = 9.380499 GHz; **f)** $\mathbf{H_4L^{ox}}$/copper(II)/base 1:2:5, ν = 9.379982 GHz **g)** $\mathbf{H_4L^{ox}}$/copper(II)/base 1:2:2, carbonate added, presumably the carbonato-bridged complex $[\mathbf{H_2L^{ox}}Cu^{II}_2(\mu\text{-}CO_3)]$, ν = 9.426234 GHz

The EPR spectra of solutions with a $\mathbf{H_4L^{ox}}$/copper(II)/base ratio of 1:2:3 or higher show a time-dependent conversion to the spectrum of the carbonato-bridged complex (see Figure 4.41 g). This spectrum can also be obtained when carbonate is added to a solution of $\mathbf{H_4L^{ox}}$/copper(II)/base in a ratio of 1:2:2. These spectra are very similar to the one of the

carbonato-bridged complex of $\mathbf{H_4L^4}$ [$\mathbf{H_2L^4}Cu^{II}_2(\mu\text{-}CO_3)$] (see Figure 4.14 d). Considering the structural likeness of the cyclic pseudo peptides it is feasible, that the carbonate complexes have a similar coordination sphere, an assumption that is supported by the performed DFT calculations (see Section 4.4.4)

A satisfactory simulation of the dinuclear copper(II) complexes of $\mathbf{H_4L^{ox}}$ could not be obtained so far. The EPR spectra are suggestive of a stable outside coordinated complex $[(\mathbf{H_4L^{ox}})_2Cu^{II}]^{2+}$ that is present in solutions that contain up to three equivalents of base. Furthermore, $\mathbf{H_4L^{ox}}$ shows a high cooperativity and the stability of the formed dinuclear complexes seems to strongly depend on the degree of deprotonation of the macrocycle. The mononuclear copper(II) complex $[\mathbf{H_3L^{ox}}Cu^{II}]^{+}$ could only be detected after spectra subtraction and this emphasizes the strong cooperative effect. The dinuclear copper(II) complexes show a fast conversion to the carbonato-bridged complex $[\mathbf{H_2L^{ox}}Cu^{II}_2(\mu\text{-}CO_3)]$.

4.4.4 DFT Calculations

The DFT calculations of cyclic pseudo octapeptides are quite time consuming. Therefore, not all geometry optimizations were finished by the time this thesis was written. Structures of the outside coordinated complexes have not been calculated due to their immense computational costs.

The experimental results, especially the fact that the mononuclear copper(II) complex of $\mathbf{H_4L^{ox}}$, *i.e.* $[\mathbf{H_3L^{ox}}Cu^{II}]^{+}$ could only be detected in traces are suggestive of a complementary effect of $\mathbf{H_4L^{ox}}$. Complementarity could also be observed for the cyclic pseudo hexapeptide $\mathbf{H_3L^2}$ (see Section 3.2.2), the pseudo octapeptide $\mathbf{H_4L^4}$ and was reported previously for some of the natural cyclic pseudo peptides.[103, 167] These findings were reproduced by the performed DFT calculations of the copper(II) complexes of $\mathbf{H_4L^{ox}}$ (G09, B3LYP/6-31g* (C,H,N,O)/ TZVP (Cu)). When the structures of the mono-, and the dinuclear copper(II) complexes of $\mathbf{H_4L^{ox}}$, $[\mathbf{H_3L^{ox}}Cu^{II}(H_2O)_2]^{+}$ and $[\mathbf{H_2L^{ox}}Cu^{II}_2(H_2O)_3]^{2+}$, are compared, it emerges that the coordination of the first copper(II) ion leads to a substantial reorganization of the macrocycle, while the coordination of the second copper hardly leads to any change. An overlay plot of the

mono- and the dinuclear complex is depicted in Figure 4.42, the structural parameters are given in Table 4.13.

In the mononuclear complex, the coordination sphere of copper(II) was completed by two water molecules and a square pyramidal coordination polyhedron of copper(II) is adopted in the optimized structure, consistent with the recorded and simulated EPR spectrum. Interestingly, the adopted conformation of the macrocycle in the mononuclear complex is nearly identical to that of $\mathbf{H_4L^4}$ and this is reflected in the nearly identical EPR spin Hamiltonian parameters of the two complexes (see page 119). The high stability of the outside coordinated copper(II) complexes of $\mathbf{H_4L^{ox}}$ suggests that possibly another conformation of the macrocycle might be important, as an outside coordination could not be observed for other C_4-symmetric pseudo peptides. Potentially, it is similar to the one adopted in the solid state of $\mathbf{H_4L^{ox}}$, where two oxazole rings are oriented in a parallel fashion (see Figure 4.7). The NMR spectra strongly indicate a C_4-symmetric conformation in solution and this contradicts the idea that a different folding of the macrocycle is important for the formation of an outside coordinated complex. Thus, it is assumed that the outside coordination might be correlated to electronic effects as the electronics in imidazole and oxazole rings are known to be different and thus influence the macrocycle in a different way (see Section 1.3). The fact the an outside coordination could neither be observed with one of the imidazole containing pseudo peptides nor with the thiazole and oxazoline containing $\mathbf{H_4L^{ascA}}$ (see Section 4.5) emphasizes the importance of oxazole rings for the outside coordination.

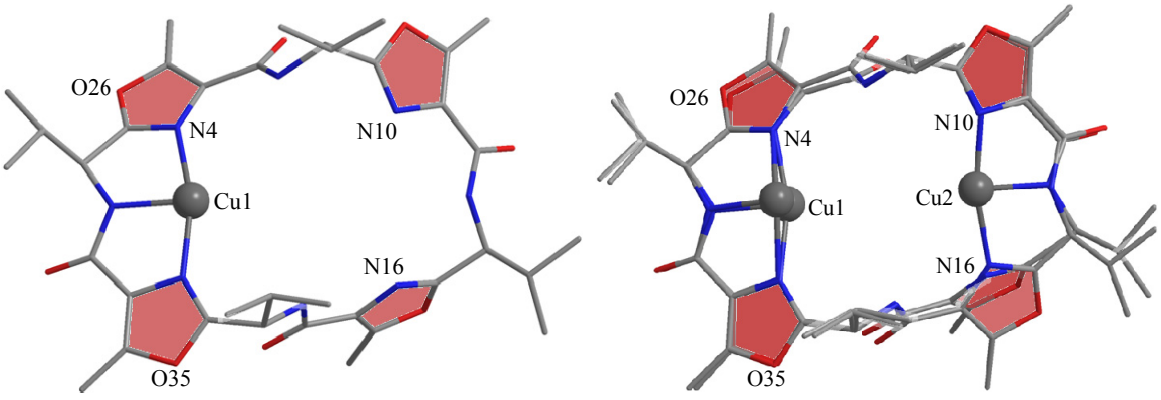

Figure 4.42. Top view of the DFT calculated structure of $[\mathbf{H_3L^{ox}}Cu^{II}]^+$ (left) and of the overlay plot of the DFT calculated structures of the mono- and dinuclear copper(II) complex of $\mathbf{H_4L^{ox}}$ $[\mathbf{H_3L^{ox}}Cu^{II}]^+$ and $[\mathbf{H_2L^{ox}}Cu^{II}_2]^{2+}$, respectively. Hydrogen atoms and solvent molecules are omitted for clarity.

Table 4.13. Selected angles and distances of the DFT [a] optimized structures of the copper(II) complexes of $\mathbf{H_4L^{ox}}$.

	$[\mathbf{H_3L^{ox}}Cu^{II}(H_2O)_2]^+$	$[\mathbf{H_2L^{ox}}Cu^{II}_2(H_2O)_3]^{2+}$	$[\mathbf{H_2L^{ox}}Cu^{II}_2(OH)]^+$	$[\mathbf{H_2L^{ox}}Cu^{II}_2(OH)_2]$	$[\mathbf{H_2L^{ox}}Cu^{II}_2(\mu\text{-}CO_3)]$
α [N4-N10-N16-N22] [b]	25	17	14	18	10
β [N35–N22–N10–N29], [N26–N4–N16–N32] [b]	0/3	0/5	3/3	5/0	11/4
∠ (Cu1-O1-Cu2)	-	164	122	157/107	-
ρ					
N1-N13/N7-N19	8.83/5.76	8.90/5.84	9.10/5.95	8.72/6.31	8.89/6.41
N22-N4/N4-N10/N10-N16/N16-N22	4.13/ 5.45/4.13/5.47	4.06/5.56/4.02/5.53	4.05/5.63/4.18/5.83	4.29/5.73/4.37/5.50	4.30/5.88/4.71/5.77
N4-N16/N10-N22	6.73/6.89	6.66/6.86	7.09/6.88	7.21/6.83	6.91/7.73
Cu1-Cu2	-	5.25	5.41	5.14	5.18
Cu1-O1/Cu2-O1	2.03	2.05/3.24	1.91/4.14	1.84/3.38	-
Cu1-O2/Cu2-O2	2.37	4.06/2.36	5.79/2.32	4.23/1.86	-
Cu1-O3/Cu2-O3	-	4.31/3.36	3.45/2.07	-	-
$Cu1\text{-}N_{het}/N_{amide}/N_{het}$	2.08/1.95/2.07	2.05/1.94/2.04	2.10/1.93/2.10	2.17/1.90/2.17	2.17/1.93/2.19
$Cu2\text{-}N_{het}/N_{amide}/N_{het}$	-	2.06/1.93/2.05	2.10/1.93/2.13	2.18/1.95/2.30	2.19/1.96/2.69
Cu^{II} coordination sphere	distorted square pyramidal	distorted square planar/ distorted tetragonal	distorted square pyramidal	distorted square planar/ distorted tetragonal	distorted square planer/ distorted tetragonal

Units: d [Å] ∠ [°] a) G09, B3LYP/6-31g* (C,H,N,O)/TZVP (Cu); b) see Figure 4.4 for atom numbers.

For the dinuclear copper(II) complexes, the dihydroxo complex was calculated. This complex could not be seen in the ESI-MS spectra, the UV-vis spectra and especially the CD spectra at four equivalents of base are very similar to those of **H_4L^4** (see Section 4.2.1). This indicates that possibly **H_4L^{ox}** also forms a dihydroxo species. The calculated dinuclear complexes of **H_4L^{ox}** were found to have a nearly identical conformation of the macrocycle as the respective complexes of **H_4L^4** (see Appendix I for overlay plots). It is hard to compare the EPR spectra as the resolution in the recorded spectra of **H_4L^{ox}** unfortunately is quite low and the presence of the outside coordinated copper(II) complex complicates the interpretation. The copper-copper distances in the calculated dinuclear complexes range from 5.14 Å in the dihydroxo complex to 5.41 Å in the terminal hydroxo complex. Interestingly, in the dihydroxo and in the carbonato-bridged complex one of the Cu2-N_{het} bonds is elongated. This effect is larger in the carbonato-bridged complex and has also been observed for the carbonato-bridged complex of **H_4L^4**.

The DFT calculations suggest that in presence of base, the copper(II) coordination chemistry and the formed complexes of **H_4L^{ox}** are nearly identical to those of **H_4L^4**.

The cyclic pseudo octapeptide **H_4L^{ox}** was expected to have a similar coordination chemistry as **H_4L^4**. However, it was found that at low base concentrations **H_4L^{ox}** preferably coordinates copper(II) from the outside of the macrocycle, thereby forming unusual complexes with a **H_4L^{ox}**/copper(II) 2:1 ratio. Yet, at high base concentrations the coordination chemistry was found to be very similar to that of **H_4L^4** and the natural cyclic pseudo peptides. **H_4L^{ox}** is preorganized for the coordination of copper(II), shows a cooperative effect and readily reacts with CO_2 to the corresponding stable carbonato-bridged complexes. Indications for the existence of the equivalent of the pink species of **H_4L^4** were found, but could not be definitely identified. **H_4L^{ox}** seems to be a potential model system for natural cyclic peptides, however only at high base concentrations. It is worth testing if the reaction of **H_4L^{ox}** with CO_2 is catalytic in contrast to the reaction of the dinuclear copper(II) complexes of **H_4L^4** with CO_2.

4.5 Copper(II) Coordination Chemistry of H_4L^{ascA}

4.5.1 ESI-MS Experiments

$\mathbf{H_4L^{ascA}}$ is nearly identical to the natural cyclic pseudo octapeptide ascidiacyclamide. The only difference is the *L*-amino acid, that links the thiazole and the oxazoline unit. In the natural cyclic peptide, the linking *L*-amino acid is isoleucine while in the synthetic cyclic peptide $\mathbf{H_4L^{ascA}}$ the heterocycles are linked by *L*-valine (see Figure 4.43). Both cyclic pseudo octapeptides have two different N_{het}-N_{amide}-N_{het} binding sites (TAO, see Figure 4.43), that differ in the configuration at C_α and in case of ascidiacyclamide additionally in the amino acid residue. Two different binding sites were also present in $\mathbf{H_4L^{rs}}$. However, unlike $\mathbf{H_4L^{rs}}$ the binding sites of $\mathbf{H_4L^{ascA}}$ and ascidiacyclamide are not enantiomeric. This is a result of the additional stereogenic centers that are induced by the oxazoline rings. From previous studies it is known that ascidiacyclamide has a high cooperativity and this is also expected for $\mathbf{H_4L^{ascA}}$.[167]

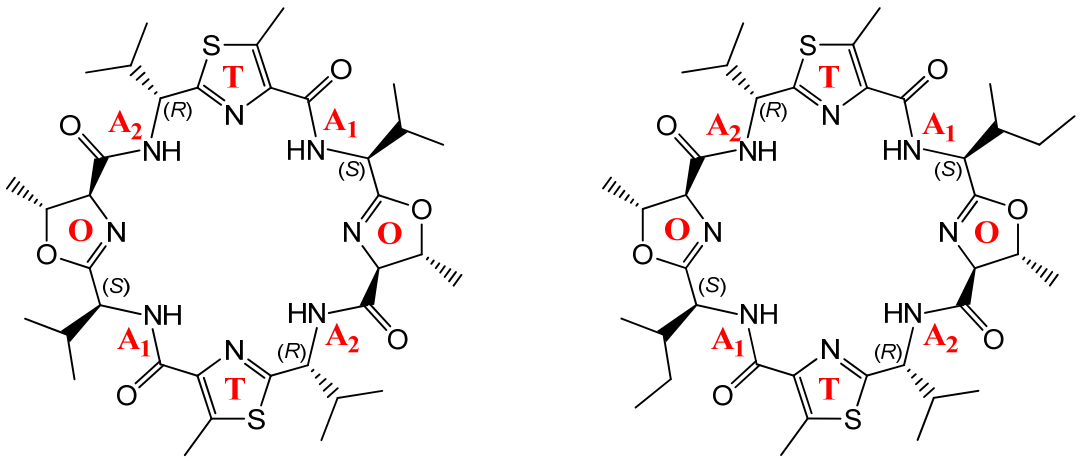

Figure 4.43. Chemical structure and binding sites of $\mathbf{H_4L^{ascA}}$ (left) and ascidiacyclamide (right). A = amide-, T = thiazole-, O = oxazoline nitrogen atom.

The ESI-MS experiments with various ratios of $\mathbf{H_4L^{ascA}}$/copper(II)/base revealed that the copper(II) coordination chemistry of $\mathbf{H_4L^{ascA}}$ is similar to that of $\mathbf{H_4L^4}$. An outside co-ordination, as it was found for the oxazole containing macrocycles $\mathbf{H_4L^{ox}}$ and $\mathbf{H_3L^2}$, could not be observed (see Section 4.4 and Section 3.2.3, respectively). The representative species present in methanolic solutions of $\mathbf{H_4L^{ascA}}$ are listed in Table 4.14. A high amount of

methoxide bridged dinuclear complex was detected, *i.e.* $[\mathbf{H_2L^{ascA}}Cu^{II}_2(\mu\text{-OMe})]^+$. The methoxide is sterically more demanding than hydroxide and this indicates that the macrocyclic backbone of $\mathbf{H_4L^{ascA}}$ is more flexible than the one of the far studied macrocycles. The higher flexibility is caused by the incorporation of oxazoline rings that, in contrast to the imidazole and oxazole rings of the other studied macrocycles include a single bond that enlarges the flexibility of the macrocycle. Solutions that contain the hydroxo complex $[\mathbf{H_2L^{ascA}}Cu^{II}_2(OH)]^+$ show a time-dependent conversion of the hydroxo complex to the (bi)carbonato-bridged complexes $[\mathbf{H_2L^{ascA}}Cu^{II}_2(\mu\text{-}HCO_3)]^+$ and $[\mathbf{H_2L^{ascA}}Cu^{II}_2(\mu\text{-}CO_3)]$. Addition of carbonate to dinuclear complex solutions also leads to the formation of carbonato-bridged complexes. Indications for the formation of a non-charged species, such as the dihydroxo complex seen with $\mathbf{H_4L^4}$ (see Section 4.2.1 and Section 4.3.1) have not been observed but cannot be excluded.

Table 4.14: Molecular formula, experimental and calculated masses of the observed mono- and dinuclear copper(II) complexes of $\mathbf{H_4L^{ascA}}$.

species	molecular formula	experimental	calculated
$[\mathbf{H_5L^{ascA}}]^+$	$C_{36}H_{53}N_8O_6S_2^+$	757.35423	757.3524
$[\mathbf{H_4L^{ascA}}Na]^+$	$C_{36}H_{52}N_8O_6S_2Na^+$	779.33460	779.33434
$[\mathbf{H_3L^{ascA}}Cu^{II}]^+$	$C_{36}H_{51}CuN_8O_6S_2^+$	818.26756	818.26635
$[\mathbf{H_3L^{ascA}}Cu^{II}(OH_2)]^+$	$C_{36}H_{53}CuN_8O_7S_2^+$	836.26228	836.267291
$[\mathbf{H_2L^{ascA}}Cu^{II}_2(OH)]^+$	$C_{36}H_{51}Cu_2N_8O_7S_2^+$	897.18972	897.19087
$[\mathbf{H_2L^{ascA}}Cu^{II}_2(\mu\text{-OMe})]^+$	$C_{37}H_{53}Cu_2N_8O_7S_2^+$	911.20586	911.20652
$[\mathbf{H_2L^{ascA}}Cu^{II}_2(\mu\text{-}HCO_3)]^+$	$C_{37}H_{51}Cu_2N_8O_9S_2^+$	941.18131	941.18070
$[\mathbf{H_2L^{ascA}}Cu^{II}_2(CO_3)Na]^+$	$C_{37}H_{50}Cu_2N_8NaO_9S_2^+$	963.16386	963.16264

From the ESI-MS experiments the copper(II) complexation equilibria depicted in Figure 4.44 are assumed. Addition of copper(II) to a solution of $\mathbf{H_4L^{ascA}}$ leads to the formation of mono- and dinuclear complexes. The fact that dinuclear complexes can be observed in absence of base highlights the high cooperativity of $\mathbf{H_4L^{ascA}}$. Again the addition of base is mandatory to obtain a complete complexation of copper(II) to the cyclic pseudo peptide. When three equivalents of base are added the dominating signals are those of the hydroxo complex, $[\mathbf{H_2L^{ascA}}Cu^{II}_2(OH)]^+$, and the methoxide bridged complex $[\mathbf{H_2L^{ascA}}Cu^{II}_2(\mu\text{-OMe})]^+$. The hydroxo complex is presumably able to react with atmospheric CO_2 to the carbonato-

bridged complex, indicating that the role of the cyclic pseudo octapeptides in the *ascidian's* metabolism might indeed be correlated to the capture of CO_2. A reaction of the methoxide bridged complex with CO_2 could not be observed.

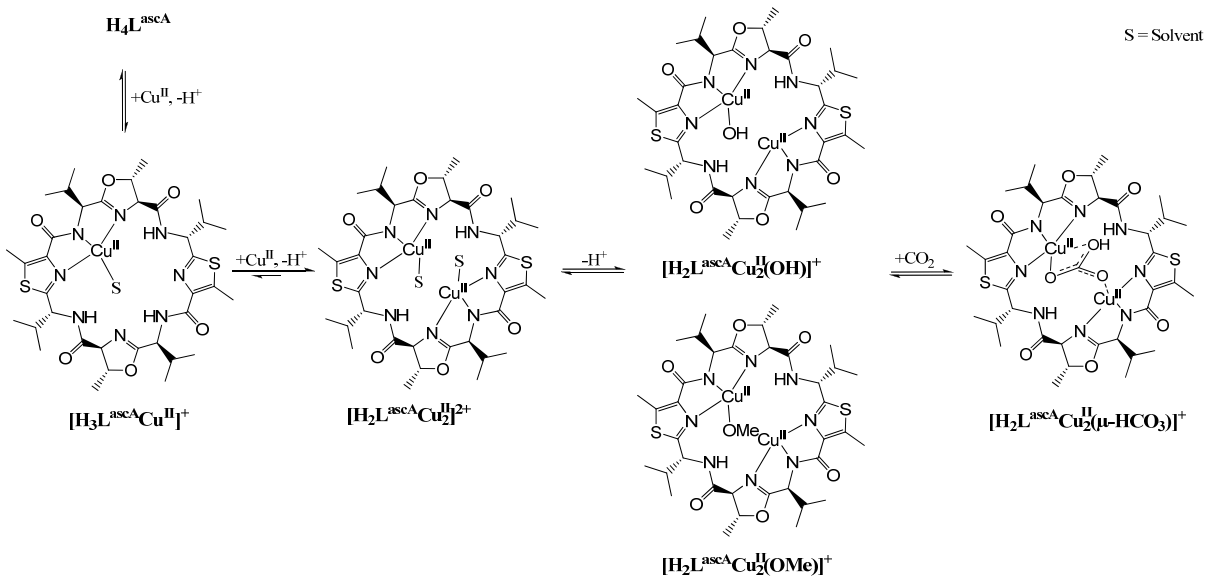

Figure 4.44. Assumed copper(II) complexation equilibria of $\mathbf{H_4L^{ascA}}$ (solvent = methanol).

4.5.2 CD and UV-vis Spectroscopy

The copper(II) coordination to $\mathbf{H_4L^{ascA}}$ can nicely be followed by CD- and UV-vis spectroscopy. The UV-vis spectra of a titration of up to two equivalents of copper(II) to a $\mathbf{H_4L^{ascA}}$ solution show an absorption band at 686 nm that shifts to 666 nm during the titration (see Figure 4.45). This is a clear indication for the coordination of copper(II) to the binding motif of $\mathbf{H_4L^{ascA}}$. The observed absorption maximum is similar to those of the dinuclear copper(II) complexes of $\mathbf{H_4L^4}$ (λ_{max} = 674 nm) and $\mathbf{H_4L^{rs}}$ (λ_{max} = 685 nm). A deviation is expected as $\mathbf{H_4L^{ascA}}$ is the only ligand that also forms methoxide bridged complexes. In the CD spectra the formation of Cotton effects in the range ≥ 400 nm further supports a coordination of copper(II) in the binding site. The negative Cotton effect at 314 nm and the positive Cotton effect at 380 nm reflect the conformational change in the macrocycle backbone that occurs upon coordination of copper(II) to the binding site.

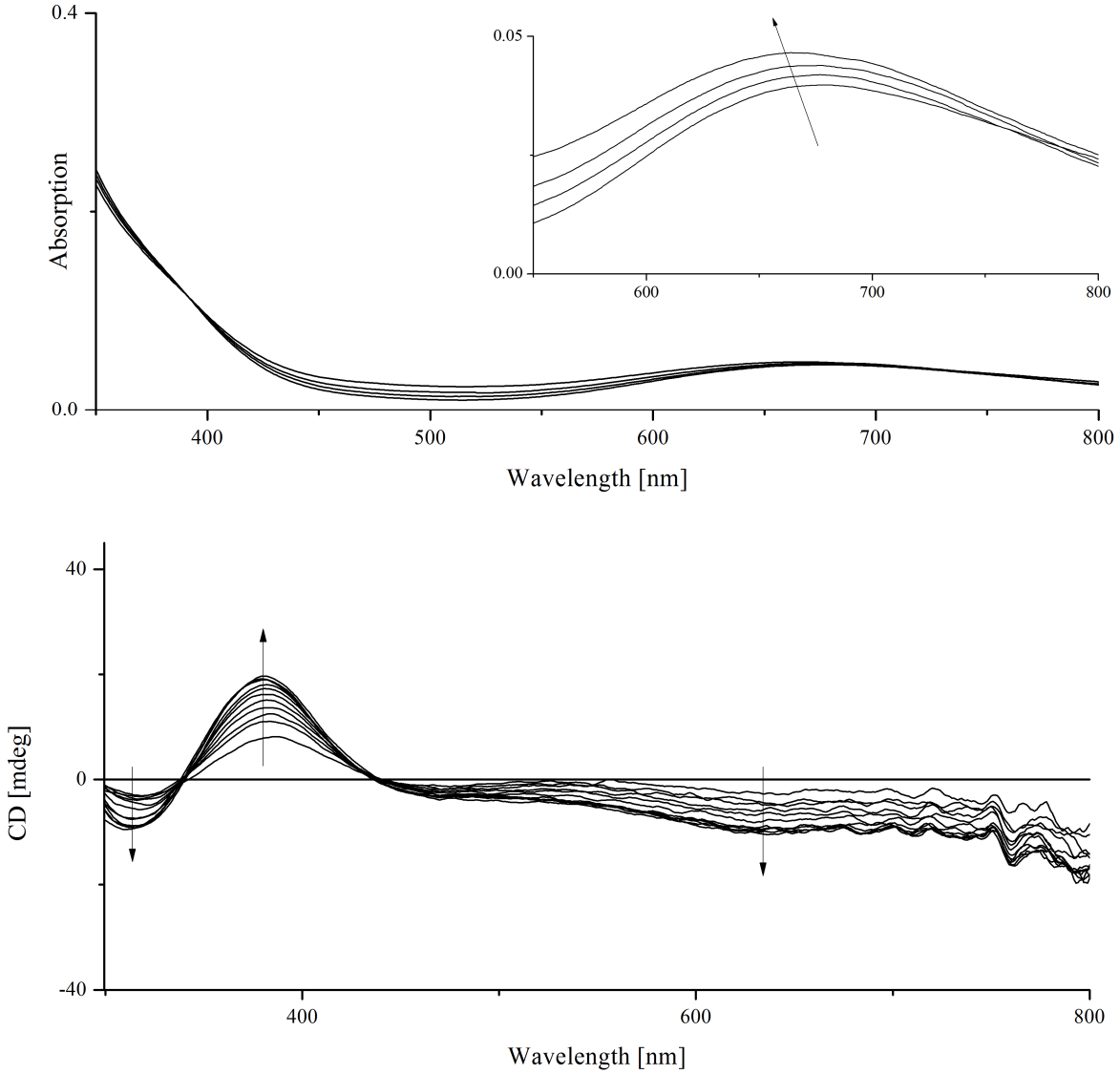

Figure 4.45. UV-vis (top) and CD titration (bottom) of 0-2 eq of copper(II), in 0.2 eq steps, to a solution of $\mathbf{H_4L^{ascA}}$.

Addition of base leads to an increase of the observed absorptions in the CD and UV-vis spectra. Up to one equivalent of base, the bands in the UV-vis spectrum linearly increase. Thereafter, the absorption maximum is shifted to a higher wavelength (703 nm, see Figure 4.46 top). Possibly this is the effect of an increased amount of the methoxide bridged complex. The negative Cotton effect at ~650 nm increases in intensity up to one equivalent of copper and stays constant after that. The fact that it is not shifted during the titration, indicates a similar or identical coordination sphere in the mono- and dinuclear copper(II) complexes. The positive Cotton effect at 379 nm increases in intensity up to one equivalent of base and decreases in intensity from one to two equivalents of base. This suggests an ongoing change

in the macrocyclic backbone during the formation of the complexes. However, this does not seem to effect the coordination environment of copper(II) (constant neg. effect at 679 nm). The exact reasons for the observed non linear behavior are not clear yet. They might be correlated to the enhanced asymmetry and flexibility of the cyclic pseudo peptide.

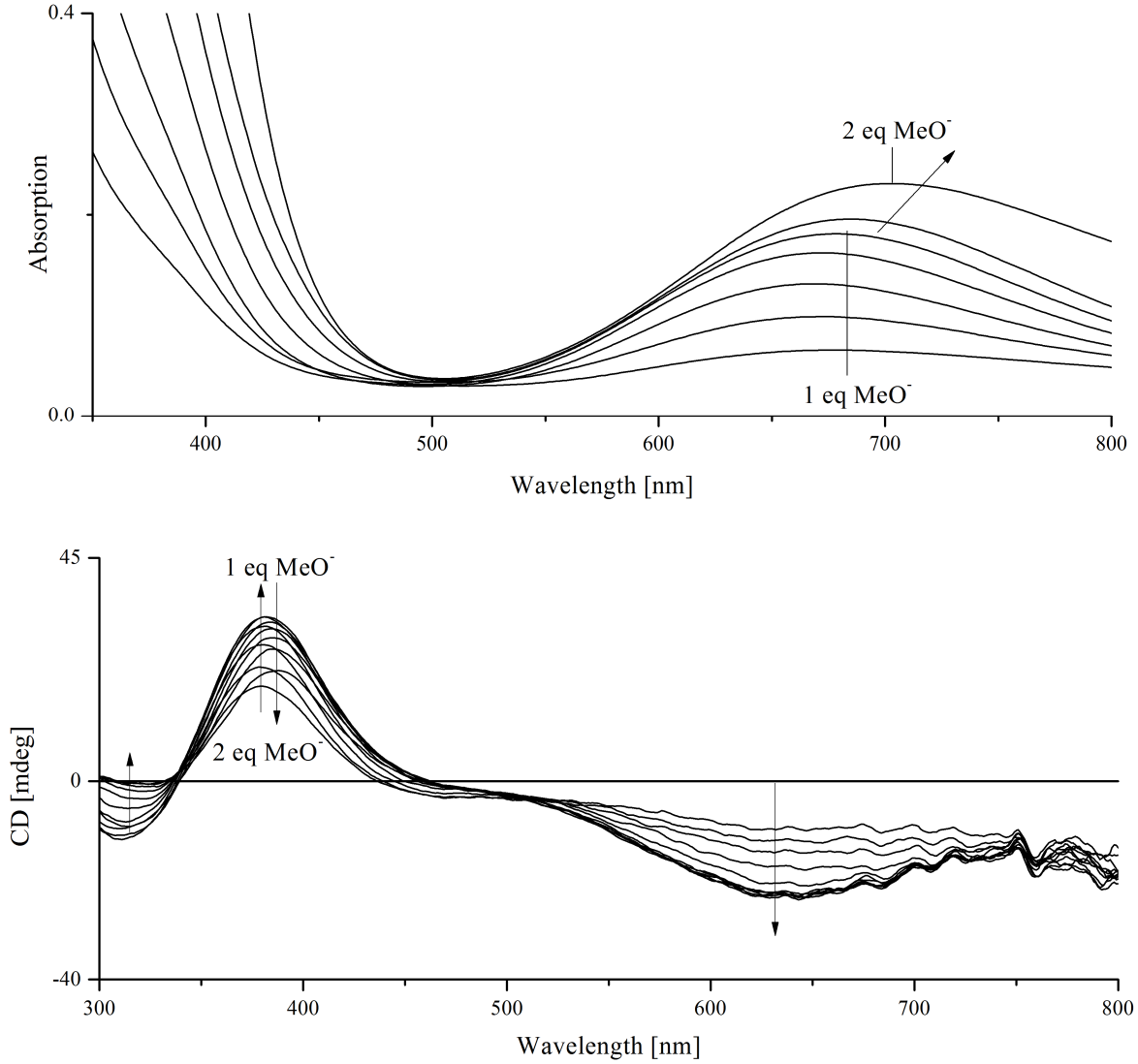

Figure 4.46. UV-vis (top) and CD (bottom) spectra of the titration of 0-2 eq of base (MeO^-), in 0.1 eq steps, to a $\mathbf{H_4L^{ascA}}$/copper(II) 1:2 solution ($c(\mathbf{H_4L^{ascA}})$ = 1.25 mM, methanol).

When a third equivalent of base is added the formation of a dinuclear hydroxo complex and a methoxide bridged complex can be observed in the ESI-MS spectra and accordingly the absorption band in the UV-vis spectra is shifted to higher wavelength (722 nm), while the Cotton effects in the CD spectra are intensified (see Figure 4.47). The consistency of the CD spectra indicates that there is no change in the coordination sphere at the copper(II), again a

slightly rearrangement of the macrocyclic backbone, as the Cotton effect at 379 nm is intensified.

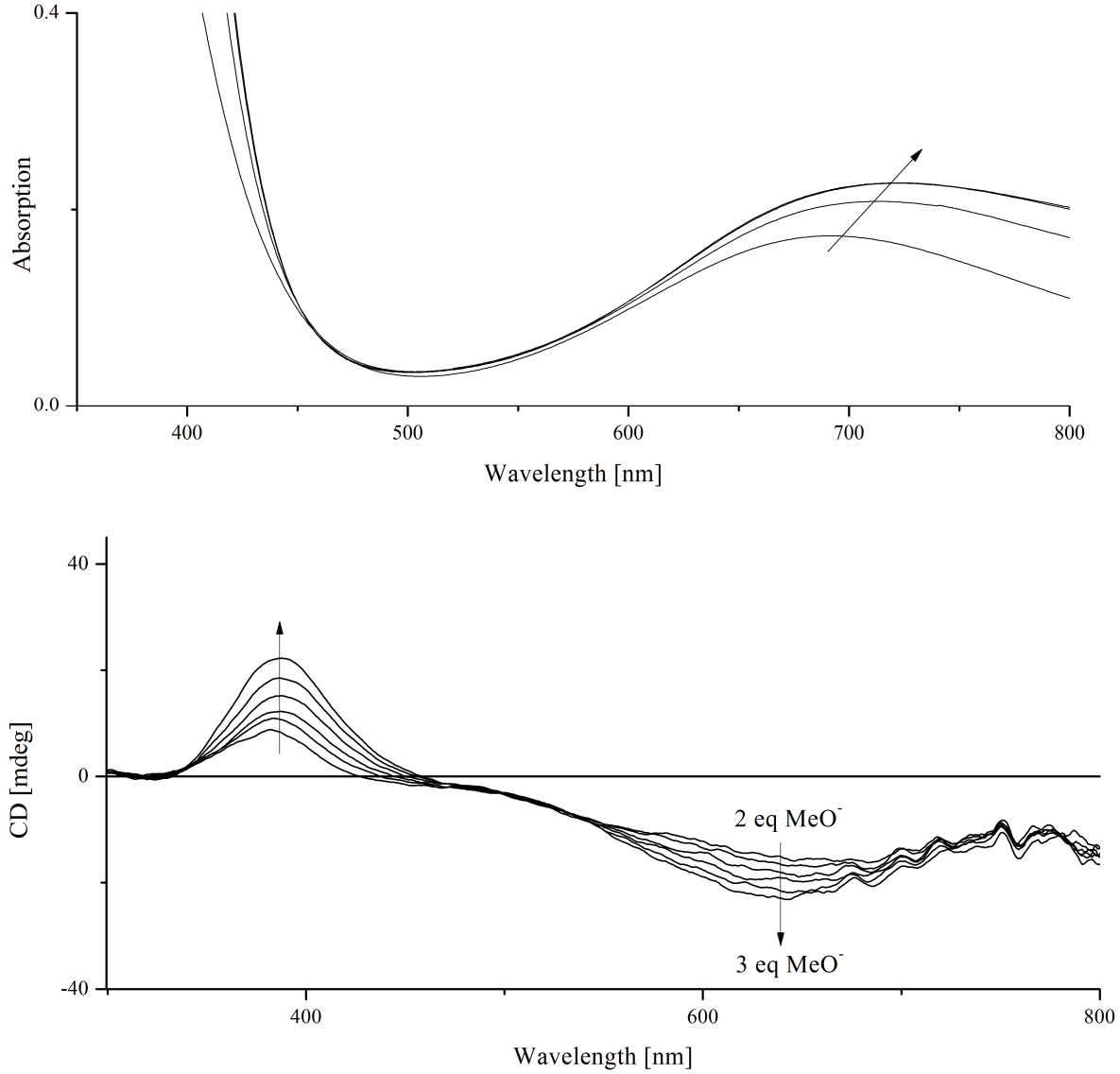

Figure 4.47. UV-vis (top) and CD (bottom) spectra of the titration of 2-3 eq of base (MeO^-), in 0.2 eq steps, to a $\mathbf{H_4L^{ascA}}$/copper(II) 1:2 solution (c = 1.25 mM, methanol).

Addition of more than three equivalents of base does not lead to a change in the CD or UV-vis spectra, indicating that no dihydroxo species, as observed for $\mathbf{H_4L^4}$ (see Section 4.2.1) and $\mathbf{H_4L^{ox}}$ (see Section 4.4.4) is formed with $\mathbf{H_4L^{ascA}}$. This observation also strongly suggests that there is no formation of a pink species (see Section 4.2.2, page 73). When the solutions are exposed to air a time-dependent shift to lower wavelength (690 nm) can be observed in the UV-vis spectra and this shift can be correlated to the formation of the carbonato-bridged species that can also be observed in the ESI-MS and in the EPR spectra (see Figure 4.49 f).

4.5.3 EPR Experiments

EPR spectra were recorded for solutions with various $\mathbf{H_4L^{ascA}}$/copper(II)/base ratios in order to further prove and investigate the putative equilibria. The recorded spectra are consistent with the assumed equilibria (see Figure 4.44) and suggest that the reaction of the dinuclear copper(II) complexes with atmospheric CO_2 is fast. The high cooperativity of $\mathbf{H_4L^{ascA}}$ is reflected in the recorded EPR spectra, as traces of a dinuclear complex could even be detected in absence of base (see Figure 4.49 a, arrow). Satisfactory simulations of the dinuclear spectra could not be obtained so far.

The experimental first and second derivative spectrum of the mononuclear copper(II) complex $[\mathbf{H_3L^{ascA}}Cu^{II}]^+$ together with their simulations are depicted in Figure 4.48. The spectra were simulated with the program package X-Sophe-Sophe-XeprView,[122] using the spin Hamiltonian described in Eq. 3.7.

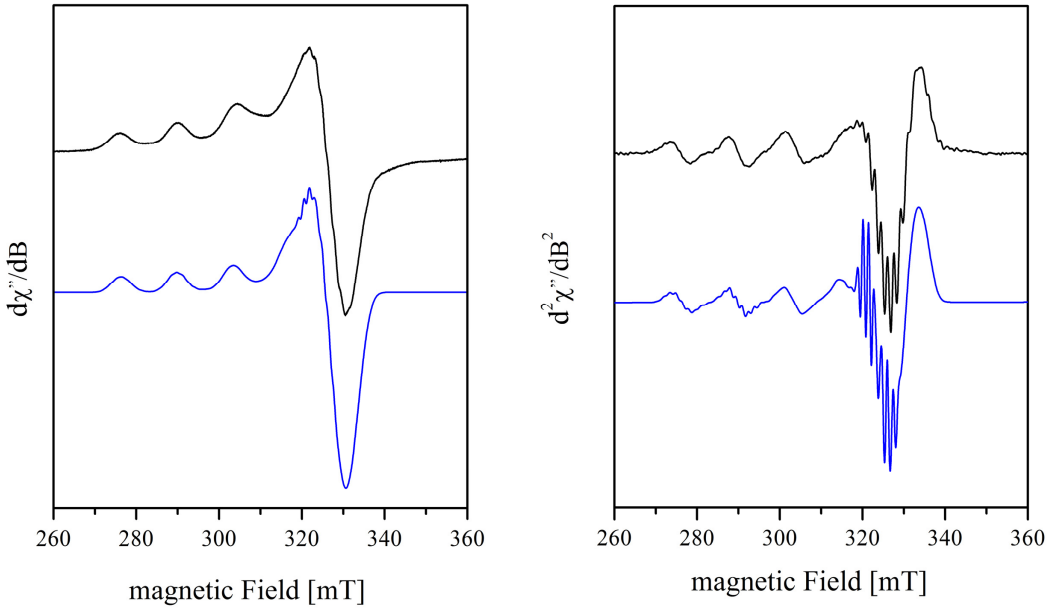

Figure 4.48. Experimental (black) and simulated (blue) first (left) and second derivative (right) X-Band EPR spectra, methanol, T = 110 K, $c(\mathbf{H_4L^{ascA}})$ = 1.25 mM, ν = 9.420872 GHz, of the mononuclear copper(II) complex $[\mathbf{H_3L^{ascA}}Cu^{II}]^+$.

The derived spin Hamiltonian parameters are suggestive of a distorted square pyramidal or six fold coordinated copper(II) center and are listed together with those of the other

investigated macrocycles in Table 4.15. The influence of the different macrocycles emerges when the A_z(Cu) tensors are compared. The A_z tensors of the imidazole and oxazole containing macrocycles are in the range of ~160 · 10^{-4} cm^{-1} while the one of $\mathbf{H_4L^{ascA}}$ is substantially lower (139 · 10^{-4} cm^{-1}). This difference reflects the disparities between the studied systems. The A_z(Cu) tensors of the natural cyclic pseudo peptides are in the range of 140 · 10^{-4} cm^{-1}, thus similar to $\mathbf{H_4L^{ascA}}$. The similarities of the complexes indicate that the synthesized cyclic pseudo peptides are potential model systems for the natural metabolites.

Table 4.15. Anisotropic spin Hamiltonian parameters of mononuclear copper(II) complexes of $\mathbf{H_4L^4}$, $\mathbf{H_4L^{ox}}$, $\mathbf{H_4L^{ascA}}$, and of the dinuclear bridged complexes of $\mathbf{H_4L^{rs}}$, $[\mathbf{H_2L^{rs}}Cu^{II}_2(H_2O)]^{2+}$ and $[\mathbf{H_2L^{rs}}Cu^{II}_2(\mu\text{-}OH)]^{+}$, respectively.

	$[\mathbf{H_3L^4}Cu^{II}]^+$	$\mathbf{H_4L^{rs}}$ water bridged	$\mathbf{H_4L^{rs}}$ hydroxo-bridged	$[\mathbf{H_3L^{ox}}Cu^{II}]^+$	$[\mathbf{H_3L^{ascA}}Cu^{II}]^+$
g_x	2.090	2.072	2.050	2.085	2.046
g_y	2.050	2.046	2.054	2.065	2.077
g_z	2.260	2.258	2.260	2.256	2.269
A_x (^{63}Cu)	14.2	4.02	12.69	20.0	11.31
A_y (^{63}Cu)	15.1	4.42	9.23	20.0	11.72
A_z (^{63}Cu)	169	166.9	161.6	163.0	139.77
A_x (^{14}N) – N_{het} *)	14.3	8.08	6.98	-	9.65
A_y (^{14}N) – N_{het} *)	12.5	11.63	9.00	-	12.69
A_z (^{14}N) – N_{het} *)	13.1	10.50	10.00	-	15.20
A_x (^{14}N) – N_{amide}	12.1	15.46	13.37	-	11.59
A_y (^{14}N) – N_{amide}	15.6	13.08	12.85	-	7.90
A_z (^{14}N) – N_{amide}	10.2	13.50	12.00	-	13.00

a) the resolution of the spectra was too low to extract the superhyperfine coupling constants *) simulated spectra included two magnetically identical heterocyclic nitrogen nuclei.

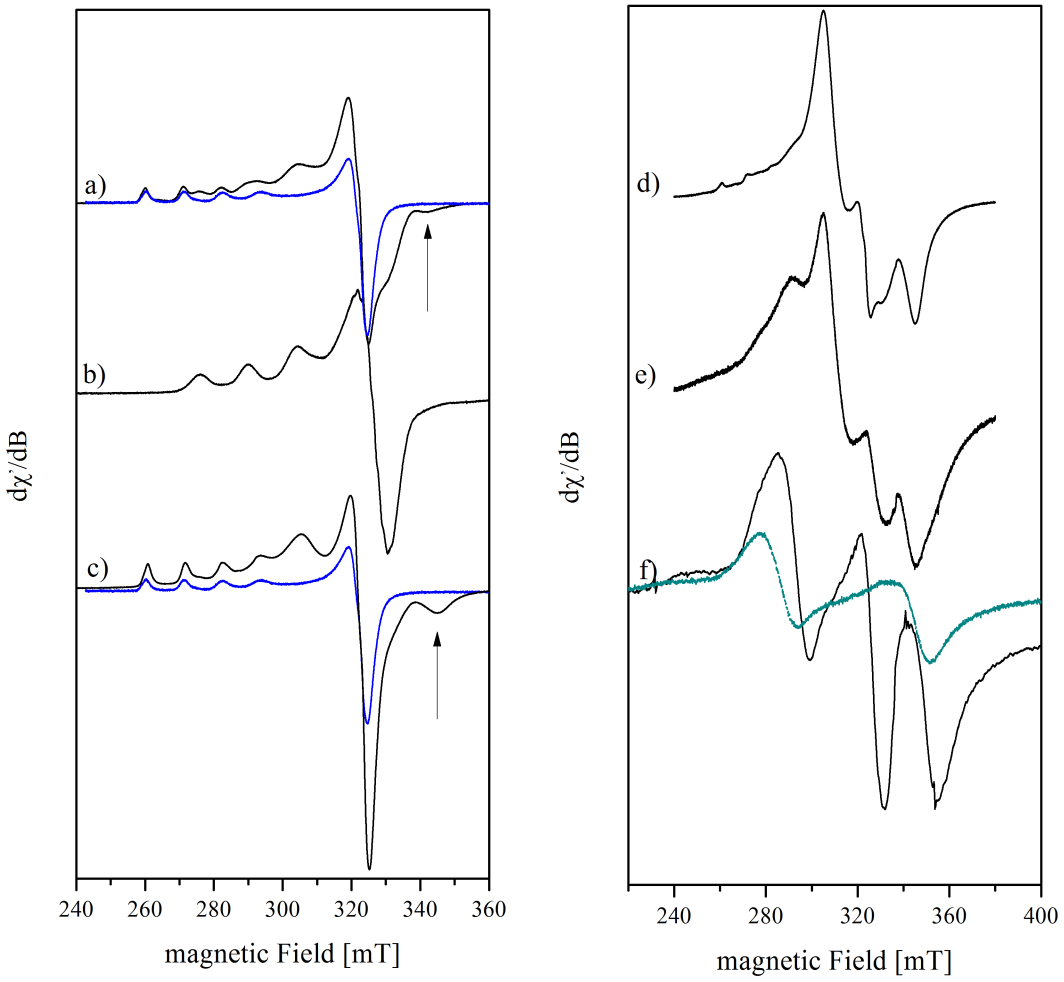

Figure 4.49. Experimental X-Band EPR spectra, methanol, T = 110 K, "free" Cu^{II} $[Cu^{II}(MeOH)_n]^{2+}$ (blue). **a)** $\mathbf{H_4L^{ascA}}$/copper(II)/base 1:1:0, ν = 9.447809 GHz; **b)** $\mathbf{H_4L^{ascA}}$/copper(II)/base 1:1:1 ν = 9.420872 GHz; **c)** $\mathbf{H_4L^{ascA}}$/copper(II)/base 1:2:1 ν = 9.452139 GHz; **d)** $\mathbf{H_4L^{ascA}}$/copper(II)/base 1:2:2 ν = 9.444581 GHz; **e)** $\mathbf{H_4L^{ascA}}$/copper(II)/base 1:2:3 ν = 9.452139 GHz; **f)** $\mathbf{H_4L^{ascA}}$/copper(II)/base 1:2:3 after 1h exposure to air (black), ν = 9.421352 GHz and carbonato complex of ascidiacyclamide (turquoise) ν = 9.4721 GHz

When more than two equivalents of base are present in the solution, signals of the mononuclear complex can no longer be observed and the spectra are consistent with dinuclear coupled copper(II) complexes. The spectra that are recorded with three equivalents of base (see Figure 4.49 e) are slightly different to those that were recorded with two equivalents of base (see Figure 4.49 d). This could indicate a structural rearrangement of the complex, *e.g.* upon formation of a hydroxo complex. However, when the spectra are compared to the one of the carbonato-bridged species depicted in Figure 4.49 f it seems likely that the spectrum is actually caused by the superposition of the dinuclear spectrum in Figure 4.49 d and the carbonato-bridged complex (Figure 4.49 f). The measured solutions were not completely CO_2 free and the observed spectra indicate that the dinuclear copper(II) complexes of $\mathbf{H_4L^{ascA}}$ react

fast with CO_2. This assumption is supported by the fact that exposure of a solution that contains three equivalents of base within one hour leads to a complete conversion to the carbonato-bridged species (Figure 4.49 f). The similarities of the EPR spectra of the carbonato-bridged complex of $\mathbf{H_4L^{ascA}}$ and the carbonato-bridged complex of ascidiacyclamide (Figure 4.49 f, turquoise) indicate that their adopted conformation is alike and this highlights the potential of the synthetic pseudo peptide as a model system for the natural cyclic pseudo peptides. When the EPR spectra of the copper(II) complexes of $\mathbf{H_4L^{ascA}}$ are compared to those of the other studied cyclic pseudo octapeptides ($\mathbf{H_4L^4}$, see Figure 4.14; $\mathbf{H_4L^{rs}}$, see Figure 4.24; and $\mathbf{H_4L^{ox}}$, see Figure 4.41) it emerges that the spectra of $\mathbf{H_4L^{ascA}}$ cover a wider range of the magnetic field. This is thought to arise from the structural difference, as $\mathbf{H_4L^{ascA}}$ (and also the natural cyclic pseudo peptides) is substantially more flexible.

The here performed experiments provided an initial insight into the copper(II) coordination chemistry of $\mathbf{H_4L^{ascA}}$. It is so far the structurally closest macrocycle in comparison to the natural cyclic pseudo peptides. No indications were found for an outside coordination of copper(II) and this highly suggest that this coordination mode is only present in oxazole containing pseudo peptides such as $\mathbf{H_4L^{ox}}$ and $\mathbf{H_3L^2}$. $\mathbf{H_4L^{ascA}}$ was found to be highly preorganized, to have a high cooperativity and to readily react with atmospheric CO_2. The alikeness of its EPR spectra to those of ascidiacyclamide indicates that it is a very good model system. However, its synthesis is expensive. Evidence for a pink species has not been found and it might be that this is a feature of C_4-symmetric macrocycles.

In further experiments it will be of interest to simulate the obtained dinuclear EPR spectra to gain a detailed structural knowledge of the adopted structures that then shall be verified by computational methods. It is also of interest whether the reaction of $\mathbf{H_4L^{ascA}}$ with CO_2 is catalytic or not, as the structural differences of $\mathbf{H_4L^{ascA}}$ and $\mathbf{H_4L^4}$ might lead to the inhibition of catalysis. So far the experimental findings strengthen the idea of the involvement of the copper(II) complexes of natural cyclic pseudo octapeptides in CO_2 fixation and probably transport of carbonate into the *ascidian's* organism.

4.6 Summary and Outlook

The copper(II) coordination chemistry of the investigated cyclic pseudo octapeptides was found to be versatile and different to that of the smaller cyclic pseudo hexapeptides (see Chapter 3.3). The high preference for the formation of dinuclear complexes, that had been observed for the smaller macrocycles $\mathbf{H_3L^{1\text{-}3}}$ and $\mathbf{H_3L^{wa}}$, is even stronger pronounced as the macrocycles are larger and enable the coordination of two copper(II) ions in the preferred N_{het}-N_{amide}-N_{het} binding motif. Two novel cyclic pseudo octapeptides, $\mathbf{H_4L^{4\text{-}bn}}$ and $\mathbf{H_4L^{rs}}$, have been synthesized and characterized and the copper(II) coordination chemistry of the cyclic pseudo octapeptides $\mathbf{H_4L^4}$, $\mathbf{H_4L^{rs}}$,$\mathbf{H_4L^{ox}}$, and $\mathbf{H_4L^{ascA}}$ has been investigated. The differences of the studied macrocycles allowed the investigation of the influence of incorporated heterocycle and the stereochemistry at C_α. The latter was found to have a substantial influence on the adopted conformation of the macrocycle and is observable when the X-ray structures of $\mathbf{H_4L^{rs}}$, $\mathbf{H_4L^4}$ and $\mathbf{H_4L^{4\text{-}bn}}$ are compared (see Chapter 4.1). The combination of imidazole rings and an alternating R^*- and S^*-configuration in the macrocycle seems to significantly alter the copper(II) coordination chemistry of the cyclic pseudo octapeptides. Although quite different to the natural cyclic pseudo peptide ascidiacyclamide, the macrocycles $\mathbf{H_4L^4}$ and $\mathbf{H_4L^{ox}}$, with all S^*-configured stereocenters were found to be a suitable model system for the natural pseudo peptides. Both macrocycles correctly reproduce many of the features found in the natural systems, *e.g.* cooperativity, preorganization for copper(II) or reaction with CO_2, while for $\mathbf{H_4L^{rs}}$ a different coordination chemistry was observed.

Similar to the natural pseudo octapeptides, $\mathbf{H_4L^4}$ preferably forms dinuclear complexes that are able to react with atmospheric CO_2 to the respective carbonato-bridged complexes. Experiments with labeled water and CO_2 revealed that this reaction is reversible. From a structural point of view the all S^*-configuration of $\mathbf{H_4L^4}$ leads to a different folding of the macrocycle, compared to the natural cyclic peptides, and this is expected to have some influences on the coordination chemistry. The geometry of the copper(II) complexes of $\mathbf{H_4L^4}$ was initially studied by a combination of EPR spectra simulations and DFT calculation. The derived copper-copper distances from DFT calculation and EPR simulation significantly deviate and therefore the possibility of different conformations of the macrocycle was studied by MM methods. It is unlikely that the macrocycle adopts another structure than the cone like

shape observed in the crystal structure and the deviation between experimental and computational distances is thought to be caused by the simulation of local rather than a global minimum. From the recorded EPR spectra it emerges that the carbonato-bridged complex of $\mathbf{H_4L^4}$ adopts a slightly different conformation than the carbonato complex of the natural macrocycle ascidiacyclamide. The carbonato-bridged complex of $\mathbf{H_4L^4}$ rearranges to a pink species upon exposure to air. This species is strongly ferromagnetically coupled and could not be fully characterized yet. Indications for such a species could also be observed with the oxazole containing macrocycle $\mathbf{H_4L^{ox}}$ but are missing for $\mathbf{H_4L^{rs}}$ and $\mathbf{H_4L^{ascA}}$. It is possible that the pink species can only be formed with an all S^*-configuration of the macrocycles. A species that is equivalent to the pink species of $\mathbf{H_4L^4}$ has not been reported for the natural pseudo peptides. Yet, it is possible that this species is present but has not been discovered as a result of its complex observability. The reaction of the dinuclear copper(II) complexes of $\mathbf{H_4L^4}$ with atmospheric CO_2 was found to be not catalytic.

The coordination chemistry of $\mathbf{H_4L^{ox}}$ is very similar to that of the natural systems, yet only at high base concentrations. At low base concentrations, the huge influence of the incorporated oxazole rings on the copper(II) coordination chemistry of a cyclic pseudo peptide (see also coordination chemistry $\mathbf{H_3L^2}$, Chapter 3.2.3) can be observed with $\mathbf{H_4L^{ox}}$. Copper(II) is not coordinated in the usual N_{het}-N_{amide}-N_{het} binding motif but at the outside of the macrocyclic system, by the oxygen atoms of the amide bond. This unusual coordination mode could not be observed for any of the other investigated pseudo octapeptides and has been further investigated by EPR and NMR experiments. At low base concentrations the outside coordinated complex has a higher stability than the mono- or dinuclear complexes. At high base concentrations the degree of deprotonation of $\mathbf{H_4L^{ox}}$ increases and thus the coordination in the "normal" binding motif is (re)enabled. $\mathbf{H_4L^{ox}}$ exhibits a high cooperativity where the formation of mononuclear complexes can hardly be observed. The dinuclear copper(II) complexes react fast with atmospheric CO_2 and the EPR spectra are suggestive of a nearly identical conformation of the carbonato complex to that of $\mathbf{H_4L^4}$. This assumption was reflected in the performed DFT calculations.

$\mathbf{H_4L^{rs}}$ has the same stereochemistry as the natural pseudo octapeptides and was thus expected to have a copper(II) coordination chemistry that is closer to that of the natural systems. Surprisingly, it was found that its coordination chemistry remarkably differs from that of the other cyclic pseudo peptides. It does show a high cooperativity, yet the dinuclear copper(II) complexes have interesting EPR features. In the bridged complexes the copper(II)

centers are set up in a so called magic angle and this results in an EPR spectrum with mononuclear features. A reaction with CO_2 or added carbonate could not be observed and the formation of carbonato-bridged species can be excluded. It emerges that the combination of an alternating configuration at C_α and imidazole heterocycles leads to a quite rigid macrocycle that cannot form carbonato-bridged species due to the thus induced steric strain. This finding might explain the presence of oxazoline rings in the natural cyclic pseudo peptides. Each oxazoline ring introduces an additional single bond that enlarges the flexibility of the macrocycle and thus might (re)enable the formation of carbonato-bridged complexes, what seems to be more difficult with an alternating R^*- and S^*- configuration. Suitable crystals were obtained from the free macrocycle $\mathbf{H_4L^{rs}}$ and the cation $[\mathbf{H_2L^{rs}}Cu^{II}_2(\mu\text{-}OH)(H_2O)_2]^+$. These revealed a very short copper(II) copper(II) distance in the solid state. The copper(II) centers in the crystal were found to be oriented in an magic angle.

The molecular setup of $\mathbf{H_4L^{ascA}}$ is very close to the natural cyclic pseudo peptide ascidiacyclamide. Initial experiments suggest that its copper(II) coordination chemistry is nearly identical to that of ascidiacyclamide and when its chemistry is compared to that of $\mathbf{H_4L^4}$, the potential of $\mathbf{H_4L^4}$ as a model system (see above) is highlighted. From the EPR spectrum of the carbonato-bridged complex it emerges that the structures are nearly identical. $\mathbf{H_4L^{ascA}}$ exhibits the highest cooperativity and the fastest reaction with atmospheric CO_2, strengthening the involvement of cyclic pseudo peptides in CO_2 capture and transport. Further experiments, simulations, and DFT calculations with the copper(II) complexes of $\mathbf{H_4L^{ascA}}$ shall be used to gain further insight into the copper(II) coordination chemistry of the fascinating molecules.

A DFT study of the carbonato complexes of $\mathbf{H_4L^{rs}}$ should reveal whether the inexistence of carbonato-bridged species is of sterical or energetical origin. Further DFT calculations are also needed for the pseudo peptides $\mathbf{H_4L^{ox}}$ and $\mathbf{H_4L^{ascA}}$ to gain a more detailed insight into their complexation equilibria. These results can then be used to simulate the measured EPR spectra of the dinuclear complexes. The exact metabolic purpose of patellamides is still under investigation, although the here presented results emphasize the correlation of the dinuclear copper(II) complexes of cyclic pseudo peptides to CO_2. This suggests a relation to the hydrolysis and/or transport of CO_2 in the *ascidan's* metabolism.

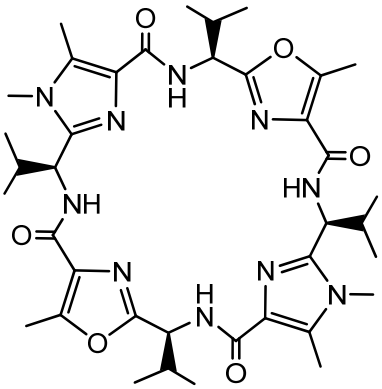

$\mathbf{H_4L^{mio}}$

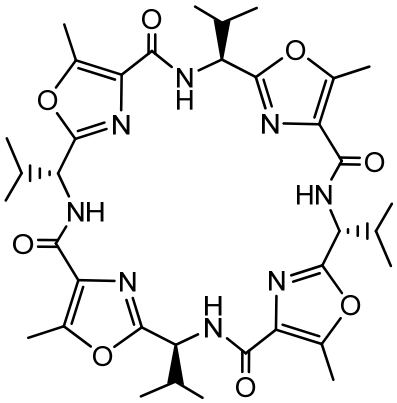

$\mathbf{H_4L^{ox\text{-}rs}}$

Figure 4.50. Chemical structure of new cyclic pseudo octapeptides $\mathbf{H_4L^{mio}}$ and $\mathbf{H_4L^{ox\text{-}rs}}$.

One interesting question that evolved during our studies is the effect of the oxazole rings. How many oxazole units are needed to enable the outside conformation? And is the outside coordination influenced by the stereochemistry at C_α? A detailed investigation of the copper(II) coordination chemistry of the cyclic pseudo octapeptides $\mathbf{H_4L^{mio}}$ and $\mathbf{H_4L^{ox\text{-}rs}}$ should answer these questions. (see Figure 4.50).

5 Experimental Section

5.1 Materials and Instruments

Materials

All solvents (absolute) and reagents (purum grade) were obtained commercially (Aldrich, Fluka) and were used without further purification. Labeled water was obtained commercially from . Labeled carbon dioxide was obtained commercially from Sigma Aldrich. The macrocycles $\mathbf{H_3L^2}$, $\mathbf{H_3L^3}$, and $\mathbf{H_4L^{ox}}$ were prepared in the group of Prof. Dr. G. Haberhauer (Institute of Organic Chemistry, University of Duisburg Essen) and used without further purification. The macrocycle $\mathbf{H_3L^{wa}}$ was prepared by Dr. Björn Seibold and used without further purification.

Chromatography

Reactions were monitored by TLC on silica gel 60 F254 thin-layer plates (POLYGRAM® SIL G/UV, Macherey-Nagel). Detection was accomplished with UV-light at a wavelength of $\lambda = 254$ nm. Flash chromatography was performed using silica gel 60 (230–400 mesh) obtained from Macerey-Nagel.

DFT and MM Calculations

DFT calculations were performed with Gaussian 03,[119] Gaussian 09,[163] TURBOMOLE,[166] ORCA,[120] and MAG-ReSpect.[127] Geometry optimization were performed using the B3LYP[130, 135, 138] hybrid functional in combination with the basis sets 6-31g*[138] (C, H N, O, S) and TZVP[136] (Cu). A frequency calculation was performed subsequent to the geometry optimization to confirm the structures as a minimum on the potential surface. Molecular mechanics calculations and MD simulations were performed with the program package Macromodel,[160] using a modified Amber force field.[161-162] No electrostatic interactions or partial charges were considered in the molecular mechanics calculations. For the conformational search, a 100 ps molecular dynamics (MD) simulation was performed at a range of different temperatures (300 K to 800 K). A multiple minimization was performed on the obtained structures of the MD simulation to give 4 structures. Calculations were run on a Linux cluster.

EPR Spectra

Continuous-wave X-band (ca. 9 GHz) EPR spectra were recorded with a Bruker Biospin Elexsys E500 EPR spectrometer fitted with a super high Q cavity. The magnetic field and the microwave frequency were calibrated with a Bruker ER 041XK Teslameter and a Bruker microwave frequency counter, respectively. A flow-through cryostat in conjunction with a Eurotherm (B-VT-2000) variable-temperature controller provided temperatures of 127–133 K at the sample position in the cavity. For lower temperatures (48–52 K), an Oxford Instruments ESR 900 flow-through cryostat in conjunction with an ITC4 temperature controller was employed. Spectrometer tuning, signal averaging, and visualization were accomplished with BrukerTs Xepr (version 2.4b.12) software. The EPR spectra of the mono- and dinuclear complexes were simulated with the XSophe-Sophe-XperView[122] (version 1.1.4) and Molecular Sophe[123] (version 2.0.91) computer simulation software suites on a personal computer, running with the Mandriva Linux v2007.0 operating system.

ITC Measurements

ITC experiments were performed with a MicroCal VP-ITC instrument. All experiments were carried out in solutions containing 0.1 M (n-Bu_4N)(ClO_4) to keep the ionic strength constant. Seven micro liters of a 2 mM $Cu(CF_3SO_3)_2$ MeOH solution were added in 29 steps by an injection syringe into the reaction vessel (V = 1.4232 mL), which contained a 0.1 mM cyclic pseudo hexapeptide solution. The ITC measurements were performed by Yuki Katod in the Laboratories of Prof. Toshiaki Taura at the University of Aichi Prefecture.

IR Spectra

IR spectra were measured with a Perkin Elmer 16C FTIR instrument from samples in KBr pellets.

Mass Spectrometry

High-resolution electrospray ionization mass spectrometry (ESI-MS) was performed with a 9.4 T Bruker ApexQe Qh-ICR hybrid instrument with an Apollo II MTP ion source in the positive and negative-ion electrospray ionization (ESI) mode. Sample solutions in methanol at concentrations of 10^{-4}–10^{-5}M were admitted to the ESI interface by means of a syringe pump at 5 $mLmin^{-1}$ and sprayed at 4.5 kV with a desolvation gas flow of 2.0 $Lmin^{-1}$ at 25°C and a nebulizer gas flow of 1.0 $Lmin^{-1}$. The ions were accumulated in the storage hexapole for

0.1-1.0 s and then transferred into the ICR cell. Trapping was achieved at a sidekick potential of -4.0 V and trapping potentials of roughly 1 V. The mass spectra were acquired in the broadband mode with 1M data points. Typically, 16 transients were accumulated for one magnitude spectrum. External mass calibration was performed on [arginine$_n$+H]$^+$ cluster ions prior to analysis. A mass accuracy of 1 ppm was achieved. The instrument was controlled by Bruker ApexControl 2.0.0.beta software and data analysis was performed using Bruker DataAnalysis 3.4 software.
Nominal masses were recorded on a Bruker QSTAR qQTOF instrument. An Agilent 1100 microbore HPLC was interfaced to the electrospray ionization source for LC-MS.

MCD Measurements

MCD spectra were recorded on an instrument based on a high through-put / high resolution Jobin Yvon 750s monochromator and an Oxford Instruments SpectroMag superconducting magnet equipped with an SM4 Cryostat and a Blue PMT (vis) and Si APD (UV) detector, respectively. The MCD spectra were recorded by Dr. Marc Riley in a methanol/glycerol 1:1 mixture at various temperatures and fields.

Melting Points:

Melting points were determined in capillary tubes and are uncorrected

Microanalyses

Elemental microanalyses were performed at the microanalytical laboratory of the University of Heidelberg**.**

NMR Spectroscopy

^{1}H and ^{13}C-NMR spectra were recorded with a Bruker 200 MHz DRX, a Bruker Avance 400 MHz, or a Bruker 900-MHz Avance-III spectrometer. All chemical shifts (δ) are given in ppm relative to TMS. The spectra were referenced to deuterated solvents, indicated in brackets in the analytical data.

Spectophotometric Titrations

Spectrophotometric titrations were performed in methanol at 25.0°C on 2 cm^3 samples at a cyclic pseudo peptide concentration of 1.25 mM. Copper(II)triflate and base (*n*-Bu$_4$N)(OMe)

were added stepwise in 0.1 (10µL) or 0.2 (20 µL) equivalents steps. The recorded spectra were corrected for the dilution factor.
UV-vis/NIR spectra were recorded with a JASCO V-570 spectrophotometer.
CD spectra were recorded with a JASCO J-710 spectropolarimeter.

Stopped Flow Measurements

Stopped flow measurements were performed with a P.D.1 photodiode-array stopped-flow spectrometer from Applied Photophysics. Experiments were performed in acetonitrile at constant ionic strength (μ = 0.2 M, $NaClO_4$). For the blind experiments 220µL of a solution of inidicator (chlor phenol red, c = 0.1 mM) and buffer (3,5-lutidine, c = 0.2M) was mixed with 220µL of a CO_2-saturated solution at room temperature. After mixing, the rapid absorbance change at 573 nm was recorded and the absorption change correlated to the amount of hydrolyzed CO_2.
In the catalysis experiments a buffered (3,5-lutidine, c = 0.2M, μ = 0.2 M, $NaClO_4$) acetonitrile solution of $\mathbf{H_4L^4}$/copper(II) 1:2 ($c(\mathbf{H_4L^4})$ = 1.25 mM), containing 0.1mM indicator was prepared 30 min prior to the experiment. The formation of the hydroxo complex $[\mathbf{H_2L^4}Cu^{II}_2(OH)]^+$ was tested by an EPR experiment. 220µL of the macrocycle containing solution were mixed with 220µL of a CO_2-saturated solution at room temperature and the rapid absorbance change at 573 nm was recorded and the absorption change correlated to the amount of hydrolyzed CO_2.

X-ray Crystallography

A suitable crystal was mounted with perfluorinated polyether oil on the tip of a glass fiber and cooled immediately on the goniometer head to 200 K. Data collections were performed using a STOE IPDS diffractometer with $Mo_{K\alpha}$ radiation (λ=0.71073 Å). The structure was solved by Prof. Dr. Linti and refined using the Bruker AXS SHELXTL 5.1 program package.[168] Refinement was in full-matrix least-squares against F^2. All non-carbon hydrogen atoms were taken from a difference Fourier map and refined with free isotopic U values; carbon–hydrogen atoms were included as riding models with fixed isotropic U values in the final refinement.

5.2 Syntheses

General Procedure for the Cleavage of the Methyl Ester Group:

The protected compound (1 equiv.) was dissolved in methanol/dioxane (10:7, 0.08 M), followed by slow addition of 2 M NaOH solution (10 equiv.) at 0 °C. Stirring was continued until TLC showed the consumption of all starting material, and then brine, 1 M HCl solution (until a pH of 1 was reached), and DCM were added. The aqueous phase was repeatedly extracted with DCM; the organic layers were combined, dried with $MgSO_4$, and concentrated in vacuo to give the acid compound. Remaining dioxane was removed through repetitive stripping with EtOAc. The acid compound was used in the next step without further purification.

General Procedure for the Cleavage of the Boc Group:

The Bocprotected compound (1 equiv.) was dissolved in ethyl acetate (0.1 M) and the solution was cooled to 0 °C. TFA (10 ml/mmol starting material) was added at that temperature. The ice bath was removed after 30 min and stirring was continued at room temperature for three hours. The mixture was concentrated in vacuo to provide a quantitative yield of the trifluoroacid salt. Remaining solvent and TFA were removed through repetitive stripping with EtOAc. The resulting salt was then washed with icecold DCM.

5.2.1 Synthesis of the Cyclic Pseudo Peptides H_3L^1 and H_4L^4

(*E*)-methyl 2-(hydroxyimino)-3-oxobutanoate (1):

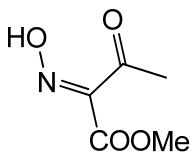

1

molecular formula: $C_5H_7NO_4$
molecular mass: 145.11 g/mol

An aqueous solution of 148.5 g (2.15 mol, 2.5 eq) sodium nitrite is slowly added to an icebath cooled solution of 100 g methyl acetoacetate (0.86 mol, 1 eq) in 140 mL glacial acetic acid.

The temperature should not exceed -5 °C. The reaction mixture is stirred for three hours at -5 °C, for 1.5 hours at room temperature and is subsequently poured on 800 g ice. The water phase is extracted several times with 400 mL diethyl ether. The combined organic layers are washed several times with saturated $NaHCO_3$ solution until the pH a neutral pH is reached, dried over $MgSO_4$ and concentrated in vacuo to yield 109.1 g (89 %) of **1** as yellowish oil that slowly crystallizes to a yellowish solid.

$C_5H_7NO_4$: calcd. (%): C 41.38, H 4.86, N 9.65; found (%): C 41.15, H 5.02, N 9.54 (20507). - **^{1}H-NMR** (200 MHz, $CDCl_3$): δ = 2.41 (s, 3H, $COCH_3$); 3.90 (s, 3H, CO_2CH_3) ppm. - **^{13}C-NMR** (50 MHz, $CDCl_3$): δ = 25.4 (CH_3CO); 52.9 (CO_2CH_3); 150.9 ($CNOH$); 162.1 (CO_2CH_3); 193.9 ($COCH_3$) ppm. - **EI-HR MS:** *m/z* calcd. for $C_5H_7NO_4^+$ 145.0375, found 145.0364 – **M.P.**: 28°C

1-methoxy-1,3-dioxobutan-2-aminium chloride (2):

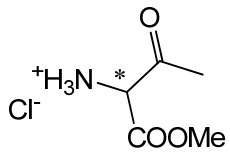

2

molecular formula: $C_5H_{10}ClNO_3$

molecular mass: 167.59 g/mol

10.0 g Palladium on charcoal (10 %) are suspended in a solution of 20 g of **1** (0.14 mol, 1eq) in 300 mL ethanol. 330 mL (0.42 mol, 3 equiv.) 1.25 M HCl in methanol are added dropwise. The reaction mixture is stirred under a H_2-atmosphere for 48 h. After removal of the H_2-atmosphere, the reaction mixture is filtered over celite and the solvent evaporated at ambient temperature. The crude product is covered with ethyl acetate and recrystallizes at -18 °C. Washing with cold dichloromethane yields 18.2 g (78 %) **2** as a colorless solid.

$C_5H_{10}ClNO_3$: calcd. (%): C 35.83, H 6.01, N 8.36, Cl 21.15; found (%): C 35.79, H 5.99, N 8.24, Cl 20.96 (22360). - **^{1}H-NMR** (200 MHz, DMSO-d_6): δ = 2.38 (s, 3H, $COCH_3$); 3.80 (s, 3H, CO_2CH_3), 5.29 (s, 1H, $CHNH_3$), 9.01 (s, 3H, NH_3) ppm. - **^{13}C-NMR** (50 MHz, DMSO-d_6) δ = 28.2 (CH_3CO); 53.6 (CH_3CO); 61.2 (CNH_3); 164.2 (CO_2CH_3); 196.7 ($COCH_3$) ppm. - **FAB-HR MS**: *m/z* calcd. for $C_5H_{10}NO_3^+$ 132.0655, found 132.0676. - **Mp.**: decomposition at T > 45°C.

Methyl 2-((*S*)-2-(tert-butoxycarbonylamino)-3-methylbutanamido)-3-oxobutanoate (3):

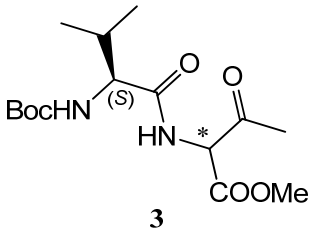

3

molecular formula: $C_{15}H_{26}N_2O_6$

molecular mass: 330.38 g/mol

The synthesis was performed according to literature procedures.[48, 67] (*S*)-Boc-Val-OH (10.4 g, 47.8 mmol, 1eq) is dissolved in 400 mL THF, NMM (3.4 g, 47.8 mmol, 1eq) is added and the solution is cooled to -25°C. Subsequently isobutyl chloroformate (6.8 g, 47.8 mmol, 1 eq) is added, during which the reaction mixture is maintained at -25°C. After 35 min, the ammonium chloride salt **2** (9.82 g, 95.6 mmol, 2 eq), followed by a second equivalent of NMM (3.4 g, 47.8 mmol, 1eq) are added at -25°C and stirring is continued for 20 h as the mixture is allowed to warm to room temperature. The solvent is evaporated, the residue dissolved in ethyl acetate, and then washed with water and brine. The combined organic layers are dried over $MgSO_4$ and concentrated in vacuo. After recrystallization from ethyl acetate 14.64 g of **3** are obtained as colorless crystals (92 %).

$C_{15}H_{26}N_2O_6$: calcd. (%): C 54.53, H 7.93, N 8.48; found (%): C 54.37, H 7.96, N 8.56 (22263). **- ^{1}H-NMR** (200 MHz, $CDCl_3$): δ = 0.90 (d, ^3J = 6.9 Hz, 3H, CHC$\underline{H}_3$); 0.91 (d, ^3J = 6.9 Hz, 3H, CHC$\underline{H}_3$); 0.96 (d, ^3J = 6.8 Hz, 6H, CHC$\underline{H}_3$); 1.42 (s, 9H, C(C$\underline{H}_3$)$_3$); 1.43 (s, 9H, C(C$\underline{H}_3$)$_3$); 2.10-2.28 (m, 2H, C$\underline{H}$(CH$_3$)$_2$); 2.36 (s, 6H, COC$\underline{H}_3$); 3.79 (s, 6H, CO$_2$C$\underline{H}_3$); 4.06 (m, 2H, NHC$\underline{H}$CO); 5.04 (m, 2H, N$\underline{H}$CO$_2$); 5.23 (d, ^3J = 6.3 Hz, 2H, C$\underline{H}$CO$_2$); 7.12 (d, ^3J = 6.3 Hz, 1H, N$\underline{H}$); 7.16 (d, ^3J = 6.3 Hz, 1H, N$\underline{H}$) ppm. **- ^{13}C-NMR** (50 MHz, $CDCl_3$): δ = 17.2, 17.4 (CH(C$\underline{H}_3$)$_2$); 18.9, 19.0 (CH(C$\underline{H}_3$)$_2$); 27.7, 27.8 (CO$\underline{C}H_3$); 28.1 ($\underline{C}$(CH$_3$)$_3$); 30.7, 30.9 ($\underline{C}$H(CH$_3$)$_2$); 53.0, 53.1 (CO$_2\underline{C}H_3$); 59.0, 59.2 (NH$\underline{C}$HCO); 62.6, 62.7 (NH$\underline{C}$HCO$_2$); 79.6, 79.7 ($\underline{C}$(CH$_3$)$_3$); 155.6 (NH$\underline{C}$OC(CH$_3$)$_3$); 166.2, 166.3 ($\underline{C}$O$_2$CH$_3$); 171.5, 175.5 (NH$\underline{C}$O); 198.1, 198.2 ($\underline{C}$OCH$_3$) ppm. **- FAB-HR MS**: *m/z* calcd. For $C_{15}H_{27}N_2O_6^+$ 331.1689, found 331.1670. **– M.P.**: 109-112°C.

(*S*)- methyl 2-(1-(*tert*-butoxycarbonylamino)-2-methylpropyl)-1,5-dimethyl-imidazole-4-carboxylate (4):[48, 67]

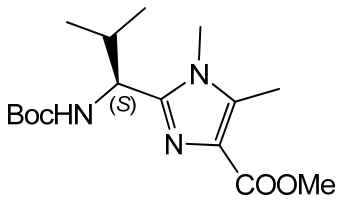

4

molecular formula: $C_{16}H_{27}N_3O_4$

molecular mass: 325.40 g/mol

The synthesis was performed according to literature procedures.[48, 67] Both glacial acedic acid (19.8 mL, 346 mmol) and NH_2Me in MeOH (8 M, 15.2 mL, 123.2 mmol) were added to a solution of **3** (10.0 g, 30.2 mmol) in xylenes (400 mL) at room temperature. The solution was stirred at 155°C with azeotropic removal of water for 8 h and then cooled to room temperature. The solvent was concentrated, and the residue was dissolved in AcOEt, and then washed with saturated $NaHCO_3$ solution and brine. The organic layer was dried over Na_2SO_4 and concentrated in vacuo. Purification was achieved by performing chromatography with silica gel (petroleum ether/ethyl acetate 1:3) to provide 5.5 g of **6** (16.9 mmol, 54%) as a white solid.

$C_{16}H_{27}N_3O_4$: calcd. (%): C 59.06, H 8.36, N 12.91; found (%): C 58.94, H 8.40, N 13.15 (22237). **- ^{1}H-NMR** (200 MHz, $CDCl_3$): δ = 0.81 (d, ^3J = 6.7 Hz, 3H, CHC$\underline{H}_3$); 1.00 (d, ^3J = 6.7 Hz, 3H, CHC$\underline{H}_3$); 1.39 (s, 9H, C(C$\underline{H}_3$)$_3$); 2.10-2.35 (m, 1H, C$\underline{H}$(CH$_3$)$_2$); 2.52 (s, 3H, $C_{het}C\underline{H}_3$); 3.55 (s, 3H, NC$\underline{H}_3$); 3.87 (s, 3H, $CO_2C\underline{H}_3$); 4.52 (dd, ^3J = 9.26 Hz, 1H, $C_\alpha\underline{H}$); 5.45 (d, ^3J = 9.5 Hz, 1H, N$\underline{H}CO_2$) ppm. **- ^{13}C-NMR** (50 MHz, $CDCl_3$): δ = 10.2 ($C_{het}\underline{C}H_3$); 18.5, 19.5 (CH($\underline{C}H_3$)$_2$); 28.2 ($\underline{C}$(CH$_3$)$_3$); 30.2 ($\underline{C}$H(CH$_3$)$_2$); 33.1 (N$\underline{C}H_3$); 51.3 ($CO_2\underline{C}H_3$); 52.1 ($\underline{C}_\alpha$); 79.3 ($\underline{C}$(CH$_3$)$_3$); 127.5 ($\underline{C}_{het}CO_2$); 136.0 ($\underline{C}_{het}NCH_3$), 148.5 ($\underline{C}_{azole}$); 155.6 ($\underline{C}O_2NH$); 164.3 ($\underline{C}O_2CH_3$) ppm. **- FAB-HR MS**: *m/z* calcd. for $C_{16}H_{28}N_3O_4^+$ 326.2074, found 326.2061. – **M.P.**: 122 °C.

(*S*)-2-(1-(*tert*-butoxycarbonylamino)-2-methylpropyl)-1,5-dimethyl-imidazole-4-carboxylic acid (5):

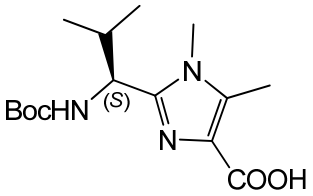

5

molecular formula: $C_{15}H_{25}N_3O_4$

molecular mass: 311.38 g/mol

Compound **4** (2.04g, 6.26 mmol) was converted into **5**, using 31 mL NaOH in 80 mL of a dioxane/methanol mixture as described above in the general procedure for the cleavage of the methyl ester group. Yield: 1.9 g (97%).

$C_{15}H_{25}N_3O_4$: calcd. (%): C 57.86, H 8.09, N 13.49; found (%): C C 57.86, H 8.09, N 13.49 **^{1}H-NMR** (200 MHz, $CDCl_3$): δ = 0.74 (d, ^3J = 6.7 Hz, 3H, CHC<u>H</u>$_3$); 1.11 (d, ^3J = 6.6 Hz, 3 H, CHC<u>H</u>$_3$); 1.35 (s, 9H, C(C<u>H</u>$_3$)$_3$); 2.48-2.62 (m, 1H, C<u>H</u>(CH$_3$)$_2$); 2.58 (s, 3H, C_{het}C<u>H</u>$_3$); 3.67 (s, 3H, NC<u>H</u>$_3$); 4.55 (dd, ^3J = 9.33 Hz 1H, C_α<u>H</u>); 7.40 (s, 1H, N<u>H</u>CO$_2$); 10.67 (s, 1H, CO$_2$<u>H</u>) ppm. **- ^{13}C-NMR** (50 MHz, $CDCl_3$): δ = 9.7 (C_{het}<u>C</u>H$_3$); 19.4, 19.6 (CH(<u>C</u>H$_3$)$_2$); 28.2 (<u>C</u>(CH$_3$)$_3$); 31.8 (<u>C</u>H(CH$_3$)$_2$); 32.3 (N<u>C</u>H$_3$); 52.6 (<u>C</u>$_\alpha$); 79.9 (<u>C</u>(CH$_3$)$_3$); 123.4 (C_{het}<u>C</u>O$_2$); 135.1 (C_{het}<u>C</u>NCH$_3$); 149.0 (C_{azole}); 156.2 (<u>C</u>O$_2$NH); 161.3 (<u>C</u>O$_2$H) ppm. **- ESI-HR MS** (CH$_3$OH): *m/z* calcd. for $C_{15}H_{26}N_3O_4^+$ 312.19178, found 312.19200. **- M.P.**: 99 -102 °C.

1-(4-carboxy-1,5-dimethyl-imidazole-2-yl)-(*S*)-1-isopropylmethyl-ammonium trifluoroacetat (6):

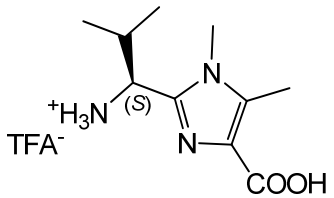

6

molecular formula: $C_{12}H_{18}F_3N_3O_4$

molecular mass: 325.13 g/mol

Compound **5** (1.9 g, 6.10 mmol) was converted into **6**, using 18 mL TFA in 120 mL DCM as described above in the general procedure for the cleavage of the Boc group. Yield: quantitative.

$C_{12}H_{18}F_3N_3O_4$: **^{1}H-NMR** (200 MHz, DMSO-D6): δ = 0.83 (d, ^3J = 6.7 Hz, 3H, CHC$\underline{H}_3$); 0.98 (d, ^3J = 6.7 Hz, 3H, CHC$\underline{H}_3$); 2.15-2.32 (m, 1H, C$\underline{H}$(CH$_3$)$_2$); 2.47 (s, 3H, $C_{het}C\underline{H}_3$); 3.57 (s, 3H, NC$\underline{H}_3$); 4.42 (m, 1H, $C_\alpha\underline{H}$); 8.49 (s, 1H, CN$\underline{H}_3$); 10.67 (s, 1H, $CO_2\underline{H}$) ppm. - **^{13}C-NMR** (50 MHz, DMSO-D6) δ = 9.9 ($C_{het}\underline{C}H_3$); 18.2, 18.2 (CH($\underline{C}H_3$)$_2$); 30.7 ($\underline{C}$H(CH$_3$)$_2$); 31.8 (N$\underline{C}H_3$); 51.0 ($\underline{C}_\alpha$); 124.4 ($\underline{C}_{het}NCH_3$); 136.9 ($\underline{C}_{het}CO_2$); 143.6 (C_{azole}); 164.3 ($\underline{C}O_2H$) ppm. - **ESI-HR MS** (CH$_3$OH): *m/z* calcd. for $C_{10}H_{19}N_3O_2^+$ 212.13935, found 212.13988.

Cyclic pseudo hexapeptide H_3L^1 and cyclic pseudo octapeptide H_4L^4:[48, 67]

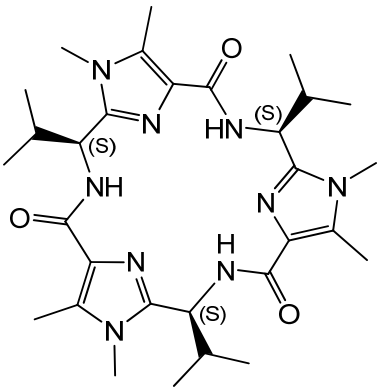

H_3L^1

molecular formula: $C_{30}H_{45}N_9O_3$

molecular mass: 579.77 g/mol

The synthesis was performed according to literature procedures.[48, 67] EDIPA (4.63 g, 35.82 mmol) and FDPP (3.89 g, 10.15 mmol) were added at room temperature to a suspension of **6** (1.94 g, 5.97 mmol) in acetonitrile (130 mL) and the mixture was stirred at room temperature for 3 days. The solvent was evaporated and the residue was dissolved in EtOAc, then extracted with water and brine, dried with $MgSO_4$, and concentrated in vacuo. Flash chromatography on silica gel (DCM/EtOAc/MeOH, 75:25:6) gave **H_3L^1** (235 mg, 35%) as a white solid, followed by **H_4L^4** (173 mg, 15%) as a white solid

$C_{30}H_{45}N_9O_3\cdot(H_2O)$: calcd. (%): C 60.28, H 7.93, N 21.09; found (%): C 60.10, H 8.00, N 20.29 (25434). - **^{1}H-NMR** (400 MHz, $CDCl_3$): δ = 1.08 (m, 6H, CHC$\underline{H}_3$); 2.07-2.17 (m, 1H, C$\underline{H}$(CH$_3$)$_2$); 2.56 (s, 3H, $C_{Het}C\underline{H}_3$); 3.52 (s, 3H, NC$\underline{H}_3$); 5.14 (dd, ^3J = 9.2, 6.14 Hz, 1H, $C_\alpha\underline{H}$); 8.43 (d, ^3J = 9.2 Hz, 1H, N$\underline{H}CO_2$) ppm. - **^{13}C-NMR** (100 MHz, CDCl3): δ = 9.6 ($C_{het}\underline{C}H_3$); 18.0, 19.5 (CH($\underline{C}H_3$)$_2$); 30.2 ($\underline{C}$H(CH$_3$)$_2$); 34.8 (N$\underline{C}H_3$); 49.6 ($\underline{C}_\alpha$H); 129.5 ($\underline{C}_{het}$CONH); 132.0 ($\underline{C}_{het}NCH_3$); 146.9 ($\underline{C}_{azole}$); 163.4 ($\underline{C}$ONH) ppm. - **IR** (KBr): ν = 3378, 2962, 2873, 1656,

1593, 1519 cm^{-1}. - **FAB-HR MS:** *m/z* calcd. for $C_{30}H_{46}N_9O_3^+$ 580.3718, found 580.3723. - **M.P.**: > 250°C.

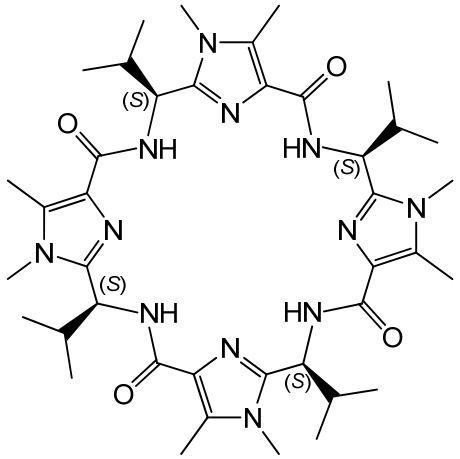

H_4L^4

molecular formula: $C_{40}H_{60}N_{12}O_4$

molecular mass: 772.98 g/mol

$C_{40}H_{60}N_{12}O_4 \cdot (H_2O)_3$ (772.98): calcd. (%): C 58.02, H 7.91, N 20.30; found (%): C 57.56, H 7.91, N 19.80 (28822). - **^{1}H-NMR** (500 MHz, $CDCl_3$): δ = 0.85 (d, ^3J = 6.6 Hz, 3H, CHC<u>H</u>$_3$); 1.10 (d, ^3J = 6.7 Hz, 3H, CHC<u>H</u>$_3$); 2.39-2.51 (m, 1H, C<u>H</u>$(CH_3)_2$); 2.47 (s, 3H, C_{het}C<u>H</u>$_3$); 3.61 (s, 3H, NC<u>H</u>$_3$); 4.89 (dd, ^3J = 9.5, 9.5 Hz, 1H, C_α<u>H</u>); 7.52 (d, ^3J = 9.4 Hz, 1H, N<u>H</u>CO_2). - **^{13}C-NMR** (125 MHz, CDCl3): δ = 9.8 (C_{het}<u>C</u>H_3); 19.2, 19.8 (CH(<u>C</u>$H_3)_2$); 30.1 (<u>C</u>$H(CH_3)_2$); 32.6 (N<u>C</u>H_3); 49.7 (<u>C</u>HC_{Het}); 129.3 (<u>C</u>$_{het}$CONH); 131.9(<u>C</u>$_{het}$NCH_3); 147.1 (<u>C</u>$_{azole}$); 163.7 (<u>C</u>ONH). - **FAB-HR MS:** *m/z* calcd. for $C_{40}H_{61}N_{12}O_4^+$ 773.4939, found 773.4880. – **M.P.**: 150-152°C.

5.2.2 Synthesis of the Cyclic Pseudo Octapeptide $H_4L^{4\text{-bn}}$

(*S*)-1-(4-(methoxycarbonyl)-1,5-dimethyl-imidazol-2-yl)-2-methylpropan-1-aminium trifluoro acetate (7):

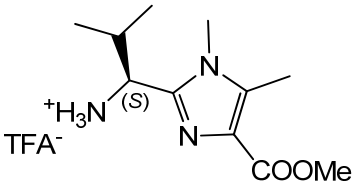

7

molecular formula: $C_{13}H_{20}F_3N_3O_4$

molecular mass: 339.31 g/mol

Compound **4** (5 g, 15.4 mmol) was converted into **7**, using 46.1 mL TFA in 460 mL DCM as described above in the general procedure for the cleavage of the Boc group. Yield: quantitative.

$C_{13}H_{20}F_3N_3O_4$ (339.31): **^{1}H-NMR** (200 MHz, DMSO-d_6): δ = 0.83 (d, ^3J = 6.8 Hz, 3H, CHC$\underline{H}_3$); 0.96 (d, ^3J = 6.7 Hz, 3H, CHC$\underline{H}_3$); 2.09-2.33 (m, 1H, C$\underline{H}$(CH$_3$)$_2$); 2.48 (s, 3H, $C_{het}C\underline{H}_3$); 3.57 (s, 3H, NC$\underline{H}_3$); 3.75 (s, 3H, $CO_2C\underline{H}_3$); 4.42 (m, 1H, $C_\alpha\underline{H}$); 8.44 (m, 1H, CN$\underline{H}_3$). - **^{13}C-NMR** (50 MHz, DMSO-d_6) δ = 9.9 ($C_{Het}\underline{C}H_3$); 18.1, 18.2 (CH($\underline{C}H_3$)$_2$); 30.7 ($\underline{C}$H(CH$_3$)$_2$); 31.8 (N$\underline{C}$H$_3$); 51.0 ($CO_2\underline{C}H_3$); 127.5 ($\underline{C}_{het}$CONH); 136.7 ($\underline{C}_{het}$NCH$_3$); 143.6 ($\underline{C}_{azole}$); 164.3 ($\underline{C}O_2CH_3$). - **ESI-HR MS**: *m/z* calcd. for $C_{11}H_{21}N_3O_2^+$ 226.15500, found 226.15514.

Methyl 2-((*S*)-2-(benzyloxycarbonylamino)-3-methylbutanamido)-3-oxobutanoate (8): [48, 67]

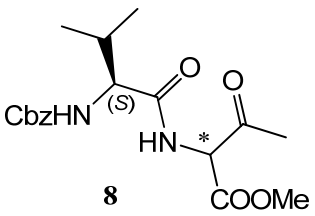

8

molecular formula: $C_{18}H_{24}N_3O_6$

molecular mass: 364.3926 g/mol

The synthesis was performed according to literature procedures.[48, 67] (*S*)-Cbz-Val-OH (16.49 g, 65.64 mmol, 1eq) were dissolved in 400 mL THF, NMM (6.6 g, 65.6 mmol, 1eq) is

added and the solution is cooled to -25°C. Subsequently isobutyl chloroformate (8.97 g, 65.64 mmol, 1 eq)was added, during which the reaction mixture was maintained at -25°C. After 35 min, the ammonium chloride salt **2** (11.0 g, 65.64 mmol, 1 eq), followed by a second equivalent of NMM (6.6 g, 65.6 mmol, 1eq) were added at -25°C and stirring was continued for 20 h as the reaction mixture was allowed to warm to room temperature. The solvent was evaporated, the residue dissolved in ethyl acetate, and then washed with water and brine. The combined organic layers were dried over $MgSO_4$ and concentrated in vacuo. After recrystallization from ethyl acetate 19.8 g of **8** were obtained as colorless crystals (82 %).

$C_{18}H_{24}N_2O_6$ (364.391) calcd. (%): C 59.33, H 6.64, N 7.69; found (%): C 58.89, H 6.72, N 7.70 (22264). - **^{1}H-NMR** (200 MHz, $CDCl_3$) δ = 0.83-0.93 (m, 6H, CH-($C\underline{H}_3$)$_2$); 2.04-2.17 (m, 1H, $C\underline{H}$-(CH_3)$_2$), 2.30 (s, 3H, $COC\underline{H}_3$), 3.73 (s, 3H, $CO_2C\underline{H}3$); 4.10 (m, 1H, $C\underline{H}$-$CH(CH_3)_2$); 5.04 (s, 2H, $C\underline{H}_2$-Ar); 5.21 (d, $^3J_{H,H}$ = 5.5 Hz, 1H, $N\underline{H}CHCO_2$); 5.32 (d, $^3J_{H,H}$ = 7.8Hz, 1H, $N\underline{H}$-CH_2-Ar); 7.05 (d, $^3J_{H,H}$ = 6.1Hz, 1H, $N\underline{H}$-CO); 7.27 (m, 5H C_{Ar}) ppm. - **^{13}C-NMR** (50 MHz, $CDCl_3$) δ = 16.7, 17.6 (CH-($\underline{C}H_3$)$_2$); 19.0, 19.3 (CH-($\underline{C}H_3$)$_2$), 28.0, 28.2 ($CO\underline{C}H_3$); 31.2, 31.3 ($\underline{C}$H-(CH_3)$_2$); 53.3, 53.5 ($CO_2\underline{C}H_3$); 59.9, 62.9 (NH$\underline{C}$HCO); 63.1, 67.3 ($\underline{C}H_2$-Ar); 128.03, 128.2, 128.3, 128.64, 128.69, 136($\underline{C}_{ar}$);, 156.5($\underline{C}O_2$NH); 166.1, 166.3 ($\underline{C}O_2CH_3$); 171($\underline{C}$ONH); 197.7, 197.9 ($\underline{C}OCH_3$) ppm. - **FAB-HR MS**: calcd for $C_{18}H_{25}N_2O_6^+$ 365.178, found 365.178

(*S*)-methyl 2-(1-(benzyloxycarbonylamino)-2-methylpropyl)-5-methyl-1H-imidazole-4-carboxylate (9):[65]

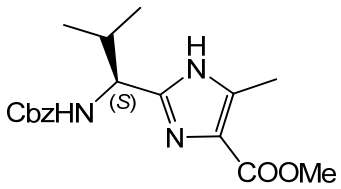

9

molecular formula: $C_{18}H_{23}N_3O_4$

molecular mass: 345.39 g/mol

The synthesis was performed according to literature procedures.[65] To a slurry of dipeptide **8** (9.7 g, 26.6 mmol) in 200 mL xylene, 6.07 g TFA (53 mmol, 2eq) and 7 M ammonia in methanol (7.6 mL, 53 mmol) were added. The mixture was heated under intensive reflux with a Dean–Stark trap for 8 h. After completion of the reaction, volatiles were removed in a rotary evaporator. The residual solid was subjected to column chromatography on silica gel (petrol ether/ethyl acetate 1:1) to obtain 4.4 g (49%) of **9** as a white fluffy solid.

$C_{18}H_{23}N_3O_4$ (345.1688) calcd. (%): C 62.59, H 6.71, N 12.17; found (%): C 62.44, H 6.74, N 11.88 (22277). - **^{1}H-NMR** (200 MHz, $CDCl_3$) δ = 0.79 (d, $^3J_{H,H}$ = 6.7Hz, 3H, CH(C<u>H</u>$_3$)$_2$); 0.93 (d, $^3J_{H,H}$ = 6.7Hz, 3H, CH-(C<u>H</u>$_3$)$_2$); 2.03-2.17 (m, 1H, C<u>H</u>(CH$_3$)$_2$), 2.41 (s, 3H, C_{het}C<u>H</u>$_3$), 3.80 (s, 3H, CO_2C<u>H</u>$_3$); 4.44 (d, $^3J_{H,H}$ = 7.9Hz 1H, C_α<u>H</u>); 5.03 (d, $^1J_{H,H}$ = 3.4Hz 2H, C<u>H</u>$_2$Ar); 7.29 (m, 5H C_{Ar}<u>H</u>) ppm. - **^{13}C-NMR** (50 MHz, $CDCl_3$) δ = 19.1 (<u>C</u>H$_3$C$_{het}$); 19.6 ((<u>C</u>H$_3$)$_2$CH); 33.9 (<u>C</u>H(CH$_3$)$_2$); 51.7 (CO_2<u>C</u>H$_3$); 56.8 (C_α); 67.8 (<u>C</u>H$_2$C$_{Ar}$); 128.9 (C_{Ar}); 129.0 (C_{het}); 129.4 (C_{Ar}); 138.1 (C_{Ar}); 142.2 (C_{Ar}); 150.2 (C_{het}); 158.3 (C_{het}); 164.3 (<u>C</u>OOCH$_3$) ppm. - **FAB-HR MS**: calcd for $C_{18}H_{24}N_2O_6^+$ 346.176, found 346.208

(*S*)-methyl 2-(1-(*tert*-butoxycarbonylamino)-2-methylpropyl)-5-methyl-1H-imidazole-4-carboxylate (10):[65]

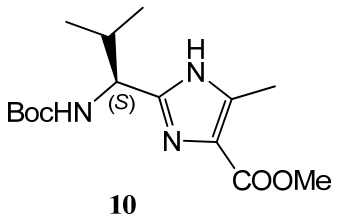

10

molecular formula: $C_{15}H_{25}N_3O_4$

molecular mass: 311.376 g/mol

The synthesis was performed according to literature procedures.[65] Di-tert-butyldicarbonate (Boc_2O) (2.75 g,11.6 mmol) and $Pd(OH)_2$ (0.43 g) were added to a solution of 9 (3.62 g, 10.5 mmol) in 200 mL THF at room temperature. The solution was stirred under an H_2 atmosphere at room temperature for 1 d, then filtered, and the solvent was removed in vacuo. Flash chromatography with silica gel (petroleum ether/ethyl acetate: 2:3) gave 2.96 g of **10** (9.30 mmol, 89%) as a white solid.

$C_{15}H_{25}N_3O_4$ (311.317) calcd. (%): C 47.86, H 8.09, N 14.4; found (%): C 57.37, H 8.11, N 13.14 (22238). - **^{1}H-NMR** (200 MHz, $CDCl_3$) δ = 0.81 (d, $^3J_{H,H}$ = 6.7 Hz, 3H, CH(C<u>H</u>$_3$)$_2$); 0.98 (d, $^3J_{H,H}$ = 6.5 Hz, 3H, CH(C<u>H</u>$_3$)$_2$); 1.45 (s, 9H, C(C<u>H</u>$_3$)$_3$); 1.98-2.14 (m, 1H, C<u>H</u>(CH$_3$)$_2$), 2.47 (s, 3H, COC<u>H</u>$_3$), 3.86 (s, 3H, CO_2C<u>H</u>$_3$); 4.26-4.40 (m, br, 1H, C_α), 5.62-5.84 (m, 1H, BocN<u>H</u>) ppm. - **^{13}C-NMR** (50 MHz, $CDCl_3$) δ = 19.1 (<u>C</u>H$_3$C$_{het}$); 19.6 ((<u>C</u>H$_3$)$_2$CH); 28.0 (CH(<u>C</u>H$_3$)$_3$); 52.7 (CO_2<u>C</u>H$_3$); 81.38 (C_α); 86.8 (<u>C</u>(CH$_3$)$_3$); 128.2 (C_{het}); 148.8 (C_{azole}); 158.1 (<u>C</u>O$_2$CH$_3$), ppm. - **FAB-HR MS**: calcd. for $C_{15}H_{25}N_3O_4^+$ 312.1923, found 312.1944. **M.P.**: 161–162°C

(*S*)-methyl 1-benzyl-2-(1-(*tert*-butoxycarbonylamino)-2-methylpropyl)-5-methyl-imidazole-4-carboxylate (11):[65]

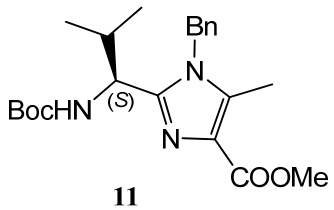

11

molecular formula: $C_{22}H_{31}N_3O_4$
molecular mass: 401.499 g/mol

The synthesis was performed according to literature procedures.[65] A solution of **10** (2.87 g, 9.3 mmol) in 180 mL DMF (400 mL) was cooled down to 0°C and both NaH (0.45 g, 11.2 mmol) and BnBr (2.07 g, 12.1 mmol) were added at this temperature. The reaction was kept at 0°C for two hours and stirring was continued for 18 hours as the reaction mixture was allowed to warm to room temperature. The reaction mixture is poured on 800g ice. The white solid is filtered, washed with water and dissolved in dichloromethane. The organic layer is washed with water and brine and dried over $MgSO_4$. The solvent was removed in vacuo. Flash chromatography with silica gel (petroleum ether/ethyl acetate: 3:1) gave 2.23 g of **11** (5.6 mmol, 60%) as a white solid.

$C_{22}H_{31}N_3O_4$ (401.499) calcd. (%): C 65.81, H 7.78, N 10.47; found (%): C 65.63, H 7.72, N 10.38 (22395). - **^{1}H-NMR** (200 MHz, MeOH-d_4) δ = 0.84 (d, $^3J_{H,H}$ = 6.7 Hz, 3H, CH(C$\underline{H}_3$)$_2$); 0.97 (d, 3H, CH(C$\underline{H}_3$)$_2$); 1.45 (s, 9H, C(C$\underline{H}_3$)$_3$); 1.98-2.15 (m, 1H, C$\underline{H}$(CH$_3$)$_2$), 2.48 (s, 3H, COC$\underline{H}_3$), 3.86 (s, 3H, $CO_2C\underline{H}_3$); 4.43 (dd, 1H, $C_\alpha\underline{H}$); 5.83 (d $^1J_{H,H}$ = 16.1 Hz, 1H, C$\underline{H}_2$Ar); 7.08-7.28 (m, 5H, $C_{ar}\underline{H}$) ppm. - **^{13}C-NMR** (50 MHz, MeOH-d_4) δ = 10,2 ($\underline{C}H_3$-C_{het}); 19,1 (($\underline{C}H_3$)$_2$CH); 19,9 (($\underline{C}H_3$)$_2$CH); 28,5 (C($\underline{C}H_3$)$_3$); 32,7 ($\underline{C}$H(CH$_3$)$_2$); 54,17 ($CO_2\underline{C}H_3$); 67,9 ($\underline{C}H_2C_{Ar}$); 80,7 ((CH$_3$)$_2\underline{C}$H); 126.6 ($\underline{C}_{Ar}$); 126.7 ($\underline{C}_{het}$); 127.2, 129.0 ($\underline{C}_{Ar}$); 130,0 ($\underline{C}_{het}$); 136,5 ($\underline{C}_{Ar}$); 137,8; 149,9 ($\underline{C}_{het}$); 157.4 ($\underline{C}O_2$NH); 164.5 ($\underline{C}O_2CH_3$) ppm. - **HR-ESI MS**: calcd. for $C_{22}H_{32}N_3O_4^+$ 402.239, found 402.219. **M.P**.: 126°C

(*S*)-1-benzyl-2-(1-(*tert*-butoxycarbonylamino)-2-methylpropyl)-5-methyl-imidazole-4-carboxylic acid (12):

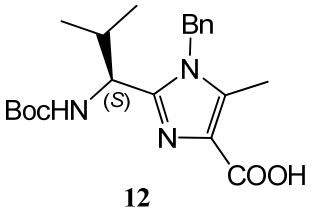

12

molecular formula: $C_{21}H_{29}N_3O_4$
molecular mass: 387.47 g/mol

Compound **11** (2.24g, 5.60 mmol) was converted into **12**, using 28 mL NaOH in 70 mL of a dioxane/methanol mixture as described above in the general procedure for the cleavage of the methyl ester group. Yield: quantitative.

$C_{21}H_{29}N_3O_4$ (387.470) calcd. (%): C 65.09, H 7.54, N 10.84; found (%): C 66.22, H 7.93, N 9.80 (22654). - **^{1}H-NMR** (200 MHz, DMSO-d_6) δ = 0.19 (d, $^3J_{H,H}$ = 6.2 Hz, 3H, CH(C$\underline{H}_3$)$_2$); 0.78 (d, $^3J_{H,H}$ = 6.4 Hz 3H, CH(C$\underline{H}_3$)$_2$); 1.38 (s, 9H, C(C$\underline{H}_3$)$_3$); 1.80-1.92 (m, 1H, C$\underline{H}$(CH$_3$)$_2$); 2.36 (s, 3H, $C_{het}C\underline{H}_3$); 4.52 (m, 1H, $C_\alpha\underline{H}$); 5.16 (d, $^1J_{H\text{-}H}$ = 16.8 Hz, 1H, C$\underline{H}_2C_{Ar}$); 5.39 (d, $^1J_{H\text{-}H}$ = 16.7 Hz, 1H, C$\underline{H}_2C_{Ar}$); 7.01-7.12 (m, 2H, $C_{Ar}\underline{H}$); 7.21-7.35 (m, 3H, $C_{Ar}\underline{H}$); 7.59 (d, $^3J_{H,H}$ = 9.8 Hz, N$\underline{H}$-(CH$_3$)$_3$) ppm. - **^{13}C-NMR** (50 MHz, DMSO-d_6) δ = 9.6 ($\underline{C}H_3C_{het}$); 19.4 (($\underline{C}H_3$)$_2$CH); 19.5 (($\underline{C}H_3$)$_2$CH); 28.1 (C($\underline{C}H_3$)$_3$); 28.6 ($\underline{C}$H(CH$_3$)$_2$); 52.1 ($CO_2\underline{C}H_3$); 66.7 ($\underline{C}_\alpha$); 78.4 ((CH$_3$)$_3\underline{C}$); 126.1 ($\underline{C}_{het}$); 127.0, 128.8 ($\underline{C}_{Ar}$); 134.2 ($\underline{C}_{azole}$); 136.0, 147.4 ($\underline{C}_{Ar}$); 154.0 ($\underline{C}_{het}$); 155.6 ($\underline{C}O_2$NH); 166.4 ($\underline{C}O_2CH_3$) ppm. - **HR-ESI MS**: calcd. for $C_{21}H_{30}N_3O_4^+$ 388.2236, found 388.2316. **M.P**.: 113°C

Methyl 2-((*S*)-1-(1-benzyl-2-((*S*)-1-(*tert*-butoxycarbonylamino)-2-methylpropyl)-5-methyl-imidazole-4-carboxamido)-2-methylpropyl)-1,5-dimethyl-imidazole-4-carboxylate (13):

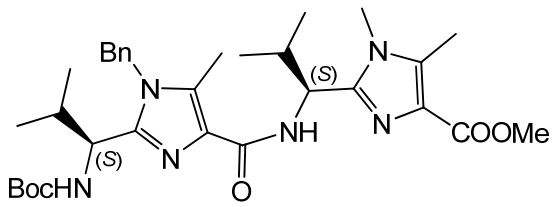

13

molecular formula: $C_{32}H_{46}N_6O_5$
molecular mass: 594.747 g/mol

EDIPA (4.87g, 37.7 mmol) and FDPP (2.10 g, 5.50 mmol) were added at room temperature to the benzyl imidazole building block **12** (1.90 g, 4.90 mmol) and the methyl imidazole building block **7** (2.10 g, 6.20 mmol) in 150 mL acetonitrile, and the mixture was stirred at room temperature for 4 days. The solvent was then evaporated and the residue dissolved in ethyl acetate. The organic layers were washed with water and brine, dried with $MgSO_4$, and concentrated in vacuo. Flash chromatography on silica gel (petrol ether/ethyl acetate 1:2) gave building block **13** (1.25 g, 43%) as a white solid.

$C_{32}H_{46}N_6O_5 \cdot$ ½ EtOAc (387.470) calcd. (%): C 63.98, H 7.82, N 13.17; found (%): C 63.69, H 7.80, N 13.50 (24297). - **^{1}H-NMR** (400 MHz, $CDCl_3$) δ = 0.71 (d, $^3J_{H,H}$ = 6.6 Hz, 3H, $CH(C\underline{H}_3)_2$); 0.92 (d, $^3J_{H,H}$ = 6.6 Hz, 3H, $CH(C\underline{H}_3)_2$); 0.96 (d, $^3J_{H,H}$ = 6.6 Hz, 3H, $CH(C\underline{H}_3)_2$); 1.13 (d, $^3J_{H,H}$ = 6.6 Hz, 3H, $CH(C\underline{H}_3)_2$); 1.38 (s, 9H, $C(C\underline{H}_3)_3$); 2.06-2.24 (m, 2H, $C\underline{H}(CH_3)_2$); 2.30 (s, 3H, $C_{het}C\underline{H}_3$); 2.38 (s, 3H, $C_{het}C\underline{H}_3$); 3.56 (s, 3H, $N_{het}C\underline{H}_3$); 3.63 (s, 3H, $N_{het}C\underline{H}_3$); 4.38 (dd, 1H, $^3J_{H,H}$ = 9.1 Hz, $C_\alpha\underline{H}$); 4.91 (dd, 1H, $^3J_{H,H}$ = 9.1 Hz, $C_\alpha\underline{H}$); 5.21 (s, 2H, $C\underline{H}_2$-Ar), 6.21 (d, $^3J_{H,H}$ = 9.4 Hz, 2H, $N\underline{H}C(CH_3)_3$); 6.94-7.26 (m, 5H, $C_{ar}\underline{H}$), 7.44 (d, 1H, $^3J_{H,H}$ = 9.6Hz, $N\underline{H}CO$) ppm. - **^{13}C-NMR** (100 MHz, $CDCl_3$) δ = 9.6, 10.2 ($\underline{C}H_3C_{het}$); 18.2, 19.4, 19.5, 19.90 ($(\underline{C}H_3)_2CH$); 28.1 ($C(\underline{C}H_3)_3$); 30.4 ($N_{imi}\underline{C}H_3$); 32.4, 32.6 ($\underline{C}H(CH_3)_2$); 46.2, 49.3 (C_α); 51.1 ($CO_2\underline{C}H_3$); 51.8 ($\underline{C}H_2Ar$); 79.4 ($(CH_3)_3\underline{C}$); 126.0($\underline{C}_{het}$); 127.4, 128.5($\underline{C}_{Ar}$); 129.1, 132.3, 132.5, 136.1, 147.3($\underline{C}_{Ar}$); 163.4 ($\underline{C}O_2NH$); 163.7($\underline{C}O_2CH_3$) ppm. - **HR-ESI MS**: calcd. for $C_{32}H_{47}N_5O_6^+$ 595.3608, found 595.3610. **M.P**.: 83°C

2-((*S*)-1-(1-benzyl-2-((*S*)-1-(*tert*-butoxycarbonylamino)-2-methylpropyl)-5-methyl-imidazole-4-carboxamido)-2-methylpropyl)-1,5-dimethyl-imidazole-4-carboxylic acid (14):

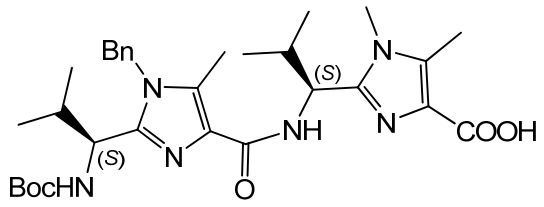

14

molecular formula: $C_{31}H_{44}N_6O_5$
molecular mass: 580.727 g/mol

Compound **13** (1.25 g, 2.11 mmol) was converted into **14**, using 11 mL NaOH in 30 mL of a dioxane/methanol mixture as described above in the general procedure for the cleavage of the methyl ester group. Yield: quantitative.

$C_{31}H_{44}N_6O_5 \cdot H_2O$ (580.727) calcd. (%): C 62.19, H 7.74, N 14.04; found (%): C 62.49, H 7.75, N 13.56 (24423). - **^{1}H-NMR** (400 MHz, $CDCl_3$) δ = 0.58 (d, $^3J_{H,H}$ = 6.3 Hz, 3H, CH(C$\underline{H}_3$)$_2$); 0.92 (d, $^3J_{H,H}$ = 6.6 Hz, 3H, CH(C$\underline{H}_3$)$_2$); 0.96 (d, $^3J_{H,H}$ = 6.6 Hz, 3H, CH(C$\underline{H}_3$)$_2$); 1.16 (d, $^3J_{H,H}$ = 6.6 Hz, 3H, CH(C$\underline{H}_3$)$_2$); 1.33 (s, 9H, C(C$\underline{H}_3$)$_3$); 2.19-2.42 (m, 2H, C$\underline{H}$(CH$_3$)$_2$); 2.52 (s, 3H, $C_{het}C\underline{H}_3$); 2.58 (s, 3H, $C_{het}C\underline{H}_3$), 2.67-2.84 (m, 2H, C$\underline{H}$(CH$_3$)$_2$); 3.56 (s, 3H, $N_{het}C\underline{H}_3$); 4.55 (dd, 1H, $^3J_{H,H}$ = 9.3 Hz, $C_\alpha\underline{H}$); 5.06 (dd, 1H, $^3J_{H,H}$ = 9.1 Hz, $C_\alpha\underline{H}$); 5.21 (d, 1H, $^1J_{H,H}$ = 16.1 Hz, C$\underline{H}_2$-Ar); 5.39 (d, 1H, $^1J_{H,H}$ = 16.1 Hz, C$\underline{H}_2$-Ar); 5.87 (d, $^3J_{H,H}$ = 8.9 Hz, 2H, N$\underline{H}$C(CH$_3$)$_3$); 7.04-7.36 (m, 5H, $C_{ar}\underline{H}$), 8.72 (d, 1H, $^3J_{H,H}$ = 8.6Hz, N$\underline{H}$CO), 11.3 (s, br, 1H, COO$\underline{H}$) ppm. - **^{13}C-NMR** (100 MHz, $CDCl_3$) δ = 9.6 ($\underline{C}H_3C_{het}$); 10.2 ($\underline{C}H_3C_{het}$); 18.2, 19.4, 19.5, 19.90 (($\underline{C}H_3$)$_2$CH); 28.1 (C($\underline{C}H_3$)$_3$); 30.4 (N$\underline{C}H_3$); 32.4, 32.6 ($\underline{C}$H(CH$_3$)$_2$); 46.2, 49.3 (C_α); 51.1 ($CO_2\underline{C}H_3$); 51.8 ($\underline{C}H_2$Ar); 79.4 ((CH$_3$)$_3\underline{C}$); 126.0($\underline{C}_{het}$); 127.4, 128.5($\underline{C}_{Ar}$); 129.1, 132.3, 132.5, 136.1, 147.3($\underline{C}_{Ar}$); 163.4 ($\underline{C}O_2$NH); 163.7($\underline{C}O_2$H) ppm. - **HR-ESI MS**: calcd. for $C_{31}H_{45}N_5O_6^+$ 581.3608, found 581.3600. **M.P**.: 112°C

(*S*)-1-(1-benzyl-4-((*S*)-1-(4-carboxy-1,5-dimethyl-imidazol-2-yl)-2-methyl-propyl-carb-amoyl)-5-methyl-imidazol-2-yl)-2-methylpropan-1-aminium trifluoro acetate (15):

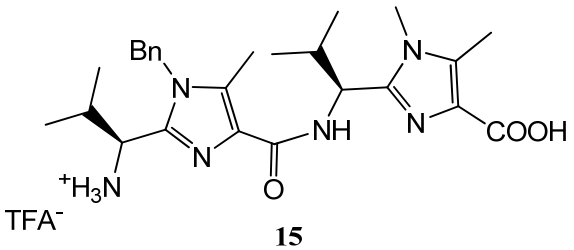

15

molecular formula: $C_{26}H_{31}N_6O_3 \cdot C_2F_3O_2$
molecular mass: 577.623 g/mol

Compound **14** (1.22 g, 2.10 mmol) was converted into **15**, using 6.3 mL TFA in 42 mL DCM as described above in the general procedure for the cleavage of the Boc group. Yield: quantitative.

$C_{26}H_{31}N_6O_3 \cdot C_2F_3O_2$ (577.623) - **^{1}H-NMR** (400 MHz, $CDCl_3$) δ = 0.67 (m, 3H, CH(C<u>H</u>$_3$)$_2$); 0.91 (d, $^3J_{H,H}$ = 5.3 Hz, 3H, CH(C<u>H</u>$_3$)$_2$); 0.99 (d, $^3J_{H,H}$ = 5.05 Hz, 3H, CH(C<u>H</u>$_3$)$_2$); 1.24 (m, 3H, CH(C<u>H</u>$_3$)$_2$); 2.19-2.29 (m, 1H, C<u>H</u>(CH$_3$)$_2$); 2.45 (s, 3H, C_{het}C<u>H</u>$_3$); 2.51-2.59 (m, 1H, C<u>H</u>(CH$_3$)$_2$); 2.54 (s, 3H, C_{het}C<u>H</u>$_3$), 3.91 (s, 3H, N_{het}C<u>H</u>$_3$); 4.45 (m, 1H, C_α<u>H</u>); 5.18-5.30 (m, 2H, C<u>H</u>$_2$-Ar); 7.04-7.36 (m, 5H, C_{ar}<u>H</u>), 8.72 (m, br, 1H, N<u>H</u>CO), 11.3 (s, br, 1H, COO<u>H</u>) 14.5-15.5 (s, br, 3H, N<u>H</u>$_3$) ppm. - **^{13}C-NMR** (100 MHz, $CDCl_3$) δ = 9.1, 9.6 (<u>C</u>H$_3$C$_{het}$); 17.3, 18.3, 18.9, 19.34 ((<u>C</u>H$_3$)$_2$CH); 31.4 (N_{imi}<u>C</u>H$_3$); 32.0 (<u>C</u>H(CH$_3$)$_2$); 47.2 (<u>C</u>H$_2$Ar); 50.7, 52.6 (C_α); 111.31, 114.21, 117.1, 119.96 (TFA); 126.0(<u>C</u>$_{het}$); 128.4, 128.5(<u>C</u>$_{Ar}$); 129.1, 134.3, 135.5, 142.1, 147.3(<u>C</u>$_{Ar}$); 160.4; 163.7(<u>C</u>O$_2$H) ppm. - **HR-ESI MS**: calcd. for $C_{26}H_{31}N_6O_3^+$ 481.293, found 481.3121.

Cyclic Pseudo Octapeptide $H_4L^{4\text{-bn}}$:

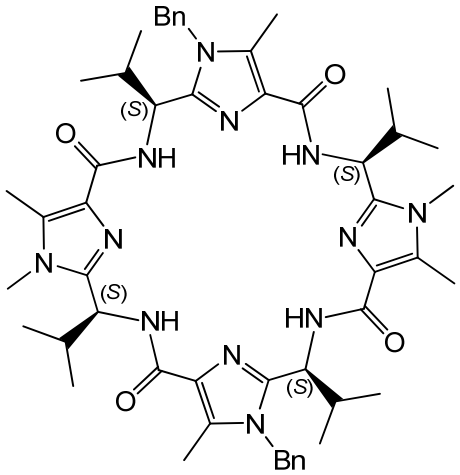

$H_4L^{4\text{-bn}}$

molecular formula: $C_{52}H_{68}N_{12}O_4$

molecular mass: 925.172 g/mol

The synthesis was performed analogous to literature procedures.[48, 67] EDIPA (1.91 g, 14.77 mmol) and FDPP (1.62 g, 4.22 mmol) were added at room temperature to a suspension of **15** (1.22 g, 2.11 mmol) in 200 mL acetonitrile and the mixture was stirred at room temperature for 3 days. The solvent was evaporated and the residue was dissolved in EtOAc, then extracted with water and brine, dried with $MgSO_4$, and concentrated in vacuo. Flash chromatography on silica gel (petrol ether/ethyl acetate 1:1) gave $\mathbf{H_4L^{4\text{-bn}}}$ in 45 % yield (880 mg, 0.95 mmol).

$C_{52}H_{68}N_{12}O_4 \cdot 2H_2O$ (925.172) calcd. (%): C 64.98, H 7.55, N 17.49; found (%): C 64.73, H 7.65, N 17.19 (24233). - **^{1}H-NMR** (400 MHz, $CDCl_3$) δ 0.67 (m, 3H, CH(C$\underline{H}_3$)$_2$); 0.91 (d, $^3J_{H,H}$ = 5.3 Hz, 3H, CH(C$\underline{H}_3$)$_2$); 0.99 (d, $^3J_{H,H}$ = 5.05 Hz, 3H, CH(C$\underline{H}_3$)$_2$); 1.24 (m, 3H, CH(C$\underline{H}_3$)$_2$); 2.19-2.29 (m, 1H, C$\underline{H}$(CH$_3$)$_2$); 2.45 (s, 3H, $C_{het}C\underline{H}_3$); 2.51-2.59 (m, 1H, C$\underline{H}$(CH$_3$)$_2$); 2.54 (s, 3H, $C_{het}C\underline{H}_3$), 3.91 (s, 3H, $N_{het}C\underline{H}_3$); 4.45 (m, 1H, $C_\alpha\underline{H}$); 5.18-5.30 (m, 2H, C$\underline{H}_2$-Ar); 7.04-7.36 (m, 5H, $C_{ar}\underline{H}$), 8.72 (m, br, 1H, N$\underline{H}$CO), 11.3 (s, br, 1H, COO$\underline{H}$) 14.5-15.5 (s, br, 3H, N$\underline{H}_3$) ppm. - **^{13}C-NMR** (100 MHz, $CDCl_3$) δ = 9.1, 9.6 ($\underline{C}H_3C_{het}$); 17.3, 18.3, 18.9, 19.34 (($\underline{C}H_3$)$_2$CH); 31.4 ($N_{imi}\underline{C}H_3$); 32.0 ($\underline{C}$H(CH$_3$)$_2$); 47.2 ($\underline{C}H_2$Ar); 50.7, 52.6 (C_α); 111.31, 114.21, 117.1, 119.96 (TFA); 126.0($\underline{C}_{het}$); 128.4, 128.5($\underline{C}_{Ar}$); 129.1, 134.3, 135.5, 142.1, 147.3($\underline{C}_{Ar}$); 160.4; 163.7($\underline{C}O_2H$) ppm. - **HR-ESI MS**: calcd. for $C_{52}H_{69}N_{12}O_4^+$ 925.3564, found 925.5564.

5.2.3 Synthesis of the Cyclic Pseudo Octapeptide H_4L^{rs}

Methyl 2-((*R*)-2-(tert-butoxycarbonylamino)-3-methylbutanamido)-3-oxobutanoate (16):

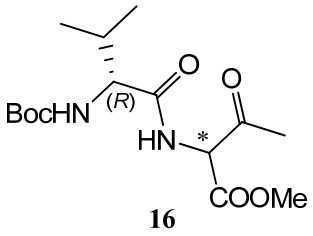

16

molecular formula: $C_{15}H_{26}N_2O_6$

molecular mass: 330.38 g/mol

The Synthesis was performed analogous to literature procedures.[48] (*R*)-Boc-Val-OH (3.5 g, 15.6 mmol, 1eq) is dissolved in 100 mL THF, NMM (1.7 g, 16.65 mmol, 1eq) is added and the solution is cooled to -25°C. Subsequently isobutyl chloroformate (2.13 g, 15.6 mmol, 1 eq) is added, during which the reaction mixture is maintained at -25°C. After 35 min, the ammonium chloride salt **2** (2.6 g, 15.6 mmol, 1 eq), followed by a second equivalent of NMM (1.7 g, 47.8 mmol, 1eq) are added at -25°C and stirring is continued for 20 h as the mixture is allowed to warm to room temperature. The solvent is evaporated, the residue dissolved in ethyl acetate, and then washed with water and brine. The combined organic layers are dried over $MgSO_4$ and concentrated in vacuo. After recrystallization from ethyl acetate 4.5 g of **16** are obtained as colorless crystals (87 %).

$C_{15}H_{26}N_2O_6$: calcd. (%): C 54.53, H 7.93, N 8.48; found (%): C 54.66, H 7.94, N 8.62 (28053). **- ^{1}H-NMR** (200 MHz, $CDCl_3$): δ = 0.87 (d, $^3J_{H,H}$ = 6.9 Hz, 3H, CHC$\underline{H}_3$), 0.88 (d, $^3J_{H,H}$ = 6.9 Hz, 3H, CHC$\underline{H}_3$), 0.93 (d, $^3J_{H,H}$ = 6.8 Hz, 6H, CHC$\underline{H}_3$); 1.39(s, 9H, C(C$\underline{H}_3$)$_3$); 1.40 (s, 9H, C(C$\underline{H}_3$)$_3$); 2.10-2.26 (m, 2H, C$\underline{H}$(CH$_3$)$_2$); 2.33 (s, 6H, COC$\underline{H}_3$); 3.76 (s, 6H, $CO_2C\underline{H}_3$); 4.0 - 4.08 (m, 2H, C$\underline{H}$CONH); 5.07 (d, $^3J_{H,H}$ = 8.1 Hz, 1H, N$\underline{H}CO_2$); 5.09 (d, $^3J_{H,H}$ = 8.6 Hz, 1H, N$\underline{H}CO_2$); 5.21 (d, $^3J_{H,H}$ = 6.3 Hz, 2H, C$\underline{H}CO_2$); 7.13 (d, $^3J_{H,H}$ = 6.3 Hz, 1H, N$\underline{H}$); 7.18 (d, $^3J_{H,H}$ = 6.5 Hz, 1H, N$\underline{H}$) ppm. **- ^{13}C-NMR** (50 MHz, $CDCl_3$): δ = 17.3, 17.5 (CH(C$\underline{H}_3$)$_2$); 19.1; 19.2 (CH(C$\underline{H}_3$)$_2$); 27.9, 28.0 (CO$\underline{C}H_3$); 28.2 ($\underline{C}$(CH$_3$)$_3$); 30.7, 30.9 ($\underline{C}$H(CH$_3$)$_2$); 53.2, 53.3 ($CO_2\underline{C}H_3$); 59.4, 59.5 (NH$\underline{C}$HCO); 62.8, 62.9 (NH$\underline{C}$HCO$_2$); 80.1 ($\underline{C}$(CH$_3$)$_3$); 155.7 (NH$\underline{C}$OC(CH$_3$)$_3$); 166.3, 166.4 ($\underline{C}O_2CH_3$); 171.6 (NH$\underline{C}$O); 198.0; 198.1 ($\underline{C}OCH_3$) ppm. **- FAB-HR MS**: *m/z* calcd. for $C_{15}H_{27}N_2O_6^+$ 331.1866, found 331.1853. **- M.P.:** 106°C.

(*R*)-methyl 2-(1-(*tert*-butoxycarbonylamino)-2-methylpropyl)-1,5-dimethyl-imidazole-4-carboxylate (17):

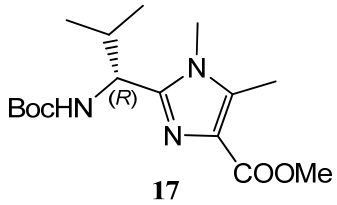

17

molecular formula: $C_{16}H_{27}N_3O_4$

molecular mass: 325.40 g/mol

The synthesis was performed analogous to the synthesis of **4**.[67] Both glacial acedic acid (7.9 mL, 33.5 mmol, 1 eq) and NH_2Me in MeOH (8 M, 6.45 mL, 62.96 mmol, 4eq) were added to a solution of **16** (5.2 g, 15.7 mmol, 1eq) in 200 mL xylenes at room temperature. The solution was stirred at 155°C with azeotropic removal of water for 8 h and then cooled to room temperature. The solvent was concentrated, and the residue was dissolved in AcOEt, and then washed with saturated $NaHCO_3$ solution and brine. The organic layer was dried over Na_2SO_4 and concentrated in vacuo. Purification was achieved by performing chromatography with silica gel (petroleum ether/ethyl acetate 1:3) to provide 3.6 g of **17** (72%) as a white solid.

$C_{16}H_{27}N_3O_4$ (325.40): calcd. (%):C 59.06, H 8.36; N 12.91; found (%): C 58.82, H 8.36, N 12.86 (28052). - **^{1}H-NMR** (200 MHz, $CDCl_3$): δ = 0.74 (d, $3J_{H,H}$ = 6.7 Hz, 3H, $CHC\underline{H}_3$), 0.93 (d, ^3J = 6.7 Hz, 3H, $CHC\underline{H}_3$), 1.31 (s, 9H, $C(C\underline{H}_3)_3$), 2.02-2.30 (m, 1H, $C\underline{H}(CH_3)_2$), 2.44 (s, 3H, $C_{het}C\underline{H}_3$), 3.48 (s, 1H, $NC\underline{H}_3$), 3.79 (s, 1H, $CO_2C\underline{H}_3$), 4.45 (dd, $^3J_{H,H}$ = 9.18 Hz, 1H, $C_\alpha\underline{H}$), 5.26 (d, $J_{H,H}$ = 9.58 Hz, 1H, N$\underline{H}$) ppm. - **^{13}C-NMR** (50 MHz, $CDCl_3$): 10.2 ($C_{het}\underline{C}H_3$); 18.5, 19.6 ($CH(\underline{C}H_3)_2$); 28.3 ($\underline{C}(CH_3)_3$); 30.3 ($N\underline{C}H_3$); 33.2 ($\underline{C}H(CH_3)_2$); 51.4 ($CO_2\underline{C}H_3$); 52.1 ($\underline{C}_\alpha$); 79.4 ($\underline{C}(CH_3)_3$); 127.5 ($\underline{C}_{het}CO_2$); 135.9 ($\underline{C}_{het}CH_3$); 148.4 ($\underline{C}_{het}N$); 155.6 (NH$\underline{C}$O); 164.2 ($\underline{C}O_2CH_3$) ppm - **ESI-HR MS**: *m/z* calcd. for $C_{16}H_{28}N_3O_4^+$ 326.2074, found 326.2075. - **M.P.:** 106°C.

(*R*)-2-(1-(*tert*-butoxycarbonylamino)-2-methylpropyl)-1,5-dimethyl-imidazole-4-carboxylic acid (18):

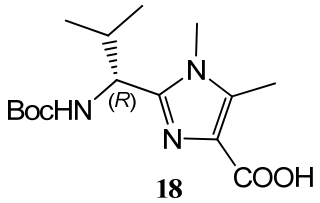

18

molecular formula: $C_{15}H_{25}N_3O_4$
molecular mass: 311.38 g/mol

Compound **17** (1.9 g, 5.8 mmol) was converted into **18**, using 29 mL NaOH in 73 mL of a dioxane/methanol mixture as described above in the general procedure for the cleavage of the methyl ester group. Yield: quantitative.

$C_{15}H_{25}N_3O_4$ (311.38): calcd. (%): C 59.06, H 8.36, N 12.91; found (%): C 58.82, H 8.36, N 12.86 (28052). - **^{1}H-NMR** (200 MHz, $CDCl_3$): δ = 0.74 (d, $^3J_{H,H}$ = 6.7 Hz, 3H, CHC$\underline{H}_3$); 1.11 (d, $^3J_{H,H}$ = 6.6 Hz, 3 H, CHC$\underline{H}_3$); 1.35 (s, 9H, C(C$\underline{H}_3$)$_3$); 2.48-2.62 (m, 1H, C$\underline{H}$(CH$_3$)$_2$); 2.58 (s, 3H, $C_{het}C\underline{H}_3$); 3.67 (s, 3H, NC$\underline{H}_3$); 4.55 (dd, $^3J_{H,H}$ = 9.33 Hz 1H, $C_\alpha\underline{H}$); 7.40 (s, 1H, N$\underline{H}CO_2$); 10.67 (s, 1H, $CO_2\underline{H}$) ppm. - **^{13}C-NMR** (50 MHz, $CDCl_3$): δ = 9.7 ($C_{het}\underline{C}H_3$); 19.4, 19.6 (CH($\underline{C}H_3$)$_2$); 28.2 ($\underline{C}$(CH$_3$)$_3$); 31.8 ($\underline{C}$H(CH$_3$)$_2$); 32.3 (N$\underline{C}H_3$); 52.6 ($\underline{C}_\alpha$); 79.9 ($\underline{C}$(CH$_3$)$_3$); 123.4 ($\underline{C}_{het}CO_2$); 135.1 ($\underline{C}_{het}NCH_3$); 149.0 (C_{azole}); 156.2 ($\underline{C}O_2NH$); 161.3 ($\underline{C}O_2H$) ppm. - **FAB-HR MS**: *m/z* cald. for $C_{15}H_{26}N_3O_4^+$ 312.2074, found 336.2088. **- M.P.:** 104 °C.

Methyl 2-((*S*)-1-(2-((*R*)-1-(*tert*-butoxycarbonylamino)-2-methylpropyl)-1,5-dimethyl-imidazole-4-carboxamido)-2-methylpropyl)-1,5-dimethyl-imidazole-4-carboxylate (19):

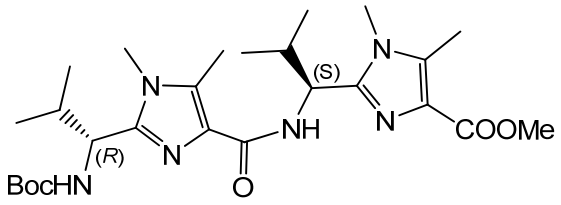

19

molecular formula: $C_{26}H_{42}N_6O_5$
molecular mass: 518.64 g/mol

EDIPA (5.7 mL, 31.2 mmol) and FDPP (3.50 g, 9.12 mmol) were added at room temperature to a solution of **18** (1.50 g, 4.80 mmol) and **7** (2.40 g, 7.20 mmol) in 150 mL acetonitrile, and the mixture was stirred at room temperature for 4 days. The solvent was then evaporated and the residue dissolved in ethyl acetate. The organic layers were washed with water and brine,

dried with $MgSO_4$, and concentrated in vacuo. Flash chromatography on silica gel (petrol ether/ethyl acetate 1:2) gave building block 13 (1.7 g, 68%) as a white solid.

$C_{26}H_{42}N_6O_5 \cdot H_2O$: calcd. (%): C 58.19, H 8.26, N 15.66, found (%): C 58.53, H 8.08, N 14.70 (26011). **- ^{1}H-NMR** (400 MHz, $CDCl_3$): δ = 0.82 (d, $^3J_{H\text{-}H}$ = 6.9 Hz, 3H, CHC$\underline{H}_3$); 0.84 (d, $^3J_{H\text{-}H}$ = 6.7 Hz, 3H, CHC$\underline{H}_3$); 0.94 (d, $^3J_{H\text{-}H}$ = 6.7 Hz, 3H, CHC$\underline{H}_3$); 1.06 (d, $^3J_{H\text{-}H}$ = 6.55 Hz, 3H, CHC$\underline{H}_3$); 1.44 (s, 9H, C(C$\underline{H}_3$)$_3$); 1.99-2.13 (m, 1H, C$\underline{H}$CH$_3$); 2.51 (s, 6H, $C_{het}C\underline{H}_3$); 2.52-2.62 (m, 1H, C$\underline{H}$CH$_3$), 3.47 (s, 3H, NC$\underline{H}_3$); 3.64 (s, 3H, NC$\underline{H}_3$); 3.85 (s, 3H, $CO_2C\underline{H}_3$); 4.51 (dd, $^3J_{H\text{-}H}$ = 8.57 Hz, 1H, $C_\alpha\underline{H}$); 4.96 (dd, $^3J_{H\text{-}H}$ = 9.85 Hz, 1H, $C_\alpha\underline{H}$); 5.36-5.22 (m, 1H, N$\underline{H}$); 7.68 (m, 1H, N$\underline{H}$) ppm. **- ^{13}C-NMR** (100 MHz, $CDCl_3$): δ = 9.7, 10.2 ($C_{het}\underline{C}H_3$); 18.1, 19.2, 19.6, 20.0 (CH$\underline{C}$H$_3$); 28.3 ($\underline{C}$CH$_3$); 30.0, 30.4 ($\underline{C}$H(CH$_3$)$_2$); 32.3, 32.9 (NCH$_3$); 52.1 ($CO_2\underline{C}H_3$); 79.5 ($\underline{C}$(CH$_3$)$_3$); 135.9, 146.9, 148.3 ($\underline{C}_{het}$); 155.7, 163.5, 163.7 ($\underline{C}$O) ppm. **- FAB-HR MS**: *m/z*. calcd. for $C_{26}H_{43}N_6O_5^+$ 519.32894 found: 519.3318– **M.P.**: 179 °C

.

2-((*S*)-1-(2-((*R*)-1-(*tert*-butoxycarbonylamino)-2-methylpropyl)-1,5-dime-thyl-imidazole-4-carboxamido)-2-methylpropyl)-1,5-dimethyl-imidazole-4-carboxylic acid (20):

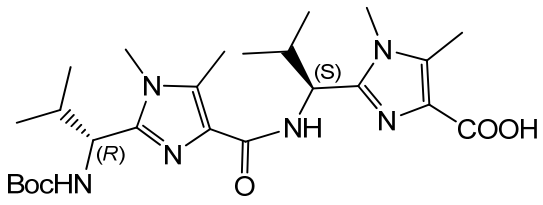

20

molecular formula: $C_{25}H_{40}N_6O_4$

molecular mass: 504.62 g/mol

Compound **19** (1.7 g, 3.26 mmol) was converted into **12**, using 33 mL NaOH in 40 mL of a dioxane/methanol mixture as described above in the general procedure for the cleavage of the methyl ester group. Yield: quantitative.

$C_{25}H_{40}N_6O4$: **^{1}H-NMR** (400 MHz, $CDCl_3$): δ = 0.82 (d, ^3J = 6.9 Hz, 3H, CHC$\underline{H}_3$); 0.84 (d, ^3J = 6.7 Hz, 3H, CHC$\underline{H}_3$); 0.94 (d, ^3J = 6.7 Hz, 3H, CHC$\underline{H}_3$); 1.06 (d, ^3J = 6.55 Hz, 3H, CHC$\underline{H}_3$); 1.44 (s, 9H, C(C$\underline{H}_3$)$_3$); 1.99-2.13 (m, 1H, C$\underline{H}$CH$_3$); 2.51 (s, 6H, $C_{het}C\underline{H}_3$); 2.52-2.62 (m, 1H, C$\underline{H}$CH$_3$), 3.47 (s, 3H, NC$\underline{H}_3$); 3.64 (s, 3H, NC$\underline{H}_3$); 3.85 (s, 3H, $CO_2C\underline{H}_3$); 4.51 (dd, ^3J = 8.57 Hz, 1H, NHC$\underline{H}$); 4.96 (dd, ^3J = 9.85 Hz, 1H, NHC$\underline{H}$); 5.36-5.22 (m, 1H, N$\underline{H}$); 7.68 (m, 1H, N$\underline{H}$) ppm. **- ^{13}C-NMR** (100 MHz, $CDCl_3$): δ = 9.4, 9.5 ($C_{het}\underline{C}H_3$); 18.2, 19.7, 19.0, 19.3 (CH$\underline{C}$H$_3$); 28.0 ($\underline{C}$CH$_3$); 30.4, 30.8 ($\underline{C}$H(CH$_3$)$_2$); 31.2, 31.9 (NCH$_3$); 78.5 ($\underline{C}$(CH$_3$)$_3$);

128.3, 130.8, 133.9, 136.8, 146.1, 148.1 ($\underline{C}_{Het}$); 155.4, 160.5, 162.3 ($\underline{C}O$) ppm. **- FAB-HR MS**: *m/z* calcd. found **– M.P.**: 217 °C .

(*R*)-1-(4-((*S*)-1-(4-carboxy-1,5-dimethyl-imidazol-2-yl)-2-methylpropylcarbamoyl)-1,5-dimethyl-imidazol-2-yl)-2-methylpropan-1-aminium trifluoro acetate (21):

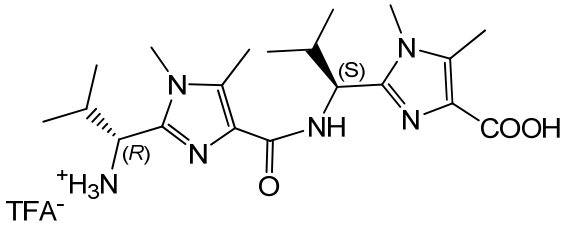

21

molecular formula: $C_{22}H_{32}F_3N_6O_4$

molecular mass: 501.52 g/mol

Compound **20** (1.5 g, 2.90 mmol) was converted into **21**, using 8.7 mL TFA in 58 mL DCM as described above in the general procedure for the cleavage of the Boc group. Yield: quantitative.

$C_{22}H_{32}F_3N_6O_4$: **^{1}H-NMR** (400 MHz, $CDCl_3$): δ = 0.82 (d, ^3J = 6.9 Hz, 3H, CHC$\underline{H}_3$); 0.84 (d, ^3J = 6.7 Hz, 3H, CHC$\underline{H}_3$); 0.94 (d, ^3J = 6.7 Hz, 3H, CHC$\underline{H}_3$); 1.06 (d, ^3J = 6.55 Hz, 3H, CHC$\underline{H}_3$); 1.44 (s, 9H, C(C$\underline{H}_3$)$_3$); 1.99-2.13 (m, 1H, C$\underline{H}$CH$_3$); 2.51 (s, 6H, C_{het}C$\underline{H}_3$); 2.52-2.62 (m, 1H, C$\underline{H}$CH$_3$), 3.47 (s, 3H, NC$\underline{H}_3$); 3.64 (s, 3H, NC$\underline{H}_3$); 3.85 (s, 3H, CO_2C$\underline{H}_3$); 4.51 (dd, ^3J = 8.57 Hz, 1H, NHC$\underline{H}$); 4.96 (dd, ^3J = 9.85 Hz, 1H, NHC$\underline{H}$); 5.36-5.22 (m, 1H, N$\underline{H}$); 7.68 (m, 1H, N$\underline{H}$) ppm. **- ^{13}C-NMR** (100 MHz, $CDCl_3$): δ = 9.4, 9.5 ($C_{Het}\underline{C}H_3$); 18.2, 19.7, 19.0, 19.3 (CH$\underline{C}H_3$); 28.0 ($\underline{C}CH_3$); 30.4, 30.8 ($\underline{C}H(CH_3)_2$); 31.2, 31.9 (NCH_3); 78.5 ($\underline{C}(CH_3)_3$); 128.3, 130.8, 133.9, 136.8, 146.1, 148.1 ($\underline{C}_{Het}$); 155.4, 160.5, 162.3 ($\underline{C}O$) ppm. **- M.P.**: > 200 °C .

Cyclic Pseudo Octapeptide H_4L^{rs}:

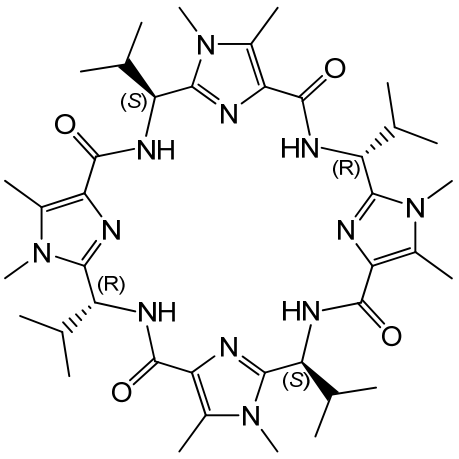

H_4L^{rs}

molecular formula: $C_{40}H_{60}N_{12}O_4$
molecular mass: 772.98 g/mol

The synthesis was performed analogous to the synthesis of **$H_4L^{4\text{-bn}}$**. EDIPA (1.87 g, 14.77 mmol) and FDPP (2.23 g, 5.8 mmol) were added at room temperature to a suspension of **21** (1.5 g, 2.11 mmol) in 150 mL acetonitrile and the mixture was stirred at room temperature for 2 days. The solvent was evaporated and the residue was dissolved in EtOAc, then extracted with water and brine, dried with $MgSO_4$, and concentrated in vacuo. Flash chromatography on silica gel (DCM/EE/MeOH 70:30:4) gave **H_4L^{rs}** in 54 % yield (302 mg, 0.95 mmol).

$C_{40}H_{60}N_{12}O_4 \bullet H_2O \bullet$ ½EtOAc: calcd. (%): C 60.45, H 7.91, N 20.14; found (%): C 60.64, H 8.00, N 20.47 (28059). **- ^{1}H-NMR** (750 MHz, $CDCl_3$): δ = 0.87 (d, $^3J_{H,H}$ = 6.75 Hz, 3H, $CH(C\underline{H}_3)_2$); 0.92 (d, $^3J_{H,H}$ = 6.76 Hz, 3H, $CH(C\underline{H}_3)_2$); 2.19-2.29 (m, 1H, $C\underline{H}CH_3$); 2.55 (s, 3H, $C_{het}C\underline{H}_3$); 3.64 (s, 3H, $NC\underline{H}_3$); 5.11-5.14 (m, 1H, $C_\alpha\underline{H}$); 8.60 (d, ^3J = 9.04 Hz, 1H, N$\underline{H}$) ppm. **-^{13}C-NMR** (175 MHz, $CDCl_3$): δ = 9.8 ($C_{het}\underline{C}H_3$); 18.7, 19.6 ($CH(\underline{C}H_3)_2$); 30.7 ($\underline{C}H(CH_3)_2$); 35.6 ($N\underline{C}H_3$); 51.0 ($NH\underline{C}H$); 130.1 ($\underline{C}_{het}CO$); 134.5 ($\underline{C}_{het}NCH_3$); 148.2 (C_{azole}); 165.4 ($NH\underline{C}O$) ppm. **- FAB-HR MS**: *m/z*. calcd. for $C_{40}H_{61}N_{12}O_4^+$ 773.4939, found 773.4944 **– M.P.**: > 250 °C.

5.2.4 Synthesis of the Cyclic Pseudo Octapeptide H_4L^{ascA}

(2*S*,3*R*)-methyl 2-((*S*)-2-(benzyloxycarbonylamino)-3-methylbutanamido)-3-hydroxybutanoate (22):[100]

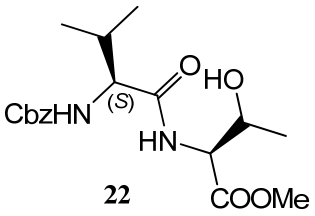

22

molecular formula: $C_{18}H_{26}N_2O_6$
molecular mass: 366.408 g/mol

The synthesis was performed according to literature.[100] (*S*)-Cbz-Val-OH (4.73 g, 17 mmol) and NMM (4.52 g, 25.6 mmol) were dissolved in 50 mL DCM and cooled to -15°C, isobutyl chloroformate (2.51 g, 25.5 mmol) was added drop wise at this temperature. Subsequently a solution of threonine methylester hydrochloride (2.8 g, 17 mmol) and NEt_3 (1.81 g, 17 mmol) in 10 mL DMF was added and stirring was continued while as the reaction mixture was allowed to warm to room temperature. 50 mL DCM were added and the organic layers washed with 1N HCl, 1 N NaOH and brine, dried over $MgSO_4$, and concentrated in vacuo. After recrystallization from hexane 4.2 g of **22** were obtained as colorless crystals (68 %).

$C_{18}H_{26}N_2O_6$ (366.41): calcd. (%): C 59.00, H 7.15, N 7.65; found (%): C 58.766, H 7.05, N 7.52 (23872). - **^{1}H-NMR** (200 MHz, $CDCl_3$): δ = 0.95 (d, $^3J_{H,H}$ = 7.0 Hz, 3H, $CH(C\underline{H}_3)_2$); 0.98 (d, $^3J_{H,H}$ = 7.0 Hz, 3H, $CH(C\underline{H}_3)_2$); 1.16 (d, $^3J_{H,H}$ = 6.4 Hz, 3H, $C_{(R)}HC\underline{H}_3$); 2.02-2.18 (m, 1H, $C\underline{H}(CH_3)_2$); 3.74 (s, 3H, $CO_2C\underline{H}_3$); 4.10 (dd, $^3J_{H,H}$ = 6.8, 8.8 Hz, 1H, $COC\underline{H}NH$); 4.34 (dq, $^3J_{H,H}$ = 6.2, 2.4 Hz, 1H, $C_{(R)}\underline{H}CH_3$); 4.61 (dd, 1H, $^3J_{H,H}$ = 2.5, 9.0 Hz, $C\underline{H}CO_2$); 5.09 (s, 2H, $C_{Ar}C\underline{H}_2$), 5.62 (d, 1H, $^3J_{H,H}$ = 7.8 Hz, $N\underline{H}$Cbz); 7.01 (d, 1H, ^3J = 8.9 Hz, $N\underline{H}CO$); 7.28-7.42 (m, 5H, $C\underline{H}_{Ar}$). - **^{13}C-NMR** (50 MHz, $CDCl_3$): δ = 18.4, 19.5 ($CH(\underline{C}H_3)_2$); 20.3 ($C_{(R)}H\underline{C}H_3$); 31.5 ($\underline{C}H(CH_3)_2$); 53.0 ($CO_2\underline{C}H_3$); 57.7 ($\underline{C}HCO_2$); 60.9 ($CO\underline{C}HNH$); 67.5 ($C_{Ar}\underline{C}H_2$); 68.5 ($C_{(R)}\underline{H}CH_3$); 128.4, 128.6, 128.9, 136.6 ($\underline{C}_{Ar}$); 156.7 ($\underline{C}O_2NH$); 171.3; 172.4 ($CH\underline{C}_{oxa}$, $\underline{C}ONH$). - **FAB-HR MS:** *m/z* calcd. for $C_{18}H_{27}N_2O_6^+$ 367.1864, found 367.1848. – **M.P.**: 135-137°C.

(4*S*,5*S*)-methyl 2-((*S*)-1-(benzyloxycarbonylamino)-2-methylpropyl)-5-methyl-4,5-dihydrooxazole-4-carboxylate (23):[100]

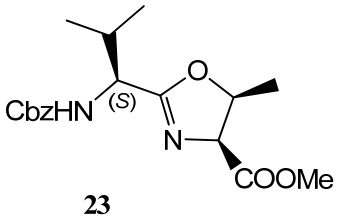

23

molecular formula: $C_{18}H_{24}N_2O_5$

molecular mass: 349.391 g/mol

The synthesis was performed according to literature.[100] A solution **22** (2.09 g, 5.72 mmol) in 40 mL of dry THF was treated with *Burgess' reagent* (1.5 g, 2.2 mmol) and heated at 75°C for 2.5 h. The reaction mixture was evaporated onto silica gel and chromatographed (EtOAc/hexanes 1:1) to yield **23** (1.13 g, 57%) as an oil:

$C_{18}H_{24}N_2O_5$ (348.39): calcd. (%): C 62.05, H 6.94, N 8.04; found (%): C 61.76, H 7.01, N 8.00 (22320). - **^{1}H-NMR** (200 MHz, $CDCl_3$): δ = 0.96 (d, $^3J_{H,H}$ = 6.9 Hz, 3H, $CH(C\underline{H}_3)_2$); 1.01 (d, $^3J_{H,H}$ = 6.9 Hz, 3H, $CH(C\underline{H}_3)_2$); 1.28 (d, $^3J_{H,H}$ = 6.3 Hz, 3H, $C_{Oxa}HC\underline{H}_3$); 2.10-2.26 (m, 1H, $C\underline{H}(CH_3)_2$); 3.73 (s, 3H, $CO_2C\underline{H}_3$); 4.39 (dd, $^3J_{H,H}$ = 9.2, 4.3 Hz, 1H, $C\underline{H}C_{Oxa}$); 4.76 (d, $^3J_{H,H}$ = 10.1 Hz, 1H, $C_{oxa}\underline{H}CO_2$); 4.85-4.99 (m, 1H, $C_{oxa}\underline{H}CH_3$); 5.05, 5.16 (^2J = 12.2 Hz, 2H, $C_{Ar}C\underline{H}_2$);, 5.54 (d, ^3J = 9.2 Hz, 1H, N<u>H</u>Cbz); 7.27-7.36 (m, 5H, $C\underline{H}_{Ar}$). - **^{13}C-NMR** (50 MHz, $CDCl_3$): δ = 16.0 ($C_{oxa}H\underline{C}H_3$); 17.0, 18.7 ($CH(\underline{C}H_3)_2$); 31.3 ($\underline{C}H(CH_3)_2$); 51.9 ($CO_2\underline{C}H_3$); 54.2 ($\underline{C}HC_{oxa}$); 66.8 ($C_{Aryl}\underline{C}H_2$); 70.7 ($\underline{C}_{oxa}HCO_2$); 78.4 ($\underline{C}_{oxa}HCH_3$); 128.0, 128.4, 136.3($\underline{C}_{Ar}$); 156.2 ($\underline{C}O_2NH$); 169.6; 170.0 ($CH\underline{C}_{oxa}$, $\underline{C}O_2CH_3$). - **FAB-HR MS:** *m/z* calcd. for $C_{18}H_{25}N_2O_5^+$ 349.1758, found 349.1745.

(2*S*,3*S*)-methyl 2-((*S*)-2-(benzyloxycarbonylamino)-3-methylbutanamido)-3-hydroxybutanoate (24):[48]

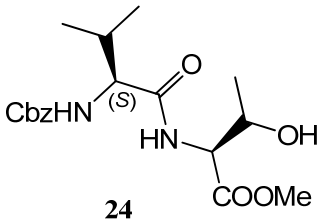

24

molecular formula: $C_{18}H_{26}N_2O_6$

molecular mass: 366.408 g/mol

The synthesis was performed according to literature.[100] A solution of **23** (1 g, 2.87 mmol) in 44 mL of dry THF was treated with 22 mL of 1 M HCl. The reaction mixture was stirred for

30 min at room temperature and then the pH was adjusted to 9.5 by the addition of solid K_2CO_3. The reaction was complete after 2 h (TLC). The organic solvent was evaporated and the aqueous layer extracted with EtOAc (2£30 mL). The combined organic extracts were washed with brine and dried over Na_2SO_4. Filtration followed by evaporation in vacuo yielded **24** (950 mg, 90%) as a colorless solid.

$C_{18}H_{26}N_2O_6$ (366.41): calcd. (%): C 59.00, H 7.15, N 7.65; found (%): C 58.66, H 7.08, N 7.64 (24812). - **^{1}H-NMR** (200 MHz, $CDCl_3$): δ = 0.93 (d, $^3J_{H,H}$ = 6.7 Hz, 3H, CH(C<u>H</u>$_3$)$_2$); 0.96 (d, $^3J_{H,H}$ = 6.7 Hz, 3H, CH(C<u>H</u>$_3$)$_2$; 1.19 (d, $^3J_{H,H}$ = 6.5 Hz, 3H, $C_{(S)}$HC<u>H</u>$_3$); 2.00-2.16 (m, 1H, C<u>H</u>(CH$_3$)$_2$); 3.75 (s, 3H, CO_2C<u>H</u>$_3$); 4.10-4.18 (m, 2H, COC<u>H</u>NH, $C_{(S)}$<u>H</u>CH$_3$); 4.66 (dd, $^3J_{H,H}$ = 3.2, 7.7 Hz, 1H, C<u>H</u>CO_2); 5.12, 5.07 ($^2J_{H,H}$ = 12.2 Hz, 2H, C_{Aryl}C<u>H</u>$_2$); 5.70 (d, $^3J_{H,H}$ = 8.7 Hz, 1H, N<u>H</u>Cbz); 7.25 (m, 1H, N<u>H</u>CO); 7.28-7.42 (m, 5H, C<u>H</u>$_{Ar}$). - **^{13}C-NMR** (50 MHz, $CDCl_3$): δ = 18.4 (CH(<u>C</u>H$_3$)$_2$); 19.3 ($C_{(S)}$H<u>C</u>H$_3$); 19.5 (CH(<u>C</u>H$_3$)$_2$); 31.6 (<u>C</u>H(CH$_3$)$_2$); 52.9(CO_2<u>C</u>H$_3$); 58.5 (<u>C</u>HCO_2); 60.8 (CO<u>C</u>HNH); 67.5 (C_{Ar}<u>C</u>H$_2$); 69.0 ($C_{(R)}$<u>H</u>CH$_3$); 128.4, 128.6, 128.9, 136.6 (<u>C</u>$_{Ar}$); 157.1 (<u>C</u>O_2NH);; 170.9; 172.5 (CH<u>C</u>$_{oxa}$, <u>C</u>ONH). - **FAB-HR MS:** *m/z* calcd. for $C_{18}H_{27}N_2O_6^+$ 367.1864, found 367.1860. – **M.P.**: 122-125 °C

(4*S*,5*R*)-methyl 2-((*S*)-1-(benzyloxycarbonylamino)-2-methylpropyl)-5-methyl-4,5-dihydrooxazole-4-carboxylate (25):[48]

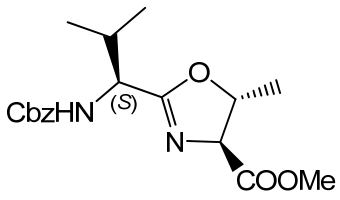

25

molecular formula: $C_{18}H_{24}N_2O_5$

molecular mass: 349.391 g/mol

The synthesis was performed according to literature.[100] A solution **24** (940 mg, 2.59 mmol) in 50 mL of dry THF was treated with *Burgess' reagent* (679 mg, 2.85 mmol) and heated at 75°C for 2.5 h. The reaction mixture was evaporated onto silica gel and chromatographed (EtOAc/hexanes 1:1) to yield **25** (700 mg, 77%) as an oil

$C_{18}H_{24}N_2O_5$ ·½ H_2O (348.39): calcd. (%): C 60.49, H 7.05, N 7.80; found (%): C 60.38, H 7.02, N 8.17 (28824). - **^{1}H-NMR** (200 MHz, $CDCl_3$): δ = 0.90 (d, $^3J_{H,H}$ = 6.9 Hz, 3H, CH(C<u>H</u>$_3$)$_2$); 0.96 (d, $^3J_{H,H}$ = 6.8 Hz, 3H, CH(C<u>H</u>$_3$)$_2$); 1.39 (d, $^3J_{H,H}$ = 6.3 Hz, 3H, C_{oxa}HC<u>H</u>$_3$); 2.05-2.21 (m, 1H, C<u>H</u>(CH$_3$)$_2$); 3.74 (s, 3H, CO_2C<u>H</u>$_3$); 4.25 (d, ^3J = 7.0 Hz, 1H, C_α<u>H</u>); 4.40

(dd, $^3J_{H,H}$ = 9.1, 4.6 Hz, 1H, $C_{oxa}\underline{H}CO_2$); 4.75-4.88 (m, 1H, $C_{oxa}\underline{H}CH_3$); 5.05, 5.12 ($^2J_{H,H}$ = 12.3 Hz, 2H, $C_{Ar}C\underline{H}_2$); 5.51 (d, 1H, $^3J_{H,H}$ = 9.2 Hz, N<u>H</u>Cbz); 7.23-7.35 (m, 5H, $C\underline{H}_{Ar}$). - **^{13}C-NMR** (50 MHz, $CDCl_3$): δ = 17.1, 18.7 ($CH(\underline{C}H_3)_2$); 20.8 ($C_{oxa}H\underline{C}H_3$); 31.6 ($\underline{C}H(CH_3)_2$); 52.5 ($CO_2\underline{C}H_3$); 54.3 ($\underline{C}HC_{oxa}$); 66.8 ($C_{Ar}\underline{C}H_2$); 74.0 ($\underline{C}_{oxa}HCO_2$); 79.6 ($\underline{C}_{oxa}HCH_3$); 128.0, 128.4, 136.3 ($\underline{C}_{Ar}$); 156.1 ($\underline{C}O_2NH$); 168.7; 171.2 ($CH\underline{C}_{oxa}$, $\underline{C}O_2CH_3$). - **FAB-HR MS:** *m/z* calcd. for $C_{18}H_{25}N_2O_5^+$ 349.1758, found 349.1748.

(4*S*,5*R*)-2-((*S*)-1-(benzyloxycarbonylamino)-2-methylpropyl)-5-methyl-4,5-dihydro-oxazole-4-carboxylic acid (26):

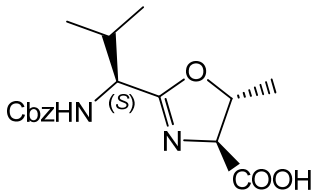

26

molecular formula: $C_{17}H_{22}N_2O_5$
molecular mass: 334.361 g/mol

Compound **25** (700 mg, 2 mmol) was converted into **26**, using 10 mL NaOH in 26 mL of a dioxane/methanol mixture as described above in the general procedure for the cleavage of the methyl ester group. Yield: quantitative.

$C_{17}H_{22}N_2O_5$ (334.37): calcd. (%): C: 61.07, H 6.63, N 8.38; found (%): 60.37, H 7.06, N 8.27 (28823). - **^{1}H-NMR** (200 MHz, $CDCl_3$): δ = 0.89 (d, 3H, $^3J_{H,H}$ = 6.8 Hz, $CH(C\underline{H}_3)_2$); 0.95 (d, $^3J_{H,H}$ = 6.8 Hz, 3H, $CH(C\underline{H}_3)$); 1.34 (d, $^3J_{H,H}$ = 6.3 Hz, 3H, $CHC\underline{H}_3$); 2.02-2.18 (m, 1H, $C\underline{H}(CH_3)_2$); 4.17 (d, $^3J_{H,H}$ = 6.9 Hz, 1H, $C_\alpha\underline{H}$); 4.46 (dd, $^3J_{H,H}$ = 9.5, 5.0 Hz, 1H, $C\underline{H}CH_3$); 4.87-5.00 (m, 1H, $C\underline{H}CO_2$); 5.05, 5.14 ($^2J_{H,H}$ = 12.6 Hz, 2H, $C_{Ar}C\underline{H}_2$); 6.85 (d, $^3J_{H,H}$ = 10.0 Hz, 1H, N<u>H</u>Cbz); 7.28-7.36 (m, 5H, $C\underline{H}_{Ar}$). - **^{13}C-NMR** (50 MHz, $CDCl_3$): δ = 17.3, 18.8 ($CH(\underline{C}H_3)_2$); 20.2 ($C_{oxa}H\underline{C}H_3$); 31.4 ($\underline{C}H(CH_3)_2$); 54.3 ($\underline{C}HC_{oxa}$); 66.7 ($C_{Ar}\underline{C}H_2$); 72.4 ($\underline{C}_{oxa}HCO_2$); 80.6 ($\underline{C}_{oxa}HCH_3$); 127.7, 128.0, 128.5, 136.5 ($\underline{C}_{Ar}$); 156.6 ($\underline{C}O_2NH$); 171.9, 172.7 ($CH\underline{C}_{oxa}$, $\underline{C}O_2H$). - **FAB-HR MS:** *m/z* calcd for $C_{17}H_{23}N_2O_5^+$ 335.1602, found 335.1647. - **M.P.**: 162°C

(*R*)-methyl 2-(1-(*tert*-butoxycarbonylamino)-2-methylpropyl)-5-methylthiazole-4-carboxylate (27):[48]

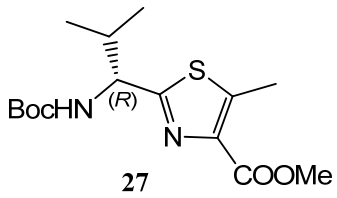

27

molecular formula: $C_{15}H_{24}N_2O_4S$
molecular mass: 328.431 g/mol

The synthesis was performed according to literature procedure.[48] *Lawesson's Reagent* (10.0 g, 24.7 mmol) was added at room temperature to a solution of **16** (5.46 g, 16.53 mmol) in 170 mL anhydrous THF. The mixture was stirred at reflux for 8 h. The solvent was removed and the residue dissolved in EtOAc, washed with water, 1 N HCl, saturated $NaHCO_3$ solution and brine, dried with MgSO4, and concentrated in vacuo. The crude product was chromatographed (petroleum ether/EtOAc: 3:1) to yield **27** (3.67 g, 70%) as a solid.

$C_{15}H_{24}N_2O_4S$ (328.43):calcd. (%): C 54.86, H 7.37, N 8.53 S 9.76; found (%): C 54.84, H 7.35, N 9.64, S 9.64 (24793). - **^{1}H-NMR** (200 MHz, $CDCl_3$): δ = 0.85 (d, $^3J_{H,H}$ = 6.9 Hz, 3H, $CH(C\underline{H}_3)_2$); 0.92 (d, $^3J_{H,H}$ = 6.8 Hz, 3H, $CH(C\underline{H}_3)_2$); 1.39 (s, 9H, $C(C\underline{H}_3)_3$); 2.24-2.45 (m, 1H, $C\underline{H}(CH_3)_2$); 2.68 (s, 3H, $C_{thia}C\underline{H}_3$); 3.87 (s, 3H, $CO_2C\underline{H}_3$); 4.75 (dd, $^3J_{H,H}$ = 5.6, 8.5 Hz, 1H, $C_\alpha\underline{H}$); 5.21 (d, $^3J_{H,H}$ = 8.6 Hz, 1H, $N\underline{H}CO_2$). - **^{13}C-NMR** (50 MHz, $CDCl_3$): δ = 13.0 ($C_{thia}\underline{C}H_3$); 17.1, 19.3 ($CH(\underline{C}H_3)_2$); 28.2 ($C(\underline{C}H_3)_3$); 33.0 ($\underline{C}H(CH_3)_2$); 52.0 ($CO_2\underline{C}H_3$); 57.7 ($\underline{C}_\alpha$); 79.9 ($\underline{C}(CH_3)_3$); 140.9, 144.3 ($\underline{C}_{thia}CH_3$, $\underline{C}_{thia}CO_2$); 155.3 ($\underline{C}O_2NH$); 162.8, 168.3 ($CH\underline{C}_{thia}$, $\underline{C}O_2CH_3$). - **FAB-HR MS**: *m/z* calcd. for $C_{15}H_{25}N_2O_4S^+$ 329.1457, found 329.1514. – **M.P.**: 111°C.

(*R*)-2-(1-(*tert*-butoxycarbonylamino)-2-methylpropyl)-5-methylthiazole-4-carboxylic acid (28):

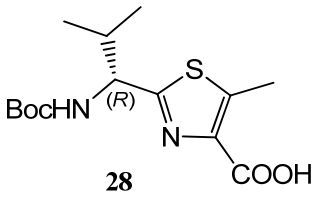

28

molecular formula: $C_{14}H_{22}N_2O_4S$
molecular mass: 314.137 g/mol

Compound **27** (1.2 g, 3.65 mmol) was converted into **28**, using 18 mL NaOH in 40 mL of a dioxane/methanol mixture as described above in the general procedure for the cleavage of the methyl ester group. Yield: quantitative.

$C_{14}H_{22}N_2O_4S$ (314.14): calcd. (%): C 53.48, H 7.05, N 8.91; found (%): C 52.99, H 7.07, N 8.71 (24857). - **^{1}H-NMR** (200 MHz, $CDCl_3$): δ = 0.91 (d, $^3J_{H,H}$ = 6.9 Hz, 3H, CHC$\underline{H}_3$); 0.96 (d, $^3J_{H,H}$ = 6.9 Hz, 3H, CHC$\underline{H}_3$); 1.42 (s, 9H, C(C$\underline{H}_3$)$_3$); 2.25-2.41 (m, 1H, C$\underline{H}$(CH$_3$)$_2$); 2.74 (s, 3H, $C_{thia}C\underline{H}_3$); 4.77 (dd, $^3J_{H,H}$ = 6.0, 7.9 Hz, 1H, $C_\alpha\underline{H}$); 5.31 (d, $^3J_{H,H}$ = 8.0 Hz, 1H, N$\underline{H}CO_2$). - **^{13}C-NMR** (50 MHz, $CDCl_3$): δ = 13.0 ($C_{thia}\underline{C}H_3$); 17.4, 19.3 (CH($\underline{C}H_3$)$_2$); 28.2 (C($\underline{C}H_3$)$_3$); 33.0 ($\underline{C}$H(CH$_3$)$_2$); 57.7 ($\underline{C}_\alpha$); 80.2 ($\underline{C}$(CH$_3$)$_3$); 140.4, 145.3 ($\underline{C}_{thia}CH_3$, $\underline{C}_{thia}CO_2$); 155.4 ($\underline{C}O_2$NH); 168.4 (CH$\underline{C}_{thia}$). - **FAB-HR MS**: *m/z* calcd. for $C_{14}H_{23}N_2O_4S^+$ 315.1373, found 315.1343. - **M.P.**: 146°C.

(*R*)-benzyl 2-(1-(*tert*-butoxycarbonylamino)-2-methylpropyl)-5-methylthiazole-4-carboxylate (29):

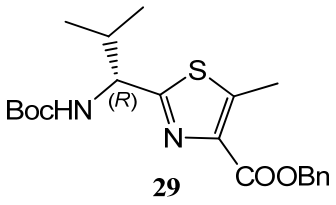

29

molecular formula: $C_{21}H_{28}N_2O_4S$

molecular mass: 404.523 g/mol

The reaction was performed analogous to literature.[48] DBU (0.48 mL, 3.26 mmol) and BnBr (0.50 mL, 4.23 mmol) were added at room temperature to a solution of **28** (1.02 g, 3.256 mmol) in 50 mL acetonitrile and the mixture was stirred at that temperature for 6 days. The solvent was evaporated and the residue was dissolved in EtOAc, extracted with water and brine, dried with MgSO4, and concentrated in vacuo. Purification was accomplished by chromatography on silica gel (petroleum ether/ethyl acetate, 2:1) to yield **29** (1.2 g, 91%) as a white solid.

$C_{21}H_{28}N_2O_4S$ (404.52): calcd. (%): C 62.35, H 6.98, N 6.93 S 7.93; found (%): C 62.14, H 6.97, N 6.76 S 7.95 (24856). - **^{1}H-NMR** (200 MHz, $CDCl_3$): δ = 0.87 (d, $^3J_{H,H}$ = 6.8 Hz, 3H, CHC$\underline{H}_3$); 0.95 (d, $^3J_{H,H}$ = 6.8 Hz, 3H, CHC$\underline{H}_3$); 1.41 (s, 9H, C(C$\underline{H}_3$)$_3$); 2.28-2.44 (m, 1H, C$\underline{H}$(CH$_3$)$_2$); 2.66 (s, 3H, $C_{Thia}C\underline{H}_3$); 4.77 (dd, $^3J_{H,H}$ = 8.7, 5.4 Hz, 1H, $C_\alpha\underline{H}$); 5.22 (d, $^3J_{H,H}$ = 8.5 Hz, 1H, N$\underline{H}CO_2$); 5.33, 5.40 ($^2J_{H,H}$ = 12.6 Hz, 2H, C$\underline{H}_2C_{Ar}$); 7.25-7.46 (m, 5H, C$\underline{H}_{Ar}$). - **^{13}C-NMR** (50 MHz, $CDCl_3$): δ = 13.0 ($C_{thia}\underline{C}H_3$); 17.2, 19.4 (CH($\underline{C}H_3$)$_2$); 28.3 (C($\underline{C}H_3$)$_3$); 33.1 ($\underline{C}$H(CH$_3$)$_2$); 57.7 ($\underline{C}HC_{thia}$); 66.6 ($C_{Ar}\underline{C}H_2$); 79.9 ($\underline{C}$(CH$_3$)$_3$); 128.2, 128.3, 128.5, 136.0 ($\underline{C}_{Ar}$); 141.1, 144.3 ($\underline{C}_{thia}CH_3$, $\underline{C}_{thia}CO_2$); 155.4 ($\underline{C}O_2$NH); 162.2, 168.0 (CH$\underline{C}_{thia}$, $\underline{C}O_2$Bn). - **FAB-HR MS**: *m/z* calcd. for $C_{21}H_{29}N_2O_4S^+$ 405.1843, found 405.1831. - **M.P.**: 74°C.

(*R*)-1-(4-(benzyloxycarbonyl)-5-methylthiazol-2-yl)-2-methylpropan-1-aminium trifluoro acetate (30):

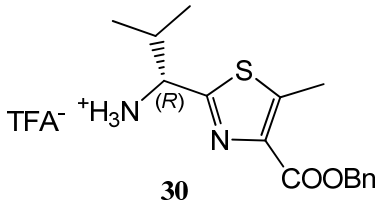

30

molecular formula: $C_{18}H_{21}F_3N_2O_2S$
molecular mass: 418.432 g/mol

Compound **29** (1.1 g, 2.7 mmol) was converted into **30**, using 8.4 mL TFA in 60 mL DCM as described above in the general procedure for the cleavage of the Boc group. Yield: quantitative.

$C_{18}H_{21}F_3N_2O_2S$ (418.43). - **^{1}H-NMR** (200 MHz, $CDCl_3$): δ = 0.89 (d, $^3J_{H,H}$ = 6.8 Hz, 3H, CHC$\underline{H}_3$); 0.95 (d, ^3J = 6.9 Hz, 3H, CHC$\underline{H}_3$); 1.76 (s, 2H, N$\underline{H}_2$); 2.07-2.23 (m, 1H, C$\underline{H}(CH_3)_2$); 2.68 (s, 3H, $C_{het}C\underline{H}_3$); 4.05 (d, $^3J_{H,H}$ = 5.3 Hz, 1H, $C_\alpha\underline{H}$); 5.33, 5.40 ($^2J_{H,H}$ = 12.4 Hz, 2H, C$\underline{H}_2C_{Ar}$); 7.24-7.46 (m, 5H, C$\underline{H}_{Ar}$). - **^{13}C-NMR** (50 MHz, $CDCl_3$): δ = 13.2 ($C_{thia}\underline{C}H_3$); 16.8, 19.3 (CH($\underline{C}H_3$)$_2$); 34.1 ($\underline{C}H(CH_3)_2$); 59.2 ($\underline{C}HC_{thia}$); 66.3 ($C_{Ar}\underline{C}H_2$); 128.0, 128.2, 128.3, 135.9 ($\underline{C}_{Ar}$); 140.4, 144.4 ($\underline{C}_{thia}CH_3$, $\underline{C}_{thia}CO_2$); 162.3, 172.8 (CH$\underline{C}_{thia}$, $\underline{C}O_2$Bn). - **FAB-HR MS**: *m/z* calcd. for $C_{16}H_{21}N_2O_2S^+$ 305.1324, found 305.1489.

Methyl 2-((1*R*)-1-((5*R*)-2-((*S*)-1-(benzyloxycarbonylamino)-2-methylpropyl)-5-methyl-4,5-dihydrooxazole-4-carboxamido)-2-methylpropyl)-5-methylthiazole-4-carboxylate (31):

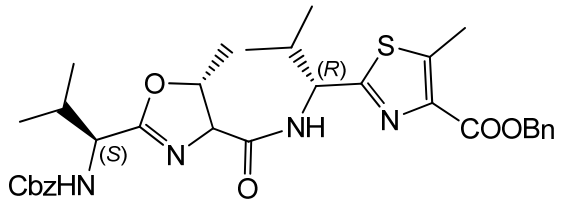

31

molecular formula: $C_{33}H_{40}N_4O_6S$
molecular mass: 620.761 g/mol

EDIPA (728 mg, 5.64 mmol) and DPPA (752 mg, 2.73 mmol) were added at room temperature to **30** (702 g, 1.67 mmol) and **26** (510 g, 1.52 mmol) in 40 mL acetonitrile, and the mixture was stirred at room temperature for 20 hours. The solvent was then evaporated and the residue dissolved in ethyl acetate. The organic layers were washed with water and

brine, dried with $MgSO_4$, and concentrated in vacuo. Flash chromatography on silica gel (DCM/EE/MeOH 75:25:2) gave **31** (550 mg, 58%) as a white solid

$C_{33}H_{40}N_4O_6S$ (620.76): **^{1}H-NMR** (400 MHz, $CDCl_3$): δ = 0.85 (d, $^3J_{H,H}$ = 6.9 Hz, 3H, $C_{val}HCHC\underline{H}_3$); 0.95 (d, $^3J_{H,H}$ = 6.8 Hz, 3H, $C_{val}HCHC\underline{H}_3$); 1.01 (d, $^3J_{H,H}$ = 6.8 Hz, 3H, $C_{val}HCHC\underline{H}_3$); 1.02 (d, $^3J_{H,H}$ = 6.8 Hz, 3H, $C_{val}HCHC\underline{H}_3$); 1.52 (d, $^3J_{H,H}$ = 6.2 Hz, 3H, $C_{oxa}HC\underline{H}_3$); 2.08-2.16 (m, 1H, $C\underline{H}(CH_3)_2$); 2.43-2.51 (m, 1H, $C\underline{H}(CH_3)_2$); 2.69 (s, 3H, $C_{thia}C\underline{H}_3$); 4.26 (d, ^3J = 7.3 Hz, 1H, $C_{oxa}\underline{H}CO$); 4.43 (dd, $^3J_{H,H}$ = 8.8, 4.8 Hz, 1H, $C_\alpha\underline{H}$); 4.78-4.84 (m, 1H, $C_{oxa}\underline{H}CH_3$); 5.10 (dd, ^3J = 9.2, 2.8 Hz, 1H, $C\underline{H}C_{thia}$); 5.16-5.20 (m, 2H, $C\underline{H}_2C_{Ar}$), 5.36-5.43 (m, 2H, $C\underline{H}_2C_{Ar}$), 5.51 (d, ^3J = 8.7 Hz, 1H, $N\underline{H}CO_2$); 7.29-7.49 (m, 11H, $N\underline{H}CO_2$, $C_{Ar}\underline{H}$). - **^{13}C-NMR** (100 MHz, $CDCl_3$): δ = 13.2 ($C_{thia}\underline{C}H_3$); 17.4, 17.8, 18.8, 19.5 ($CH(\underline{C}H_3)_2$); 21.8 ($C_{oxa}H\underline{C}H_3$); 31.3, 32.9 ($\underline{C}H(CH_3)_2$); 54.8 ($\underline{C}HC_{oxa}$); 56.2 ($\underline{C}HC_{thia}$); 66.6, 67.0 ($C_{Ar}\underline{C}H_2$); 74.3 ($\underline{C}_{oxa}HCO$); 80.7 ($\underline{C}_{oxa}HCH_3$); 128.1, 128.2, 128.2, 128.4, 128.5, 135.9, 136.2 ($\underline{C}_{Ar}$); 141.2 ($\underline{C}_{thia}CH_3$); 144.3 ($\underline{C}_{thia}CO$); 156.1 ($\underline{C}O_2NH$); 162.1 ($CH\underline{C}_{oxa}$); 164.5 ($CH\underline{C}_{thia}$); 169.0 ($C_{thia}\underline{C}O_2$); 171.2 ($C_{oxa}H\underline{C}ONH$). - **EI-HR MS:** *m/z* calcd. for $C_{33}H_{40}N_4O_6^+$ 620.2669, found 620.2689. - **M.P.**: 56 °C.

Cyclic Pseudo Octapeptide H_4L^{ascA}:

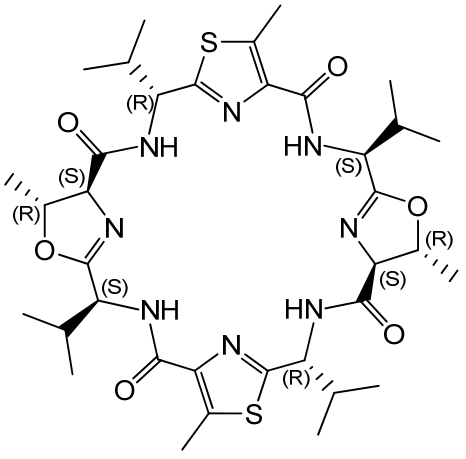

H_4L^{ascA}

molecular formula: $C_{36}H_{52}N_8O_6S_2$
molecular mass: 756.982 g/mol

Pd/C (10%, 240 mg) was added to a solution of **31** (280 mg, 0.42 mmol) in 30 mL methanol. The suspension was stirred for 1 h under an H_2 atmosphere, subsequently filtered and the solvent evaporated. The crude reaction mixture was dissolved in 30 mL acetonitrile and FDPP (327 mg, 0.85 mmol) and EDIPA (0.35 mL, 2 mmol) were added at room temperature. The mixture was stirred for 3 days. The solvent was evaporated and the residue was dissolved in

EtOAc, extracted with water and brine, dried with MgSO4, and concentrated in vacuo. Purification was accomplished by chromatography on silica gel (DCM/ethyl acetate/MEOH 75:25:2) to yield $\mathbf{H_4L^{ascA}}$ (45 mg, 28%) as a white solid

$C_{36}H_{52}N_8O_6S_2$ (756.98): **^{1}H-NMR** (400 MHz, benzene-d_6): δ = 0.76 (d, $^3J_{H,H}$ = 6.9 Hz, 6H, $C_{(S)val}HCHC\underline{H}_3$); 0.92 (d, $^3J_{H,H}$ = 6.7 Hz, 6H, $C_{(R)val}HCHC\underline{H}_3$); 0.93 (d, $^3J_{H,H}$ = 6.8 Hz, 6H, $C_{(S)val}HCHC\underline{H}_3$; 1.01 (d, $^3J_{H,H}$ = 6.3 Hz, 6H, $C_{oxa}HC\underline{H}_3$); 1.04 (d, $^3J_{H,H}$ = 6.8 Hz, 6H, $C_{(R)val}HCHC\underline{H}_3$); 1.78-1.91 (m, 4H, $C_{(S)val}HC\underline{H}(CH_3)_2$, $C_{(R)val}HC\underline{H}(CH_3)_2$); 2.57 (s, 6H, $C_{thia}C\underline{H}_3$); 4.00 (d, $^3J_{H,H}$ = 6.7 Hz, 2H, $C_{oxa}\underline{H}CO$); 4.75-4.82 (m, 2H, $C_{oxa}\underline{H}CH_3$); 5.01 (m, 2H, $C\underline{H}C_{oxa}$); 5.56 (dd, $^3J_{H,H}$ = 9.9, 7.6 Hz, 2H, $C\underline{H}C_{thia}$); 5.51 (d, $^3J_{H,H}$ = 10.0 Hz, 2H, $C_{(R)val}HN\underline{H}$); 8.50 (d, ^3J = 7.8 Hz, 2H, $C_{(S)val}N\underline{H}$). - **^{13}C-NMR** (100 MHz, benzene-d_6) δ = 12.4 ($C_{thia}\underline{C}H_3$); 17.8, 18.9, 19.0, 19.1 ($CH(\underline{C}H_3)_2$); 21.6 ($C_{oxa}H\underline{C}H_3$); 32.5, 34.4 ($\underline{C}H(CH_3)_2$); 52.8 ($\underline{C}_{(R)val}HNH$); 54.4 ($\underline{C}_{(S)val}HNH$); 73.9 ($\underline{C}_{oxa}HCO$); 81.4 ($\underline{C}_{oxa}HCH_3$); 140.7 ($\underline{C}_{thia}CH_3$); 143.7 ($\underline{C}_{thia}CO$); 162.1 ($CH\underline{C}_{oxa}$); 163.8 ($CH\underline{C}_{thia}$); 169.2 ($C_{thia}\underline{C}ONH$); 170.3 ($C_{oxa}H\underline{C}ONH$). - **ESI-HR MS:** *m/z* calcd. for $C_{36}H_{53}N_8O_6S_2^+$ 757.35240, found 757.35367.

5.2.5 Preparation of the Copper(II) Complexes of Cyclic Pseudo Peptides

The copper(II) complexes of the cyclic pseudo peptides were prepared in situ by mixing of methanolic solutions of the respective macrocycle (*c* = 1.25 mM) with a copper(II)triflate solution (*c* = 25mM) and base (*n*-Bu_4N)(OMe) (*c* = 25 mM).

The mononuclear complexes were prepared by mixing the solutions in a macrocycle/copper(II)/base ratio of 1:1:1.

The dinuclear copper(II) complexes were prepared by mixing the solutions in a macrocycle/copper(II)/base ratio of 1:2:0 or 1:2:1.

The hydroxo (bridged) complexes were prepared by mixing the solutions in a macrocycle/copper(II)/base ratio of 1:2:3.

The dinuclear carbonato bridged complexes were prepared by exposing mixed solution with a macrocycle/copper(II)/base ratio of 1:2:3 for 30min to two hours to air.

A suitable crystal for X-ray diffraction was obtained from the dinuclear copper(II) complex of $\mathbf{H_4L^{rs}}$, the cation $[\mathbf{H_2L^{rs}}Cu^{II}_2(\mu\text{-}OH)(H_2O)_2]^+$, after a complex solution was dissolved in a water/methanol mixture of 1:1 and slowly evaporated at room temperature.

[(μ-OCH_3)Cu^{II}_2(HL^1)](CF_3SO_3)

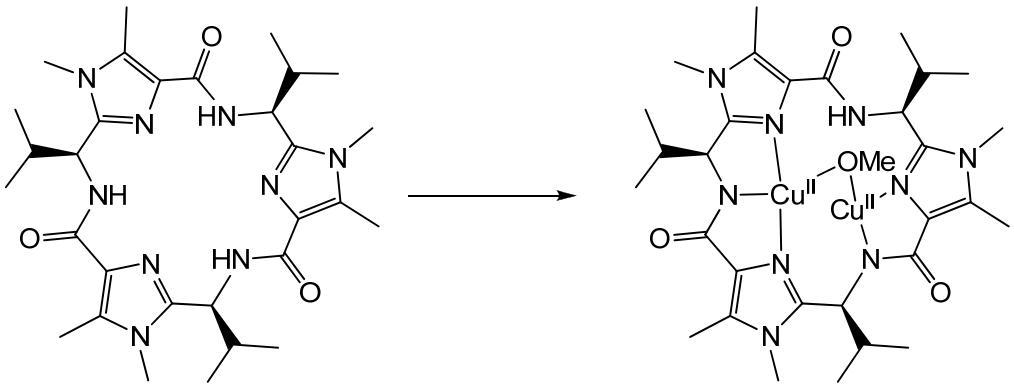

9.7 mg (2 eq) copper(II) triflate and 43 µL (3 eq) were added at room temperature to a solution of 15.36 mg (1eq) **H_3L^1**. The solution was stirred for 24 h and the solvent evaporated to yield 25.1 mg [(µ-OCH_3)Cu^{II}_2(HL^1)](CF_3SO_3) as a dark green solid.

$C_{32}H_{46}Cu_2F_3N_9O_7S \cdot 3.5\ H_2O$ (947.97): calcd. (%): C 40.54, H 5.64, N 13.30; found (%): C 40.39, H 5.47, N 13.63 (21609). - **IR** (KBr): ν = 3292, 2961, 2982, 2871, 1617, 1594, 1508. – **ESI-HR MS:** *m/z* calcd. for $C_{31}H_{46}Cu_2N_9O_4^+$ 734.22593, found 734.22459.

6. Literature

[1] Rosen, M.K.; Schreiber, S.L. *Angew. Chem., Int. Ed.* **1992**, *31,* 384.

[2] Li, C.P.; Prescott, B.; Jahnes, W.B. *Proc. Natl. Acad. Sci. U.S.A.* **1962**, *109,* 534.

[3] Nigrelli, R.F.; Stempien, M.F.; Ruggieri, G.D.; Ligouri, V.R.; Cecil, J.T. *Fed. Proc.* **1967**, *26,* 1197.

[4] Schmeer, M.R.; Huala, C.V. *Ann. N Y Acad. Sci.* **1960**, *90,* 893.

[5] Faulkner, D.J. *Nat. Prod. Rep.* **1988**, *5,* 613.

[6] Lewis, J.R. *Nat. Prod. Rep.* **1989**, *6,* 503.

[7] Fusetani, N.; Sugawara, T.; Matsunaga, S.; Hirota, H. *J. Am. Chem. Soc.* **1991**, *113,* 7811.

[8] Abbenante, G.; March, D.R.; Bergman, D.A.; Hunt, P.A.; Garnham, B.; Dancer, R.J.; Martin, J.L.; Fairlie, D.P. *J. Am. Chem. Soc.* **1995**, *117,* 10220.

[9] Abbenante, G.; Fairlie, D.P.; Gahan, L.R.; Hanson, G.R.; Pierens, G.K.; van den Brenk, A.L. *J. Am. Chem. Soc.* **1996**, *118,* 10384.

[10] Krebs, H.C. *Fortschr. Chem. Org. Naturst.* **1986**, *49,* 151.

[11] Krebs, H.C., *Recent developments in the field of marine natural products with the emphasis on biologically active compounds*, Progress in the Chemistry of Organic Natural Products. Vol. 49. Springer-Verlag: Vienna, 151, **1986**.

[12] Ogino, J.; Moore, R.E.; Patterson, G.M.L.; Smith, C.D. *J. Nat. Prod.* **1996**, *59,* 581.

[13] Ninawe, A.S. *Drug Discovery and Development* **2007**, *10,* 46.

[14] Chin, Y.W.; Balunas, M.J.; Chai, H.B.; Kinghorn, A.D. *Aaps J.* **2006**, *8,* E239.

[15] Newman, D.J.; Cragg, G.M.; Snader, K.M. *Nat. Prod. Rep.* **2000**, *17,* 215.

[16] Newman, D.J.; Cragg, G.M. *J. Nat. Prod.* **2007**, *70,* 461.

[17] Newman, D.J.; Cragg, G.M.; Snader, K.M. *J. Nat. Prod.* **2003**, *66,* 1022.

[18] O'Hanlon, L.H. *J. Natl. Cancer I.* **2006**, *98,* 662.

[19] Michael, J.P.; Pattenden, G. *Angew. Chem. Int. Edit.* **1993**, *32,* 1.

[20] Davidson, B.S. *Chem. Rev.* **1993**, *93,* 1771.

[21] Faulkner, D.J.; Newman, D.J.; Cragg, G.M. *Nat. Prod. Rep.* **2004**, *21,* 50.

[22] Wipf, P. *Chem. Rev.* **1995**, *95,* 2115.

[23] Fookes, C.J.R.; Jeffrey, S.W. *J. Chem. Soc., Chem. Commun.* **1989**, 1827.

[24] Rinehart, K.L.; Kishore, V.; Bible, K.C.; Sakai, R.; Sullins, D.W.; Li, K.M. *J. Nat. Prod.* **1988**, *51,* 1.

[25] Kustin, K.; McLeod, G.C. *Top. Curr. Chem.* **1977**, *69,* 1.

[26] Morris, L.A.; Jaspars, M. *Spec. Publ. Roy. Soc. Chem.* **2000**, *257,* 140.

[27] Morris, L.A.; Jaspars, M.; Kettenes-van den Bosch, J.J.; Versluis, K.; Heck, A.J.R.; Kelly, S.M.; Price, N.C. *Tetrahedron* **2001**, *57,* 3185.

[28] Morris, L.A.; Milne, B.F.; Jaspars, M.; Kettenes-van den Bosch, J.J.; Versluis, K.; Heck, A.J.R.; Kelly, S.M.; Price, N.C. *Tetrahedron* **2001**, *57,* 3199.

[29] Boitel, F.; Truchot, J.P. *Mar. Biol.* **1989**, *103,* 495.

[30] Schmidt, E.W.; Nelson, J.T.; Rasko, D.A.; Sudek, S.; Eisen, J.A.; Haygood, M.G.; Ravel, J. *Proc. Natl. Acad. Sci. U.S.A.* **2005**, *102,* 7315.

[31] Faulkner, D.J. *Nat. Prod. Rep.* **1984**, *1,* 551.

[32] Faulkner, D.J. *Nat. Prod. Rep.* **1984**, *1,* 251.

[33] Faulkner, D.J. *Nat. Prod. Rep.* **1986**, *3,* 1.

[34] Faulkner, D.J. *Nat. Prod. Rep.* **1987**, *4,* 539.

[35] Faulkner, D.J. *Nat. Prod. Rep.* **1990**, *7,* 269.

[36] Faulkner, D.J. *Nat. Prod. Rep.* **1991**, *8,* 97.

[37] Faulkner, D.J. *Nat. Prod. Rep.* **1992**, *9,* 323.

[38] Watters, D.J.; Van Den Brenk, A.L. *Toxicon* **1993**, *31,* 1349.

[39] Haberhauer, G.; Rominger, F. *Eur. J. Org. Chem.* **2003**, 3209.

[40] Ireland, C.; Scheuer, P.J. **1980**, *102,* 5688.

[41] Ireland, C.M.; Durso, A.R., Jr.; Newman, R.A.; Hacker, M.P. *J. Org. Chem.* **1982**, *47,* 1807.

[42] Degnan, B.M.; Hawkins, C.J.; Lavin, M.F.; McCaffrey, E.J.; Parry, D.L.; van den Brenk, A.L.; Watters, D.J. *J. Med. Chem.* **1989**, *32,* 1349.

[43] Schmitz, F.J.; Ksebati, M.B.; Chang, J.S.; Wang, J.L.; Hossain, M.B.; Van der Helm, D.; Engel, M.H.; Serban, A.; Silfer, J.A. *J. Org. Chem.* **1989**, *54,* 3463.

[44] Williams, D.E.; Moore, R.E.; Paul, V.J. *J. Nat. Prod.* **1989**, *52,* 732.

[45] Hamamoto, Y.; Endo, M.; Nakagawa, M.; Nakanishi, T.; Mizukawa, K. *J. Chem. Soc., Chem. Commun.* **1983**, 323.

[46] Wasylyk, J.M.; Biskupiak, J.E.; Costello, C.E.; Ireland, C.M. *J. Org. Chem.* **1983**, *48,* 4445.

[47] Wang, M.; Gould, S.J. *J. Org. Chem.* **1993**, *58,* 5176.

[48] Haberhauer, G.; Rominger, F. **2003**, 3209.

[49] Salomon Christine, E.; Faulkner, D.J. *J. Nat. Prod.* **2002**, *65,* 689.

[50] Hambley, T.W.; Hawkins, C.J.; Lavin, M.F.; van den Brenk, A.; Watters, D.J. *Tetrahedron* **1992**, *48,* 341.

[51] Prinsep, M.R.; Moore, R.E.; Levine, I.A.; Patterson, G.M.L. *J. Nat. Prod.* **1992**, *55,* 140.

[52] Haberhauer, G.; Rominger, F. *Tetrahedron Lett.* **2002**, *43,* 6335.

[53] Wipf, P.; Miller, C.P. *J. Am. Chem. Soc.* **1992**, *114,* 10975.

[54] Bertram, A.; Blake, A.J.; de Turiso, F.G.L.; Hannam, J.S.; Jolliffe, K.A.; Pattenden, G.; Skae, M. *Tetrahedron* **2003**, *59,* 6979.

[55] Jayaprakash, S.; Pattenden, G.; Viljoen, M.S.; Wilson, C. *Tetrahedron* **2003**, *59,* 6637.

[56] Hamada, Y.; Shibata, M.; Shioiri, T. *Tetrahedron Lett.* **1985**, *26,* 5159.

[57] Hamada, Y.; Shibata, M.; Shioiri, T. *Tetrahedron Lett.* **1985**, *26,* 5155.

[58] Ishida, T.; In, Y.; Doi, M.; Inoue, M.; Hamada, Y.; Shioiri, T. *Biopolymers* **1992**, *32,* 131.

[59] Ishida, T.; In, Y.; Shinozaki, F.; Doi, M.; Yamamoto, D.; Hamada, Y.; Shioiri, T.; Kamigauchi, M.; Sugiura, M. *J. Org. Chem.* **1995**, *60,* 3944.

[60] In, Y.; Doi, M.; Inoue, M.; Ishida, T.; Hamada, Y.; Shioiri, T. *Chem. Pharm. Bull.* **1993**, *41,* 1686.

[61] In, Y.; Doi, M.; Inoue, M.; Ishida, T. *Acta Crystallogr., Sec. C: Cryst. Struct. Comm.* **1994**, *C50,* 2015.

[62] Cusack, R.M.; Grondahl, L.; Abbenante, G.; Fairlie, D.P.; Gahan, L.R.; Hanson, G.R.; Hambley, T.W. *J. Chem. Soc., Perkin Trans. 2* **2000**, 323.

[63] Milne, B.F.; Morris, L.A.; Jaspars, M.; Thompson, G.S. *J. Chem. Soc., Perkin Trans. 2* **2002**, 1076.

[64] Haberhauer, G.; Drosdow, E.; Oeser, T.; Rominger, F. *Tetrahedron* **2008**, *64,* 1853.

[65] Pinter, A.; Haberhauer, G. *Tetrahedron* **2009**, *65,* 2217.

[66] Ishida, T.; Tanaka, M.; Nabae, M.; Inoue, M.; Kato, S.; Hamada, Y.; Shioiri, T. *J. Org. Chem.* **1988**, *53,* 107.

[67] Haberhauer, G. *Tetrahedron Lett.* **2008**, *49,* 2421.

[68] Ishida, T.; Inoue, M.; Hamada, Y.; Kato, S.; Shioiri, T. *J. Chem. Soc., Chem. Commun.* **1987**, 370.

[69] Shinozaki, F.; In, Y.; Doi, M.; Yamamoto, D.; Kamigauchi, M.; Sugiura, M.; Ishida, T.; Hamada, Y.; Shioiri, T. *Pept. Chem.* **1996**, *34th,* 405.

[70] In, Y.; Doi, M.; Inoue, M.; Ishida, T.; Hamada, Y.; Shioiri, T. *Acta Crystallogr., Sec. C: Cryst. Struct. Comm.* **1994**, *C50,* 432.

[71] van den Brenk, A.L.; Byriel, K.A.; Fairlie, D.P.; Gahan, L.R.; Hanson, G.R.; Hawkins, C.J.; Jones, A.; Kennard, C.H.L.; Moubaraki, B.; Murray, K.S. *Inorg. Chem.* **1994**, *33,* 3549.

[72] van den Brenk, A.L.; Tyndall, J.D.A.; Cusack, R.M.; Jones, A.; Fairlie, D.P.; Gahan, L.R.; Hanson, G.R. *J. Inorg. Biochem.* **2004**, *98,* 1857.

[73] Hawkins, C.J. *Pure Appl. Chem.* **1988**, *60,* 1267.

[74] van den Brenk, A.L.; Hanson, G.R.; Hawkins, C.J. **1989**, *98,* 165.

[75] van den Brenk, A.L.; Fairlie, D.P.; Hanson, G.R.; Gahan, L.R.; Hawkins, C.J.; Jones, A. *Inorg. Chem.* **1994**, *33,* 2280.

[76] Yin, X.; Moss, J.R. *Coord. Chem. Rev.* **1999**, *181,* 27.

[77] Parson, E.A.; Keith, D.W. *Science* **1998**, *282,* 1053.

[78] Kersting, B. *Angew. Chem., Int. Ed.* **2001**, *40,* 3987.

[79] Chen, J.-M.; Wei, W.; Feng, X.-L.; Lu, T.-B. *Chem. - Asian J.* **2007**, *2,* 710.

[80] Dussart, Y.; Harding, C.; Dalgaard, P.; McKenzie, C.; Kadirvelraj, R.; McKee, V.; Nelson, J. *J. Chem. Soc., Dalton Trans.* **2002**, 1704.

[81] Garcia-Espana, E.; Gavina, P.; Latorre, J.; Soriano, C.; Verdejo, B. *J. Am. Chem. Soc.* **2004**, *126,* 5082.

[82] Bazzicalupi, C.; Bencini, A.; Bencini, A.; Bianchi, A.; Corana, F.; Fusi, V.; Giorgi, C.; Paoli, P.; Paoletti, P.; et al. *Inorg. Chem.* **1996**, *35,* 5540.

[83] Sola, M.; Lledos, A.; Duran, M.; Bertran, J. *J. Am. Chem. Soc.* **1992**, *114,* 869.

[84] Kimura, E. *Acc. Chem. Res.* **2001**, *34,* 171.

[85] Parkin, G. *Chem. Rev.* **2004**, *104,* 699.

[86] Hartmann, M.; Clark, T.; van Eldik, R. *J. Am. Chem. Soc.* **1997**, *119,* 7843.

[87] Leitner, W. *Coord. Chem. Rev.* **1996**, *153,* 257.

[88] Kitajima, N.; Hikichi, S.; Tanaka, M.; Morooka, Y. *J. Am. Chem. Soc.* **1993**, *115,* 5496.

[89] Company, A.; Jee, J.-E.; Ribas, X.; Lopez-Valbuena Josep, M.; Gomez, L.; Corbella, M.; Llobet, A.; Mahia, J.; Benet-Buchholz, J.; Costas, M.; van Eldik, R. *Inorg. Chem.* **2007**, *46,* 9098.

[90] Palmer, D.A.; Van Eldik, R. *Chem. Rev.* **1983**, *83,* 651.

[91] Escuer, A.; Mautner, F.A.; Penalba, E.; Vicente, R. *Inorg. Chem.* **1998**, *37,* 4190.

[92] Mao, Z.-W.; Heinemann, F.W.; Liehr, G.; van Eldik, R. *J. Chem. Soc., Dalton Trans.* **2001**, 3652.

[93] Wipf, P.; Venkatraman, S.; Miller, C.P.; Geib, S.J. *Angew. Chem., Int. Edit.* **1994**, *33,* 1516.

[94] Grondahl, L.; Sokolenko, N.; Abbenante, G.; Fairlie, D.P.; Hanson, G.R.; Gahan, L.R. *J. Chem. Soc. Dalton* **1999**, 1227.

[95] Freeman, D.J.; Pattenden, G.; Drake, A.F.; Siligardi, G. *J. Chem. Soc. Perk. T. 2* **1998**, 129.

[96] Comba, P.; Cusack, R.; Fairlie, D.P.; Gahan, L.R.; Hanson, G.R.; Kazmaier, U.; Ramlow, A. *Inorg. Chem.* **1998**, *37,* 6721.

[97] Bernhardt, P.V.; Comba, P.; Fairlie, D.P.; Gahan, L.R.; Hanson, G.R.; Lötzbeyer, L. *Chem. - Eur. J.* **2002**, *8,* 1527.

[98] Hamada, Y.; Shibata, M.; Shioiri, T. *Tetrahedron Lett.* **1985**, *26,* 6501.

[99] Hamada, Y.; Kato, S.; Shioiri, T. *Tetrahedron Lett.* **1985**, *26,* 3223.

[100] Wipf, P.; Miller, C.P.; Grant, C.M. *Tetrahedron* **2000**, *56,* 9143.

[101] Sokolenko, N.; Abbenante, G.; Scanlon, M.J.; Jones, A.; Gahan, L.R.; Hanson, G.R.; Fairlie, D.P. *J. Am. Chem. Soc.* **1999**, *121,* 2603.

[102] Haberhauer, G.; Pinter, A.; Oeser, T.; Rominger, F. *Eur. J. Org. Chem.* **2007**, 1779.

[103] Seibold, B., Ruprecht Karls Universität, **2008**.

[104] Haberhauer, G.; Oeser, T.; Rominger, F. *Chem. - Eur. J.* **2005**, *11,* 6718.

[105] Stanwell, C.; Gescher, A.; Watters, D. *Biochem. Pharmacol.* **1993**, *45,* 1753.

[106] Van den Brenk, A.L., PhD Thesis, University of Queensland (AU), **1994**.

[107] Comba, P.; Gahan, L.R.; Haberhauer, G.; Hanson, G.R.; Noble, C.J.; Seibold, B.; van den Brenk, A.L. *Chem. - Eur. J.* **2008**, *14,* 4393.

[108] Comba, P.; Dovalil, N.; Haberhauer, G.; Taura, T.; Kato, Y. *J. Biol. Chem.* **2010**, *15,* 1129.

[109] Chen, A.S.C.; Wadsö, I. **1982**, *6,* 307.

[110] Saboury, A.A. **2004**, *77,* 997.

[111] Sivaraja, V.; Kumar, T.K.S.; Rajalingam, D.; Graziani, I.; Prudovsky, I.; Yu, C. **2006**, *91,* 1932.

[112] Tinoco, A.D.; Valentine, A.M. **2005**, *127,* 11218.

[113] Creagh, A.L.; Tiong, J.W.C.; Tian, M.M.; Haynes, C.A.; Jeferies, W.A. **2005**, *280,* 15735.

[114] Wiseman, T.; Williston, S.; Brandts, J.; Lin, L. **1989**, *179,* 131.

[115] Spinc, C.; Wadsö, I. **1976**, *23,* 1.

[116] Di Natale, G.; Damante, C.A.; Nagy, Z.; Osz, K.; Pappalardo, G.; Rizzarelli, E.; Sovago, I. *J. Inorg. Biochem.* **2008**, *102,* 2012.

[117] Inoue, M.B.; Velazquez, E.F.; Ruiz-Lucero, A.; Inoue, M.; Raitsimring, A.; Fernando, Q. *Inorg. Chem.* **1999**, *38,* 834.

[118] Krot, K.A.; de Namor, A.F.D.; Aguilar-Cornejo, A.; Nolan, K.B. *Inorg. Chim. Acta.* **2005**, *358,* 3497.

[119] Frisch, M.J.; Trucks, G.W.; Schlegel, H.B.; Scuseria, G.E.; Robb, M.A.; Cheeseman, J.R.; Montgomery, J.J.A.; Vreven, T.; Kudin, K.N.; Burant, J.C.; Millam, J.M.; S. S. Iyengar, J.T.; Barone, V.; Mennucci, B.; Cossi, M.; Scalmani, G.; N. Rega; Petersson, G.A.; Nakatsuji, H.; Hada, M.; Ehara, M.; Toyota, K.; Fukuda, R.; Hasegawa, J.; Ishida, M.; Nakajima, T.; Honda, Y.; O. Kitao; Nakai, H.; Klene, M.; Li, X.; Knox, J.E.; Hratchian, H.P.; Cross, J.B.; Adamo, C.; Jaramillo, J.; Gomperts, R.; Stratmann, R.E.; Yazyev, O.; Austin, A.J.; Cammi, R.; Pomelli, C.; Ochterski, J.W.; Ayala, P.Y.; Morokuma, K.; Voth, G.A.; Salvador, P.; Dannenberg, J.J.; Zakrzewski, V.G.; Dapprich, S.; Daniels, A.D.; Strain, M.C.; Farkas, O.; Malick, D.K.; Rabuck, A.D.; Raghavachari, K.; Foresman, J.B.; Ortiz, J.V.; Cui, Q.; Baboul, A.G.; Clifford, S.; Cioslowski, J.; Stefanov, B.B.; Liu, G.; Liashenko, A.; Piskorz, P.; Komaromi, I.; Martin, R.L.; Fox, D.J.; Keith, T.; Al-Laham, M.A.; Peng, C.Y.; Nanayakkara, A.; Challacombe, M.; P. M. W. Gill; Johnson, B.; Chen, W.; Wong, M.W.; Gonzalez, C.; Pople, J.A. *Gaussian 03, Revision B.03*, Gaussian, Inc., Pittsburgh PA, **2003**

[120] Neese, F. *J. Chem. Phys.* **2001**, *115,* 11080.

[121] Neese, F. *Coordin. Chem. Rev.* **2009**, *253,* 526.

[122] Hanson, G.R.; Gates, K.E.; Noble, C.J.; Griffin, M.; Mitchell, A.; Benson, S. *J. Inorg. Biochem.* **2004**, *98,* 903.

[123] Hanson, G.R.; Noble, C.J.; Benson, S. *Biol. Magn. Res.* **2008**, *28,* 105.

[124] Pilbrow, J.R., *Transition Ion Electron Paramegnetic Resonance*. Clarendon Press: Oxford, **1990**.

[125] Mabbs, F.E.; Collison, D.C., *Electron Paramagnetic Resonance of Transition Metal Compounds*. Elsevier: Amsterdam, **1992**.

[126] Abragam, A.; Bleaney, E., *Electron Paramagnetic Resonance of Transition Ions*. Claredon Press: Oxford, **1970**.

[127] Malkin, V.G.; Malkina, O.L.; Reviakine, R.; Arbouznikov, A.F.; Kaupp, M.; Schimmelpfennig, B.; Malkin, I.; Helgaker, T.; Ruud, H. *MAG-ReSpect 1.2*,

[128] Perdew, J.P.; Burke, K.; Ernzerhof, M. *Phys. Rev. Lett.* **1996**, *77,* 3865.

[129] Perdew, J.P.; Burke, K.; Ernzerhof, M. *Phys. Rev. Lett.* **1998**, *80,* 891.

[130] Becke, A.D. *Phys. Rev. A* **1988**, *38,* 3098.

[131] Perdew, J.P.; Chevary, J.A.; Vosko, S.H.; Jackson, K.A.; Pederson, M.R.; Singh, D.J.; Fiolhais, C. *Phys. Rev. B* **1993**, *48,* 4978.

[132] Perdew, J.P.; Chevary, J.A.; Vosko, S.H.; Jackson, K.A.; Pederson, M.R.; Singh, D.J.; Fiolhais, C. *Phys. Rev. B* **1992**, *46,* 6671.

[133] Perdew, J.P.; Burke, K.; Wang, Y. *Phys. Rev. B* **1996**, *54,* 16533.

[134] Tao, J.M.; Perdew, J.P.; Staroverov, V.N.; Scuseria, G.E. *Phys. Rev. Lett.* **2003**, *91,*

[135] Lee, C.T.; Yang, W.T.; Parr, R.G. *Phys. Rev. B* **1988**, *37,* 785.

[136] Schafer, A.; Huber, C.; Ahlrichs, R. *J. Chem. Phys.* **1994**, *100,* 5829.

[137] Adamo, C.; Barone, V. *Chem. Phys. Lett.* **1997**, *274,* 242.

[138] Schafer, A.; Horn, H.; Ahlrichs, R. *J. Chem. Phys.* **1992**, *97,* 2571.

[139] W. J. Hehre; R. Ditchfield; Pople, J.A. *J. Chem. Phys.* **1972**, *56,* 2257.

[140] W. Kutzelnigg; U. Fleischer; Schindler, M., *The IGLO-Method: Ab Initio Calculation and Interpretation of NMR Chemical Shifts and Magnetic Susceptibilities*. Springer-Verlag: Heidelberg, **1990**.

[141] Ahlrichs, J. *unpublished results*

[142] Wachters, A. *J. Chem. Phys.* **1969**, *52,* 1033.

[143] Kaupp, M.; Reviakine, R.; Malkina, O.L.; Arbuznikov, A.; Schimmelpfennig, B.; Malkin, V.G. *J. Comput. Chem.* **2002**, *23,* 794.

[144] Barone, V., *Recent Advances in Functional Methods, Part I*, ed. D.P. Chong. World Scientific Publ. Co.: Singapore, **1996**.

[145] van Vleck, J.H., *The Theory of Electric and Magnetic Susceptibility*. Oxford University Press: Oxford, **1932**.

[146] Heisenberg, W. *Z. Phys.* **1928**, *49,* 619.

[147] Dirac, P.A.M. *Proc. R. Soc. Lond. A* **1929**, *123,* 714.

[148] Comba, P.; Hausberg, S.; Martin, B. *J. Phys. Chem A* **2009**, *113,* 6751.

[149] Noodleman, L.; Davidson, E.R. *Chem. Phys.* **1986**, *109,* 131.

[150] Soda, T.; Kitagawa, Y.; Onishi, T.; Takano, Y.; Shigeta, Y.; Nagao, H.; Yoshioka, Y.; Yamaguchi, K. *Chem. Phys. Lett.* **2000**, *319,* 223.

[151] Ruiz, E.; Cano, J.; Alvarez, S.; Alemany, P. *J. Comput. Chem.* **1999**, *20,* 1391.

[152] Neese, F.; Solomon, E.I. *Inorg. Chem.* **1999**, *38,* 1847.

[153] Osborne, G.A.; Stephens, P.J. *J. Chem. Phys.* **1972**, *56,* 609.

[154] Piepho, S.B.; Schatz, P.N., *Group Theory in Spectroscopy with Application to Magnetic Circular Dichroism*. Wiley: New York, **1983**.

[155] Stephens, P.J. *J. Chem. Phys.* **1970**, *52,* 3489.

[156] Stephens, P.J. *Chem. Phys. Lett.* **1968**, *2,* 241.

[157] Gibbons, B.H.; Edsall, J.T. *J. Biol. Chem.* **1963**, *238,* 6.

[158] *Jaguar, version 6.5*, Schrödinger, LLC, New York, NY, **2006**

[159] Hay, P.J.; Wadt, W.R. *J. Chem. Phys.* **1985**, *82,* 270.

[160] Mohamadi, F.; Richards, N.G.J.; Guida, W.C.; Liskamp, R.; Lipton, M.; Caufield, C.; Chang, G.; Hendrickson, T.; Still, W.C. *J Comput Chem* **1990**, *11,* 440.

[161] Cornell, W.D.; Piotr Cieplak; Christopher I. Bayly; Ian R. Gould; Kenneth M. Merz, J.; David M. Ferguson; David C. Spellmeyer; Thomas Fox; Caldwell, J.W.; Kollman, P.A. *J. Am. Chem. Soc.* **1995**, *117,* 5179.

[162] Scott J. Weiner; Peter A. Kollman; David A. Case; U. Chandra Singh; Caterina Ghio; Giuliano Alagona; Salvatore Profeta, J.; Weinerl, P. *J. Am. Chem. Soc.* **1984**, 765.

[163] Frisch, M.J.; Trucks, G.W.; Schlegel, H.B.; Scuseria, G.E.; Robb, M.A.; Cheeseman, J.R.; Scalmani, G.; Barone, V.; Mennucci, B.; Petersson, G.A.; Nakatsuji, H.; Caricato, M.; Li, X.; Hratchian, H.P.; Izmaylov, A.F.; Bloino, J.; Zheng, G.; Sonnenberg, J.L.; Hada, M.; Ehara, M.; Toyota, K.; Fukuda, R.; Hasegawa, J.; Ishida, M.; Nakajima, T.; Honda, Y.; Kitao, O.; Nakai, H.; Vreven, T.; Montgomery, J., J. A.; ; Peralta, J.E.; Ogliaro, F.; Bearpark, M.; Heyd, J.J.; Brothers, E.; Kudin, K.N.; Staroverov, V.N.; Kobayashi, R.; Normand, J.; Raghavachari, K.; Rendell, A.; Burant, J.C.; Iyengar, S.S.; Tomasi, J.; Cossi, M.; Rega, N.; Millam, N.J.; Klene, M.; Knox, J.E.; Cross, J.B.; Bakken, V.; Adamo, C.; Jaramillo, J.; Gomperts, R.; Stratmann, R.E.; Yazyev, O.; Austin, A.J.; Cammi, R.; Pomelli, C.; Ochterski, J.W.; Martin, R.L.; Morokuma, K.; Zakrzewski, V.G.; Voth, G.A.; Salvador, P.; Dannenberg, J.J.; Dapprich, S.; Daniels, A.D.; Farkas, Ö.; Foresman, J.B.; Ortiz, J.V.; Cioslowski, J.; Fox, D.J. *Gaussian 09, Revision A.02*, Gaussian, Inc., Wallingford CT, **2009**

[164] Dunning, J.T.H.; Hay, P.J., eds. *Modern Theoretical Chemistry*. ed. H.F. Schaefer. 1976, Plenum: New York. 1.

[165] Poupko, R.; Luz, Z. **1972**, *57,* 3311.

[166] Ahlrichs, J. *Turbomole V5-9-1*, University of Karlsruhe, Karlsruhe, **2007**

[167] Morris, L.A.; Milne, B.F.; Thompson, G.S.; Jaspars, M. *J. Chem. Soc., Perkin Trans. 2* **2002**, 1072.

[168] Sheldrick, G.M., **1994**.

Appendices

A Abbreviations

µL	Microliters
Å	Ångström
Ala	Alanine
Bn	Benzyl
Boc	Tertbutylcarboxycarbonyl
Bu	Butyl
c	Concentration
Calcd.	Calculated
Cbz	Carboxybenzyl
CD	Circular Dichroism
CT	Charge Transfer
CW	Continuous Wave
d	Days
DCM	Dichloromethane
DFT	Density Functional Theory
DMF	*N,N'*-Dimethylformamide
DMSO	Dimethyl sulfoxide
DPPA	Diphenylphosphorylazide
e.s.d	Estimated Standard Deviation
EDIPA	N,N-diisopropylethylamine
EPR	Electron Paramagnetic Resonance
eq	Equivalents
Eq.	Equation
ESI	Electrospray Ionisation
Et_2O	Diethylether
EtOAc	Ethyl Acetate
EtOH	Ethanol
FAB	Fast Atom Bombardment
FDPP	Pentafluorophenyl diphenylphosphinate
G03	Gaussian 03
G09	Gaussian 09
h	Hours

HF	Hartree Fock
HR	High resolution
Ile	Isoleucine
IR	Infrared
M.P.	Melting Point
MCD	Magnetic Circular Dichroism
MD	Molecular Dynamics
Me	Methyl
MeOH	Methanol
mL	Milliliters
mM	Millimolar
MM	Molecular Mechanics
MS	Mass Spectrometry
NaOH	Sodium Hydroxide
neg.	Negative
NMM	N-methyl Morpholine
NMR	Nuclear Magnetic Resonance
Otf	Trifluoromethane sulfonate
PCM	Point Charge Model
Phe	Phenylalanine
pos.	Positive
ppm	Parts Per Million
RMS	Root Mean Square
RMSD	Root Mean Square Deviation
SH	Spin Hamiltonian
SOC	Spin Orbit Coupling
THF	Tetrahydrofuran
UV-vis	Ultraviolet / visible
Val	Valine
VH	Variable Field
vs.	Versus
VT	Variable Temperature
ΔA	Absorption

B ITC Data

Fit for the mono- and dinuclear copper(II) complexes of $\mathbf{H_3L^1}$ $[\mathbf{H_2L^1}Cu^{II}(solvent)_2]^+$ (left) and $[\mathbf{HL^1}Cu^{II}_2(OMe)]^+$ (right).

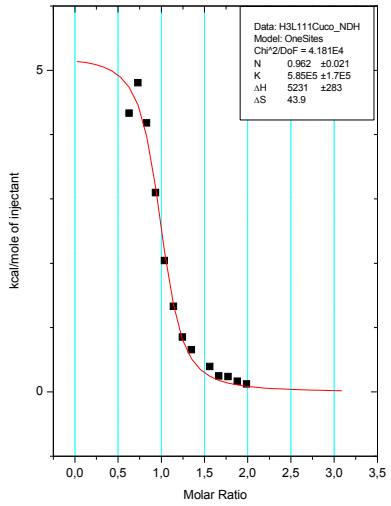

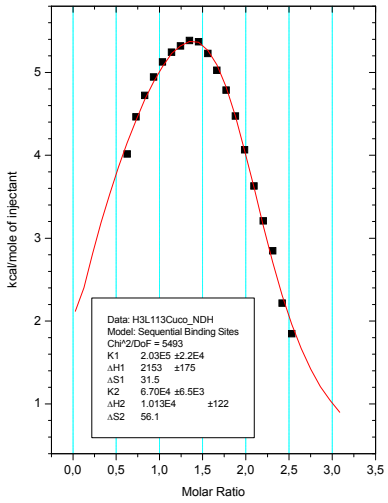

Fit for the mono- and dinuclear copper(II) complexes of $\mathbf{H_3L^2}$ $[\mathbf{H_2L^2}Cu^{II}(solvent)_2]^+$ (left) and $[\mathbf{HL^2}Cu^{II}_2(OMe)]^+$ (right).

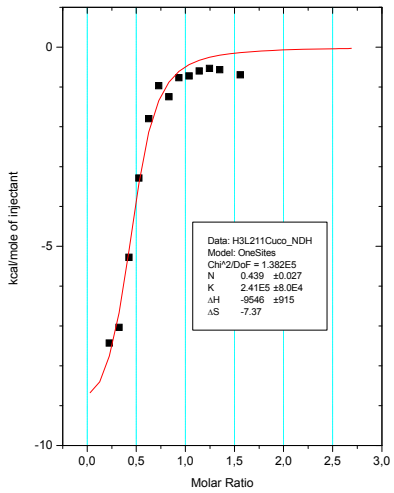

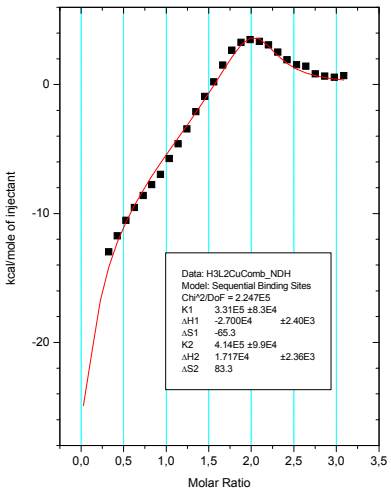

Fit for the mono- and dinuclear copper(II) complexes of $\mathbf{H_3L^3}$ $[\mathbf{H_2L^3}Cu^{II}(solvent)_2]^+$ (left) and $[\mathbf{HL^3}Cu^{II}_2(OMe)]^+$ (right).

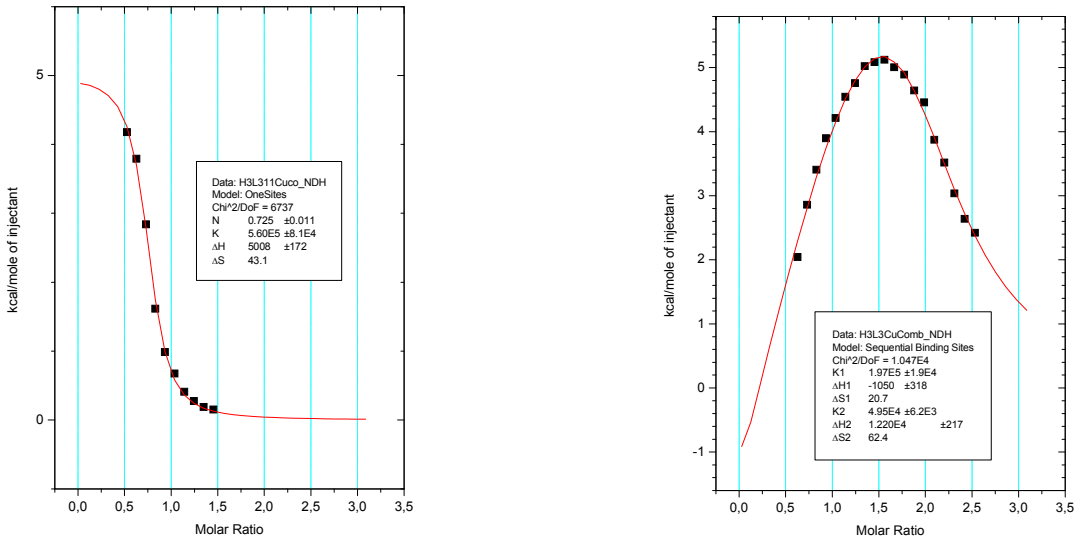

C DFT Calculated Structures of the Dinuclear Copper(II) complexes of $\mathbf{H_3L^2}$ and $\mathbf{H_3L^3}$

Topview of DFT calculated (G03, B3LYP/6-31g*) mononuclear copper(II) complexes of $\mathbf{H_3L^2}$ (a), $\mathbf{H_3L^3}$ (b), and $\mathbf{H_3L^{wa}}$ (c).

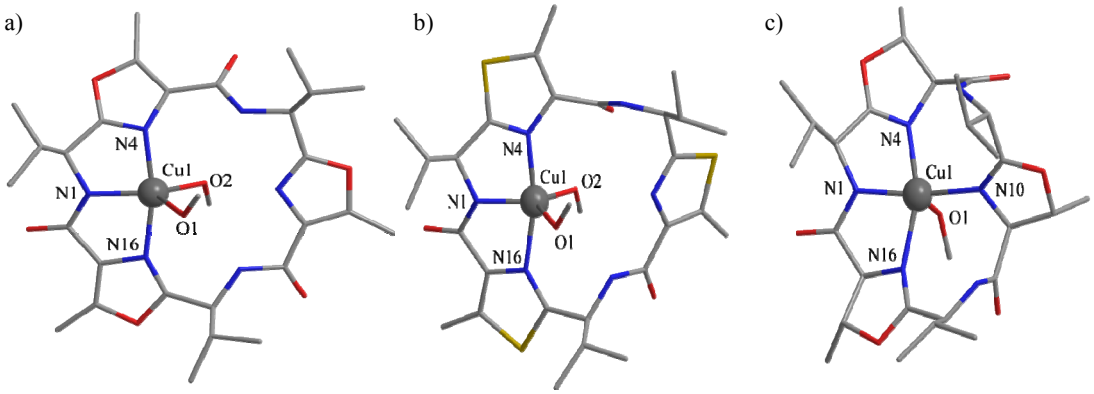

Topview of the DFT calculated structures (G03, B3LYP/6-31g*) methanol bridged dinuclear complexes of $\mathbf{H_3L^2}$ (a), $\mathbf{H_3L^3}$ (b), and $\mathbf{H_3L^{wa}}$ (c).

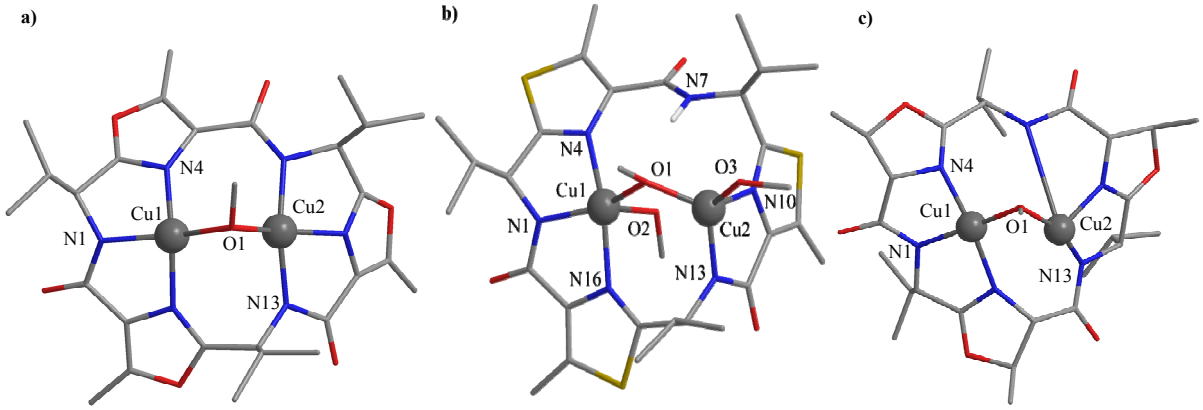

D Calculated *g* and *A* tensors of $H_3L^{2,3}$ and H_3L^{wa}

Calculated *g* and *A* tensors with various combinations of functionals and basis sets: tables and visualizations. See in text (Chapter 3) for references. Wachters[142] basis set was solely applied on copper.

H_3L^2:

	Experimental *g* values			Experimental *A* tensors [10^{-4} cm^{-1}]		
Functional / Basis set	$g_x = 2.083$	$g_y = 2.034$	$g_z = 2.279$	$A_x = 15$	$A_y = 17$	$A_z = 153$
MAG-ReSpect[127]	2.081	2.095	2.292	19	4	182
BHLYP / TZVP[136] Wachters[142]	2.092	2.102	2.319	9	31	314
BHLYP / IGLO-II[140] Wachters	2.081	2.101	2.305	1	17	298
BHLYP / EPR-II[141] Wachters	2.060	2.142	2.304	21	72	305
BHLYP / 6-311g*[139] Wachters	2.085	2.100	2.304	11	33	311
B40LYP / IGLO-II Wachters	2.086	2.097	2.302	21	72	305
BHLYP / IGLO-II Wachters SOC	2.061	2.143	2.305	15	66	291

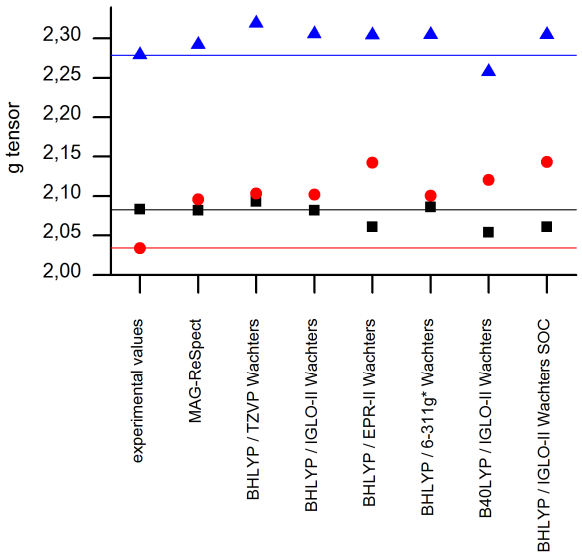

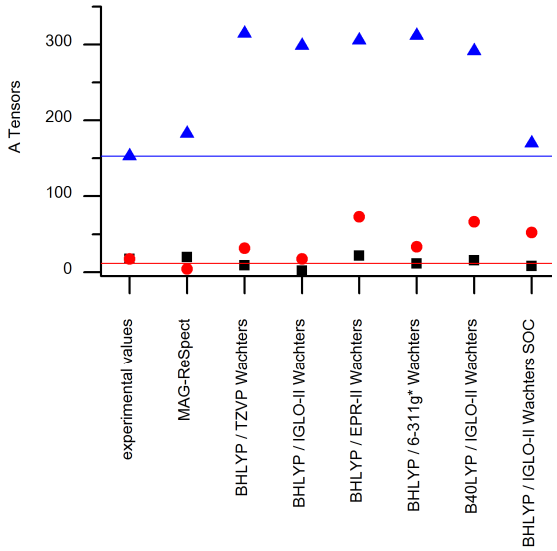

H_3L^3:

Functional / Basis set*)	Experimental *g* values			Experimental *A* tensors [10^{-4} cm^{-1}]		
	$g_x = 2.082$	$g_y = 2.037$	$g_z = 2.263$	$A_x = 15$	$A_y = 19$	$A_z = 150$
MAG-ReSpect	2.082	2.096	2.295	35	25	166
B38LYP / IGLO-II Wachters	2.070	2.083	2.244	9	28	289
B38LYP / IGLO-II Bauschlicher	2.071	2.085	2.257	100	120	175
BHLYP / 6-311g* IGLO-II Wachters	2.088	2.099	2.305	11	31	311
BHLYP / 6311g* Wachters	2.081	2.102	2.306	18	18	298
BHLYP / EPR II Wachters	2.087	2.099	2,302	109	31	310
BHLYP / IGLO-II Wachters	2.081	2.101	2.305	2	17	298
BHLYP / IGLO-II grid5	2.086	2.099	2.302	10	31	310
BHLYP / IGLO-II grid5 SCF tight	2.086	2.099	2.302	11	31	311
BHLYP / IGLO-II Kaupp	2.089	2.100	2.309	12	31	305
BHLYP / IGLO-II SOCFlag 1,3,3,5	2.086	2.099	2.302	10	31	310
BHLYP / TZV[136] Wachters	2.086	2.109	2.322	2	15	300
BHLYP / TZV IGLO-II Wachters	2.088	2.099	2.306	10	30	310
BHLYP / TZVP[136] Wachters	2.086	2.109	2.322	3	15	300
BHLYP / IGLO-II Wachters	2.086	2.099	2.302	11	31	310
BHLYP / IGLO-II Wachters SOC	2.086	2.098	2.300	12	30	176

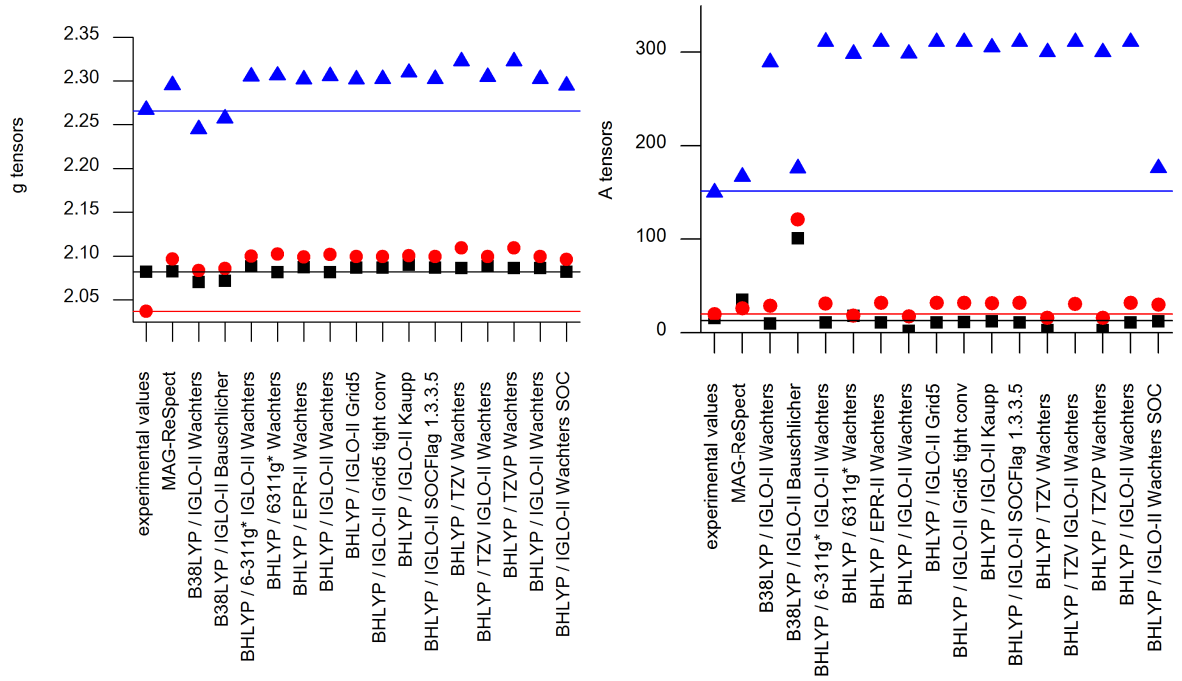

H_3L^{wa}:

Functional / Basis set*)	Experimental g values			Experimental A tensors [10^{-4} cm^{-1}]		
	$g_x = 2.083$	$g_y = 2.051$	$g_z = 2.267$	$A_x = 14$	$A_y = 16$	$A_z = 175$
BHLYP / EPR-II Wachters	2,072	2,097	2,298	0	35	303
BHLYP / IGLO-II Wachters	2,091	2,101	2,324	8	16	302
BHLYP / IGLO-II Partridge	2,095	2,110	2,344	0	13	296
MAG-ReSpect BHLYP IGLO-II	2,090	2,094	2,311	not determined		

E MCD Data: Fits of the VTVH Curves

VTVH curves of $[\mathbf{H_1L^1}Cu_2^{II}(\mu\text{- }OHCH(CH_2OH)_2)]^{2+}$

Fit assuming an isolated S = ½ species (e.g. monomeric impurity):

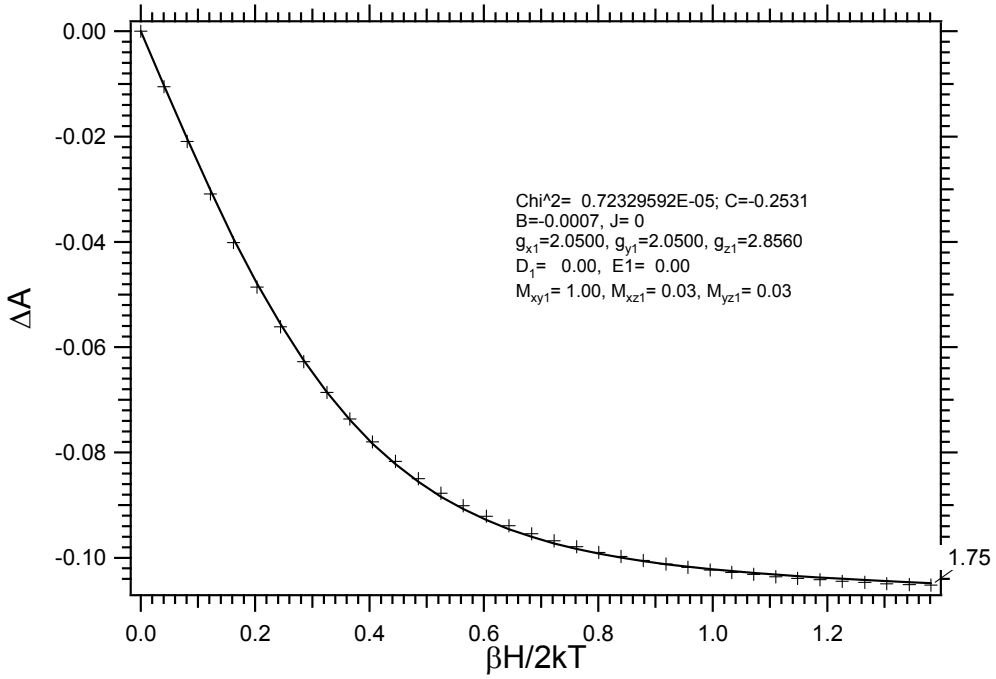

Fit assuming an anitferromagnetically coupled species with small *J*:

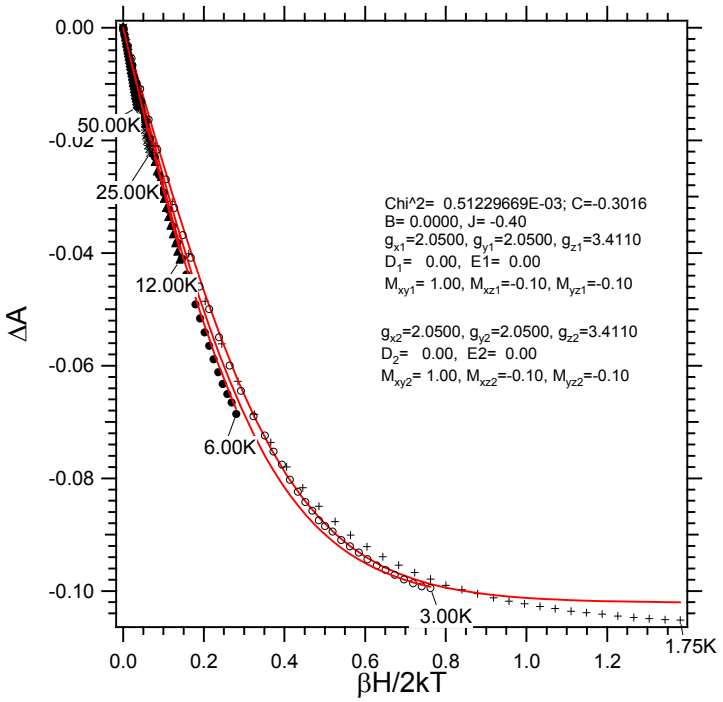

F Crystallographic Data

	$\mathbf{H_4L^{4\text{-}bn}}$	$\mathbf{H_4L^{rs}}$	$[\mathbf{H_2L^{rs}}Cu^{II}_2(\mu\text{-}OH)(H_2O)_2]^+$
Identification code	nd1	nd4a	nd8b
Empirical formula	C26 H41 N6 O5	C40 H60 N12 O4	C40 H62 Cu2 N12 O7, Cl O4, 2(H2 O)
Formula weight	517.65	773.00	1085.58
Temperature / Wavelength	200(2) K / 71.073 pm	200(2) K / 71.073 pm	200(2) K / 71.073 pm
Crystal system	Tetragonal	Tetragonal	Monoclinic
Space group	P 41 21 2	I -4	P 2 / c
Unit cell dimensions	a = 16.824(2) pm, α = 90°. b = 16.824(2) pm, β = 90°. c = 20.119(4) pm, γ = 90°.	a = 19.861(3) pm, α = 90°. b = 19.861(3) pm, β = 90°. c = 6.9222(14)pm. γ = 90°.	a = 11.876(2) pm , α = 90°. b = 11.599(2) pm, β = 102.09 (3). c = 18.240(4) pm, γ = 90°.
Volume	5694.5(16) nm^3	2730.4(8)nm^3	2456.8(8) nm^3
Z	8	2	2
Absorption coefficient	0.085 mm^{-1}	0.063 mm^{-1}	0.993 mm^{-1}
F(000)	2232	832	1138
Crystal size	0.2 x 0.02 x 0.02 mm^3	0.3 x 0.21 x 0.11 mm^3	0.2 x 0.06 x 0.05 mm^3
Theta range for data collection	1.58 to 22.38	2.90 to 28.12	2.57 to 30.47
Index ranges	-17 ≤ h ≤ 17, -17 ≤ k ≤ 18, -20 ≤ l ≤ 21	-26 ≤ h ≤ 26, -26≤ k ≤ 29, -9 ≤ l ≤ 9	-16 ≤ h ≤ 16, -16≤ k ≤ 17, -24 ≤ l ≤ 25
Reflections collected	29980	13373	29065
Independent reflections	3651 [R(int) = 0.0450]	3313 [R(int) = 0.0450]	3384 [R(int) = 0.0503]
Completeness to theta = 22.62°	99.6%	99.6%	91.5%
Refinement method		Full-matrix least-squares on F2	
Data / restraints / parameters	3651 / 9 / 371	3316 / 0 / 132	6841 / 0 / 324
Goodness-of-fit on F^2	0.863	1.13	0.847
Final R indices [I>2sigma(I)]	R1 = 0.0450, wR2 = 0.0994	R1 = 0.1749, wR2 = 0.3757	R1 = 0.1206, wR2 = 0.1262
R indices (all data)	R1 = 0.0761, wR2 = 0.1085	R1 = 0.1288, wR2 = 0.3577	R1 = 0.0503, wR2 = 0.1015
Absolute structure parameter	-1 (2)	6 (6)	-1 (2)
Largest diff. peak and hole	0.269 d -0.310 e.$Å^{-3}$	1.613 d -0.534e.$Å^{-3}$	0.578 and -0.612e. $Å^{-3}$

G NMR and EPR Spectra of the Pink Species of H_4L^4

NMR spectra (200 MHZ, MeOH-d_4) of $\mathbf{H_4L^4}$ (green) and the pink species. NMR signals: δ = 0.85 (d, ^3J = 6.6 Hz, 3H, CHC$\underline{H}_3$); 1.10 (d, ^3J = 6.7 Hz, 3H, CHC$\underline{H}_3$); 2.39-2.51 (m, 1H, C$\underline{H}$(CH$_3$)$_2$); 2.47 (s, 3H, C$_{het}$C$\underline{H}_3$); 3.61 (s, 3H, NC$\underline{H}_3$); 4.94 (dd, ^3J = 9.5, 9.5 Hz, 1H, C$_\alpha$$\underline{H}$) ppm.

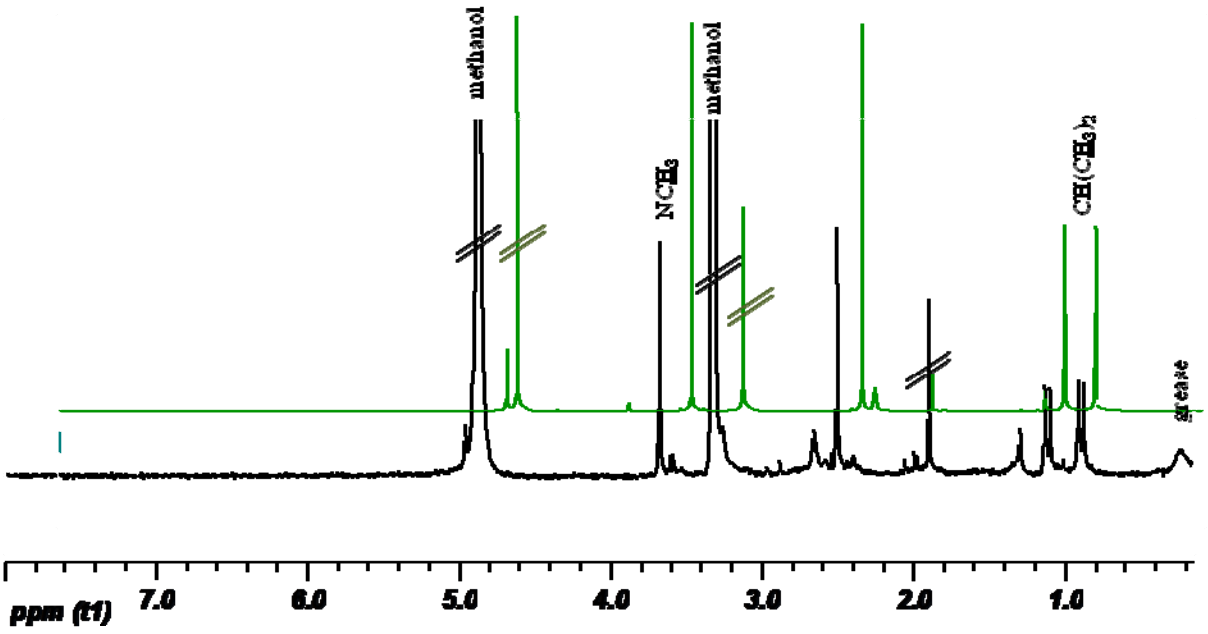

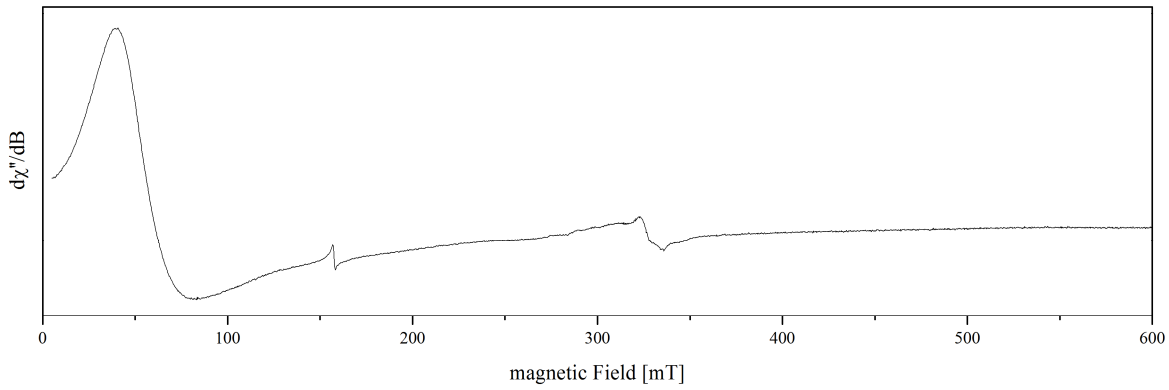

H Anisoptropic Spin Hamiltonian Parameters of the Dinuclear Copper(II) Complexes of $^{H}_{4}{}^{L4}$

Parameters [a]		$[\mathbf{H_2L^4}Cu_2]^{2+}$ [b]	$[\mathbf{H_2L^4}Cu_2(OH)]^{+}$ [c]	$[\mathbf{H_2L^4}Cu_2(OH)_2]$ [d]	$[\mathbf{H_2L^4}Cu_2(^{13}CO_3)]$ [e]
Cu 1	g_x	2.05	2.0855	2.0049	2.0215
	g_y	2.09	2.0732	2.1128	2.1920
	g_z	2.20	2.1760	2.212	2.1924
A_x		20	42.742	35.917	45
A_y		30	54.523	26.876	45
A_z		155	48.225	169.838	111.2339
α		0	0.000	129.671	0
β		0	90.000	86.962	0
γ		0	0.000	143.146	0
X		0	0.000	2.71258	0.0
Y		0	0.000	0.480993	0.0
Z		0	0.000	0.262991	0.0
Cu 2	g_x	2.08	2.0520	1.9923	2.0211
	g_y	2.10	2.0748	2.1462	2.1914
	g_z	2.15	2.1753	2.1948	2.1930
A_x		30	28.526	29.402	9.1233
A_y		50	79.599	24.316	47.51394
A_z		140	160.366	156.481	93.34469
α		30	0.000	129.472	0
β		5	90.000	173.592	0
γ		30	0.000	160.457	0
X		-5.49910	0.000	-2.53655	0.0
Y		-0.154500	0.000	-0.2352	0.0
Z		0.217100	4.473	-0.7078	4.259
J [f]		-20	-20	-20	-20
R		5.223	4.473	4.9691	4.259

a) Units:X,Y,Z, R [Å], A [$10^{-4}cm^{-1}$], J [cm^{-1}], Line width parameters [Units: dA, lw, $10^{-4}cm^{-1}$; dJ, cm^{-1}; dr, Å];
b) Line width parameters for the two Cu(II) centers: $LW_{x1,y1,z1} = 15$; $LW_{x2,y2,z2} = 15$.
c) Line width parameters for the two Cu(II) centers: $dg_{x1}=0.002$, $dg_{y1}=0.002$, $dg_{z1}=0.002$, $dA_{x1}=1.0$, $dA_{y1}=1.0$, $dA_{z1}=1.0$; $dg_{x2}=0.002$, $dg_{y2}=0.002$, $dg_{z2}=0.002$, $dA_{x2}=1.0$, $dA_{y2}=1.0$, $dA_{z2}=1.0$, dJ=0.00 $dr^{-3}=0.000885$; $lw_x = 41.514791$, $lw_y=18.359317$, $lw_z=11.978638$.
d, e) Line width parameters for the two Cu(II) centers: $dg_{x1}=0.000018$, $dg_{y1}=0.000023$, $dg_{z1}=0.000000$, $dA_{x1}=49.670672$, $dA_{y1}=86.721661$, $dA_{z1}=44.414936$; $dg_{x2}=0.025879$, $dg_{y2}=0.000000$, $dg_{z2}=0.026824$, $dA_{x2}=59.283464$, $dA_{y2}=88.877275$, $dA_{z2}=13.504909$, dJ=0.00 $dr^{-3}=0.00$; $lw_x=0.001997$, $lw_y=30.310447$, $lw_z=31.107599$. The unresolved hyperfine coupling arises from contributions of A, lw, dg, and dA.
f) $H = J\, S_1.S_2$

I DFT Calculated Structures of the Copper(II) Complexes of Cyclic Pseudo Octapeptides

Dihydroxo complex of $\mathbf{H_4L^4}$, top and side view $[\mathbf{H_2L^4}Cu^{II}_2(OH)_2]$

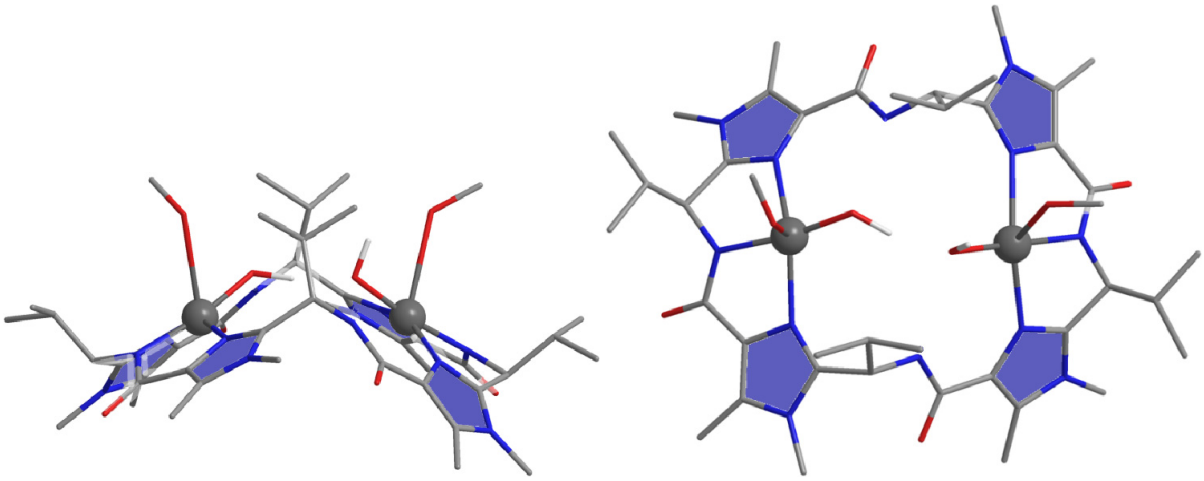

Overlay Plots of the DFT Calculated Structures of the Dinuclear Copper(II) Complexes of $\mathbf{H_4L^{ox}}$ and $\mathbf{H_4L^4}$:

$[\mathbf{H_2L^4}Cu^{II}_2]^{2+}$ (orange) *vs* $[\mathbf{H_2L^{ox}}Cu^{II}_2]^{2+}$ (black). Top (left) and sideview (right).

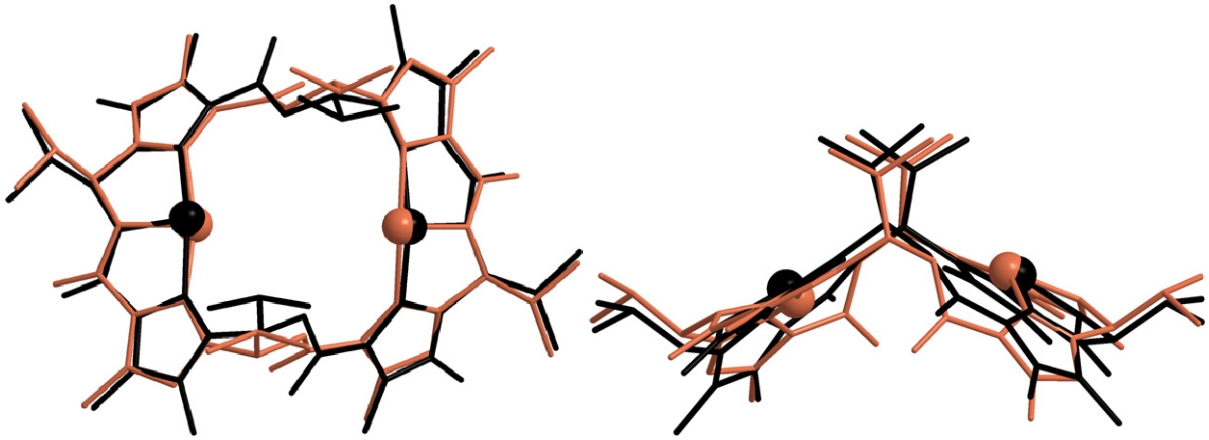

$[\mathbf{H_2L^4}Cu^{II}_2(\mu\text{-}CO_3)]^{2+}$ (orange) *vs* $[\mathbf{H_2L^{ox}}Cu^{II}_2(\mu\text{-}CO_3)]^{2+}$ (black). Top (left) and sideview (right).

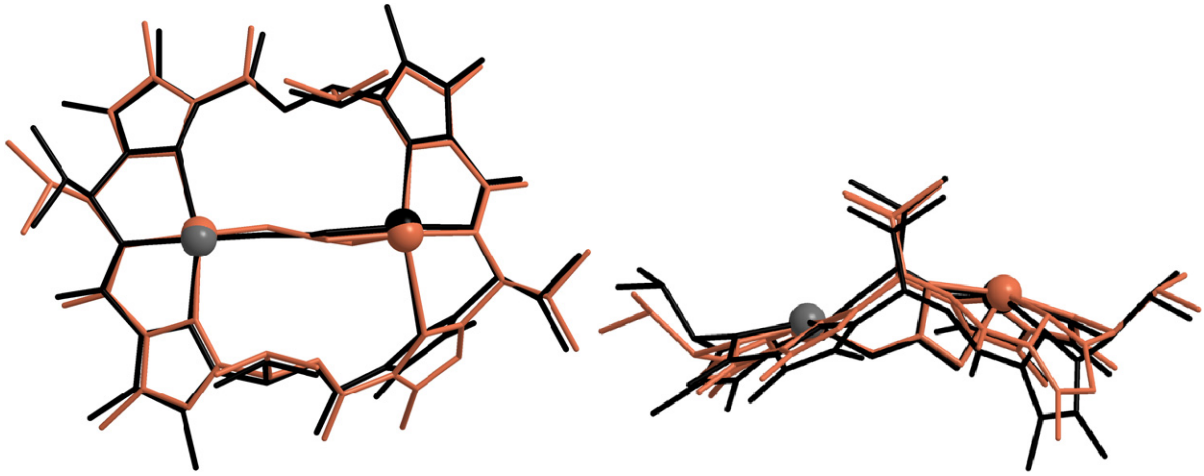

Top (left) and side view (right) of the overlay plots of the DFT calculated structures of the mononuclear copper(II) complex $[\mathbf{H_3L^{rs}}Cu^{II}_s(H_2O)_2]^+$, calculated with (Gaussian 09, B3LYP/6-31g*/TZVP, PCM, methanol) and without a solvation model.

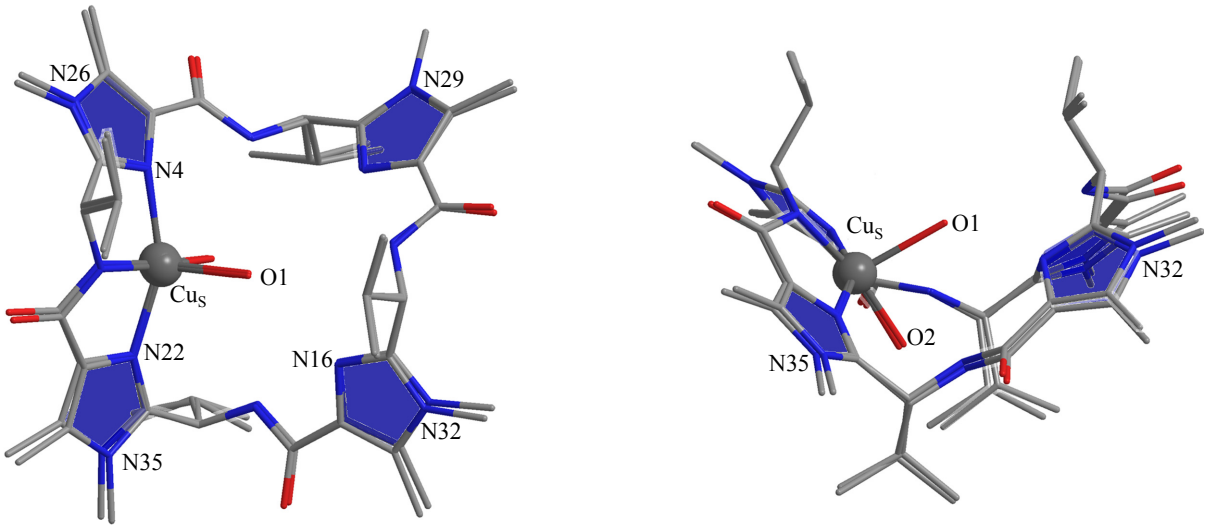

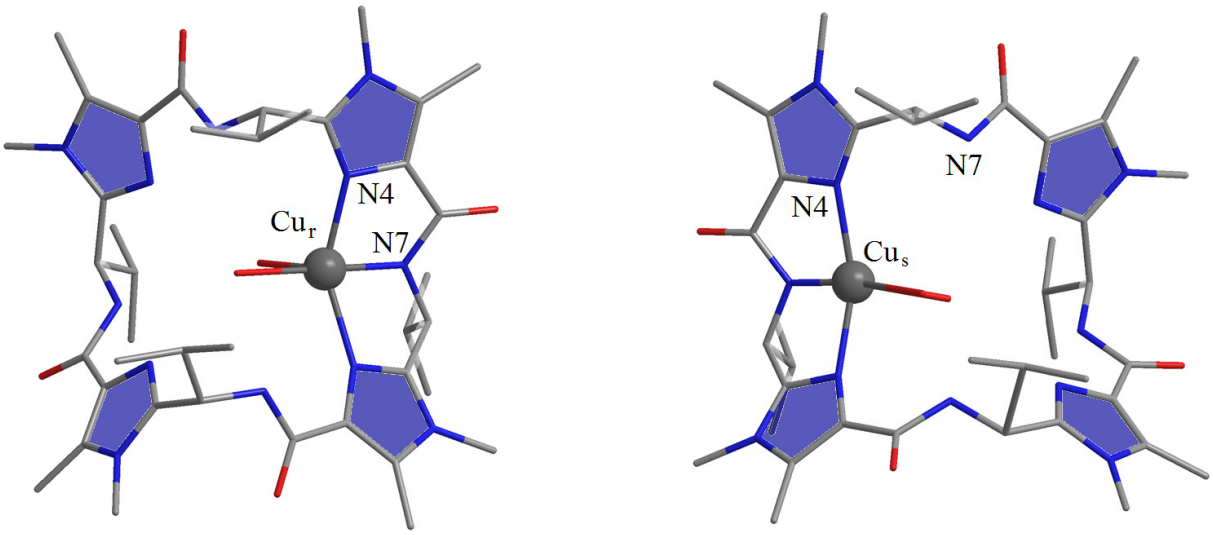

J UV-vis and CD Spectra of H_4L^{ascA}

Titration of 1-2 eq of base to an H_4L^{ascA} : copper(II) 1:2 solution

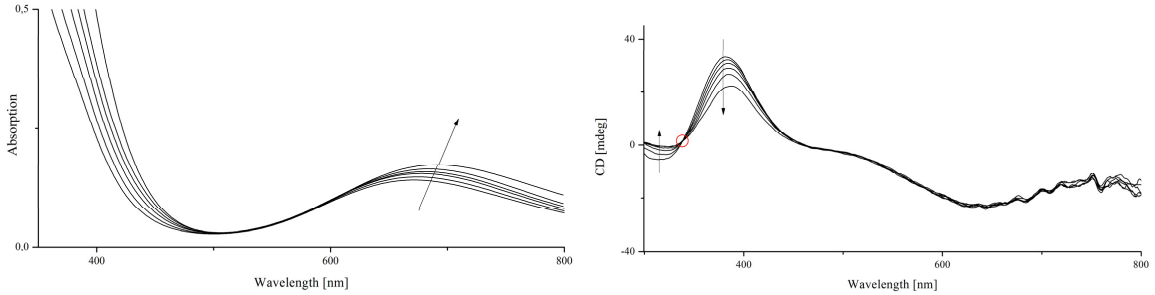

Titration of 2-3 equivalents of base an H_4L^{ascA} : copper(II) 1:2 solution

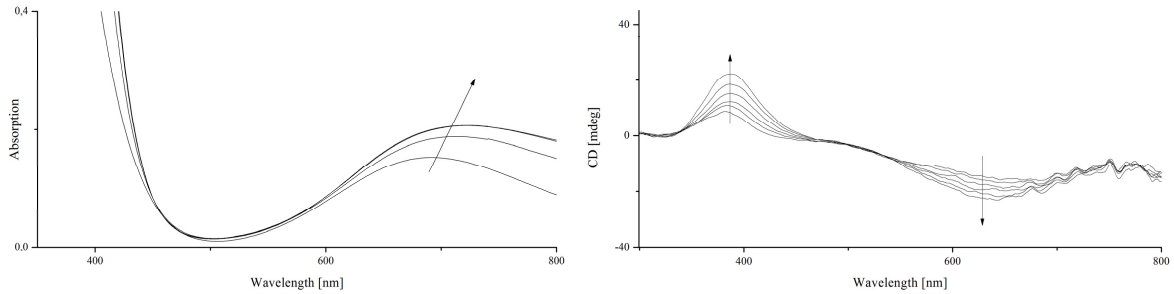

Erklärungen gemäß § 8 (3) b) und c) der Prüfungsordnung:

a) Ich erkläre hiermit an Eides statt, dass ich die vorliegende Arbeit selbst verfasst und mich dabei keiner anderen als der von mir bezeichneten Quellen und Hilfen bedient habe.

b) Ich erkläre hiermit an Eides statt, dass ich an keiner anderen Stelle ein Prüfungsverfahren beantragt bzw. diese Dissertation in dieser oder anderer Form bereits anderweitig als Prüfungsarbeit verwendet oder einer anderen Fakultät als Dissertation vorgelegt habe.

Heidelberg, 5. Oktober 2010

(Nina Dovalil)